Design of Nanocarrier Impregnated Transdermal Patch for the Sustained Release of Analgesic Drugs

Thesis submitted by

Sourav Adhikary

Doctor of Philosophy (Science)

School of Materials Science & Nanotechnology

Faculty of Interdisciplinary Studies, Law & Management (FISLM)

Jadavpur University

Kolkata-700032

India

2024

JADAVPUR UNIVERSITY

KOLKATA – 700032, INDIA

INDEX NO: D-7/ISLM/106/19

1. TITLE OF THE THESIS:

Design of Nanocarrier Impregnated Transdermal Patch for the Sustained Release of Analgesic Drugs

2. NAME, DESIGNATION & INSTITUTION OF SUPERVISORS:

Dr. Rajib Dey

Professor

Metallurgical and Material Engineering Department

Jadavpur University

Kolkata-700032

Dr. Mahua Ghosh Chaudhuri

Associate Professor

School of Materials Science and Nanotechnology

Jadavpur University

Kolkata-700032

3. LIST OF PUBLICATION:

- Adhikary, S., Al Hoque, A., Ray, M., Paul, S., Hossain, A., Goswami, S., & Dey, R. (2023). Investigation of Paracetamol Entrapped Nanoporous Silica Nanoparticles in Transdermal Drug Delivery System. Applied biochemistry and biotechnology, 195(8), 4712–4727. https://doi.org/10.1007/s12010-023-04576-w

- Adhikary, S., Al Hoque, A., Ray, M. et al. Tailored Transdermal Drug Delivery System for Pain Management: Development and Evaluation of Clonidine Hydrochloride/Sodium Montmorillonite Composite Patch. BioNanoSci. 14, 1651–1664 (2024). https://doi.org/10.1007/s12668-024-01402-3

4. LIST OF PATENTS: NIL

5. LIST OF PRESENTATIONS IN NATIONAL /INTERNATIONAL:

- Poster presentation at the *International Conference on Nano Science and Technology (ICONSAT)* on March 5-7, 2020. Venue: Biswa Bangla Convention Centre, New Town, Kolkata.

- Paper presentation at *METALLIX'24*, the annual national symposium for Metallurgical and Material Engineering students at Jadavpur University, on March 15-16, 2024.

- Paper presentation at the *International Conference on Nonferrous Metals & Material Science 2024* on March 29-30, 2024. Venue: Biswa Bangla Convention Centre, New Town, Kolkata.

STATEMENT OF ORIGINALITY

I, Sourav Adhikary, registered on 5th November 2019 do hereby declare that this thesis entitled "**Design of Nanocarrier Impregnated Transdermal Patch for the Sustained Release of Analgesic Drugs**" contains literature survey and original research work done by the undersigned candidate as part of Doctoral studies.

All information in this thesis have been obtained and presented in accordance with existing academic rules and ethical conduct. I declare that, as required by these rules and conduct, I have fully cited and referred all materials and results that are not original to this work.

I also declare that I have checked this thesis as per the "Policy on Anti Plagiarism, Jadavpur University, 2019", and the level of similarity as checked by iThenticate software is **7%**.

Signature of Candidate: Sourav Adhikary.

Date: 22/11/2024.

Certified by Supervisor(s):

(Signature with date, seal)

1. Rajib Dey 22/11/24

Professor
Metallurgical & Material Engg. Dept.
Jadavpur University
Kolkata - 700032

2. Mahua Ghosh Chaudhuri 22/11/24

Dr. (Ms) Mahua Ghosh Chaudhuri
Associate Professor
School of Materials Science and Nano Technology
Jadavpur University
Kolkata-700 032, India

CERTIFICATE FROM THE SUPERVISORS

This is to certify that the thesis entitled "**Design of Nanocarrier Impregnated Transdermal Patch for the Sustained Release of Analgesic Drugs**" submitted by **Sourav Adhikary**, for the award of **PhD (Science)** degree of Jadavpur University is absolutely based on his own work under the supervision of **Dr. Rajib Dey** and **Dr. Mahua Ghosh Chaudhuri** and that neither this thesis nor any part of the same has been submitted for any degree/diploma or any other academic award anywhere before.

Rajib Dey 22/11/24

Dr. Rajib Dey

Professor

Metallurgical and Material Engineering Department

Jadavpur University

Kolkata-700032

Professor
Metallurgical & Material Engg. Dept.
Jadavpur University
Kolkata - 700032

Mahua Ghosh Chaudhuri 22/11/24

Dr. Mahua Ghosh Chaudhuri

Associate Professor

School of Materials Science and Nanotechnology

Jadavpur University

Kolkata-700032

Dr. (Ms) Mahua Ghosh Chaudhuri
Associate Professor
School of Materials Science and Nano Technology
Jadavpur University
Kolkata-700 032, India

Dedicated

to

My Family

Acknowledgement

I would like to take this opportunity to express my gratitude to every individual who has remained by my side throughout this entire journey. My entire PhD journey has been a rollercoaster ride of learning, happiness, struggle, and frustration. Without the constant support and guidance of all these people, this journey would not have been possible.

Firstly, I would like to acknowledge the contribution of Dr. Rajib Dey, Professor, Metallurgical and Material Engineering Department, Jadavpur University, Kolkata who has not only been my technical mentor but also been my friend, philosopher, and guide. During my toughest times, his motivation and guidance have been a blessing. My other co-guides, Dr. Mahua Ghosh Chaudhuri, Associate Professor, School of Materials Science and Nanotechnology, Jadavpur University, Kolkata and Late Dr. (Dr.) Subrata Goswami, Directorate of ESI (MB) Scheme, Department of Labour, Government of West Bengal has also supported in the best way possible. From a student of Chemistry to a PhD scholar in the field of Nanobiotechnology – this transition would have been difficult without their thorough supervision. It was the vision of Late Dr. (Dr.) Subrata Goswami to develop such an innovative approach to pain treatment which I have tried to develop through my research. I hope that in the future such formulations will be available commercially and his dream will turn into reality.

I would also like to express respect and admiration towards ex-professor Dr. Gopes Chandra Das of the Metallurgical and Material Engineering Department, Jadavpur University, Kolkata and Dr. Biswajit Mukherjee of the Department of Pharmaceutical Technology, Jadavpur University, Kolkata. Their academic wisdom has been a boon for me in my research work.

I also owe my success to all the professors and lab technicians of this department without whom my journey would have been incomplete.

My special thanks to all my lab seniors and juniors Dr. Maharshi Ghosh Dastidar, Amit Kumar Bhandary, Dr. Pritha Pal, Arnab Swarnakar, Dr. Bitan Kumar Sarkar, Dr. Ahana Banerjee, Santosh Khan, Alakananda Chatterjee, Ayan Pal, Subham Bose, Sanjib Mondal, Swastik Paul for their constant support throughout my journey. In the toughest of my times, they acted as pillars of support and the brotherhood I developed with them will remain forever even beyond my research journey.

Also, my special thanks to Ashique Al Hoque (Ashique Da) and Manisheeta Ray (Moni), Research Fellows of the Department of Pharmaceutical Technology, Jadavpur University, Kolkata for making me understand the pharmaceutical aspects that were the backbone of my research work.

Pursuing a PhD in a completely different field has been a challenging task for me and in this reference I need to acknowledge Manisheeta Ray (Moni) for clearing my doubts without any hesitation and supporting me in every way possible. Her presence has truly helped me to overcome the hurdles with ease.

One name that I need also to mention is Debadrita De, Senior Chemist, IRS, ONGC, Ahmedabad. Our friendship, which started in my graduation days, remains unchanged even today. She was the first to spot this research project advertisement for me and even accompanied me during my interview in this department just to motivate and support me. Such feelings are hard to describe in words. From the bottom of my heart, I thank her for staying by my side.

I am forever indebted to my parents and family members for bearing with all my frustrations throughout my journey. My tenure as a research scholar consisted of several struggles and hardships but I always find peace in my home. When all my friends opted for a job, my decision to pursue a PhD appeared as a shock for everybody except my parents who have never forced

me to set aside my aspirations of doing a PhD and supported me in every way possible. Today on the verge of completing my PhD, I dedicate my success to them.

Finally, I gratefully acknowledge the Department of Higher Education, Science & Technology and Biotechnology, Government of West Bengal (File no: ST/P/S&T/6G-32/2017) for funding me during my initial phase of research work (2018-2021).

Sourav Adhikary

List of Contents

List of Figures

Chapter 5B: Drug Delivery by Montmorillonite Nanoclay-Based Transdermal Patch

List of Tables

Chapter 6: Overall Conclusion, Limitations, IPR Issues and Future Scope of Work

Chapter: 1
Introduction

1.1. Nanoscience and Nanotechnology:

Nowadays in the field of research and development, nanoscience and nanotechnology have received much more attention. The term “nano” was invented from the Greek word “nanos” which means “dwarf.” Therefore, a tiny object comes to mind whenever we think about nanoscience or nanotechnology. Nanoscience involves a lot of theories regarding functionality, properties, and different phenomena shown by the materials whose dimensions are measured within the nanoscale whereas nanotechnology deals with the development, application, and implication of such nano-sized material. These materials are called nanomaterials with at least one dimension in the 1-100 nm range. Nanomaterials are categorized based on their dimensions: zero, one, two, and three-dimensional. Zero-dimensional nanomaterials, like nanoparticles, have all dimensions under 100 nm. One-dimensional nanomaterials, such as nanotubes and nanowires, have only one dimension outside the nanoscale. Two-dimensional nanomaterials, like ultrathin films, have two dimensions larger than 100 nm. Three-dimensional nanomaterials, including nanocomposites, have no dimensions confined to the nanoscale but display nanoscale features [1]. Nanotechnology has become a driving force behind a new industrial revolution in both the private and public sectors. It has been applied to IT and communications in developing sensors, quantum computing, photonics, and novel communications [2]. Furthermore, nanotechnology is being incorporated to develop solar cells and fuel cells as clean, affordable, renewable energy sources to decrease the energy consumption and toxicity burden on the environment [3]. It also has an application in medical science and healthcare to make a precise solution for preventing the disease, diagnosis, and treatment [4].

1.2. Nanobiotechnology:

Nanobiotechnology is nothing but a liaison between nanotechnology and biology. This technical approach towards biology allows a scientist to think and create some devices or materials that can be used for biological research. The application of nanophotonics to manipulate the molecular processes in living cells, imaging of biological membranes, biomolecules and tissues etc. are the major topics for nanobiotechnology researchers. Recently, the topic of synthesis of nanoparticles using microorganisms has been of great interest [5]. Also in the food sector, the pesticide delivery systems through nanoencapsulation, the use of biosensors to detect and quantify organic compounds, etc. led to the applications of nanobiotechnology [6]. Besides, nanobiotechnology has led to the optimization of the drug delivery system, for effectively serving the currently available bioactive tool. The nanomedicines have become well appreciated since the nano-sized particles can move more freely, can enter the cell membrane easily in the human body than larger materials, and could be utilized as delivery agents for encapsulating therapeutic drugs along with delivering them to the target diseased cells with control as well as sustained release [7].

1.3. Nanotechnology in the Drug Delivery:

A drug is a chemical substance that is used to prevent or cure a disease or to lessen its symptoms. However, due to the low solubility (hydrophobicity) of the drug molecules and their lack of specificity, an effective concentration of the drug at the target site cannot be achieved. Therefore, patients need to take high doses of drugs to achieve the desired therapeutic level for treating a particular disease. As a result of this, some undesired interactions occur between the drug molecules and healthy cells & tissues in the case of conventional drug delivery which is known as the side effects of the drug. To overcome these problems, different polymeric devices such as microspheres [8], and nanoparticles [9] have been designed as a biocompatible nano

drug carrier [10]. Various nanodevices like carbon nanotubes (CNT) [11] and quantum dots [12] have been reported for this purpose. Also, nanoclay [13] and layered double hydroxide (LDH) [14] particles can serve as nano drug carriers. The advantages associated with these nanotechnology-based drug delivery systems are [15]:

- They can protect drugs from degradation with time in the physiological environment.
- Controlled as well as sustained release of drugs from nanoparticles can be achieved.
- Maximum patient compliance at a minimal dose and side effects are observed.
- They reduce treatment expenses.
- They allow the delivery of insoluble drugs as well as drugs that are difficult to administer.
- The drug does not lose its therapeutic efficacy while in circulation throughout the bloodstream in the human body.
- They improve the bioavailability of the drugs.
- They can permeate the skin barrier.
- They can be used at specific target sites for drug delivery.

1.4. Difference between Conventional and Modified Release Dosage Forms:

Conventional drug delivery systems release the drug instantly, in which the release of the drug cannot be controlled and an effective concentration cannot be maintained at the target site for a longer period. The oral route is mainly preferred among other administration routes of drugs like parental, nasal, transmucosal, transdermal, etc. The formulations for conventional oral drug delivery could be a tablet, a pill, or a capsule. In the case of conventional dosage forms, (A) the dosing interval is relatively short which means that maintaining the amount of drug in the blood for a long duration of time, is so important that every three, four or six hours, depending upon the type of dosage form we must take the second dose. Therefore, a presence

of large bands and valleys in the drug level is observed i.e., the drug level may exceed the maximum toxic concentration (MTC) or may remain below the minimum effective concentration (MEC) of the drug for which the drug then shows the side effects and (B) if we miss the dose once or twice, the effect of the drug will be diluted [16]. Hence to overcome the above-mentioned problems the conceptualization of a modified release dosage form occurred. Modified release is classified mainly into two categories: controlled release and delayed release. Again, the controlled release is of three types: sustained, extended, and prolonged release [17]. Sometimes all these releases are interchangeably used by some authors for the same purpose which is sustained release. The difference between the controlled and sustained release is so much confusing. Generally, it can be said that the controlled release is exhibited by those systems that can deliver the drugs or any therapeutic material at predetermined rates over a certain period. The sustained release systems mainly release the drug very slowly over an extended period. So, the basic concept, in brief, is if the systems succeed in maintaining the constancy of the drug levels in the blood or any target site, it must be considered a controlled-release system. However, it will be regarded as a sustained release system (Fig 1.1) if it fails to preserve consistency while prolonging the period of action beyond what is possible with conventional delivery. One more important thing is that the sustained release may or may not be controlled. Sustained-release dosage forms have many advantages [18] that include:

(1) Patient compliance is enhanced because the frequency of intake of doses is reduced.

(2) The total amount of drug for administration is lessened and thus

(2a) the availability of the drug becomes maximized with minimum dose,

(2b) side effects of the drug are diminished or sometimes eliminated.

(3) Absorption of the drug molecules is controlled to a greater extent so that high blood levels can be observed for a long time after administration.

(4) The blood level variation in the case of several doses of conventional delivery is minimized.

Also, the sustained release dosage form has a few disadvantages like (a) increased cost, (b) occurrence of dose dumping, (c) poor in vitro and in vivo correlation, (d) the drugs having very short or very long half-life is not suitable for this purpose [18].

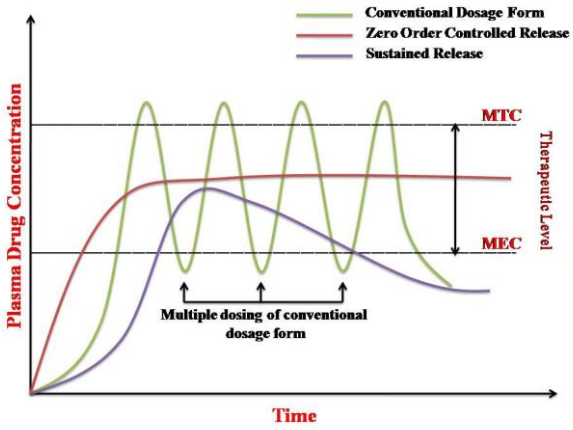

Fig 1.1 Plasma concentration profile for conventional, controlled, and sustained release formulations

1.5. Routes of Drug Administration via Skin and Their Importance over Conventional Route:

There are various ways to administer the drugs through the skin such as intramuscular (IM), intravenous (IV), subcutaneous (SC), and transdermal to avoid first-pass metabolism as well as to increase the bioavailability of the drugs, and gastric irritation that occurs in most preferred conventional route of drug administration i.e., oral route. Additionally, the drug administration via skin requires less frequent dosing compared to oral medications, leading to better patient adherence to treatment regimens. However, IM injections may cause discomfort, particularly when administering high dosages of drugs that irritate muscle tissue, IV injection necessitates vein puncture, which may be painful and increase the risk of thrombosis, haemorrhage, or infection, and SC injections may induce redness, swelling, or irritation [19]. On the other hand, the transdermal route offers a convenient, painless, and effective alternative to injections for

the delivery of medications, particularly for drugs that require controlled, sustained release or are associated with injection-related issues such as pain, needlestick injuries, and poor patient compliance.

1.6. Importance of Transdermal Drug Delivery System (TDDS):

The Transdermal Drug Delivery System (TDDS) got great attention among the routes owing to a few advantages [20]:

- They provide sustained release of the drugs at the site of application, thereby dosing frequency gets reduced.
- Anxiety and pain associated with injections can be avoided.
- Patients may administer TDDS on their own. This improves convenience, especially for patients who need to take medications over an extended period.
- Patient compliance is largely increased due to its non-invasive and user-friendly nature.
- TDDS can lead to cost savings by minimizing the requirement for healthcare professional involvement in drug administration.

However, there are certain limitations in TDDS [20]:

- Skin irritation may occur.
- Delivery of the ionic drug molecules and macromolecules is not possible.
- Not suitable for patients having very low blood flow on peripheral sites etc.

1.7. History of Transdermal Patches:

The concept of transdermal delivery dates to ancient times when medicinal substances were applied to the skin to treat various ailments. Ancient civilizations, including the Egyptians and Greeks, used poultices and salves made from herbs and other natural substances for therapeutic

purposes. The modern history of transdermal patches began in the 19th century with experiments in drug delivery through the skin. In 1887, a German physician named Paul Ehrlich conducted experiments on skin permeability and observed that certain dyes could penetrate the skin. The first documented use of transdermal delivery for therapeutic purposes occurred in the early 20th century. The transdermal system, made of scopolamine drug was approved in the USA (1979) for the treatment of motion sickness. In 1984, a transdermal patch containing nicotine was approved by the United States Food and Drug Administration (FDA) [21]. Over the years, advancements in materials science and drug delivery technology have led to improvements in transdermal patch design. Patches have become thinner, more flexible, and better at controlling drug release rates. Currently, different types of transdermal patches for different purposes like contraception, pain relief (cancer or chronic), urinary incontinence, hormone replacement, etc. are available in the market and all of those are FDA-approved.

1.8. Components of Transdermal Patches:

Transdermal patches are made of different components [20]:

- A backing film that protects the patch from moisture uptake which subsequently protects the patch from the bulkiness of the material and microbial contamination.
- A reservoir that is nothing but a polymeric matrix.
- Drug molecules.
- Suitable solvents in which the drugs are completely solubilised or dispersed.
- Semi-permeable membrane (in case of multi-layered type or reservoir type transdermal patches) which is used to control the release of the drug.
- Adhesive material that keeps the components of the patch adhered as well as adheres the patch to the skin.

- ⍟ Penetration enhancer for increasing the permeation of the drug molecules through the skin.
- ⍟ Plasticizers that are used to enhance the flexibility and lower the brittleness of the patch.
- ⍟ Liner that is removed before use.

1.9. Definition and Classification of Pain:

In this research work, only pain management has been focused as pain is the common reason for people to consult doctors. Pain is nothing but an early warning system that protects us from the environment around us and ourselves. There are many pain detectors (nerve cells) in most areas of the human body. Those detectors are called "nociceptors" and are stretched from our spinal cord to every organ of the body. Nociceptors can conduct electrical signals like other nerve cells through which the information is sent back to the brain from the located area. Unlike other nerve cells, nociceptors give a response only when something happens that could cause damage. For example, no pain will be felt if the tip of a needle is gently touched. Instead of the pain, a metallic nature will be felt for which the normal nerve cells are responsible. But by pushing harder to the tip of the needle, the nociceptor threshold is crossed and then pain is felt consequently (**nociceptive pain**) [22]. Certain chemicals produced by the damaged cells are responsible for lowering the nociceptors' threshold to a point where just a touch can cause pain. This is where a set of classes of drugs such as opioid and non-opioid drugs (analgesic, anti-inflammatory drugs) come in. Another two types of pain that make people uncomfortable:

- ❖ **Neuropathic pain** that originates from damage to the nerves or other portions of the nervous system. This pain may lead to mobility issues [22].
- ❖ **Radicular pain** occurs when the spinal nerves get compressed or inflamed. People who suffer from this pain may experience muscle weakness, numbness, and tingling [22].

1.10. Requirement for the Transdermal Patches of Pain-Relief Drugs:

There is an increased chance of adverse effects such as gastrointestinal, hepatic, and renal problems when using oral medications for a prolonged period. Because of this, more attention has been placed on alternatives to traditional medications, such as pain relief transdermal Patches. The FDA-approved pain relief patches have grown in popularity in recent years. The active ingredients found in pain relief patches available already on the market include [23]:

- ☞ Methyl Salicylate (A topical analgesic used in patches for muscle and joint pain).
- ☞ Menthol (An analgesic used in patches for muscle and joint pain).
- ☞ Diclofenac (A nonsteroidal anti-inflammatory drug (NSAID) used in patches for arthritis, muscle strains, and sprains).
- ☞ Lidocaine (A local anaesthetic used in patches for post-herpetic neuralgia and other localized pain conditions).
- ☞ Capsaicin (Derived from chilli peppers, a topical analgesic and used in patches for neuropathic pain and arthritis).

1.11. Pain-Relief Drugs Chosen for the Preparation of Transdermal Patches:

Our research work has concentrated on three drugs to produce their transdermal patch formulations. The drugs are Clonidine Hydrochloride, Etoricoxib, and Paracetamol.

1.11.1. Clonidine Hydrochloride (chemical name: 2-((2,6-dichlorophenyl) amino)-2-imidazoline hydrochloride, Fig 1.2) is the first congener of an agonist of the alpha-2 adrenergic receptor. It is mostly used as an antihypertensive in the field of clinical medicine [24]. Recent research has demonstrated the importance of systemic and intrathecal clonidine in the management of acute postoperative pain [25]. CH could be a suitable active pharmaceutical ingredient (API) to prevent chronic pain as per available animal and human studies [26]. The

FDA-approved formulations of clonidine such as oral tablets [27], extended-release tablets [28], transdermal patches [29], and epidural solutions [30] are available in the market. Additionally, clonidine is frequently compounded as a topical medication. The suggested dosage for cancer pain is 30 µg/hr as a continuous epidural infusion [31]. There are clonidine transdermal patches available in dosages of 2.5, 5.0, and 7.5 mg, each of which is intended to administer 0.1, 0.2, and 0.3 mg of clonidine per day respectively for seven days to treat neuropathic pain [32]. So, an effort has been made to sustain the drug release for three to four weeks or even more than four weeks in a single dose using nanomedicine (i.e., drug-loaded nanoparticle) in transdermal drug delivery systems (TDDS) for which patient compliance (especially, cancer patients) could be largely enhanced. No such formulation of clonidine hydrochloride is available to date.

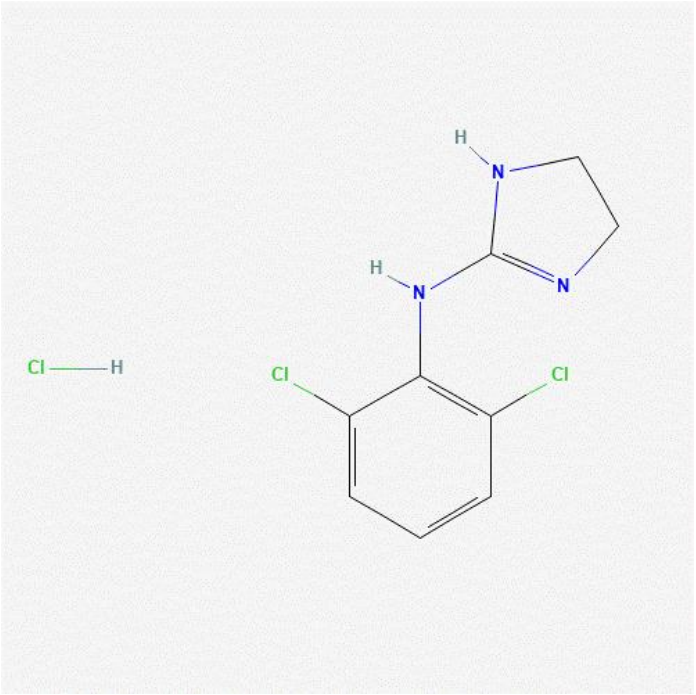

Fig 1.2. Molecular structure of clonidine hydrochloride

1.11.2. Etoricoxib (chemical name: 5-chloro-3-(4-methylsulfonyl)phenyl-2-(2-methyl-5-pyridinyl)pyridine, Fig 1.3) is an NSAID that belongs to the class of selective COX-2 inhibitors. It is used for the treatment of pain and inflammation associated with osteoarthritis,

rheumatoid arthritis, ankylosing spondylitis, acute gouty arthritis, and acute pain conditions [33]. Etoricoxib is primarily available in oral tablet formulation. As of the last update in 2024, no transdermal formulation of etoricoxib is available in the market due to its poor aqueous solubility (0.01 to 0.5 mg/mL at 25°C) [34]. Etoricoxib is normally used once a day at a dosage of 60 mg for osteoarthritis and rheumatoid arthritis. The dosage may sometimes be raised to 90 mg once a day if necessary. For ankylosing spondylitis, 90 mg of etoricoxib once a day is advised. Etoricoxib is prescribed at a dosage of 120 mg once a day, although this should only be taken during the acute phase of symptoms associated with gouty arthritis [35]. Being an NSAID, excessive levels of etoricoxib in the plasma can significantly increase the risk of gastrointestinal ulcers, heart attack, or stroke. Furthermore, high plasma concentrations of etoricoxib can lead to kidney damage and renal insufficiency [36]. These adverse effects can be eliminated if the etoricoxib is administered through only transdermal formulations. On the other hand, the low aqueous solubility may affect its bioavailability. Therefore, it has been decided to load the drug into nanoparticles before incorporating it into the transdermal matrix.

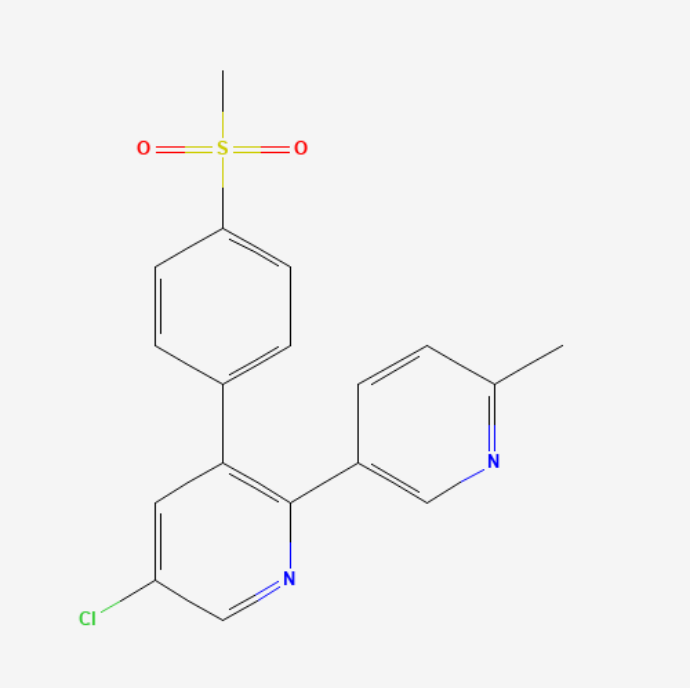

Fig 1.3. Molecular structure of etoricoxib

1.11.3. Paracetamol (acetaminophen or *p*-hydroxyacetanilide, Fig 1.4), is a non-opioid analgesic and antipyretic agent [53], that is used alone or in conjunction with opioid analgesics for moderate to severe pain. The suggested dosage for adults and children (12 years and older) is 500–1000 mg every 4-6 hours, as needed, up to a maximum of 4000 mg in 24 h [54]. The high single oral dose of paracetamol causes liver injury by generating the poisonous metabolite N-acetyl-p-benzoquinone imine (NAPQI) [37]. Apart from this toxicity, paracetamol is not administered through the oral or rectal route in children and infants suffering from gastroenteritis [38]. Additionally, young patients who often decline to take the complete dose of medication orally due to taste or other reasons may find oral administration to be impractical. Moreover, no transdermal formulations are available for paracetamol to date to avoid the problems mentioned above because it is sparingly soluble in water (14.5 mg/mL at 25°C) [39]. Henceforth, the transdermal route of administration has been chosen for paracetamol in the form of nanomedicine as an alternative route.

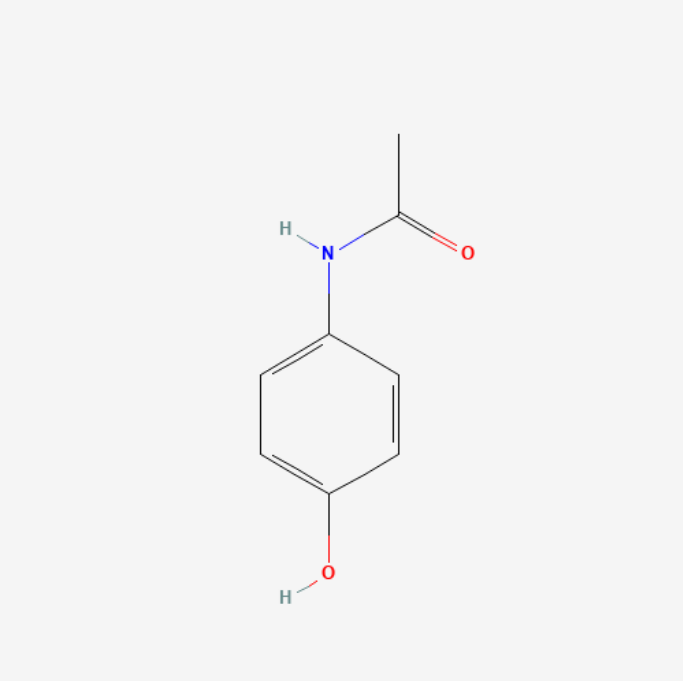

Fig 1.4. Molecular structure of paracetamol

1.12. Nanoparticles Used for the Preparation of Nanomedicines:

The major purposes for the preparation of nanomedicines (i.e., drug-loaded nanoparticles) of the above-mentioned three pain-relief drugs in our research work may be described as the nano-based systems solubilize the insoluble or poorly soluble drugs by various mechanisms like reduction of particle size to fine colloidal dimension [40], elimination of crystalline nature of the drug molecules [41], and increase in pH of the environment than the pK_a of a drug within the dosage form [40], etc.

Two potential inorganic nanocarriers have been focused on throughout the research work: Silica nanoparticles (SNPs) and Sodium montmorillonite (Na-MMT) nanoclay.

1.12.1. Silica Nanoparticles (SNPs): Nowadays, among the various nanoparticles used in the field of biomedical applications, **silica nanoparticles (SNPs)** are receiving wide attention. They are novel inorganic nano drug carriers due to their high drug loading capacity, better biocompatibility, chemical stability, tuneable pore size, porosity to the type and size of the drug molecules, and large surface area, which can be functionalized to load the suitable kind of drug molecules like hydrophilic, lipophilic and control their release [42]. Due to a strong Si-O bond, these particles are not degraded compared to other drug carriers. Hence, no external stabilization is needed during the synthesis [43]. SNPs can use shunt routes into the skin, including the hair follicles and sweat glands in the dermis layer. Therefore, they could release the drug into those hair follicles and sweat glands before being absorbed locally or systemically. The particle size between 300 and 600 nm can enter the hair follicles more efficiently than the larger as well as smaller particles [44].

1.12.2. Sodium Montmorillonite (Na-MMT) Nanoclay: Nanoclays are becoming more popular due to their improved therapeutic effects. Clay minerals have been widely used since ancient times for their potential use in various biomedical applications both as actives and excipients. The recent research regarding the effects of clay nanoparticles on cellular adhesion,

proliferation, and differentiation has provided new insight into the potential of clay minerals in the field of nanomedicine [45]. Clay minerals with a high aspect ratio of 300:1 to 1500:1 consist of negatively charged aluminosilicate layers and positively charged exchangeable ions in between the two layers to balance the net charge. Each layer of its layered structure has a thickness of around 1 nm and the basal spacing between two layers is on average 1.5-2.5 nm. The positively charged ions may be able to exchange the drug molecules in a solution that leads to the formation of a "clay-drug composite." The drug molecules in the interlayer space become stabilized via electrostatic attraction, which enhances the tendency of sustained drug release through the ion exchange phenomenon with the counter ions present in the biological environment and improves drug dissolution. This is how clay minerals can act as a drug delivery system. Not only electrostatic attraction but also other molecular interactions such as Vander Waals interaction, hydrogen bonding, etc. occur between the clay and drug molecules depending upon the nature of the clay mineral and the functional group present in drug molecules [46]. The cation exchange capacity (CEC) varies from clay to clay. For example, the smectite group of clay minerals has higher CEC compared to that of kaolin, talc, etc. minerals. Owing to biocompatibility, high CEC, large surface area, and swellability, the smectite group of minerals is highly recommended for pharmaceutical applications. From the structural point of view, it is seen that the Kaolin group of minerals (e.g., kaolinite and halloysite) have a 1:1 layered structure where the octahedral alumina sheet and tetrahedral silica sheet are stacked together by hydrogen bonding [47]. Smectite minerals (e.g., montmorillonite) have a 2:1 layered structure where the octahedral sheet composed of octahedrally coordinated Al, Mg, or Fe atoms with hydroxyl ion or oxygen atoms is sandwiched between two tetrahedral silica sheets [48]. Nanoclay particles may passively diffuse through the spaces between skin cells (keratinocytes) in the stratum corneum, which is the outermost layer of the skin. Besides, nanoclay particles with appropriate surface properties

may interact with the lipid-rich structure of the stratum corneum to move through the skin barrier [49]. While nanoclay particles may be too large to pass through sweat ducts, they may still be small enough to enter hair follicles. Thus, they could potentially diffuse into deeper layers of the skin via hair follicles [50].

1.13. Drug Release Study:

Drug release experiments are essential in pharmaceutical research and development to understand how drugs are released from various delivery systems over time. These experiments help assess the efficacy, safety, and performance of drug formulations. *In vitro* release studies involve evaluating the release of drugs from various delivery systems, such as transdermal patches, nanoparticles, or implants, in simulated physiological conditions outside the body [51]. *Ex vivo* permeation studies involve measuring the penetration of drugs through biological membranes, such as skin or mucosal tissues, using excised tissue samples [52]. Keeping all these factors in mind, *in vitro* drug release experiments from the nanomedicines and *ex vivo* skin permeation experiments of the drugs as nanomedicine released from the transdermal patches have been conducted in our research work.

1.14. Drug Release Kinetics:

Drug release kinetics are necessary for ensuring the efficacy, safety, and patient acceptance of medications. By controlling the rate and pattern of drug release, pharmaceutical scientists can design drug delivery systems that deliver drugs in a manner that maximizes therapeutic benefit while minimizing adverse effects. Because of this reason, it also has been decided to apply several kinetic models to the drug dissolution data for the determination of the best fit kinetic model accompanied by drug release in both burst and sustained periods [53].

1.15. Methods to Assay the Analgesic Activity of the Drugs on Rodents:

There are different methods to measure analgesic activities in mice or rats [54]. These are:

- **Hot plate method** in which the time of reactions (licking and jumping on Eddy's hot plate at 50-55℃) is recorded at definite time intervals after administration of the drug.
- **Tail flick method** where the reaction times (usually a cut-off time of 10-15 seconds are taken to avoid heat injury) at time intervals after the drug administration are recorded by locating the tip of the tail on a heat source (the nichrome wire present in analgesiometer or warm water).
- **Tail immersion test** in which the time of reaction i.e. tail withdrawal from the hot water (50-55℃) is recorded every 30 minutes after the administration.

Since the hot-plate and tail-flick methods are the most used and reliable approaches for assessing the pain-relieving effects of drugs in mice as well as rats by measuring their response to a thermal nociceptive stimulus according to the literature [55, 56], these two methods have been chosen to execute *in vivo* analgesic study using a pre-designed animal model for inspection the performances of the prepared transdermal patches.

So, in summary, the chosen pain relief drugs have been entrapped into the above-mentioned two nanocarriers, called "nanomedicine." Those nanomedicines have been delivered from the prepared transdermal patches which is an innovative approach to administer the drug molecules through the skin. The long-term analgesic effect of the drugs released from the patches as nanomedicines has been examined. Moreover, a suitable kinetic model associated with *ex vivo* drug release study from each transdermal formulation has been established.

Reference:

1. Murr, L. E. (2015). Handbook of materials structures, properties, processing and performance. *Handbook of Materials Structures, Properties, Processing and Performance*, 1–1152. https://doi.org/10.1007/978-3-319-01815-7

2. Goodnick, S., Korkin, A., Krstic, P., Mascher, P., Preston, J., & Zaslavsky, A. (2010). Editorial: Semiconductor nanotechnology: Novel materials and devices for electronics, photonics and renewable energy applications. *Nanotechnology*, *21*(13), 19–21. https://doi.org/10.1088/0957-4484/21/13/130201

3. Ahmadi, M. H., Ghazvini, M., Nazari, M. A., Ahmadi, M. A., Pourfayaz, F., Lorenzini, G., & Ming, T. (2019). Renewable energy harvesting with the application of nanotechnology: A review. *International Journal of Energy Research*, *43*(4), 1387–1410. https://doi.org/10.1002/er.4282

4. Yezdani, U., Khan, M. G., Kushwah, N., Verma, A., & Khan, F. (2018). Aplication of nanotechnology in diagnosis and treatment of various diseases and its future advances in medicine. *World Journal of pharmacy and pharmaceutical sciences*, *7*(11), 1611–1633. https://doi.org/10.20959/wjpps201818-12703

5. Zhang, X., Yan, S., Tyagi, R. D., & Surampalli, R. Y. (2011). Synthesis of nanoparticles by microorganisms and their application in enhancing microbiological reaction rates. *Chemosphere*, *82*(4), 489–494. https://doi.org/10.1016/j.chemosphere.2010.10.023

6. Singh, T., Shukla, S., Kumar, P., Wahla, V., & Bajpai, V. K. (2017). Application of nanotechnology in food science: Perception and overview. *Frontiers in Microbiology*, *8*(AUG), 1–7. https://doi.org/10.3389/fmicb.2017.01501

7. Patra, J. K., Das, G., Fraceto, L. F., Campos, E. V. R., Rodriguez-Torres, M. D. P., Acosta-Torres, L. S., … Shin, H. S. (2018). Nano based drug delivery systems: Recent developments and future prospects 10 Technology 1007 Nanotechnology 03 Chemical Sciences 0306 Physical Chemistry (incl. Structural) 03 Chemical Sciences 0303 Macromolecular and Materials Chemistry 11 Medical and He. *Journal of Nanobiotechnology*, *16*(1), 1–33. https://doi.org/10.1186/s12951-018-0392-8

8. Yavuz, B., Kondolot Solak, E., & Oktar, C. (2023). Preparation of biocompatible microsphere-cryogel composite system and controlled release of mupirocin. *International Journal of Polymeric Materials and Polymeric Biomaterials*. https://doi.org/10.1080/00914037.2022.2163638

9. Al Hoque, A., Dutta, D., Paul, B., Kumari, L., Ehsan, I., Dhara, M., … Ganguly, S. (2023). ΔPSap4#5 surface-functionalized abiraterone-loaded nanoparticle successfully inhibits carcinogen-induced prostate cancer in mice: a mechanistic investigation. *Cancer Nanotechnology*, *14*(1). https://doi.org/10.1186/s12645-023-00223-5

10. Gunasekaran, T., Haile, T., Nigusse, T., & Dhanaraju, M. D. (2014). Nanotechnology: An effective tool for enhancing bioavailability and bioactivity of phytomedicine. *Asian Pacific Journal of Tropical Biomedicine*, *4*(Suppl 1), S1–S7. https://doi.org/10.12980/APJTB.4.2014C980

11. Tan, J. M., Karthivashan, G., Arulselvan, P., Fakurazi, S., & Hussein, M. Z. (2014). Characterization and in vitro sustained release of silibinin from ph responsive carbon nanotube-based drug delivery system. *Journal of Nanomaterials*, *2014*. https://doi.org/10.1155/2014/439873

12. Matea, C. T., Mocan, T., Tabaran, F., Pop, T., Mosteanu, O., Puia, C., … Mocan, L. (2017). Quantum dots in imaging, drug delivery and sensor applications. *International Journal of Nanomedicine*, *12*, 5421–5431. https://doi.org/10.2147/IJN.S138624

13. Bediako, E. G., Nyankson, E., Dodoo-Arhin, D., Agyei-Tuffour, B., Łukowiec, D., Tomiczek, B., … Efavi, J. K. (2018). Modified halloysite nanoclay as a vehicle for sustained drug delivery. *Heliyon*, *4*(7). https://doi.org/10.1016/j.heliyon.2018.e00689

14. Ameena Shirin, V. K., Sankar, R., Johnson, A. P., Gangadharappa, H. V., & Pramod, K. (2021). Advanced drug delivery applications of layered double hydroxide. *Journal of Controlled Release*, *330*, 398–426. https://doi.org/10.1016/J.JCONREL.2020.12.041

15. Farokhzad, O. C., & Langer, R. (2009). Impact of Nanotechnology on Hair Attributes. *ACS Nano*, *3*(1), 1–7.

16. Geraili, A., Xing, M., & Mequanint, K. (2021, October 1). Design and fabrication of drug-delivery systems toward adjustable release profiles for personalized treatment. *VIEW*. John Wiley and Sons Inc. https://doi.org/10.1002/VIW.20200126

17. Wheless, J. W., & Phelps, S. J. (2018, July 1). A clinician's guide to oral extended-release drug delivery systems in epilepsy. *Journal of Pediatric Pharmacology and Therapeutics*. Pediatric Pharmacy Advocacy Group, Inc. https://doi.org/10.5863/1551-6776-23.4.277

18. Rajendra Gadekar, M., Barge, V., & Neharkar Sheshrao, N. (2021). *A REVIEW ON SUSTAINED RELEASE DRUG DELIVERY SYSTEM*. *International Journal of Creative Research Thoughts* (Vol. 9). Retrieved from www.ijcrt.org

19. Kwatra, S., Taneja, G., & Nasa, N. (2012). Alternative Routes of Drug Administration-Transdermal, Pulmonary & Parenteral. *Indo Global Journal of Pharmaceutical Sciences*, *2*(4), 409–426.

20. Sharma, N. (2018). Organic & Medicinal Chem IJ A Brief Review on Transdermal Patches. *Organic and Medicinal Chemistry International Journal*, *7*(2). https://doi.org/10.19080/OMCIJ.2018.07.555707

21. Prausnitz, M. R., & Langer, R. (2008, November). Transdermal drug delivery. *Nature Biotechnology*. https://doi.org/10.1038/nbt.1504

22. Świeboda, P., Filip, R., Prystupa, A., & Drozd, M. (2013). *Assessment of pain: types, mechanism and treatment*. *Ann Agric Environ Med* (Vol. 1). Retrieved from www.aaem.pl

23. Nalamachu, S., & Gudin, J. (2020). Characteristics of analgesic patch formulations. *Journal of Pain Research*, *13*, 2343–2354. https://doi.org/10.2147/JPR.S270169

24. Kumar, A., Maitra, S., Khanna, P., & Baidya, D. K. (2014, January). Clonidine for management of chronic pain: A brief review of the current evidences. *Saudi Journal of Anaesthesia*. https://doi.org/10.4103/1658-354X.125955

25. Singh, R., Chopra, N., Choubey, S., Tripathi, R., Prabhakar, & Mishra, A. (2014). Role of Clonidine as adjuvant to intrathecal bupivacaine in patients undergoing lower abdominal surgery: A randomized control study. *Anesthesia: Essays and Researches*, *8*(3), 307. https://doi.org/10.4103/0259-1162.143119

26. Roh, D. H., Kim, H. W., Yoon, S. Y., Seo, H. S., Kwon, Y. B., Han, H. J., … Lee, J. H. (2008). Intrathecal clonidine suppresses phosphorylation of the n-methyl-D-aspartate receptor NR1 subunit in spinal dorsal horn neurons of rats with neuropathic pain. *Anesthesia and Analgesia*, *107*(2), 693–700. https://doi.org/10.1213/ane.0b013e31817e7319

27. Vasseur, B., Dufour, A., Houdas, L., Goodwin, H., Harries, K., Emul, N. Y., & Hutchings, S. (2017). Comparison of the Systemic and Local Pharmacokinetics of Clonidine Mucoadhesive Buccal Tablets with Reference Clonidine Oral Tablets in Healthy Volunteers: An Open-Label Randomised Cross-Over Trial. *Advances in Therapy*, *34*(8), 2022–2032. https://doi.org/10.1007/s12325-017-0585-9

28. Jain, R., Segal, S., Kollins, S. H., & Khayrallah, M. (2011). Clonidine extended-release tablets for pediatric patients with attention-deficit/hyperactivity disorder. *Journal of the American Academy of Child and Adolescent Psychiatry*, *50*(2), 171–179. https://doi.org/10.1016/j.jaac.2010.11.005

29. Weber, M. A., Drayer, J. I. M., McMahon, F. G., Hamburger, R., Shah, A. R., & Kirk, L. N. (1984). Transdermal Administration of Clonidine for Treatment of High BP. *Archives of Internal Medicine*, *144*(6), 1211–1213. https://doi.org/10.1001/archinte.1984.00350180139020

30. Roelants, F., Lavand'homme, P. M., & Mercier-Fuzier, V. (2005). *Epidural Administration of Neostigmine and Clonidine to Induce Labor Analgesia Evaluation of Efficacy and Local Anesthetic-sparing Effect*. *Anesthesiology* (Vol. 102). Retrieved from www.anesthesiology.org.

31. Ackerman, L. L., Follett, K. A., & Rosenquist, R. W. (2003). Long-term outcomes during treatment of chronic pain with intrathecal clonidine or clonidine/opioid combinations. *Journal of Pain and Symptom Management*, *26*(1), 668–677. https://doi.org/10.1016/S0885-3924(03)00144-1

32. Chen, S., & Vidt, D. G. (n.d.). *Patient acceptance of transdermal clonidine A retrospective review of 25 patients*. Retrieved from www.ccjm.org

33. D Martina, S., Vesta, K. S., & Ripley, T. L. (2005, May). Etoricoxib: A highly selective COX-2 inhibitor. *Annals of Pharmacotherapy*. https://doi.org/10.1345/aph.1E543

34. Alzweiri, M., Sallam, M., Al-Zyoud, W., & Aiedeh, K. (2018). Stability study of etoricoxib a selective cyclooxygenase-2 inhibitor by a new single and rapid reversed phase HPLC method. *Symmetry*, *10*(7). https://doi.org/10.3390/sym10070288

35. Birmingham, B., & Buvanendran, A. (2014). Nonsteroidal Anti-inflammatory Drugs, Acetaminophen, and COX-2 Inhibitors. *Practical Management of Pain: Fifth Edition*, 553-568.e5. https://doi.org/10.1016/B978-0-323-08340-9.00040-2

36. Altman, R., Bosch, B., Brune, K., Patrignani, P., & Young, C. (2015, May 30). Advances in NSAID development: Evolution of diclofenac products using pharmaceutical technology. *Drugs*. Springer International Publishing. https://doi.org/10.1007/s40265-015-0392-z

37. Mazaleuskaya, L. L., Sangkuhl, K., Thorn, C. F., Fitzgerald, G. A., Altman, R. B., & Klein, T. E. (2015). PharmGKB summary: Pathways of acetaminophen metabolism at the therapeutic versus toxic doses. *Pharmacogenetics and Genomics*, *25*(8), 416–426. https://doi.org/10.1097/FPC.0000000000000150

38. Sintov, A. C., Krymberk, I., Gavrilov, V., & Gorodischer, R. (2010). Transdermal delivery of paracetamol for paediatric use: effects of vehicle formulations on the percutaneous penetration. *Journal of Pharmacy and Pharmacology*, *55*(7), 911–919. https://doi.org/10.1211/0022357021486

39. Jyoti Sen, D., & Patel, J. G. (2016). Logarithmic Partition Coefficient Comparison Study and Molecular Weight of Synthesized Prodrugs of Ibuprofen+Paracetamol, Diclofenac Sodium+Paracetamol and Ibuprofen+Diclofenac Sodium. *American Journal of Advanced Drug Delivery*, *04*(05), 1–5. https://doi.org/10.21767/2321-547x.1000003

40. Sareen, S., Joseph, L., & Mathew, G. (2012). Improvement in solubility of poor water-soluble drugs by solid dispersion. *International Journal of Pharmaceutical Investigation*, *2*(1), 12. https://doi.org/10.4103/2230-973x.96921

41. Naik, D. R., & Raval, J. P. (2016). Amorphous polymeric binary blend pH-responsive nanoparticles for dissolution enhancement of antiviral drug. *Journal of Saudi Chemical Society*, *20*, S168–S177. https://doi.org/10.1016/j.jscs.2012.09.020

42. Bharti, C., Gulati, N., Nagaich, U., & Pal, A. (2015). Mesoporous silica nanoparticles in target drug delivery system: A review. *International Journal of Pharmaceutical Investigation*, *5*(3), 124. https://doi.org/10.4103/2230-973x.160844

43. Kwon, S., Singh, R. K., Perez, R. A., Neel, E. A. A., Kim, H. W., & Chrzanowski, W. (2013). Silica-based mesoporous nanoparticles for controlled drug delivery. *Journal of Tissue Engineering*, *4*(1), 1–18. https://doi.org/10.1177/2041731413503357

44. Akram, M. W., Jamshaid, H., Rehman, F. U., Zaeem, M., Khan, J. zeb, & Zeb, A. (2022). Transfersomes: a Revolutionary Nanosystem for Efficient Transdermal Drug Delivery. *AAPS PharmSciTech*, *23*(1). https://doi.org/10.1208/s12249-021-02166-9

45. Viseras, C., Carazo, E., Borrego-Sánchez, A., García-Villén, F., Sánchez-Espejo, R., Cerezo, P., & Aguzzi, C. (2019). Clay minerals in skin drug delivery. *Clays and Clay Minerals*, *67*(1), 59–71. https://doi.org/10.1007/s42860-018-0003-7

46. Damato, A., Vianello, F., Novelli, E., Balzan, S., Gianesella, M., Giaretta, E., & Gabai, G. (2022, May 10). Comprehensive Review on the Interactions of Clay Minerals With Animal Physiology and Production. *Frontiers in Veterinary Science*. Frontiers Media S.A. https://doi.org/10.3389/fvets.2022.889612

47. Zhang, Y., Long, M., Huang, P., Yang, H., Chang, S., Hu, Y., … Mao, L. (2016). Emerging integrated nanoclay-facilitated drug delivery system for papillary thyroid cancer therapy. *Scientific Reports*, *6*. https://doi.org/10.1038/srep33335

48. Park, J. H., Shin, H. J., Kim, M. H., Kim, J. S., Kang, N., Lee, J. Y., … Kim, D. D. (2016, July 1). Application of montmorillonite in bentonite as a pharmaceutical excipient in drug delivery systems. *Journal of Pharmaceutical Investigation*. Springer Netherlands. https://doi.org/10.1007/s40005-016-0258-8

49. Kim, M. H., Choi, G., Elzatahry, A., Vinu, A., Choy, Y. Bin, & Choy, J. H. (2016). Review of clay-drug hybrid materials for biomedical applications: Administration routes. *Clays and Clay Minerals*, *64*(2), 115–130. https://doi.org/10.1346/CCMN.2016.0640204

50. Palmer, B. C., & DeLouise, L. A. (2016, December 1). Nanoparticle-enabled transdermal drug delivery systems for enhanced dose control and tissue targeting. *Molecules*. MDPI AG. https://doi.org/10.3390/molecules21121719

51. Weng, J., Tong, H. H. Y., & Chow, S. F. (2020). In vitro release study of the polymeric drug nanoparticles: Development and validation of a novel method. *Pharmaceutics*, *12*(8), 1–18. https://doi.org/10.3390/pharmaceutics12080732

52. Tas, C., Ozkan, Y., Okyar, A., & Savaser, A. (2007). In vitro and ex vivo permeation studies of etodolac from hydrophilic gels and effect of terpenes as enhancers. *Drug Delivery*, *14*(7), 453–459. https://doi.org/10.1080/10717540701603746

53. Pal, P. (2021). In vitro release kinetics study of Diallyl Disulphide entrapped into mesoporous silica matrix & evaluation of its antimicrobial activity, *6*(2), 148–157. https://doi.org/10.22034/nmrj.2021.02.006

54. Fan, S.-H., Ali, N. A., & Basri, D. F. (2014). Evaluation of Analgesic Activity of the Methanol Extract from the Galls of *Quercus infectoria* (Olivier) in Rats. *Evidence-Based Complementary and Alternative Medicine*, *2014*, 976764. https://doi.org/10.1155/2014/976764

55. Hestehave, S., Munro, G., Pedersen, T. B., & Abelson, K. S. P. (2017). Antinociceptive effects of voluntarily ingested buprenorphine in the hot-plate test in laboratory rats. *Laboratory Animals*, *51*(3), 264–272. https://doi.org/10.1177/0023677216668553

56. Modi, A. D., Parekh, A., & Pancholi, Y. N. (2023). Evaluating pain behaviours: Widely used mechanical and thermal methods in rodents. *Behavioural Brain Research*, *446*. https://doi.org/10.1016/j.bbr.2023.114417

Chapter: 2
Literature Review

2.1. Nanomaterials: The materials cannot be seen through our naked eyes in the nanoworld. Even these materials cannot be manipulated or touched by hands or any other tools we use. They are very tiny and approximately comparable to the size of atoms and molecules. Bulk materials' properties are independent of size but when a material is reduced to nano dimension, its properties depend on the size. The nanomaterials have a large fraction of atoms on the surface, high surface energy, a minimal number of imperfections compared to those of bulk materials etc [1]. The chemical properties are changed due to the increase of the exposed surface area of nanoparticles. The optical properties of nanomaterials are also different from the bulk material, for example, due to the increased band gap of semiconductor particles, the absorption peak shifted towards a shorter wavelength [2]. Besides, the electrical conductivity changes when the materials are nano-scale [3]. Based on the number of dimensions, nanomaterials are classified into four categories. (i) zero, (ii) one, (iii) two and (iv) three-dimensional nanomaterials. Zero dimensional nanomaterials have all the dimensions within the nanoscale which means all the dimensions are smaller than 100 nm. Generally, zero-dimensional nanomaterials are nanoparticles. When one of the dimensions is outside the nanoscale, it is called one-dimensional nanomaterial. This category includes nanotubes, nanofibers, nanorods, nanotapes, nanowires etc. Similarly, if any two of the dimensions are larger than 100 nm, then those nanomaterials are called two-dimensional. This class exhibits ultrathin layer, ultrathin film. In the case of three-dimensional nanomaterials, all the dimensions are not confined to the nanoscale but exhibit the features at the nanoscale. This class represents nanocomposites, inorganic-organic hybrid nanocomposites, nanoporous and nanocrystalline materials [4]. Nanocomposite materials are nothing but a matrix-filler combination where nanoparticles, nanotubes, nanowires etc. acting as a filler are dispersed in the polymer matrix [5]. Nanoporous materials have pores in the range of 0.5-100 nm. There are three types of nanoporous materials based on pore size: microporous (below 2 nm), mesoporous (between 2 and 50 nm), and

macroporous (beyond 50 nm) [6]. Nano-sized crystals are the main ingredient to form the consolidated nanocrystalline materials having high mechanical strength [6].

2.2. Methods to Synthesize the Nanomaterials: There are mainly two approaches through which the nanomaterials can be synthesized: (i) Top-down approach and (ii) Bottom-up approach [7]. In the former case, the nano-sized materials are obtained by reducing the size of bulk materials with the help of different techniques like electron beam lithography (EBL), photolithography, ball-milling etc. The second approach involves several ways of accumulation of atoms and molecules in a controlled manner such as physical vapour deposition (PVD), chemical vapour deposition (CVD), sol-gel technique etc. to prepare the nanomaterials of different shapes and sizes. In the case of lithography techniques, a pattern is transferred onto a reactive polymer film, also described as a photoresist polymer which in turn is used to replicate on top of the underlying thin film of the desired substrate [8]. This method is widely used to prepare integrated circuits. Ball milling is another top-down approach where the balls are rotated around a horizontal axis inside the material-filled container with a high energy and then it is allowed to fall on the material with gravity force and kinetic energy to produce the nano-sized material. Generally, ceramic, and metallic nanomaterials are produced with the help of this technique [9]. PVD is a physical process where the source material, either in liquid or solid state, is first evaporated to bring the molecules in a gaseous state and then it is deposited or condensed on the substrate to form a thin film. In CVD, the precursor molecules, as a gaseous compound are involved in chemical interaction or decomposition on the substrate surface to deposit the desired thin film on the substrate [4]. Finally, the sol-gel process is used to prepare various types of nanomaterials like porous materials, thin films, fine powders etc. A liquid sol (colloidal state of the solution) is completely transformed into a solid gel phase in the process. Silicon alkoxides or metal alkoxides/chlorides are used mainly as a precursor

which on hydrolysis followed by condensation produces the oxo or hydroxo bridged polymeric network of gel phase [10].

2.3. Nanotechnology in Drug Delivery Systems: In drug delivery, nanotechnology has been demonstrated by the nanomaterials which show inimitable properties *in vitro* as well as *in vivo*. The cells absorb the nanoparticles more effectively than bulky materials and therefore could be used as an effective drug delivery system. The development of an ideal drug delivery system is based upon a few factors such as interactions of nanomaterials with the biological environment, mechanism of drug action, the site where the drugs will be released from the system, drug retention, drug administration, stability of the drugs in the living cells etc [11][12]. There are two ways through which the nanomaterials, acting as a nanocarrier, deliver drugs: (i) passive and (ii) self-delivery. In the former case, either the drug molecules are physically encapsulated in the inner cavity of the carrier or the drug molecules are attached to the nanocarrier by chemical conjugation. The physical encapsulation is stabilized by non-covalent interaction, especially the hydrophobic effect between nanocarrier and drug molecules. Porous nanoparticles and nanocapsules have the hydrophobicity to stabilize the encapsulated drug. When these nanocarriers are disassembled at the target site of action, drug molecules come out from the system consequently. In the case of chemical conjugation, it is so important to say that the conjugation must be cleavable. If the drug molecules cannot be cleaved from the carrier at the right time, then their bioactivity and bioavailability will diminish with time. Besides, if the drug molecules are separated too early then they will not be able to reach the target site of action with an adequate dose, which is called a “burst release.” In the latter case, the drug molecules are self-assembled reversibly to produce supramolecular nanostructure [13][14][15]. A few nano drug carriers are reviewed below focusing on their both targeting and sustained drug delivery application.

(2.3.1) Mesoporous Silica Nanoparticles (MSNs): In the era of nanotechnology, mesoporous silica nanoparticles having honeycomb structure, have become the novel inorganic drug carrier due to their high drug loading capacity, better biocompatibility, chemical stability, porosity and tunable pore size to the type and size of the drug molecules and large surface area which can be functionalized to load the suitable type of drug molecules such as hydrophobic, hydrophilic, positive or negative charged and control their release [16][17]. These particles also do not get degraded compared to other drug carriers like liposomes because of the existence of strong Si-O bonds and therefore no external stabilization is needed during the synthesis of MSNs [18]. They could be synthesized using different methods like the sol-gel method, hydrothermal method, microwave synthesis method, template-assisted synthesis method etc. The sol-gel method is described above in the section "Methods to synthesize the nanomaterials." Low-temperature environments and easily controlled experiments using simple equipment are the advantages of this method over other techniques. In the hydrothermal process the surfactants (acting as a templating agent), acid or base catalyst and the precursor of silica are mixed to make the solution homogeneous. The solution is then transferred to an autoclave and heated to obtain the hydrogel. The hydrothermal process is not as simple as a sol-gel method. It requires high temperature and high pressure and the reaction takes a long time to complete [19]. Microwave synthesis is the rapid one to prepare mesoporous silica nanoparticles where the successive hydrothermal process is carried out under the microwave oven which can provide high localized heating [20]. Template template-assisted technique is another approach to synthesising these nanoparticles where the surfactant molecules are used as the directing agent of structure and after the precipitation of the silica framework around the template surfactant molecules are eliminated by the process of calcinations [21]. The drug molecules could be loaded into the mesopores either by in-situ entrapment during the synthesis of MSNs or through immersion of MSNs in the aqueous or alcoholic drug solution [22][23]. **T. Moodley** and **M.**

Singh (2019) reported on in vitro delivery of 5-fluorouracil (anti-cancer drug) using polymeric mesoporous silica nanoparticles as drug carriers [24]. **J. Ke, Y. Wang et al. (2020)** synthesized core-shell mesoporous silica nanoparticles and loaded indomethacin (NSAID) in silica nanocarrier to do in vitro and in vivo release study [25]. **M. Shahriarinour et al. (2019)** worked on the entrapment of thymol in SBA-15 mesoporous nanoparticles to study its antibacterial activity [26].

(2.3.2) Liposomes: Liposomes are bilayered vesicles having a diameter in the range of 0.01-5.0 μm and have the potential to encapsulate the hydrophilic as well as hydrophobic drugs are formed by the hydration of phospholipids (unsaturated fatty acids) in excess aqueous medium [27]. Phospholipids are prone to oxidation to form cyclic peroxidise and hydroperoxidases which are toxic through free radical formation. This degradation of liposomes is prevented by adding anti-oxidants like butylated hydroxyl toluene (BHT) or by protecting them from light [28]. Some hydrophilic groups such as polyethylene glycol (PEG), monogangliosides etc. are used to coat the liposome surface to reduce the interaction with blood and cell components and opsonisation consequently. There are different techniques to synthesize the liposomes, a few of which are mentioned below. First comes the "ether injection method" where a diethyl ethereal solution of lipid is injected into the aqueous solution of the drug to be encapsulated at the temperature of 55℃ to 65℃ under reduced pressure and finally the ether is removed under vacuum [29]. The second method is the "ethanol injection method" in which the ethanolic solution of the lipid is injected in distilled water and after that liposomes are separated by removing excess ethanol and water [30]. But this method has a disadvantage which is the formation of an azeotropic mixture of ethanol and water for which the complete removal of ethanol is not possible. The third method gives the liposomes having high aqueous space to-lipid ratio and hence high loading efficiency of water-soluble drugs. The name of this method is "reverse phase evaporation method" where the inverted micelle is centrifuged through the

barrier of buffered aqueous phase containing water-soluble drugs and organic phase such as diethyl ether, isopropyl ether of the mixture of chloroform and isopropyl ether containing the phospholipids [31]. **A. Paavola et al. (2000)** investigated in vitro control release of ibuprofen using liposomal systems [32]. **Daniele R. de Araujo et al. (2004)** worked on the preparation of unilamellar liposomes for control delivery of bupivacaine and mepivacaine prolonging their anaesthetic effect [33].

(2.3.3) Quantum Dots (QDs): Quantum Dots are nothing but nanocrystals of semiconducting materials having the diameter of the particles between 2 to 10 nm [34]. They have exclusive optical properties which make them luminescent nanocarriers or probes for biomedical applications. The tumour especially small-sized tumours in the body cannot be located and removed easily due to lack of bioluminescence. QDs resolve the above-mentioned problem targeting the cancer cells specifically along with imaging those cells in vivo [35]. Several core/shell quantum dots such as CdTe/ZnS, CdSe/ZnS etc. are synthesized for the above-mentioned purposes [36][37]. The synthesis of core/shell structure involves two steps: first, the core is made by heating the solution of precursors such as Me_2Cd and $(TMS)_2Se$ or $(TMS)_2S$ in TOPO-TOP solvent. Second, the solution of Me_2Zn and $(TMS)_2S$ in TOPO-TOP solvent is added to the colloidal solution of CdSe or CdS. The thin layered shell of the high band, non-toxic materials like ZnS, ZnSe etc is used to reduce the toxicity of QDs which makes them more promising for biological applications [38]. There are mainly two ways to put together the drug molecules and quantum dots into nanoparticle formulations for drug delivery: (a) conjugation of the drugs to the surface of QDs. In this case, the local factors like the biological pH as well as enzymes trigger the cleavage of the drugs from the surface. (b) Encapsulation of the drug molecules in polymer nanoparticles containing hydrophilic or hydrophobic QDs. The choice of QDs taken here depends on the nature of the polymer. The polymers that must be biocompatible are used to inhibit the degradation of QDs in a physiological environment.

Subsequently, the release of the drug molecules happened either upon degradation of the polymer at low pH or through the diffusion process from the polymer [39]. Currently, researchers are working on cadmium-free QDs as well, for example, $CuInS_2$, InP etc. which is found to be non-toxic compared to Cd-based QDs and hence more suitable for in vivo applications [39]. **Q. Yuan et al. (2010)** synthesized the anti-cancer drug "doxorubicin hydrochloride" loaded blue light emitting ZnO quantum dots for anti-tumour drug delivery [40]. **S. Hanada, K. Fujioka et al. (2013)** studied the cytotoxicity and biological effect of "alminoprofen" (analgesic for rheumatism) conjugated silicon quantum dots [41].

(2.3.4) Carbon Nanotubes (CNTs): It is known that graphene is a 2D graphite sheet where carbon atoms are arrayed in a regular hexagonal pattern like a honeycomb lattice. The one-dimensional carbon nanotubes are formed by rolling up the above two-dimensional graphene sheet. CNTs are of two types: (a) single-walled carbon nanotubes (SWNTs) which are made of one cylindrical tube having a diameter of approximately 0.6-2.4 nm and (b) multi-walled carbon nanotubes (MWNTs) having several concentric cylindrical tubes with an inner diameter of 1-3 nm, outer diameter in the range of 2.5-100 nm and interlayer distance is about 0.34 nm [42]. SWNTs mainly attract huge attention for having a lot of advantages which include high aspect ratio, large surface area, structural flexibility, inherent stability due to the presence of delocalized π-system of graphite sheet, high loading efficiency, prolonged circulation time and hence increased bioavailability of entrapped drug molecules [43]. **Z. Liu, K. Chen et al. (2008)** analysed that the conjugation of "SWNT and paclitaxel (cancer chemotherapy drug)" suppressed the growth of tumour cells more than clinical Taxol (cancer chemotherapy drug) in breast cancer models.

(2.3.5) Nanoclay and Layered Double Hydroxides (LDH): Clays are considered a naturally occurring major element of pharmaceutical products where they can act as either active or excipient substances. Clays have been used for a long time to serve the purpose of wound

healing, diarrhoea etc. Medicinal clays have been used to cure ulcers, infections, allergies etc. Clay minerals having a high aspect ratio in the range of 300:1 to 1500:1 consist of negatively charged aluminosilicate layers and positively charged exchangeable ions in between the two layers to balance the net charge for which they may be able to exchange the basic drug molecules in solution that leads to the formation of "clay-drug hybrid." The drug molecules in the interlayer space become stabilized via electrostatic attraction which enhances the tendency of controlled as well as sustained release of the drug molecules through ion exchange phenomenon with the counter ions present in the biological environment and improve drug dissolution. This is how the clay minerals can act as a drug delivery system. Not only electrostatic attraction but also more different types of interactions such as Vander Waals interaction, hydrogen bonding etc. occur between the clay and drug molecules depending upon the nature of the clay mineral and the functional group present in drug molecules [44][45]. The cation exchange capacity (CEC) varies from clay to clay e.g., the smectite group of clay minerals have a high cation exchange capacity compared to that of kaolin, talc etc. minerals [46]. Due to the large surface area, swellability, and biocompatibility along with high CEC, the smectite group of minerals are highly recommended for pharmaceutical applications [47]. From the structural point of view, it is seen that the Kaolin group of minerals (e.g., kaolinite and halloysite) have a 1:1 layered structure where the octahedral alumina sheet and tetrahedral silica sheet are stacked together by hydrogen bonding. Smectite minerals (e.g., montmorillonite) have a 2:1 layered structure where the octahedral sheet composed of octahedrally coordinated Al, Mg or Fe atoms with hydroxyl ion or oxygen atoms is sandwiched between two tetrahedral silica sheets. There are also other nanoclays such as bentonite, saponite, vermiculite, laponite, and hectorite that can produce a homogeneous dispersion of nanocrystals in water [48]. Sometimes the nanoclay particles are incorporated into the polymeric host carrier to achieve the slow release of the drug from the carrier either by

decreasing the porosity of the polymer or by obstructing the diffusion of the drug molecules [49]. All the properties of Layered double hydroxides (LDH) like swelling in water, layered structure, interlayer separation, ion-exchange capacity, and chemical composition make them "clay-like" materials. They are known as anionic clay due to their anion exchange properties. The main difference between the LDHs and nanoclays is that LDHs are laboratory synthesized but the nanoclays are naturally occurring inorganic materials. **Hector A Lobato-Aguilar et al. (2020)** researched on release kinetic of "chlorhexidine diacetate" (anti-bacterial agent) from montmorillonite clay [50]. **Ernest Gyan Bediako et al. (2018)** investigated the sustained release property of "sodium salicylate" (analgesic and antipyretic drug) from the modified halloysite nanotube [51]. **J. Chakraborty et al. (2013)** studied the release behaviour of methotraxate (chemotherapy agent) from the "Mg-Al LDH-methotraxate" nanohybrid system [52].

2.4. Pharmacokinetics of the Drugs: Pharmacokinetics is simply defined as the study of drug absorption, distribution, metabolism, and excretion. In our body system, the blood flows from the digestive system to arterial circulation. More specifically it starts its flow from the gut to the liver via the hepatic portal system. Thereafter, the blood enters the right-hand side of the heart via venous circulation. It goes then to the lungs through pulmonary arteries and again returns to the left-hand side of the heart. Eventually, it comes into the arterial circulation. The drugs are usually placed in different parts of this system and blood plasma concentration in arterial circulation is measured with respect to time. In the case of the oral route of the drug administration, the drug molecules move through the gastrointestinal tract are absorbed by the gut and enter arterial circulation after moving through all the above-mentioned systems. Hence it takes quite a while to achieve maximum concentration (C_{max}) in oral delivery. The time taken to achieve C_{max} is called T_{max}. But during intravenous drug administration, the drug molecules will not be involved in first-pass metabolism and therefore they will take less time to reach the

arterial circulation. As a result of this, higher C_{max} can be achieved at a shorter T_{max} compared to that of oral drug delivery. Similarly, subcutaneous, and intramuscular administration helps to achieve the peak of the drug level quickly. For the inhalation route of administration, the drug molecules are placed in the lungs directly so that the drug molecules have a very short journey i.e., only the heart to get into arterial circulation. Compared with the other two situations for the same dose it is seen that the drug concentration in the blood will be increased rapidly to reach the maximum concentration in inhalation delivery [53][54][55]. Thus, a conclusion that comes from the above explanation is to get fast relief from a disease for example pain, the analgesics should be taken by inhalation or intravenously instead of orally. But to avoid the toxicity of the drug that appeared due to higher C_{max} oral route is much more preferred over others. After absorption the drug molecules are then distributed over various compartments of the body depending on the different factors like size of the drug molecules, their ionization as well as lipophilicity, pH of the area etc. until equilibrium is attained between the compartments. These compartments are blood plasma, extra and intracellular matrix, lipids, cerebrospinal fluid (CSF), synovial fluid, peritoneum etc. In blood plasma, the drug molecules bind with the plasma proteins which are mainly reversible and therefore may be replaced by another substance or another drug molecule. The binding force involves ionic interaction, covalent interaction, hydrogen bonding, or Vander Waals force of interaction. An equilibrium exists between bounded and unbounded drug molecules in blood plasma and unbounded molecules then move to the next compartment until equilibrium is established [56]. The next step is the metabolism of the drug where the water-soluble form of the drug molecules is formed that is very easy to excrete through the kidney from a lipid-soluble form of the drug which is more suitable for the absorption and distribution process. The metabolism process takes place not only in the liver but also lungs and gut. Most often the drugs taken by oral delivery get metabolized in the liver before they reach in systemic circulation for which the concentration

of active molecules decreases. This phenomenon is called "first-pass metabolism." Metabolism occurs in two phases: cytochrome P-450 enzyme present in the endoplasmic reticulum of liver cells oxidizes the drug molecule in the first phase followed by synthesis of water-soluble glucuronide or sulphate products or conjugated product with glutathione [57]. The last process is excretion where metabolites are excreted from the body through urine or faeces. High molecular weight drugs e.g., conjugated products with glutathione are excreted preferably by faeces whereas low molecular weight metabolites that enter blood and other organs after metabolism are excreted through urine [58].

2.5. Transdermal Drug Delivery Systems (TDDS): Transdermal patches adhere to the skin and deliver a predetermined amount of drug over time. Their purpose is to deliver the drug gradually which has many benefits including increased patient compliance, fewer side effects, and extended therapeutic effects. There are variations in the transdermal patches described below [59].

[A] Singe layer drug in adhesive patches: It consists of a polymeric matrix having an adhesive property and the drug molecules dispersed in the layer. The adhesive layer is protected by the backing film and liner layer. Therefore, the adhesive layer serves three purposes here viz. adheres the layers of the patch along with the whole system to the skin and controls the release of drug molecules.

[B] Multi-layer drug in adhesive patches: These patches are very similar to the previous one but the only difference is that another drug in the adhesive layer is added and remains separated by a thin membrane (not seen in every case). Both the adhesive layers are responsible for releasing the drug molecules. Also, the whole system is surrounded by permanent backing film and temporary liner. Generally, these types of patches are used to deliver analgesic drugs, hormone therapy etc.

[C] Vapour transdermal patches: They are also composed of single-layered adhesive polymer like the first one which controls the release of vapour. Some vapour patches, available in the market contain essential oil that is mainly used for decongestion purposes. There are also some vapour patches available in the market which reduces the time of smoking to one in a month.

[D] Matrix systems: Here the adhesive layer surrounds the drug layer which contains a semisolid matrix (lipophilic or hydrophilic) along with the dispersed drug molecules. This system also has impermeable laminate backing.

[E] Reservoir patches: The rate-controlling membrane separates the adhesive layer from the drug reservoir. The drug reservoir contains a liquid solution of the drug molecules or its suspension. The entire system is backed by the backing layer and has a release liner.

The materials used to make the different parts of the transdermal patches are listed below:

(i) Hydroxypropyl methyl cellulose (HPMC) belongs to a group of cellulose ether that is used to produce the biocompatible, biodegradable hydrophilic matrix. The hydrophilic matrices offer an opportunity to develop the controlled-release dosage form. HPMC is soluble in water, specifically cold water and in 70 % ethanol but insoluble in hot water. HPMC also can swell by absorbing the water. It forms a clear film as the drug molecules are soluble in the polymer [60]. Polymethacrylate-based copolymers having an application in sustained release drug delivery (e.g., Eudragit E100, Eudragit S100, Eudragit RL PM, Eudragit RS PM, Eudragit NE 40D), ethyl cellulose, polyvinylpyrrolidone, polyvinyl alcohol etc. are also used for the fabrication of matrix type transdermal patches [61].

(ii) Polyethylene glycol is one of the polyethers that are widely used as a plasticizer to design transdermal patches. It also has a good biocompatibility. Plasticizers can mix well with the polymers and can remain in the polymers permanently. The film of the polymer will be broken in response to bending, and stretching if such a plasticizer is not used to plasticize the polymer

[62]. PEG 400 is usually used instead of the other PEGs with high molecular weight because the plasticizers having low molecular weight can enter between the film-forming polymer chains and interact with the functional groups of the chain more easily [63]. Phthalic acid esters e.g., dioctyl phthalate and aliphatic esters e.g., dioctyl adipate, more glycol derivatives e.g., propylene glycol, an ester derivative of glycerol e.g., triacetin are also used as the plasticizer.

(iii) Polysiloxane adhesive, polyisobutylene adhesive, and acrylates are the chiefly used pressure-sensitive additives. After applying the pressure, the liquid-like adhesive material is erected and then it enables the adhesion by wetting the outer surface of the skin [64].

(iv) Dimethyl sulfoxide, glycols, ethanol, fatty acids, terpenes, and surfactants are used as the penetration enhancer. They facilitate the penetration of the drug either by solubilizing the lipid present in the stratum corneum or by hydrating the stratum corneum [65].

(v) Fluoroacrylates, Fluorosilicone, ethylene vinyl acetate, aluminium foil etc. can be used as release liners. It is very important to say that the release liner must be inert towards the other ingredients of the delivery system as well as the penetration properties [66].

(vi) Polypropylene, polyethene, polyurethane etc are used to prepare the backing film. These materials are chosen for the above purpose as they are impermeable for the drug molecules and inert as well towards the other constituents [67].

Drug selection is also very important in designing the transdermal patches. Drugs should be chosen by considering different physicochemical properties associated with the drug molecules. Generally, the drug molecules having a molecular weight less than 500 Daltons, melting point less than 25℃, log P value i.e., partition coefficient value in the range between 1 to 4 indicating more lipophilic, low therapeutic index (the ratio between the dosage causes toxic effect and the dosage causes therapeutic effect) are incorporated in the transdermal patches [68][69]. Besides the absorbability, permeability and diffusibility of the drug molecules

across the outer layer of the human skin called stratum-corneum, the dose concentration as well is also taken into consideration to formulate the patches.

Ravi Teja Allena et al. (2012) prepared "metaphormine hydrochloride" (controls high blood sugar) transdermal patches using HPMC (hydrophilic polymer) and chitosan (natural polymer) to investigate their sustained release property [70]. **S.T. Prajapati et al. (2011)** made transdermal patches using PVP K30 and HPMC polymers to deliver repaglinide (an anti-diabetic drug) in a sustained manner [71]. **A. Chandra and P.K. Sharma (2009)** fabricated the reservoir-type transdermal patch using HPMC and different permeation enhancers like dimethyl sulphoxide and eucalyptus oil to investigate in vitro release of ketorolac (NSAID) [72]. **H.C. Evans and S.E. Easthope (2003)** formulated buprenorphine (opioid analgesic) loaded transdermal matrix patch [73]. **D. Hashmat et al. (2020)** studied the controlled release of lornoxicam (NSAID) from a membrane-based transdermal patch where oleic acid and propylene glycol were used as permeation enhancers [74].

2.6. Anatomy of the Skin: The skin is composed of four different tissue layers: (a) non-viable epidermis (stratum corneum): It is the outermost layer of the skin which is the first barrier to substances encountering the skin. This layer is 0.5 to 0.20 μm thick and contains 5 to 15% lipids (cholesterol, cholesteryl sulphate, glycosphingolipids, phospholipids) and 75-80% keratin protein. (b) Viable epidermis: It is situated between the dermis and the stratum corneum. The physicochemical structure of the cells of the live epidermis is comparable to that of other living tissues. The thickness of the layer is found to be 50-100 μm. Mainly, water is present (90%) in this layer. (c) Viable dermis: The dermis layer is located underneath the viable epidermis and its thickness lies between 2000 to 3000 μm. This layer is composed of the non-globular protein fibrin. (d) Hypodermis: It is the innermost layer consisting of collagen and fat tissues containing blood & lymph vessels, cutaneous nerves, and secretory pores of sweat glands. The fatty tissues present in this layer can act as a storehouse of drug molecules [75].

2.7. Drug Penetration Routes through Layers of Skin: Drug molecules can penetrate via two possible pathways (Fig 2.1): (a) transepidermal pathway in which drug molecules pass through the stratum corneum and (b) transappendegeal pathway that involves the movement of drug through hair follicles & sweat glands. Transepidermal penetration can be divided into two categories: (I) intra-cellular route which allows the passage of polar or hydrophilic molecules through keratinocytes and (II) inter-cellular route that involves diffusion of non-polar or lipophilic molecules through the matrix of lipid [75].

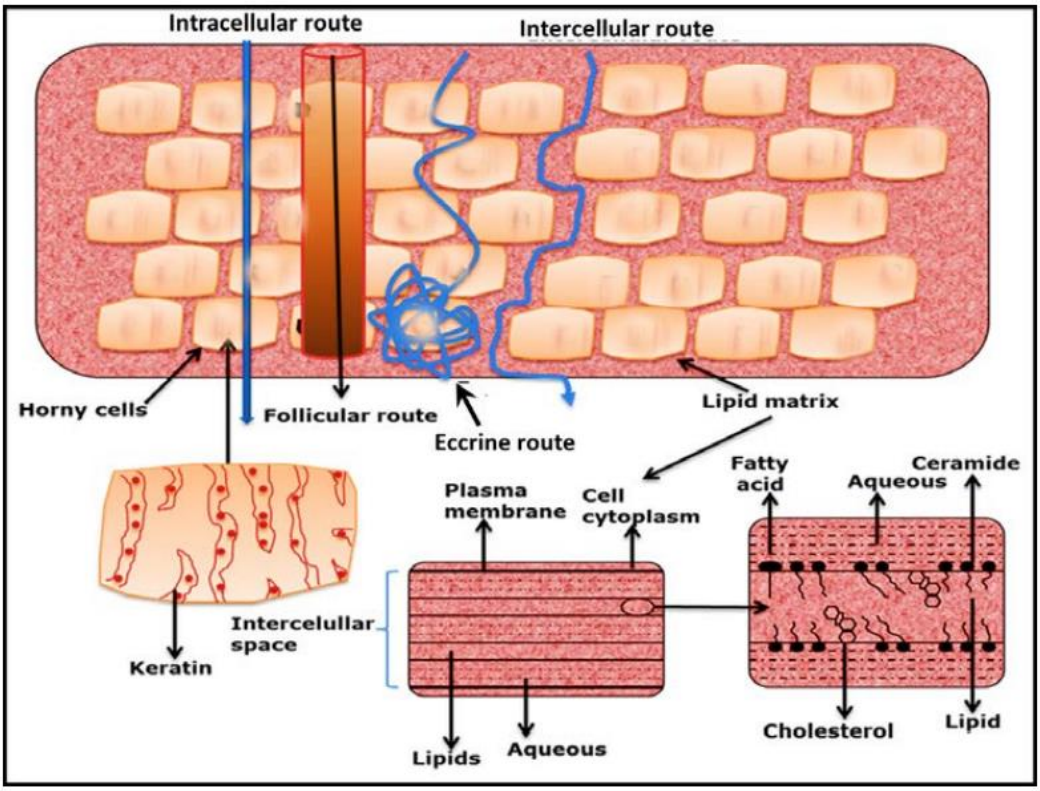

Fig 2.1. Possible pathways of drug molecule penetration [75]

2.8. Skin Permeation of Nanoparticles: The hair follicles have drawn much more attention when it comes to the absorption of nanoparticles. It is generally agreed that hair follicles are essential for the penetration of solid nanoparticles in skin that is not damaged. Hair follicles may penetrate deeply into the subcutaneous fat due to invasions of the epidermis (mostly based

on the follicle's developmental stage). An effective barrier that resembles the stratum corneum is situated in the follicle's top region and has connections in its bottom region to prevent the particles from readily entering the living cells. Rather, once entering the follicle openings, the particles will remain there until they are removed by the growth of hair or the production of sebum. Since the particles within the follicles are somewhat shielded from desquamation, cloth contact, and washing, clearance occurs much more slowly than from the stratum corneum. It makes follicles an outstanding storage site for nanoparticles that can be utilized for drug release. Additionally, follicles provide a direct route to the systemic circulation and viable skin layers for which the effective concentration of the drug in plasma may be achieved in a short period [76].

2.9. Drug Release Kinetic Study: For the optimization of controlled as well as sustained release formulation, the engineers and pharmacist with their similar aims (i.e., reduction of the dosing frequency, increasing of the therapeutic efficacy and patient compliance) worked together on mathematical modelling that helps to predict the model fitted with the release data and diffusion coefficient. These drug release kinetic models mainly describe the dissolution profile which consists of three steps: (1) The solvent molecule approaches the interface between solid and liquid, (2) an interaction occurs at the interface and (3) the solid drug molecules dissolve into the solvent and move towards the bulk solvent [77][78]. The mathematical models include zero order, first order, Higuchi model, Korsmeyrer-Peppas model, Hixon-Crowell model, Weibull model, Baker-Lonsdale model, Gompertz model, Hopfenburg model, a few of which have been described below[79]. **J. Singh et al. (2011)** showed that the "Regression Coefficient" value (R^2 value) is used as goodness of fit parameter. The calculation of the R^2 value is based on the mean value of data points which is why the R^2 value will increase with the increase in data points. Therefore, it is not promising to consider the R^2 value as the suitable indicator of the goodness of fit parameter solely in both linear and

non-linear relationships. So they used The SSR/R^2 value, where SSR stands for "Sum of Squares of Residuals" and also mentioned that the equation has the best R^2 value may not have the best SSR value and both the parameters together give proper justification of the choice of equation, not individually. However, this attempt is not taken in the pharmaceutical industries as the use of R^2 value still prevails over there [80].

(2.9.1) Zero Order Model: The release of a drug from the dosage form may be expressed as:

$$Q_t - Q_0 = k_0 t \quad \ldots (1)$$

Rearranging the eqn (1):

$$Q_t = k_0 t + Q_0 \quad \ldots (2)$$

Q_t = Concentration of drug dissolved at time t

Q_0 = Initial concentration of drug at time t=0

K_0 = Release constant whose unit is represented as concentration time^{-1}. The release data of in vitro and in vivo experiments are plotted as "cumulative percentage amount of drug released" vs. "time."

Differentiating the equation (2):

$$dQ_t/dt = k_0 \quad \ldots (3)$$

Where dQ_t/dt indicates the concentration change with time which is known as the "rate of a reaction." So, equation (3) implies that the release mechanism proceeds at a steady pace regardless of the drug's concentration when zero-order kinetics is used.

The zero-order drug release may be achieved by coating a matrix tablet containing the sparingly water-soluble drug molecules for oral delivery. Also, the above relation can be applied to describe the drug dissolution of transdermal drug delivery systems. A drug reservoir can

provide zero-order release if the material of the reservoir remains saturated with the suspension of drug molecules.

(2.9.2) First-Order Model: The following equations represent the drug release with first-order kinetics.

$$(-)\, dC_t/dt = k_1 C_t = k_1 C_0 e^{-k_1 t} \quad \ldots (4)$$

$$\text{As, } C_t = C_0 e^{-k_1 t} \quad \ldots (5)$$

Where k_1 = First order rate constant whose unit is time^{-1}.

C_t = Concentration of drug at time t

C_0 = Concentration of drug at time t=0

From the equation (4) and (5), it can be easily concluded that the release rate or the drug concentration at any instant decreases exponentially with time.

Taking "log" (base 10), the eqn (5) may be written as

$$\log C_t = \log C_0 - k_1 t/2.303 \quad \ldots (6)$$

The release data are plotted as a "log of cumulative percentage of drug remaining" vs. "time" which produces a straight line having a slope of $-k_1/2.303$.

First-order release kinetics can be achieved by incorporating the drug molecules into the porous matrices.

(2.9.3) Higuchi Model: This model is based on a few assumptions that include (a) a higher initial concentration of the drug in the matrix than the solubility of drug molecules, (b) the diffusion of the drug in one dimension from the matrix, (c) the smaller drug molecules than the thickness of the delivery system, (d) negligible swelling as well as dissolution of the matrix, and (e) constant diffusivity of the drug.

Considering all the above assumptions, the derived classical Higuchi equation is represented as:

$$Q = A\sqrt{D(2C-C_s)C_s t} \quad \ldots (7)$$

Q = Concentration of drug released per unit area A in time t.

C = Initial concentration of dug.

Cs = Solubility of the drug molecules in the matrix.

D = Diffusivity of the drug molecules.

Eqn (7) is changed to eqn (8) if the drug's concentration in a heterogeneous matrix system falls below its solubility and the drug is released via the matrix's pores.

$$Q = \sqrt{D\delta/(2C-C_s)\, C_s t} \quad \ldots (8)$$

δ = porosity of the matrix,

ζ = Tortuosity of the matrix is the ratio of the effective diffusivities in the pore space to those in the bulk material.

Simply the Higuchi equation is written as

$$Q = KH\sqrt{t} \quad \ldots (9)$$

Where, KH = Higuchi dissolution constant.

The release data obtained are plotted as “cumulative percentage of drug release” vs. “square root of time.”

For some transdermal formulations and matrix tablets carrying aqueous-soluble drugs, the Higuchi model is often used to describe the drug-dissolving phenomena.

(2.9.4) Korsmeyer- Peppas Model: A pharmaceutical dosage form follows the Higuchi model means the release of the drug is diffusion-controlled. Once it is ascertained that release data fits properly in the Higuchi equation then a question comes that which type of diffusion process occurs. To get the answer, the release data are subsequently fitted in the logarithmic form of the Korsmeyer-Peppas equation (11).

The general equation is:

$M_t/M_\infty = Kt^n$ ... (10)

M_t/M_∞ = Fraction of drug released at time t

K = Release rate constant and n = Release exponent.

Taking "log" (base 10), the equation (10) can be written as

$\log M_t/M_\infty = \log K + n \log t$ … (11)

The slope value, n (listed in Table 2.1) of the plot ($\log M_t/M_\infty$) vs. ($\log t$) characterizes the type of diffusion mechanism.

Table 2.1. The release mechanism of the drug depends on "n" values

Release Exponent (n)	Types of Diffusion
0.4	Fickian
0.4 <n<0.9	Non-Fickian (Anomalous)
0.9	Case II transport
>0.9	Super Case II transport

The transfer of molecules from an area of high concentration to one of low concentration is known as the diffusion process. In 1855, Adolf Fick stated that (i) the diffusive flux is directly proportional to the concentration gradient – known as "Fick's first law" and (ii) the concentration varies as a function of time to the change in the flux concerning position – known

as “Fick’s second law”. In a general way, it can be said that if the diffusion obeys Fick’s law, then it is called as “Fickian diffusion” otherwise it is “non-fickian diffusion” which is again classified into three categories: Anomalous, Case II transport and Super Case II transport. The major differences between fickian and non-fickian diffusion are: (i) A boundary exists in the case of non-fickian diffusion that leads to separation of the swollen region from the shiny unswollen region but such a boundary does not exist in fickian diffusion, (ii) For non-fickian diffusion a sharp front move into the polymer for which the quantity of liquid absorbed enhances linearly with time but for fickian diffusion no sharp front is present. And the solvent diffusion velocity distinguishes the three groups of non-fickian diffusion. In the case of anomalous, the magnitude of the velocity of solvent-diffusion and polymer relaxation are similar. In case II transport, the solvent-diffusion velocity is greater than polymeric relaxation; however, in super case II transport, the solvent-diffusion velocity is so high that the solvent penetration is accelerated [82].

(2.9.5) Hixon-Crowell Model: This model describes a dosage form where a change in diameter and surface area of the particle occurs on releasing of the drug from the dosage form. The fact that a particle's surface area is proportional to its volume-cube root was predicted by Hixon and Crowell with the aid of this phenomenon. Based on this fact they constructed a relationship between the release of drug and time which is expressed as following equation (12).

$$W_0^{1/3} - W_t^{1/3} = \kappa t \quad \ldots (12)$$

Where, W_t = Remaining concentration of the drug.

W_0 = Initial concentration of the drug.

κ = Constant where surface volume relation is incorporated

t = time.

In vitro and in vivo release data are plotted as “cube root of remaining drug percentage” vs. “time.” This equation is applied to tablets or other dosage forms, where the dissolution process occurs in such a way that the original geometrical shape remains constant with time.

2.10. Analgesic Drugs and their Mechanism of Action: A pain ladder was recommended by the World Health Organization (WHO) for managing analgesia, especially for cancer-related but it can be used as a general principle by doctors or medical professionals for any type of pain. The WHO provides an example of how to manage chronic pain (long-term pain) using pharmaceuticals in Tables 2.2 and 2.3. If therapy is not successful in providing the patient with enough pain relief at any stage, the patient and doctor need to proceed to the next step [83][84].

Table 2.2. WHO’s pain ladder

Steps	Types of pain	Medicines	Results
1	Mild	Non-opioid + Adjuvant	If pain persists or increases then step 2 must be adopted.
2	Moderate	Weak opioid + non-opioid + Adjuvant	If again pain persists or increases then it is important to go to step 3
3	Severe	Strong opioid + non-opioid + Adjuvant	Relief from pain.

Table 2.3. Several types of pain and drug management

Types of pain	Treatment	Remarks
Migraine	Paracetamol and NSAIDs	Triptans are often used when other medications are ineffective.
Headache	Paracetamol and NSAIDs	If headaches persist and are accompanied by fever, or vomiting then a doctor consultation is very much needed.
Menstrual Cramps	NSAIDs	Any NSAID would work.
Bone fracture, burn, wound or severe sprain	Opioids	Freedom from pain within two weeks.
Abrasions, bruises, sprains	Paracetamol and NSAIDs	Opioids are not needed for this purpose.
Post-operative severe pain	Opioids	A combination of opioids is prescribed.
Minor pain after surgery	Paracetamol and NSAIDs	Opioids are rarely used.
Pulled or strain muscle	NSAIDs	Relief from inflammation (if any). Only short-term use of NSAIDs is needed.

Muscle ache	Paracetamol and NSAIDs	Relief from inflammation (if any).
Pain from the kidney stone	Paracetamol, NSAIDs and Opioids	Opioids are necessary if the pain is severe as well as persistent.
Osteoarthritis pain	Paracetamol and NSAIDs	Medical attention is recommended if the pain continues.
Chronic back pain	Paracetamol and NSAIDs	Opioids are recommended if the pain is intense and if persists.
Gastroesophageal reflux or heartburn	Antacid, proton-pump inhibitor, H_2 antagonist	NSAIDs must be avoided as much as possible. Medical attention is proposed if heartburn continues.
Toothache	Paracetamol and NSAIDs	Opioids are necessary if the pain is severe.

It is clear from the above tables that treatment of pain is dependent on three categories of drugs: Opioids, NSAIDs and Paracetamol.

Pain can be classified depending on its severity into three parts that include “mild pain,” “mild to moderate pain” and “moderate to severe pain.” The medication universally accepted for such cases are [81]:

- *Mild Pain*: Paracetamol (acetaminophen) or a non-steroidal anti-inflammatory drug (NSAID) is sufficient.
- *(ii) Mild to Moderate Pain*: The combination of paracetamol, NSAID or paracetamol with a mild opioid may offer more relief than either medication alone.
- *(iii) Moderate to Severe Pain*: This class of pain is acute or chronic. A few drugs are more effective treating chronic pain than acute pain, while others are more appropriate for both types of pain. It is necessary to use acute pain medication to manage both the pain that follows surgery and the sudden onset of pain following an injury. On the other hand, chronic pain medication is for lessening the extent of ongoing pain. Generally, both strong and weak opioids are used to reduce moderate to severe pain.

(2.10.1) Opioids: Depending upon the definite properties and formulation, opioid medications are given as intermediate, long-acting or short analgesia. These medications can be administered orally, transdermally, intravenously, through nasal mucosa or by injection. However, opioid injections are rarely used to treat patients with chronic pain. Sometimes in the case of chronic pain, long-acting medication (extended-release medication) is combined with short-acting medication to lower the intensity of pain. Furthermore, Opioids may have side effects, particularly when the dosage is changed. Also, it has to be kept in mind that the use of opioids for prolonged periods may create an addiction for which the prescribing physician should monitor whether there is any improvement in the reduction of pain or abuse of medication by the patient. Other side effects may occur from the overuse of opioids such as hyperalgesia (excessively increased sensitivity of pain), neuronal changes, respiratory depression (in which overdose of opioids blocks carbon dioxide feedback loop inducing sleep that stimulation of brainstem by increased carbon dioxide level for increasing the respiratory rate during slow breathing) or even death [82]. A few examples of commonly used opioids are immediate-release oral formulations (Oxycodone - OxyContin, Percocet, Roxicodone;

Hydrocodone - Vicodin, Norco; Morphine - MS Contin, Roxanol, Kadian; Codeine - Tylenol with Codeine, Robitussin AC; Hydromorphone - Dilaudid; Tramadol - Ultram; Meperidine - Demerol), extended-release oral formulations (Oxycodone - OxyContin, Xtampza ER; Morphine - MS Contin, Kadian; Hydromorphone – Exalgo; Fentanyl - Duragesic *(transdermal patch)*; Actiq *(oral transmucosal lozenge)*; Fentora *(buccal tablets)*), injectable formulations (Morphine - Morphine sulfate injection; Hydromorphone - Dilaudid injection; Fentanyl - Sublimaze injection) etc. **Enno Freye et al. (2007)** showed results of effervescent morphine in faster relief of pain in patients as compared to that of immediate release [83]**. M. Afilalo et al. (2010)** assessed how well tapentadol extended-release (ER) and oxycodone controlled-release (CR) managed moderate to severe chronic knee pain associated with osteoarthritis, as well as their respective safety profiles [84]. **J.V. Pergolizzi et al. (2015)** did research on an extended-release fixed-dose combination of oxycodone/acetaminophen for acute pain treatment [85]. **Hassan Motamed et al. (2017)** attempted a clinical trial to compare intravenous fentanyl vs lidocaine for the management of renal colic pain [86]. **Samara Mayer et al. (2020)** initiated injectable diacetylmorphine and hydromorphone treatment in Vancouver, Canada [87]**. Xianzheng Zeng et al. (2023)** investigated the safety and short-term effectiveness of patient-controlled subcutaneous analgesia for moderate to severe cancer pain when provoked by hydromorphone [88]. **Lasse Härkänen et al. (2023)** measured buprenorphine levels in plasma and CSF with low-dose transdermal patch administration in osteoarthritis patients [89]. **Cecilie Hasselø Thaulow et al. (2023)** suggested dose-specific concentration ranges for fentanyl, morphine, and oxycodone for the treatment of pain [90]. **Marina Ayres Delgado et al. (2023)** focused on preclinical investigation using a postoperative pain model to observe how ketamine, lidocaine, and ascorbic acid work to reverse hyperalgesia brought on by fentanyl that is not glutamate-dependent [91]. **A. Roger et al. (2024)** compared the intra-operative use of methadone and morphine in paediatric patients having posterior spinal fusion [92]**. Flora**

Bahrami et al. (2024) used digital patient twins with physics-based technology to customize the transition from oral morphine to transdermal fentanyl patches according to patient physiology [93].

(2.10.2) Non-Opioids:

(2.10.2.1) Non-steroidal Anti-inflammatory Drugs (NSAIDs): NSAIDs are broadly used for the treatment of inflammatory conditions like arthritis, tendonitis and bursitis. Patients having kidney or liver disease asthma or high blood pressure must consult with their physicians to take NSAIDs as the overuse of NSAIDs harms the body such as gastrointestinal problems, renal side effects, and cardiac side effects. Generally, the mechanism of action of NSAIDs is based upon the inhibition of an enzyme called cyclooxygenase (COX) which is responsible for catalyzing the formation of "prostaglandins" having various functions in the body including the regulation of inflammation and "thromboxanes" from "arachidonic acid." Therefore, it can also be said that the anti-inflammatory effect occurs in the body by preventing the synthesis of prostaglandins. "Phospholipase A2", an enzyme is released from the damaged cells which converts phospholipids into arachidonic acid in the cell membrane. COX has two isoforms: COX-1 & COX-2 in which COX-1 is induced throughout the human body and produces prostaglandins and thromboxane that stimulate normal body functions such as protecting the stomach mucosa from the acidic environment, platelet accumulation, preservation of renal blood-circulation etc. In contrast, COX-2 isoform is induced only at sites of inflammation, not all the tissues of the body. COX-2-derived prostaglandins facilitate fever, pain, and inflammation. Most NSAIDs are non-selective COX inhibitors (traditional NSAIDs) which means that they can inhibit both COX-1 and COX-2. As a result of this, the production of prostaglandin in the stomach gets reduced and consequently the risk of stomach or duodenum ulceration increases. Selective COX-2 inhibitors have been developed to avoid the risk of gastrointestinal ulcers but unfortunately, they cause thrombosis which increases the risk of

heart attack to a large extent. Selective COX-2 inhibitors are costlier than traditional NSAIDs and are prescribed for extended conditions (e.g., arthritis) [94][95]. Some commonly used traditional NSAIDs are aspirin, ibuprofen, naproxen, and a few COX-2 inhibitors' names are celecoxib, etoricoxib, rofecoxib, and valdecoxib**.** The transdermal formulations available in the market are the Diclofenac patch, Ketoprofen patch, Ibuprofen patch, and Piroxicam patch. **Sinodukoo E. Okafo et al. (2020)** worked on the formulation and assessment of diclofenac sodium sustained-release matrix tablets using gum from *Brachystegia eurycoma* [96]. **G. Yurtdaş-Kırımlıoğlu et al. (2021)** synthesised ibuprofen-entrapped microspheres & studied their in vitro release profile, stability, and thermal properties [97]. **Paula Ossowicz-Rupniewska et al. (2022)** studied structural changes of ibuprofen released from a matrix-type transdermal patch on permeation of the skin barrier [98]. **T. Taguchi et al. (2023)** showed that diclofenac sodium patch is effective for low back pain [99]. **Saeede Zadsirjan et al. (2023)** compared the analgesic efficacy between ibuprofen oral tablets and ketoprofen transdermal patches in patients suffering from post-endodontic pain [100].

(2.10.2.2) Paracetamol: It has been observed that the negative impacts of opioids and NSAIDs on the human body for use over an extended period surpass their advantages. Therefore, to avoid the above-mentioned problems, paracetamol (acetaminophen) can be used as an alternative. It's a non-opioid antipyretic and analgesic that may be taken alone for mild to moderate pain or in conjunction with an opioid analgesic for more severe pain. The suggested dosage for adults and children (12 years and above) is 500–1000 mg every 4-6 hours, as needed, up to a maximum of 4000 mg in 24 h [104]. Unlike NSAIDs, paracetamol has been pointed out not to diminish tissue-inflammation. The actual mechanism of action is not clear but it can be explained as the inhibition of synthesis of prostaglandin at the site where the concentration of peroxide is low. The enzyme called "prostaglandin H2 synthase", also known as cyclooxygenase (COX) is responsible for catalyzing the formation of prostanoids

(prostaglandins and thromboxanes) from arachidonic acid (produced from phospholipids in the cell membrane by an enzyme called phospholipase A2 released from damaged cells) has two active sites: COX (cyclooxygenase) and POX (peroxidise) sites. During the formation of prostanoids, first an unstable intermediate hydroperoxide, "prostaglandin G2" is produced at the COX site which is then transformed to "prostaglandin H2" via POX. Paracetamol exhibits a substantial suppression of prostaglandin formation in unharmed cells with low amounts of arachidonic acid by preventing POX's physiological regeneration. Moreover, prostaglandin synthesis is weakly inhibited in shattered cells, where the concentration of hydroperoxide is high. This peroxide-dependent COX inhibition explains why paracetamol acts differently in the brain (where peroxide concentrations are low) and peripheral sites of inflammation (where peroxide levels are high). Hence, paracetamol has weak anti-inflammatory activity but highly effective analgesic and antipyretic properties [101]**.** Some common formulations of paracetamol available in different markets are tablets (Calpol, Crocin, Dolo, Paracetamol with various generic brands), liquid suspension (Calpol, Dolo Drops, P-125, Fevago, Pyrigesic), effervescent tablets (Panadol Advance Effervescent, Calpol Fastmelts, Paracetamol Effervescent with various generic brands). **A. Sintov et al. (2010)** attempted to produce a transdermal patch of paracetamol varying the amounts of constituents of the patch for paediatric use only [102]. **M. Jalili et al. (2016)** presented that when it comes to acute limb injuries, intravenous paracetamol seems to provide a superior analgesic effect than intravenous morphine [103]. **Fatemehshima Hadipourzadeh et al. (2021)** examined the effects of combining paracetamol with a continuous dexmedetomidine infusion pump for pain relief after heart surgery in adults [104]. **Andri Marulitua Lubis et al. (2021)** observed that the combination of ibuprofen and paracetamol is more effective in lowering the total amount of morphine required after total knee arthroplasty [105].

(*2.10.2.3) Herbal Drugs:* Nutraceuticals prepared from plants are used to get effective pain relief. Herbal medications are becoming popular day by day because of very few side effects exerted by them. People have used herbs, and essential oils such as ginger, turmeric, capsaicin, rosemary essential oil, lavender essential oil, peppermint essential oil, eucalyptus essential oil, and cloves as natural pain relievers for hundreds of years. **Patrick B. Wilson (2015)** said in his review paper that 2g of ginger/day can reduce muscle pain from exercise and prolonged running if it is taken at least five days [106]. **P. Anand and K. Bley (2011)** found that capsaicin reduces the sensitivity of skin to pain by the process of defunctionalisation of nociceptor fibres [107]. **B. Ali et al. (2015)** investigated that essential oils are also responsible for giving relief from muscle pain, headache, swollen joints etc. because of their skin permeability properties [108]. **A. Alqareer et al. (2006)** researched on anaesthetic behaviour of clove gel as an alternative to benzocaine gel which is used to reduce the pain of needle insertion by dentists generally [109]. Yet there are some problems associated with these medications including the lack of knowledge of their biological action and potential interactions with other nutraceutical products and prescribed medications, less clinical studies etc. Among these herbs, turmeric is a very common herbal remedy and usually “the turmeric paste in slaked lime” had been used by our forefathers as a traditional ayurvedic medicine for the treatment of wounds and inflammation in different parts of our body. Not many clinical studies have been conducted on the said mixture but it has been known to all that it can lower the pain and inflammation that is prevalent in our body without any major side effects. Researchers have suggested that curcumin, which is the most active component of turmeric, may be employed for the treatment of colitis, arthritis, chronic neurodegenerative disease, and cancer. The yellow colour of the turmeric appears for this curcumin compound. IUPAC name of the curcumin is 1, 7-bis (4-hydroxy-3-methoxyphenyl)-1, 6-heptadiene-3, 5-dione which is almost insoluble in water and remains as a bis-keto form in neutral and acidic condition and predominates as enolate form at

a pH greater than 8. But in alkaline medium curcumin molecules degrade into different species like vanillic acid, ferulic acid, and acetone. Its degradation can be prevented by an antioxidant like ascorbic acid, human blood etc. Commercially available curcumin contains 17% demethoxy curcumin and 3% bisdemethoxycurcumin along with pure curcumin [110]. Like NSAIDs, curcumin can show anti-inflammatory action by any one of the following pathways including inhibition of prostaglandin synthesis, inhibition of COX, inhibition of LOX, inhibition of metabolism of arachidonic acid or inhibition of cytokines (tumour necrosis factor) etc. Evidence suggests that curcumin induces anti-inflammatory action through the inhibition of the eicosanoid pathway predominantly. Among the active arachidonic acid metabolites such as leukotrienes (LTs), hydroxy eicosatetraenoic acids (HETEs), lipoxins etc. mediated by lipoxygenase (LOX), leukotrienes that include LTB4 and cysteinyl LTs (LTC4, LTD4, LTE4) are potent mediators of inflammation [111]. Many researchers have already worked on the inhibitory effects of curcumin on LTs using in vitro and in vivo model systems [112–114].

2.11. Study of Analgesic Activities: There are different methods to measure central and peripheral analgesic activities [115, 116].

- *Hot plate method:* Eddy and Leimbach are the discoverers of this method in which the mice were positioned on a hot-plate having a temperature of 55±2°C to observe the pain (either licking of forepaws or jumping). The time of reactions (licking and jumping) are recorded at definite time intervals after administration of the drug.
- *Tail flick method:* It is another approach to calculate the analgesic activity which was explained by D'amour and Smith in 1941. Here the reaction latencies are measured with the help of an analgesiometer in which the nicrome wire is the source of heat. Like the hot plate method, the reaction times (usually a cut-off time of 10-15 seconds taken to avoid the heat injury) at time intervals after the drug administration are recorded by locating the tip of the tail on the heat source.

- *Tail immersion test:* This is also a thermal test to evaluate the nociceptive reaction in mice or in other words to evaluate the potential of compounds. The lower portion of the tail of mice is immersed in hot water where the temperature is maintained at nearly 55°C. Next, the time of reaction i.e. tail withdrawal from the hot water is recorded every 30 minutes after the administration of the drug up to 2-3 h.
- *Acetic acid-induced writhing method*: In this method, the pain sensation is created by injecting the acetic acid solution into the peritoneal cavity of an animal. A standard analgesic drug, test sample and vehicle are injected before intraperitoneal administration of acetic acid solution. After that, the numbers of abdominal constrictions (writhes) are recorded from 5-10 mins after injecting the acetic acid solution up to 20-30 mins and the percentage of protection is calculated using the following formula-

  % protection = $(\eta_c-\eta_t / \eta_c) \times 100$

  Where, η_c = number of writhing in control

  And η_t = number of writhing in test animal.

2.12. Conclusion: The employment of nanotechnology in drug delivery systems to achieve enhanced solubility as well as sustained release of drugs has been elaborated. Furthermore, this review has demonstrated that transdermal drug delivery heralds a new era in drug delivery innovation, promising to redefine treatment standards and improve therapeutic outcomes for patients worldwide. Also, it has been shown that the drug release kinetic models serve as indispensable tools for formulation optimization, dosage regimen design, and therapeutic efficacy prediction. This review has highlighted the pivotal role of various analgesic drugs in pain management offering insights into their mechanism of action and recent formulations available in the market. Moreover, accurate and reproducible assessments of pain relief

efficacy by different methods have been discussed which is essential for evaluating the therapeutic potential of novel analgesic agents and guiding clinical decision-making processes.

Reference:

1. Gatoo, M. A., Naseem, S., Arfat, M. Y., Mahmood Dar, A., Qasim, K., & Zubair, S. (2014). Physicochemical properties of nanomaterials: Implication in associated toxic manifestations. *BioMed Research International*, *2014*. https://doi.org/10.1155/2014/498420

2. Singh, M., Goyal, M., & Devlal, K. (2018). Size and shape effects on the band gap of semiconductor compound nanomaterials. *Journal of Taibah University for Science*, *12*(4), 470–475. https://doi.org/10.1080/16583655.2018.1473946

3. Ganguly, S., Halder, K., Hoque, N., Das, S., & G Dastidar, S. (2015). A Comparative Study Between Electrical Properties of Bulk and Synthesized Nano Material of Zinc Sulphide. *American Journal of Research Communication*, *3*(3), 69–80.

4. Murr, L. E. (2015). Handbook of materials structures, properties, processing and performance. *Handbook of Materials Structures, Properties, Processing and Performance*, 1–1152. https://doi.org/10.1007/978-3-319-01815-7

5. Hári, J. A., & Pukánszky, B. A. (2011). Nanocomposites: Preparation, Structure, and Properties. *Applied Plastics Engineering Handbook*, 109–142. https://doi.org/10.1016/B978-1-4377-3514-7.10008-X

6. Crocker, A. G., Elvidge, A. M., & Flewitt, P. E. J. (1987). Structure and properties of polycrystalline materials. *Physica Scripta*, *1987*(T19B), 344–349. https://doi.org/10.1088/0031-8949/1987/T19B/004

7. Iqbal, P., Preece, J. A., & Mendes, P. M. (2012). Nanotechnology: The "Top-Down" and "Bottom-Up" Approaches. *Supramolecular Chemistry*. https://doi.org/10.1002/9780470661345.smc195

8. Tselev, A., Hatton, K., Fuhrer, M. S., Paranjape, M., & Barbara, P. (2004). A photolithographic process for fabrication of devices with isolated single-walled carbon nanotubes. *Nanotechnology*, *15*(11), 1475–1478. https://doi.org/10.1088/0957-4484/15/11/017

9. Piras, C. C., Fernández-Prieto, S., & De Borggraeve, W. M. (2019). Ball milling: A green technology for the preparation and functionalisation of nanocellulose derivatives. *Nanoscale Advances*, *1*(3), 937–947. https://doi.org/10.1039/c8na00238j

10. Parashar, M., Shukla, V. K., & Singh, R. (2020). Metal oxides nanoparticles via sol–gel method: a review on synthesis, characterization and applications. *Journal of Materials Science: Materials in Electronics*, *31*(5), 3729–3749. https://doi.org/10.1007/s10854-020-02994-8

11. Sharma, K. (2017). Nanomaterials for drug delivery. *Advances in Personalized Nanotherapeutics*, 57–77. https://doi.org/10.1007/978-3-319-63633-7_5

12. Rizvi, S. A. A., & Saleh, A. M. (2018). Applications of nanoparticle systems in drug delivery technology. *Saudi Pharmaceutical Journal*, *26*(1), 64–70. https://doi.org/10.1016/j.jsps.2017.10.012

13. Patra, J. K., Das, G., Fraceto, L. F., Campos, E. V. R., Rodriguez-Torres, M. D. P., Acosta-Torres, L. S., … Shin, H. S. (2018). Nano based drug delivery systems: Recent developments and future prospects 10 Technology 1007 Nanotechnology 03 Chemical Sciences 0306 Physical Chemistry (incl. Structural) 03 Chemical Sciences 0303 Macromolecular and Materials Chemistry 11 Medical and He. *Journal of Nanobiotechnology*, *16*(1), 1–33. https://doi.org/10.1186/s12951-018-0392-8

14. Lu, H., Wang, J., Wang, T., Zhong, J., Bao, Y., & Hao, H. (2016). Recent Progress on Nanostructures for Drug Delivery Applications. *Journal of Nanomaterials*, *2016*. https://doi.org/10.1155/2016/5762431

15. Yadav, S., Sharma, A. K., & Kumar, P. (2020). Nanoscale Self-Assembly for Therapeutic Delivery. *Frontiers in Bioengineering and Biotechnology*, *8*(February), 1–24. https://doi.org/10.3389/fbioe.2020.00127

16. Bharti, C., Gulati, N., Nagaich, U., & Pal, A. (2015). Mesoporous silica nanoparticles in target drug delivery system: A review. *International Journal of Pharmaceutical Investigation*, *5*(3), 124. https://doi.org/10.4103/2230-973x.160844

17. Narayan, R., Nayak, U. Y., Raichur, A. M., & Garg, S. (2018). Mesoporous silica nanoparticles: A comprehensive review on synthesis and recent advances. *Pharmaceutics*, *10*(3), 1–49. https://doi.org/10.3390/pharmaceutics10030118

18. Kwon, S., Singh, R. K., Perez, R. A., Neel, E. A. A., Kim, H. W., & Chrzanowski, W. (2013). Silica-based mesoporous nanoparticles for controlled drug delivery. *Journal of Tissue Engineering*, *4*(1), 1–18. https://doi.org/10.1177/2041731413503357

19. Yu, Q., Hui, J., Wang, P., Xu, B., Zhuang, J., & Wang, X. (2012). Hydrothermal synthesis of mesoporous silica spheres: Effect of the cooling process. *Nanoscale*, *4*(22), 7114–7120. https://doi.org/10.1039/c2nr31834b

20. Kamarudin, N. H. N., Jalil, A. A., Triwahyono, S., & Timmiati, S. N. (2016). Sintesis partikel nano silika berliang meso dibantu gelombang mikro sebagai medium penyebaran ubat. *Malaysian Journal of Analytical Sciences*, *20*(6), 1382–1389. https://doi.org/10.17576/mjas-2016-2006-17

21. Jiao, Y., Guo, J., Shen, S., Chang, B., Zhang, Y., Jiang, X., & Yang, W. (2012). Synthesis of discrete and dispersible hollow mesoporous silica nanoparticles with tailored shell thickness for controlled drug release. *Journal of Materials Chemistry*, *22*(34), 17636–17643. https://doi.org/10.1039/c2jm31821k

22. Chakraborty, S., Biswas, S., Sa, B., Das, S., & Dey, R. (2014). In vitro & in vivo correlation of release behavior of andrographolide from silica and PEG assisted silica gel matrix. *Colloids and Surfaces A: Physicochemical and Engineering Aspects*, *455*(1), 111–121. https://doi.org/10.1016/j.colsurfa.2014.04.046

23. Zhu, M., Zhu, Y., Zhang, L., & Shi, J. (2013). Preparation of chitosan/mesoporous silica nanoparticle composite hydrogels for sustained co-delivery of biomacromolecules and small chemical drugs. *Science and Technology of Advanced Materials*, *14*(4). https://doi.org/10.1088/1468-6996/14/4/045005

24. Moodley, T., & Singh, M. (2019). Polymeric mesoporous silica nanoparticles for enhanced delivery of 5-fluorouracil in vitro. *Pharmaceutics*, *11*(6). https://doi.org/10.3390/pharmaceutics11060288

25. Ke, J., Wang, Y., Wang, L., Yang, B., Gou, K., Qin, Y., … Li, H. (2020). Synthesis and characterization of core-shell mesoporous silica nanoparticles with various shell thickness as indomethacin carriers: In vitro and in vivo evaluation. *Microporous and Mesoporous Materials*, *297*(July 2019), 110043. https://doi.org/10.1016/j.micromeso.2020.110043

26. Shahriarinour, M., Divsar, F., & Eskandari, Z. (2019). Synthesis, characterization, and antibacterial activity of thymol loaded SBA-15 mesoporous silica nanoparticles. *Inorganic and Nano-Metal Chemistry*, *49*(6), 182–189. https://doi.org/10.1080/24701556.2019.1624569

27. Monteiro, N., Martins, A., Reis, R. L., & Neves, N. M. (2014). Liposomes in tissue engineering and regenerative medicine. *Journal of the Royal Society Interface*, *11*(101). https://doi.org/10.1098/rsif.2014.0459

28. Yadav, D., Sandeep, K., Pandey, D., & Dutta, R. K. (2017). Liposomes for Drug Delivery. *Journal of Biotechnology & Biomaterials*, *07*(04). https://doi.org/10.4172/2155-952x.1000276

29. Deamer, D. W. (1978). Preparation and Properties of Ether-Injection Liposomes. *Annals of the New York Academy of Sciences*, *308*(1), 250–258. https://doi.org/10.1111/j.1749-6632.1978.tb22027.x

30. Charcosset, C., Juban, A., Valour, J. P., Urbaniak, S., & Fessi, H. (2015). Preparation of liposomes at large scale using the ethanol injection method: Effect of scale-up and injection devices. *Chemical Engineering Research and Design*, *94*(January), 508–515. https://doi.org/10.1016/j.cherd.2014.09.008

31. Shi, N.-Q., & Qi, X.-R. (2021). Preparation of Drug Liposomes by Reverse-Phase Evaporation, 37–46. https://doi.org/10.1007/978-3-662-49320-5_3

32. Paavola, A., Kilpeläinen, I., Yliruusi, J., & Rosenberg, P. (2000). Controlled release injectable liposomal gel of ibuprofen for epidural analgesia. *International Journal of Pharmaceutics*, *199*(1), 85–93. https://doi.org/10.1016/S0378-5173(00)00376-8

33. de Araujo, D. R., Cereda, C. M. S., Brunetto, G. B., Pinto, L. M. A., Santana, M. H. A., & de Paula, E. (2004). Encapsulation of mepivacaine prolongs the analgesia provided by sciatic nerve blockade in mice. *Canadian Journal of Anesthesia*, *51*(6), 566–572. https://doi.org/10.1007/BF03018399

34. Wagner, A. M., Knipe, J. M., Orive, G., & Peppas, N. A. (2019). Quantum dots in biomedical applications. *Acta Biomaterialia*, *94*, 44–63. https://doi.org/10.1016/j.actbio.2019.05.022

35. Fang, M., Peng, C. W., Pang, D. W., & Li, Y. (2012). Quantum dots for cancer research: current status, remaining issues, and future perspectives. *Cancer Biology and Medicine*, *9*(3), 151–163. https://doi.org/10.7497/j.issn.2095-3941.2012.03.001

36. Zhao, Y., Zhang, Y., Qin, G., Cheng, J., Zeng, W., Liu, S., … Qu, H. (2017). In vivo biodistribution and behavior of CdTe/ZnS quantum dots. *International Journal of Nanomedicine*, *12*, 1927–1939. https://doi.org/10.2147/IJN.S121075

37. Lee, B. H., Suresh, S., & Ekpenyong, A. (2019). Fluorescence intensity modulation of CdSe/ZnS quantum dots assesses reactive oxygen species during chemotherapy and radiotherapy for cancer cells. *Journal of Biophotonics*, *12*(2), 1–9. https://doi.org/10.1002/jbio.201800172

38. Brkić, S. (2018). Applicability of Quantum Dots in Biomedical Science. *Ionizing Radiation Effects and Applications*. https://doi.org/10.5772/intechopen.71428

39. Yong, K. T., Wang, Y., Roy, I., Rui, H., Swihart, M. T., Law, W. C., … Reynolds, J. L. (2012). Preparation of quantum dot/drug nanoparticle formulations for traceable targeted delivery and therapy. *Theranostics*, *2*(7), 681–694. https://doi.org/10.7150/thno.3692

40. Yuan, Q., Hein, S., & Misra, R. D. K. (2010). New generation of chitosan-encapsulated ZnO quantum dots loaded with drug: Synthesis, characterization and in vitro drug delivery response. *Acta Biomaterialia*, *6*(7), 2732–2739. https://doi.org/10.1016/j.actbio.2010.01.025

41. Hanada, S., Fujioka, K., Futamura, Y., Manabe, N., Hoshino, A., & Yamamoto, K. (2013). Evaluation of anti-inflammatory drug-conjugated silicon quantum dots: Their cytotoxicity and biological effect. *International Journal of Molecular Sciences*, *14*(1), 1323–1334. https://doi.org/10.3390/ijms14011323

42. Zhang, W., Zhang, Z., & Zhang, Y. (2011). The application of carbon nanotubes in target drug delivery systems for cancer therapies. *Nanoscale Research Letters*, *6*, 1–22. https://doi.org/10.1186/1556-276X-6-555

43. Hadidi, N., Kobarfard, F., Nafissi-Varcheh, N., & Aboofazeli, R. (2013). PEGylated single-walled carbon nanotubes as nanocarriers for cyclosporin A delivery. *AAPS PharmSciTech*, *14*(2), 593–600. https://doi.org/10.1208/s12249-013-9944-2

44. Carretero, M. I., & Pozo, M. (2009). Clay and non-clay minerals in the pharmaceutical industry: Part I. Excipients and medical applications. *Applied Clay Science*, *46*(1), 73–80. https://doi.org/10.1016/J.CLAY.2009.07.017

45. Venkata, P., Kumari, K., Rao, Y. S., & Akhila, S. (2019). GSC Biological and Pharmaceutical Sciences Role of nanocomposites in drug delivery, *08*(03), 94–103.

46. Huggett, J. M. (2004). Clay Minerals. *Encyclopedia of Geology*, (i), 358–365. https://doi.org/10.1016/B0-12-369396-9/00273-2

47. Kim, M. H., Choi, G., Elzatahry, A., Vinu, A., Choy, Y. Bin, & Choy, J. H. (2016). Review of clay-drug hybrid materials for biomedical applications: Administration routes. *Clays and Clay Minerals*, *64*(2), 115–130. https://doi.org/10.1346/CCMN.2016.0640204

48. Ani, T. Al. (2018). Clay and clay mineralogy, (September).

49. Sohani, O. R., Phatak, A. A., & Chaudhari, P. D. (2015). Use of nanocomposites in drug delivery systems. *Pharma Times*, *47*(4), 33–35.

50. Lobato-Aguilar, H. A., Lizama-Uc, G., Uribe-Calderon, J. A., Cauich-Rodriguez, J., Rodriguez-Fuentes, N., & Cervantes-Uc, J. M. (2020). Antibacterial properties and release kinetics of chlorhexidine diacetate from montmorillonite and palygorskite clays. *Journal of Biomaterials Applications*, *34*(8), 1052–1058. https://doi.org/10.1177/0885328219891710

51. Bediako, E. G., Nyankson, E., Dodoo-Arhin, D., Agyei-Tuffour, B., Łukowiec, D., Tomiczek, B., … Efavi, J. K. (2018). Modified halloysite nanoclay as a vehicle for sustained drug delivery. *Heliyon*, *4*(7). https://doi.org/10.1016/j.heliyon.2018.e00689

52. Chakraborty, J., Roychowdhury, S., Sengupta, S., & Ghosh, S. (2013). Mg-Al layered double hydroxide-methotrexate nanohybrid drug delivery system: Evaluation of efficacy. *Materials Science and Engineering C*, *33*(4), 2168–2174. https://doi.org/10.1016/j.msec.2013.01.047

53. Rhodes, C. T., Dekker, M., & Francisco, S. (1978). SCIENTIFIC C O M M E N T A R Y Effect of Route of Administration and Distribution on Drug Action 1, *6*(6).

54. Ahmed, T. A. (n.d.). Pharmacokinetics of Drugs Following IV Bolus , IV Infusion , and Oral Administration.

55. Erd, F., Anna, L., Farkas, D., Bajza, Á., & Gizurarson, S. (2018). Evaluation of intranasal delivery route of drug administration for brain targeting, *143*(October), 155–170. https://doi.org/10.1016/j.brainresbull.2018.10.009

56. Bohnert, T., & Gan, L. (2013). Plasma Protein Binding : From Discovery to Development INTRODUCTION TO FREE DRUG THEORY — WHY IS PLASMA PROTEIN BINDING, (April), 1–42. https://doi.org/10.1002/jps

57. Tools, C. (2017). Drug Metabolism in Preclinical Drug Development: A Survey of the Discovery Process, Toxicology, and Computational Tools, 556–565. https://doi.org/10.2174/1389200218666170316093301

58. Kok-yong, S., & Lawrence, L. (n.d.). Drug Distribution and Drug Elimination.

59. Al Hanbali, O. A., Khan, H. M. S., Sarfraz, M., Arafat, M., Ijaz, S., & Hameed, A. (2019, June 1). Transdermal patches: Design and current approaches to painless drug delivery. *Acta Pharmaceutica*. Sciendo. https://doi.org/10.2478/acph-2019-0016

60. Huichao, W., Shouying, D., Yang, L., Ying, L., & Di, W. (2014). The application of biomedical polymer material hydroxy propyl methyl cellulose (HPMC) in pharmaceutical preparations, *6*(5), 155–160.

61. Prabhakara, P., Koland, M., Vijaynarayana, K., Nm, H., Shankar, G., & Ahmed, M. G. (2010). Preparation and evaluation of Transdermal patches of Papaverine hydrochloride Preparation and evaluation of Transdermal patches of Papaverine hydrochloride, (January).

62. Ozsoy, Y. (2012). Plasticizers in Transdermal Drug Delivery Systems, (March).

63. Honary, S., & Orafai, H. (2002). The Effect of Different Plasticizer Molecular Weights and Concentrations on Mechanical and Thermomechanical Properties of Free Films, *28*(6), 711–715.

64. Horstmann, M., Sciences, M., Sciences, P., Ag, A. P., Pharmacist, I., Hospital, P. A., … Therapeutics, R. (n.d.). Transdermal patches: history, development and pharmacology 1, 1–64. https://doi.org/10.1111/bph.13059

65. Article, R. (2009). Chemical Penetration Enhancers for Transdermal Drug Delivery Systems, *8*(09921227045), 173–179.

66. Wokovich, A. M., Shen, M., Doub, W. H., Machado, S. G., & Buhse, L. F. (2010). Release Liner Removal Method For Transdermal Drug Delivery Systems (TDDS), *99*(7), 3177–3187. https://doi.org/10.1002/jps

67. Prabhakar, D., Sreekanth, J., & Jayaveera, K. N. (2013). REVIEW ARTICLE TRANSDERMAL DRUG DELIVERY PATCHES : A REVIEW, *3*(4), 213–221.

68. Jeong, W. Y., Kwon, M., Choi, H. E., & Kim, K. S. (2021). Recent advances in transdermal drug delivery systems: a review. *Biomaterials Research*, *25*(1), 1–15. https://doi.org/10.1186/s40824-021-00226-6

69. Alkilani, A. Z., Mccrudden, M. T. C., & Donnelly, R. F. (2015). Transdermal Drug Delivery: Innovative Pharmaceutical Developments Based on Disruption of the Barrier Properties of the stratum corneum, 438–470. https://doi.org/10.3390/pharmaceutics7040438

70. Allena, R. T., Yadav, H. K. S., Sandina, S., & M, S. C. P. (2019). Preparation and evaluation of transdermal patches of metformin hydrochloride using natural polymer for sustained release PREPARATION AND EVALUATION OF TRANSDERMAL PATCHES OF METFORMIN HYDROCHLORIDE USING NATURAL POLYMER FOR SUSTAINED RELEASE, (January 2012).

71. Prajapati, S. T., Patel, C. G., & Patel, C. N. (2011). Formulation and Evaluation of Transdermal Patch of Repaglinide, *2011*. https://doi.org/10.5402/2011/651909

72. Chandra, A., Sharma, P. K., & Irchhiaya, R. (2009). Effect of alcohols and enhancers on permeation enhancement of ketorolac, (March). https://doi.org/10.4103/0973-8398.49173

73. Evans, H. C., & Easthope, S. E. (2010). Transdermal Buprenorphine, *63*(19), 1999–2010.

74. Hashmat, D., Harris, M., Id, S., Ali, F. R., & Siddiqui, F. (2020). Lornoxicam controlled release transdermal gel patch : Design , characterization and optimization using co-solvents as penetration enhancers, 1–23. https://doi.org/10.1371/journal.pone.0228908

75. Shahzad, Y., Louw, R., Gerber, M., & Du Plessis, J. (2015, March 28). Breaching the skin barrier through temperature modulations. *Journal of Controlled Release*. Elsevier B.V. https://doi.org/10.1016/j.jconrel.2015.01.019

76. Ghasemiyeh, P., & Mohammadi-Samani, S. (2020). Potential of nanoparticles as permeation enhancers and targeted delivery options for skin: Advantages and disadvantages. *Drug Design, Development and Therapy*, *14*, 3271–3289. https://doi.org/10.2147/DDDT.S264648

77. Gupta, S., & Kumar, P. (2012). *Drug Delivery Using Nanocarriers: Indian Perspective*. *Proceedings of the National Academy of Sciences India Section B - Biological Sciences* (Vol. 82). https://doi.org/10.1007/s40011-012-0080-7

78. Main mechanisms to control the drug release. (2015). *Strategies to Modify the Drug Release from Pharmaceutical Systems*, 37–62. https://doi.org/10.1016/B978-0-08-100092-2.00004-7

79. Mathematical models of drug release 5. (2015). https://doi.org/10.1016/B978-0-08-100092-2.00005-9

80. Singh, J., & Kaur, H. (2011). Prediction of in vitro Drug Release Mechanisms from Extended Release Matrix Tablets using SSR / R2 Technique, (April). https://doi.org/10.3923/tasr.2011.400.409

81. Kaye, A. D., Baluch, A., & Scott, J. T. (2010). Pain Management in the Elderly Population : A Review, 179–187.

82. Status, C., & Directions, F. (2009). HHS Public Access, *16*(5), 405–416. https://doi.org/10.1037/a0013628.Opioids

83. Freye, E., Levy, J. V., & Braun, D. (2007). Effervescent morphine results in faster relief of breakthrough pain in patients compared to immediate release morphine sulfate tablet. *Pain Practice*, *7*(4), 324–331. https://doi.org/10.1111/j.1533-2500.2007.00157.x

84. Afilalo, M., Etropolski, M. S., Kuperwasser, B., Kelly, K., Okamoto, A., Hove, I. Van, … Haeussler, J. (2010). Efficacy and Safety of Tapentadol Extended Release Compared with Oxycodone Controlled Release for the Management of Moderate to Severe Chronic Pain Related to Osteoarthritis of the Knee. *Clinical Drug Investigation*, *30*(8), 489–505. https://doi.org/10.2165/11533440-000000000-00000

85. Pergolizzi, J. V, Taylor, R., & Raffa, R. B. (2015). The Potential Role of an Extended-Release, Abuse-Deterrent Oxycodone/Acetaminophen Fixed-Dose Combination Product for the Treatment of Acute Pain. *Advances in Therapy*, *32*(6), 485–495. https://doi.org/10.1007/s12325-015-0213-5

86. Motamed, H., & Verki, M. M. (2019). Intravenous lidocaine compared to fentanyl in renal colic painmanagement; a randomized clinical trial. *Archives of Academic Emergency Medicine*, *7*(1). https://doi.org/10.22037/emergency.v5i1.18894

87. Mayer, S., Fowler, A., Brohman, I., Fairbairn, N., Boyd, J., Kerr, T., & McNeil, R. (2020). Motivations to initiate injectable hydromorphone and diacetylmorphine treatment: A qualitative study of patient experiences in Vancouver, Canada. *International Journal of Drug Policy*, *85*, 102930. https://doi.org/https://doi.org/10.1016/j.drugpo.2020.102930

88. Zeng, X., Zhu, J., Li, J., Chen, C., Sang, L., Liu, M., … Liu, H. (2023). Patient Controlled Subcutaneous Analgesia of Hydromorphone Versus Morphine to Treat Moderate and Severe Cancer Pain: A Randomized Double-Blind Controlled Trial. *Journal of Pain and Symptom Management*. https://doi.org/10.1016/j.jpainsymman.2023.09.018

89. Härkänen, L., Hakomäki, H., Huopio, J., Kokki, H., Korhonen, S., Lehtonen, M., … Kokki, M. (2023). Buprenorphine plasma and cerebrospinal fluid concentrations in osteoarthritis patients during low-dose transdermal patch dosing. *European Journal of Clinical Pharmacology*, *79*(12), 1709–1711. https://doi.org/10.1007/s00228-023-03583-4

90. Thaulow, C. H., Helland, A., Kongsgaard, U. E., & Høiseth, G. (2023). Oxycodone, Morphine, and Fentanyl in Patients With Chronic Pain: Proposal of Dose-Specific Concentration Ranges. *Therapeutic Drug Monitoring*, *45*(6). Retrieved from https://journals.lww.com/drug-monitoring/fulltext/2023/12000/oxycodone,_morphine,_and_fentanyl_in_patients_with.9.aspx

91. Delgado, M. A., Ferreira, L. A., Gomes, B. J. D. S., Leite, I. K. O., Gomez, M. V., & Castro-Junior, C. (2023). Preclinical study in a postoperative pain model to investigate the action of ketamine, lidocaine, and ascorbic acid in reversing fentanyl-induced, non-glutamate-dependent hyperalgesia. *Pain Reports*, *8*(2), E1062. https://doi.org/10.1097/PR9.0000000000001062

92. Fons, R. A., Hainsworth, K. R., Michlig, J., Jablonski, M., Czarnecki, M. L., & Weisman, S. J. (n.d.). Perioperative methadone for posterior spinal fusion in adolescents: Results from a double-blind randomized-controlled trial. *Pediatric Anesthesia*, *n/a*(n/a). https://doi.org/https://doi.org/10.1111/pan.14843

93. Bahrami, F., Rossi, R. M., De Nys, K., Joerger, M., Radenkovic, M. C., & Defraeye, T. (2024). Implementing physics-based digital patient twins to tailor the switch of oral morphine to transdermal fentanyl patches based on patient physiology. *European Journal of Pharmaceutical Sciences*, *195*, 106727. https://doi.org/10.1016/j.ejps.2024.106727

94. Osafo, N., Agyare, C., Obiri, D. D., & Antwi, A. O. (n.d.). Mechanism of Action of Nonsteroidal Anti- Inflammatory Drugs, *2*.

95. Budenholzer, B. R., Enhancement, C., Division, N. S., & Health, G. (2002). Are selective COX 2 inhibitors superior to traditional NSAIDs?, *325*(July).

96. Okafo, S. E., Avbunudiogba, J. A., & Ejomafuvwe, E. (2020). Formulation and evaluation of sustained release diclofenac sodium matrix tablets produced using *Brachystegia eurycoma* gum. *Journal of Pharmacy & Bioresources*, *17*(1), 34–43. https://doi.org/10.4314/jpb.v17i1.7

97. Yurtdaş-Kırımlıoğlu, G., Süzen-Demircioğlu, Y., Berkman, M. S., Metinoğlu-Örüm, S., & Altun, E. (2021). Synthesis, spectroscopic, thermal properties, in vitro release, and stability studies of ibuprofen-loaded microspheres cross-linked with hexachlorocyclotriphosphazene/octachlorocyclotetraphosphazene. *Polymer Bulletin*, *78*(11), 6221–6250. https://doi.org/10.1007/s00289-020-03422-x

98. Ossowicz-Rupniewska, P., Bednarczyk, P., Nowak, M., Nowak, A., Duchnik, W., Kucharski, Ł., … Czech, Z. (2022). Evaluation of the Structural Modification of Ibuprofen on the Penetration Release of Ibuprofen from a Drug-in-Adhesive Matrix Type Transdermal Patch. *International Journal of Molecular Sciences*, *23*(14). https://doi.org/10.3390/ijms23147752

99. Taguchi, T., Yamaguchi, S., Terahara, T., Okawa, K., & Inakura, H. (2023). Systemically Acting Diclofenac Sodium Patch for Control of Low Back Pain: A Randomized, Double-Blind, Placebo-Controlled Study in Japan. *Pain and Therapy*, *12*(2), 529–542. https://doi.org/10.1007/s40122-023-00478-1

100. Zadsirjan, S., Toghrolian, A., & Zargar, N. (2023). Analgesic Efficacy of Ketoprofen Transdermal Patch versus Ibuprofen Oral Tablet on Postendodontic Pain in Patients with Irreversible Pulpitis: A Randomized Clinical Trial. *Pain Research and Management*, *2023*, 8549655. https://doi.org/10.1155/2023/8549655

101. Sharma, C. V, Bs, M. B., Mehta, V., & Ffpmrca, F. (2013). Paracetamol : mechanisms and updates, 2–7. https://doi.org/10.1093/bjaceaccp/mkt049

102. Sintov, A. C., Krymberk, I., Gavrilov, V., & Gorodischer, R. (2010). Transdermal delivery of paracetamol for paediatric use: effects of vehicle formulations on the percutaneous penetration. *Journal of Pharmacy and Pharmacology*, *55*(7), 911–919. https://doi.org/10.1211/0022357021486

103. Jalili, M., Noori, A. M., Sedaghat, M., & Safaie, A. (2016). Efficacy of intravenous paracetamol versus intravenous morphine in acute limb trauma. *Trauma Monthly*, *21*(1). https://doi.org/10.5812/traumamon.19649

104. Hadipourzadeh, F., Mousavi, S. M., Heydarpur, A., Sadeghi, A., & Ferasat-Kish, R. (2021). Evaluation of the adding paracetamol to dexmedetomidine in pain management after adult

cardiac surgery. *Anesthesiology and Pain Medicine*, *11*(3). https://doi.org/10.5812/aapm.110274

105. Lubis, A. M., Maruanaya, S., Tantri, A. R., Andribert, L., Pontoh, P., Nastassia, N., … Ifran, S. (n.d.). The Use of Combination Paracetamol and Ibuprofen in Postoperative Pain after Total Knee Arthroplasty, a Randomized Controlled Trial. Retrieved from www.painphysicianjournal.com

106. Wilson, P. B. (n.d.). *GINGER (ZINGIBER OFFICINALE) AS AN ANALGESIC AND ERGOGENIC AID IN SPORT: A SYSTEMIC REVIEW*. Retrieved from www.nsca.com

107. Anand, P., & Bley, K. (2011). Topical capsaicin for pain management: Therapeutic potential and mechanisms of action of the new high-concentration capsaicin 8 patch. *British Journal of Anaesthesia*. Oxford University Press. https://doi.org/10.1093/bja/aer260

108. Ali, B., Al-Wabel, N. A., Shams, S., Ahamad, A., Khan, S. A., & Anwar, F. (2015). Essential oils used in aromatherapy: A systemic review. *Asian Pacific Journal of Tropical Biomedicine*, *5*(8), 601–611. https://doi.org/https://doi.org/10.1016/j.apjtb.2015.05.007

109. Alqareer, A., Alyahya, A., & Andersson, L. (2006). The effect of clove and benzocaine versus placebo as topical anesthetics. *Journal of Dentistry*, *34*(10), 747–750. https://doi.org/10.1016/j.jdent.2006.01.009

110. Lee, W., Loo, C., Bebawy, M., Luk, F., & Mason, R. S. (2013). Curcumin and its Derivatives : Their Application in Neuropharmacology and Neuroscience in the 21 st Century, 338–378.

111. Rao, C. V. (n.d.). Regulation of cox and lox by curcumin, 213–226.

112. Gouthamchandra, K., Sudeep, H. V., Chandrappa, S., Raj, A., Naveen, P., & Shyamaprasad, K. (2021). Efficacy of a standardized turmeric extract comprised of 70% bisdemothoxy-curcumin (Reverc3) against lps-induced inflammation in raw264.7 cells and carrageenan-induced paw edema. *Journal of Inflammation Research*, *14*, 859–868. https://doi.org/10.2147/JIR.S291293

113. Farooqui, A. A. (2016). Effects of Curcumin on Neuroinflammation in Animal Models and in Patients with Alzheimer Disease. In A. A. Farooqui (Ed.), *Therapeutic Potentials of Curcumin for Alzheimer Disease* (pp. 259–296). Cham: Springer International Publishing. https://doi.org/10.1007/978-3-319-15889-1_7

114. Fan, Z., Li, J., Liu, J., Jiao, H., & Liu, B. (2018). Anti-Inflammation and Joint Lubrication Dual Effects of a Novel Hyaluronic Acid/Curcumin Nanomicelle Improve the Efficacy of Rheumatoid Arthritis Therapy. *ACS Applied Materials & Interfaces*, *10*(28), 23595–23604. https://doi.org/10.1021/acsami.8b06236

115. Hestehave, S., Munro, G., Pedersen, T. B., & Abelson, K. S. P. (2017). Antinociceptive effects of voluntarily ingested buprenorphine in the hot-plate test in laboratory rats. *Laboratory Animals, 51*(3), 264–272. https://doi.org/10.1177/0023677216668553

116. Modi, A. D., Parekh, A., & Pancholi, Y. N. (2023). Evaluating pain behaviours: Widely used mechanical and thermal methods in rodents. *Behavioural Brain Research, 446*. https://doi.org/10.1016/j.bbr.2023.114417

Chapter: 3
Statement of the Problem

The research gaps in the field of Transdermal Drug Delivery Systems (TDDS) identified through the extended literature survey are summarized below.

- The epidural solution of clonidine is available for cancer pain [1], transdermal patches of clonidine are available in different dosages, which are intended to be administered for seven days to treat neuropathic pain [2], but there is no availability of the extended-release transdermal patches of clonidine to date for treating several pains mentioned earlier. The demand for such transdermal patches should increase in the upcoming years because patients suffering from cancer and neuropathic pain often face numerous challenges and disruptions in their daily lives due to their illness and treatment. Extended-release transdermal patches can help those patients maintain a sense of normalcy by allowing them to engage in activities and social interactions without the constant interruption of pain or the need for frequent medication doses.

- Transdermal patches of diclofenac are already available in the market. Both diclofenac and etoricoxib are members of the Non-Steroidal Anti-Inflammatory Drug (NSAID) family and are used as pain and inflammation relievers. However, the transdermal formulations of etoricoxib have not been developed yet. The non-selective COX inhibitor diclofenac raises the risk of renal damage, cardiovascular events, and gastrointestinal side effects. [3, 4]. Etoricoxib is a selective COX-2 inhibitor and may have a lower risk of causing harm compared to traditional NSAIDs like diclofenac [3]. Therefore, the transdermal patches of etoricoxib must be made highly desirable for patients requiring long-term pain management. The primary cause for the lack of such formulation might be the very poor aqueous solubility of etoricoxib [logarithm of the partition coefficient (log P) = 2.79, aqueous solubility = 0.01 to 0.5 mg/mL at 25°C] [4].

- The transdermal paracetamol patches are not as commonly available in the market as other formulations like oral tablets or liquid suspensions. The exact mechanism of action is not fully understood to date but it is believed to inhibit the production of prostaglandins in the brain [5, 6]. This is why, Paracetamol is often considered safer than NSAIDs for people with gastrointestinal issues or cardiovascular risks. The development of transdermal administration techniques for this drug is still under investigation [9]. The interest of patients, especially children and infants who suffer stomach irritation or ulcers associated with oral paracetamol must be developed in its transdermal option in future. The main reason behind the unavailability of such formulations could be high doses and low aqueous solubility as well [logarithm of the partition coefficient (log P) = 0.48 to 0.52, aqueous solubility = 14.5 mg/mL at 25°C] [7].

The skin permeation, release duration, and solubility in the body fluid of these drugs could be enhanced with the help of nanotechnology [8–12]. Therefore, an attempt could be made to deliver these drugs as "nanomedicine" i.e. drug-loaded nanoparticles from the transdermal patches through skin layers.

Based on the above-mentioned research gaps, the objectives of the present thesis are given as under.

☞ **Objectives:**

1. To entrap the drugs [Clonidine Hydrochloride (CH), Etoricoxib (EB), and Paracetamol (PM)] in two different nanocarriers: silica nanoparticles (SNPs) and sodium montmorillonite (Na-MMT) nanoclay.
2. To characterize the bare nanoparticles and nanomedicines (i.e., drug-loaded nanocarriers) by Brunauer-Emmett-Teller (BET)-Barrett-Joyner-Halenda (BJH)

analysis, Dynamic Light Scattering (DLS), Scanning Electron Microscopy (SEM), High-resolution Transmission Electron Microscopy (HR-TEM), X-Ray Diffraction (XRD).

3. To study *in vitro* drug release patterns from the nanomedicines (i.e., the drug-loaded SNPs and drug/Na-MMT composites) at two different pH (5.5 and 7.4) of the release medium.
4. To fabricate the matrix-type transdermal patches incorporating the nanomedicines mentioned above.
5. To characterize the bare and nanomedicine-loaded transdermal patches by Fourier Transform Infrared Spectroscopy (FTIR) and scanning Electron Microscopy (SEM).
6. To study skin irritation caused by the materials of the transdermal patches on mice and rats.
7. To perform *ex vivo* skin permeation study of the nanomedicines released from the transdermal patches.
8. To determine the *ex vivo* drug release kinetics and the release mechanism.
9. To analyze the performance of the patches via two different *in vivo* analgesic activities (Hot-Plate and Tail-Flick methods) on mice and rats.

Reference:

1. Roelants, F., Lavand'homme, P. M., & Mercier-Fuzier, V. (2005). *Epidural Administration of Neostigmine and Clonidine to Induce Labor Analgesia Evaluation of Efficacy and Local Anesthetic-sparing Effect*. *Anesthesiology* (Vol. 102). Retrieved from www.anesthesiology.org.
2. Behrman, A., & Goertemoeller, S. (2007). A Sticky Situation: Toxicity of Clonidine and Fentanyl Transdermal Patches in Pediatrics. *Journal of Emergency Nursing*, *33*(3), 290–293. https://doi.org/10.1016/j.jen.2007.02.004
3. D Martina, S., Vesta, K. S., & Ripley, T. L. (2005, May). Etoricoxib: A highly selective COX-2 inhibitor. *Annals of Pharmacotherapy*. https://doi.org/10.1345/aph.1E543

4. Alzweiri, M., Sallam, M., Al-Zyoud, W., & Aiedeh, K. (2018). Stability study of etoricoxib a selective cyclooxygenase-2 inhibitor by a new single and rapid reversed phase HPLC method. *Symmetry*, *10*(7). https://doi.org/10.3390/sym10070288

5. Saliba, S. W., Marcotegui, A. R., Fortwängler, E., Ditrich, J., Perazzo, J. C., Muñoz, E., … Fiebich, B. L. (2017). AM404, paracetamol metabolite, prevents prostaglandin synthesis in activated microglia by inhibiting COX activity. *Journal of Neuroinflammation*, *14*(1). https://doi.org/10.1186/s12974-017-1014-3

6. Greco, A., Antonietta Ajmone-Cat, M., Nicolini, A., Sciulli, M. G., & Minghetti, L. (2003). *Paracetamol Effectively Reduces Prostaglandin E 2 Synthesis in Brain Macrophages by Inhibiting Enzymatic Activity of Cyclooxygenase But Not Phospholipase and Prostaglandin E Synthase*.

7. Jyoti Sen, D., & Patel, J. G. (2016). Logarithmic Partition Coefficient Comparison Study and Molecular Weight of Synthesized Prodrugs of Ibuprofen+Paracetamol, Diclofenac Sodium+Paracetamol and Ibuprofen+Diclofenac Sodium. *American Journal of Advanced Drug Delivery*, *04*(05), 1–5. https://doi.org/10.21767/2321-547x.1000003

8. Agrawal, Y., & Patel, V. (2011). Nanosuspension: An approach to enhance solubility of drugs. *Journal of Advanced Pharmaceutical Technology & Research*, *2*(2), 81. https://doi.org/10.4103/2231-4040.82950

9. Sareen, S., Joseph, L., & Mathew, G. (2012). Improvement in solubility of poor water-soluble drugs by solid dispersion. *International Journal of Pharmaceutical Investigation*, *2*(1), 12. https://doi.org/10.4103/2230-973x.96921

10. Naik, D. R., & Raval, J. P. (2016). Amorphous polymeric binary blend pH-responsive nanoparticles for dissolution enhancement of antiviral drug. *Journal of Saudi Chemical Society*, *20*, S168–S177. https://doi.org/10.1016/j.jscs.2012.09.020

11. Gupta, S., & Kumar, P. (2012). *Drug Delivery Using Nanocarriers: Indian Perspective*. *Proceedings of the National Academy of Sciences India Section B - Biological Sciences* (Vol. 82). https://doi.org/10.1007/s40011-012-0080-7

12. Ghasemiyeh, P., & Mohammadi-Samani, S. (2020). Potential of nanoparticles as permeation enhancers and targeted delivery options for skin: Advantages and disadvantages. *Drug Design, Development and Therapy*, *14*, 3271–3289. https://doi.org/10.2147/DDDT.S264648

Chapter: 4
Materials and Methods

4.1. Materials: 4'-Hydroxyacetanilide (i.e., paracetamol, PM), etoricoxib (EB), montmorillonite K 10 (MMT K 10), phosphate buffer solution (PBS, pH 7.4), sodium acetate buffer solution (pH 5.5), and tetraethylorthosilicate (TEOS) were purchased from Sigma-Aldrich. Clonidine hydrochloride (CH) was purchased from Tokyo Chemical Industry India Pvt. Ltd. Polyvinyl alcohol (PVA) was purchased from Himedialabs. Di-n-butyl phthalate was purchased from Ranbaxy Laboratories Limited. Ethylcellulose (EC) and polyvinylpyrrolidone (PVP) were purchased from Loba Chemie Pvt. Ltd. All reagents were of A.R. grade.

4.2. Methods:

The following block diagram may portray the overall methodologies covered in the thesis:

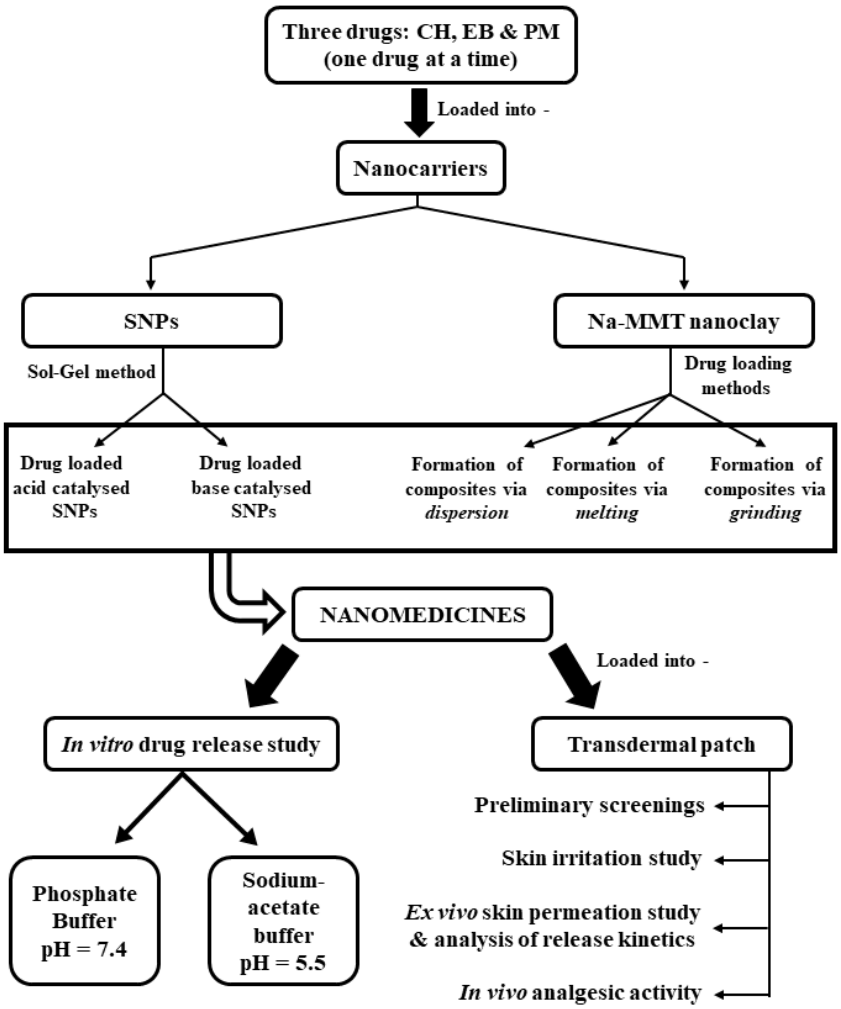

4.2.1. Synthesis of SNPs: SNPs were synthesized by acid (i.e., HCl) and base (i.e., NH_4OH) catalysed sol-gel method at room temperature (37℃) [1, 2]. This method involves a series of hydrolysis of the silica precursor, tetraethylorthosilicate (TEOS), followed by polycondensation of the hydrolysed products. Deionised water, ethanol, and TEOS were taken in a volume ratio of 1:2:1. The mixture of a catalyst (0.1 M HCl during acid catalysis and 0.1 M NH_4OH during base catalysis), deionized water, and ethanol was magnetically stirred at 350 rpm followed by the dropwise addition of TEOS for 1 h. Then the resulting colloidal solution was dried at 40℃. After the gel formation, it was calcined at 550℃ for 3 h and ground to white silica powder form by mortar and pestle. In the rest of the thesis, bare acid and base-catalysed SNPs have been designated as P1 and P2.

4.2.2. Drug Loading Procedure into SNPs: 5 mg of SNPs were added to 5 mL of ethanolic solution of the drug (in the case of EB and PM) and 5 mL of aqueous solution of CH. After that, the suspension was gently stirred for 24 h to achieve equilibrium. The resulting solution was centrifuged at 7000 rpm for 30 minutes after loading, and the quantity of drug that remained in the supernatant phase was measured by a UV-visible spectrophotometer at its maximum wavelength (λ_{max}). In the rest of the thesis, drug-loaded acid and base-catalysed SNPs have been designated as R1 and R2 for CH; S1 and S2 for EB; T1 and T2 for PM drug respectively. Percentage drug loading capacity and loading efficiency were determined using the formula:

$$\%\ \textbf{Loading Capacity} = \frac{\textbf{Drug loaded in SNPs}}{\textbf{Weight of SNPs}} \times \mathbf{100} \qquad \ldots (\boldsymbol{i})$$

$$\%\ \textbf{Loading Efficieny} = \frac{\textbf{Drug Added Initially} - \textbf{Drug Present in the Supernatant}}{\textbf{Drug Added Initially}} \times \mathbf{100} \qquad \ldots \textbf{\textit{(ii)}}$$

4.2.3. Modification of MMT K 10: MMT K 10 was treated with NaCl to enhance the cation exchange capacity (CEC), and the resulting Na-MMT dispersion was washed with deionised

water via centrifugation until the $AgNO_3$ test revealed that all chloride had been eliminated. Na-MMT was used to prepare the drug/Na-MMT composites via three different methods: dispersion, melting, and grinding. In the rest of the thesis, the composites obtained from the dispersion, melting, and grinding methods have been designated as M1, M2, and M3 for CH; L1, L2, and L3 for EB; G1, G2, and G3 for PM drug respectively.

4.2.3.1 Dispersion Method: Na-MMT dispersion was prepared by swirling 1 g of Na-MMT powder into 100 mL of deionised water for 24 h. The drug solution (0.1% w/v) was added dropwise to the MMT dispersion within one hour at 25℃. Different pH values (1 to 12) of the resulting mixture were maintained to find the optimal pH for maximum drug loading. To eliminate the excess drug from the clay surface, the mixture was stirred for ~1 hr, centrifuged (5000 rpm, 30 mins), and washed 4-5 times with double-distilled water. Next, it was dried in the air and finely ground to powder using a mortar and pestle [3].

4.2.3.2. Melting Method: The mixture of drug and Na-MMT (1:4 w/w) was heated at the rate of 2℃/min to the melting point of the drug (CH=130℃, EB=128℃, and PM=169℃) for 4 h After that, the residue was cooled to room temperature, cleaned 4-5 times with deionised water, and dried at room temperature [4].

4.2.3.3. Grinding Method: The mixture of drug and Na-MMT (1:4 w/w) was finely ground using mortar and pestle, washed 4-5 times with de-ionized water, and dried in a desiccator [4].

4.2.4. Determination of Percentage Loading Capacity and Percentage Loading Efficiency of the three drugs in Na-MMT: Percentage drug loading capacity (eq. iii) and loading efficiency (eq. iv) for formulations M1/L1/G1 were determined from the supernatant collected after centrifugation using a UV-visible spectrophotometer. In the case of M2/L2/G2 and M3/L3/G3 formulations, percentage drug loading capacity (eq. iii) and loading efficiency (eq. v) were determined by complete extraction of the drug from clay particles. 10 mg of each formulation were immersed in 10 mL of phosphate buffer and then the whole solution was

centrifuged at 12000 rpm for 30 mins. After that, the clay particles were washed 2-3 times with phosphate buffer to extract any adhered drug. The quantity of drug present in the supernatant was analysed by UV-visible spectrophotometer.

$$\% \textbf{ Loading Capacity} = \frac{\textbf{Amount of drug present in nanoclay}}{\textbf{Amount of nanoclay}} \times \mathbf{100} \quad \ldots (\boldsymbol{iii})$$

$$\% \textbf{ Loading Efficieny} = \frac{\textbf{Drug Added Initially} - \textbf{Drug Present in the Supernatant}}{\textbf{Drug Added Initially}} \times \mathbf{100} \quad \boldsymbol{\ldots (iv)}$$

$$\% \textbf{ Loading Efficiency} = \frac{\textbf{Amount of drug released from nanoclay}}{\textbf{Amount of drug initially taken to prapare the composite}} \times \mathbf{100} \quad \ldots (\boldsymbol{v})$$

4.2.5. Preparation of Transdermal Patch: The transdermal patches of each drug *(three sets of transdermal formulations: Set-I for CH, Set-II for EB and Set-III for PM; each set contained six formulations: one was made of free drug, two formulations were comprised of drug-loaded SNPs and remaining three formulations contained drug/Na-MMT composites)* were prepared by using the polymers EC, PVA and PVP, as mentioned in Table 4.1 [5].

- First, a cylindrical glass mould was taken whose both sides were opened. One side of the mould was wrapped with aluminium foil.
- 5 mL of 4% (w/v) aqueous solution of polyvinyl alcohol (PVA) was poured on the foil, and then the mould with PVA solution was kept for drying at 50℃ for 6 h to obtain the backing membrane of the patch.
- Next, the matrix was prepared by mixing EC-PVP (weight ratio of 2:1) and the nanomedicines *(i.e., drug-loaded SNPs or drug/Na-MMT composites in which the dose of CH, EB and PM was 2mg, 60mg, and 100mg, respectively)* in 10 mL ethanol. 10% (v/v) Di-n-butyl-phthalate was utilized as a plasticiser.

- Eventually, the uniform dispersion was cast on the PVA backing membrane, and the resulting solution in the mould was allowed to dry again at 50℃ for 6 h.
- The dried patch was taken out from the mould (Fig 4.1) and stored in a desiccator for further studies.
- A few patches were prepared without nanocarrier keeping the other constituents and amount the same.

Table 4.1. Materials used to prepare different transdermal formulations

Sets	Formulations	Nanomedicines	Amount and Role of The Polymers
I	A1	Free CH present	1. Backing Membrane: 4% aqueous solution of PVA 2. Matrix: EC and PVP in a weight ratio of 2:1 3. Plasticizer: 10% (v/v) Di-n-butyl phthalate
	A2	R1	
	A3	R2	
	A4	M1	
	A5	M2	
	A6	M3	
II	B1	Free EB present	
	B2	S1	
	B3	S2	
	B4	L1	
	B5	L2	
	B6	L3	
III	C1	Free PM present	
	C2	T1	
	C3	T2	
	C4	G1	
	C5	G2	
	C6	G3	

Fig 4.1. Freshly prepared transdermal patches

4.2.6. Preliminary Screening of Transdermal Patches:

(a) Percentage Moisture Content: Each patch was weighed before being stored in a desiccator comprising activated silica for 72 h at an ambient temperature. The patches were weighed again until a steady weight was attained. The following formula (eq. vi) was used to evaluate the % moisture content.

$$\%\ \textbf{Moisture Content} = \frac{\textbf{Initial Weight} - \textbf{Final Weight}}{\textbf{Final Weight}} \times 100 \qquad \ldots (vi)$$

(b) Percentage Moisture Uptake: Initially weighed patches were exposed to 84% RH using a saturated KCl solution in a desiccator at an ambient temperature for 24 h. The patches were weighed repetitively until a constant weight was observed. Percentage-moisture uptake was evaluated using the following formula (eq. vii):

$$\%\ \textbf{Moisture Uptake} = \frac{\textbf{Final Weight} - \textbf{Initial Weight}}{\textbf{Initial Weight}} \times 100 \qquad \ldots (vii)$$

(c) Swelling Index: A strip (1 cm ×1 cm) was cut from the original patches and weighed. Next, they were immersed in PBS of pH 7.4 at 0.5, 1, 2, 3, 4, 5, and 24 h. The soaked strips were

taken out from PBS at a predetermined time, blotted to eliminate the excess solvent, and weighed immediately. The following formula (eq. viii) determined the value of the swelling index at different time intervals.

$$\% \textbf{ Swelling Index} = \frac{\textbf{Final Weight} - \textbf{Initial Weight}}{\textbf{Initial Weight}} \times \textbf{100} \qquad \ldots (\boldsymbol{viii})$$

(d) Surface pH: A strip of each patch was placed in 10 mL distilled water for 4 h. Then the pH was measured by putting the electrode on the surface of the swollen patch.

(e) Folding Endurance: (1 cm ×1 cm) of the patch was cut equally, then folded repetitively until it broke. The number of folds the strips could withstand in the same position before breaking was used to calculate the folding endurance values.

(f) Weight Uniformity: Each patch was dried at 60°C for 3 h. After that, different parts were cut out from the dried patches and weighed precisely. The average weight and the standard deviation values were obtained from the individual data.

(g) Thickness of the Patch: The width (i.e., thickness) of each patch was measured at four different locations of these patches using a vernier calliper. Similarly, the average weight and the standard deviation values were determined from the four readings.

(h) Percentage Elongation: First, the initial length of a whole patch was measured. Next, the patch was stretched until the crack was initiated and the final length was noted down after increasing its size. The following formula (eq. ix) helped to evaluate the percentage elongation.

$$\% \textbf{ Elongation} = \frac{\textbf{Increase in Length of Patch}}{\textbf{Initial Length of Patch}} \times \textbf{100} \qquad \boldsymbol{\ldots (ix)}$$

(i) Development of the Spectrophotometric Method: 5 mg of each drug was dissolved in 50 mL buffer solutions of different pH (5.5 and 7.4) individually to prepare six stock solutions. Further, each stock solution was diluted by combining 0.5 mL stock solution with 9.5 mL of respective buffer solution. The UV-Spectrophotometric analysis was repeated thrice and the λ_{max} values obtained were stated as mean ± S.D. The λ_{max} values of CH at pH 5.5 and 7.4 were

observed at 270.09 ± 0.015 nm, and 271.11 ± 0.008 nm respectively (Fig 4.2). At the same two pH, the λ_{max} values of EB were measured to be 233.57 ± 0.018 nm and 233.84 ± 0.014 nm respectively (Fig 4.3) whereas the λ_{max} values were found to be 242.97 ± 0.011 nm, and 243.09 ± 0.014 nm respectively for PM (Fig 4.4). Six sets of standard solutions for each drug at two pH were prepared via the same dilution technique to produce the calibration curve.

(j) Drug Content: Another (1 cm ×1 cm) strip from each patch was positioned in a beaker containing 100 mL PBS of pH 7.4 and vigorously stirred for 24 h. The solution was filtered, and the quantity of the drug was measured by a UV-visible spectrophotometer using λ_{max} values of the drugs.

4.2.7. Characterization: BET data were obtained by Autosorb iQ2 gas sorption instrument (Quantachrome Instruments, USA). FTIR spectra were taken using an FTIR spectroscope (Model: Prestige 22, Shimadzu). XRD patterns were collected using PAN analytical X'pert Pro diffractometer which was equipped with Cu-Kα target (λ=1.5418Å) and a nickel filter. Particle sizes were determined in dispersion employing Dynamic Light Scattering, DLS (Malvern Panalytical Ltd.). Scanning Electron Microscope (SEM), images were obtained by ZEISS EVO 18 special edition model. High-Resolution Transmission Electron Microscope (HR-TEM) images were produced by JEM-2100 Plus (200 kV). Zeta potential was measured by zetasizer nano ZS (Malvern Panalytical Ltd.).

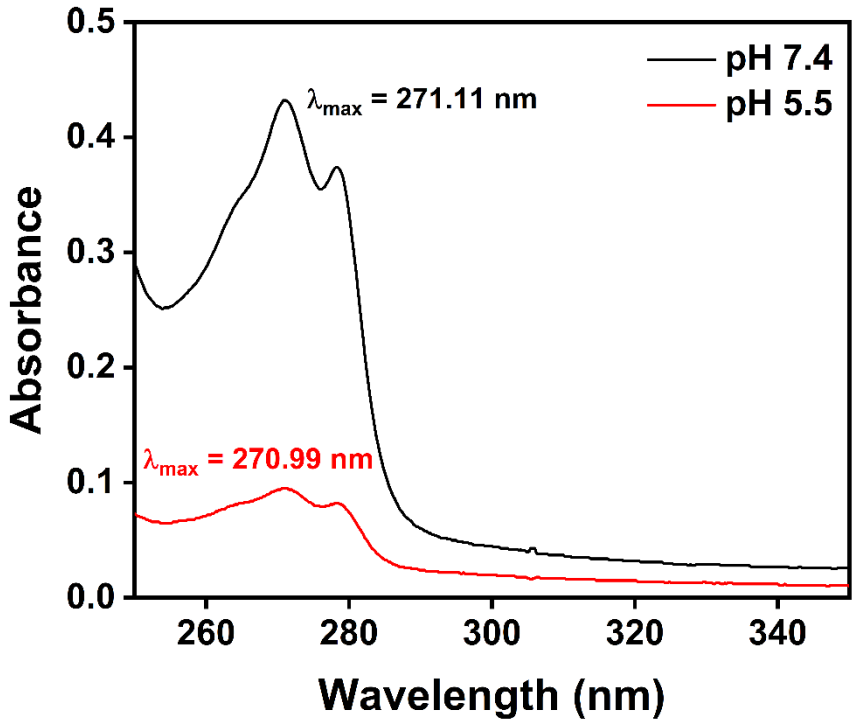

Fig 4.2. Uv-vis spectrum of clonidine hydrochloride (CH)

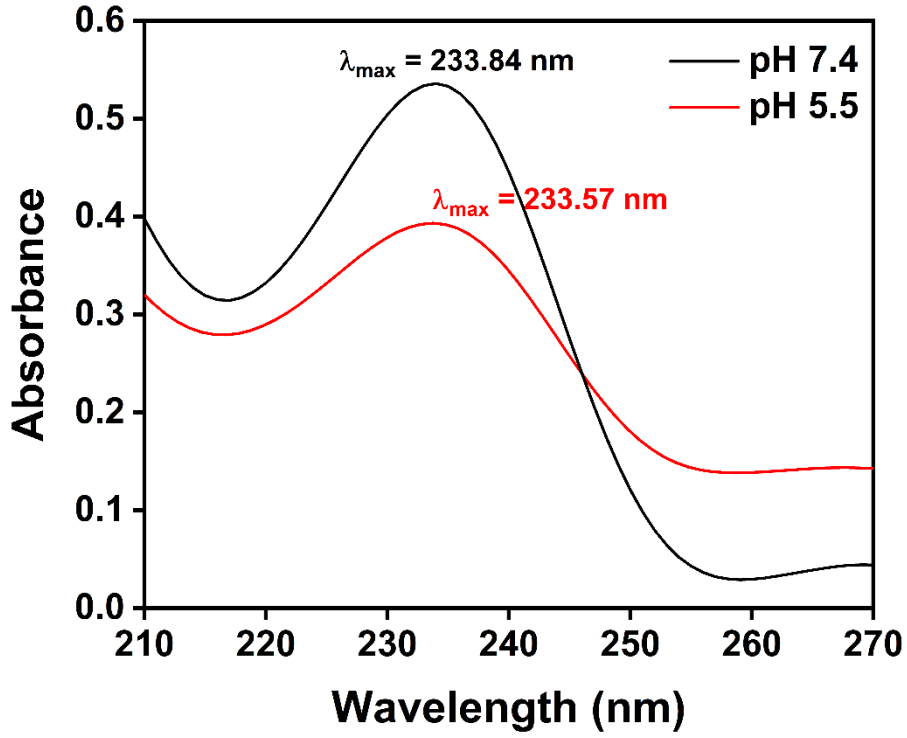

Fig 4.3. Uv-vis spectrum of etoricoxib (EB)

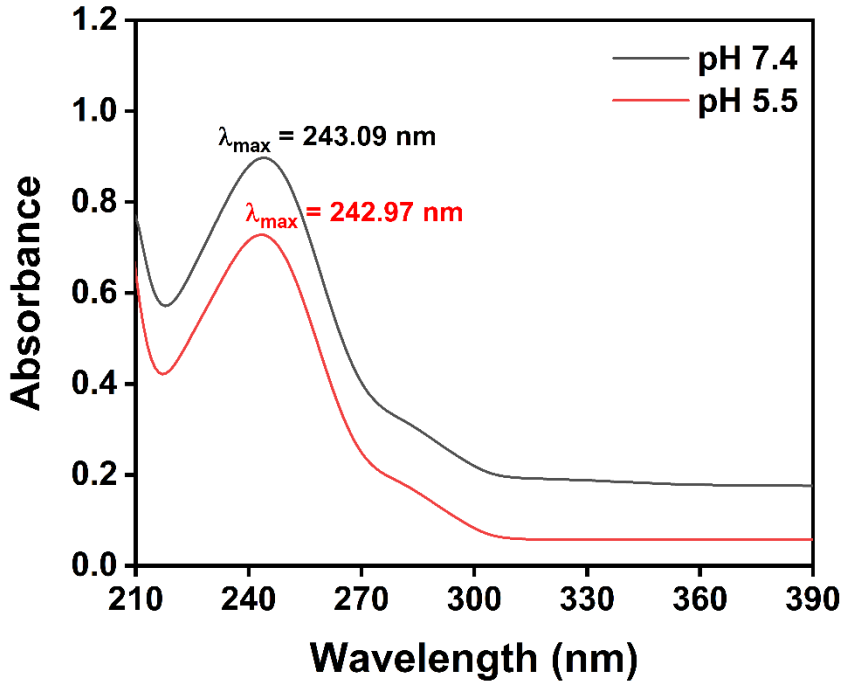

Fig 4.4. Uv-vis spectrum of paracetamol (PM)

4.2.8. *In vitro* Drug Release Study of the Drugs from Nanocarriers: 10 mg of each drug-loaded nanocarrier was exposed to phosphate buffer, PBS having pH 7.4 and sodium acetate buffer having pH 5.5. The dissolutions were performed in 500 mL of dissolution media with the help of dialysis membrane-60 (Avg. flat width-25.27 nm, Avg. diameter-15.9 nm, capacity approx.-1.99 mL/cm). At various times, 1 mL of the sample was removed, and the total volume was maintained by adding the same quantity of solvent. The amount of released drug in each sample was evaluated by a UV-visible spectrophotometer. The graphs of the percentage cumulative release against time were plotted [1].

4.2.9. Skin Irritation Test: The test was conducted on six groups U, V, W, X, Y, and Z of mice/rats (three in each group) weighing 20-25 gm for mice and 100-150 gm for rats. The transdermal patches having an area of (1 cm × 1 cm) were applied to the back of mice/rats. First, a portion of the back was shaved and cleaned with rectified spirit. In the next step, the patch adhered to that portion with the help of adhesive tape. Group U, V, W, X, Y, and Z were given transdermal formulations of free drug, drug-loaded acid-catalysed SNPs, drug-loaded base-catalysed SNPs, drug/Na-MMT composite prepared via dispersion method, drug/Na-MMT composite prepared via the melting method, and drug/Na-MMT composite prepared via grinding method respectively. Each patch was removed after 48 h, and the skin was inspected for edema (papules and wheals) and erythema (skin flushing and redness) [6].

4.2.10. *Ex vivo* Skin Permeation Study: A patch of an area (1 cm ×1 cm) was located on the stratum corneum side of the human skin soaked in PBS of pH 7.4. Subsequently, the dermis side of the skin and the patch were placed into the Franz diffusion cell such that they faced the receptor compartment, which had 90 mL of PBS at room temperature. A magnetic bead was used to constantly swirl the fluid in the receptor section at 30 to 40 rpm. To maintain overall volume, 1 mL of sample was taken from the receptor at various times and mixed with the same volume of PBS. A UV-visible spectrophotometer was eventually used to measure the quantity of drugs that permeated through the skin [9]. The graphs regarding the cumulative amount of permeated drug per square centimetre of the skin against the time were represented for eighteen transdermal formulations.

4.2.11. *Ex vivo* Drug Release Kinetic Study: The drug release kinetics was employed to identify the best-fit drug release model and the drug release mechanism. The release data obtained from the *ex vivo* skin permeation study was analysed by four kinetic models [1, 7].

- **Zero-order** equation can be represented as $A_t = A_0 + K_0t$; where, A_t = the amount of drug dissolved in release medium in time t, A_0 = initial amount of drug present in

solution (generally zero), and K_0 = zero order rate constant. The data were plotted as a percentage of cumulative drug release vs. time.

- ☞ The equation for the **first-order** model is $\log A_t = \log A_0 - k_1 t / 2.303$; where, A_t, A_0, and t bear the same meaning mentioned before. The release data were plotted as a log of the percentage of cumulative drug remaining vs. time.
- ☞ The next model is the **Higuchi equation** ($Q_t = K_H.\sqrt{t}$) in which Q_t indicates the amount of drug released in time t. Here, the data were plotted as percentage cumulative drug release vs. square root of time.
- ☞ The last model is the **Korsmeyer-Peppas equation** which is expressed as $W_t / W_\infty = K_w.t^n$ where, W_t / W_∞ = A fraction of drug released at time t, K_w = the rate constant, and n = release exponent. The data were plotted as a log of percentage cumulative drug release vs log time in which "n" acts as the slope. The value of "n" was utilized to illustrate the release mechanism; $n \leq 0.45$ implies fickian diffusion, $0.45 < n < 0.89$ corresponds to non-fickian (anomalous) diffusion, $n = 0.89$ indicates case II transport and $n > 0.89$ suggests super case II transport.

4.2.12. *In vivo* Analgesic Activity via Hot Plate Method: The analgesic activity of each drug was investigated using a hot plate whose temperature was maintained at 50±0.5℃. The mice/rats were divided into seven groups H0, H1, H2, H3, H4, H5, and H6 (Table 4.2); each group contained three mice/rats. Group H0 served as the control group whereas Group H1, H2, H3, H4, H5, and H6 received transdermal patches of free drug, drug-loaded acid-catalysed SNPs, drug-loaded base-catalysed SNPs, drug/Na-MMT composite prepared via the dispersion method, drug/Na-MMT composite prepared via the melting method, and drug/Na-MMT composite prepared via the grinding method respectively 30 mins before the experiment. The time gap between the placement of mice/rats on the hot plate and the occurrence of leaping

from the surface and the licking of paws was recorded as "latency" in seconds at different time intervals [8] up to 16 days for CH patches, 7 days for EB patches, and 2 days for PM patches.

Table 4.2. *In vivo* analgesic study

Groups of Mice/Rats (each contained three animals)	**Constituents of Transdermal Patches applied on the skin**
H0	Only saline was served, and no patch was applied
H1	Free drug
H2	Drug-loaded acid-catalysed SNPs
H3	Drug-loaded base-catalysed SNPs
H4	Drug/Na-MMT composite prepared via the dispersion method
H5	Drug/Na-MMT composite prepared via the melting method
H6	Drug/Na-MMT composite prepared via the grinding method

4.2.13. *In vivo* Analgesic Activity via Tail Flick Method: The tail (5 cm from the end) of each mouse/rat of the same group mentioned above (Table 4.2; H0 to H6) was submerged in warm water that was kept constant at 50±0.5°C. The response time in seconds (the time taken by mice/rats to flick their tail to get rid of the pain) was measured at different time intervals after the application of transdermal patches [8].

The production of pain-relief transdermal patches infused with nanomedicine utilizing the methodologies mentioned above could be a promising modality for expediting pain-relief procedures, particularly in the case of children, infants, and unconscious patients.

Reference:

1. Chakraborty, S., Biswas, S., Sa, B., Das, S., & Dey, R. (2014). In vitro & in vivo correlation of release behavior of andrographolide from silica and PEG assisted silica gel matrix. *Colloids and Surfaces A: Physicochemical and Engineering Aspects*, *455*(1), 111–121. https://doi.org/10.1016/j.colsurfa.2014.04.046

2. Selvarajan, V., Obuobi, S., & Ee, P. L. R. (2020, July 15). Silica Nanoparticles—A Versatile Tool for the Treatment of Bacterial Infections. *Frontiers in Chemistry*. Frontiers Media S.A. https://doi.org/10.3389/fchem.2020.00602

3. Datta, M. (2013). *In vitro sustained delivery of atenolol by montmorillonite Section B-Research Paper Eur*. *Chem. Bull*.

4. Madurai, S. L., Joseph, S. W., Mandal, A. B., Tsibouklis, J., & Reddy, B. S. R. (2011). Intestine-Specific, Oral Delivery of Captopril/Montmorillonite: Formulation and Release Kinetics. *Nanoscale Research Letters*, *6*(1), 1–8. https://doi.org/10.1007/s11671-010-9749-0

5. de Kumar, P., Mallick, S., Mukherjee, B., Sengupta, S., Pattnaik, S., & Chakraborty, S. (2011). Optimization of in-vitro permeation pattern of ketorolac tromethamine transdermal patches. *Iranian Journal of Pharmaceutical Research*, *10*(2), 193–201. https://doi.org/10.22037/ijpr.2011.927

6. Banerjee, S., Chattopadhyay, P., Ghosh, A., Pathak, M. P., Singh, S., & Veer, V. (2013). Acute dermal irritation, sensitization, and acute toxicity studies of a transdermal patch for prophylaxis against ({+/-}) anatoxin-a poisoning. *International journal of toxicology*, *32*(4), 308–313. https://doi.org/10.1177/1091581813489996

7. Jha, J., Chakraborty, S., Chaudhuri, M. G., & Dey, R. (2016). In Vitro Release Kinetics and Transferrin Saturation Study of Intravenous Iron Sucrose Entrapped in Poly(ethylene glycol)-Assisted Silica Xerogel. *Applied Biochemistry and Biotechnology*, *178*(7), 1351–1362. https://doi.org/10.1007/s12010-015-1951-1

8. Fan, S.-H., Ali, N. A., & Basri, D. F. (2014). Evaluation of Analgesic Activity of the Methanol Extract from the Galls of *Quercus infectoria* (Olivier) in Rats. *Evidence-Based Complementary and Alternative Medicine*, *2014*, 976764. https://doi.org/10.1155/2014/976764

Chapter: 5
Results & Discussion

Chapter: 5A

Drug Delivery by Silica Nanoparticles (SNPs)-Based Transdermal Patch

5A.1. Introduction:

Silica nanoparticles (SNPs) were synthesised by the sol-gel method in which HCl and NH_4OH were used as catalysts. The prepared acid and base-catalyzed bare SNPs were designated as P1 and P2 respectively in the rest of the thesis. Clonidine hydrochloride (CH), etoricoxib (EB), and paracetamol (PM) – three analgesic drugs were utilised to produce the corresponding nanomedicines i.e. drug-loaded nanoparticles using the nanocarriers mentioned above (P1 and P2). CH-loaded P1 and P2 formulations have been designated as R1 and R2 respectively, EB-loaded P1 and P2 formulations have been designated as S1 and S2 respectively, and PM-loaded P1 and P2 formulations have been designated as T1 and T2 respectively. The transdermal patches of these nanomedicines were prepared via the solvent-casting method. A few patches were prepared without nanocarrier keeping the other constituents and amount the same. Free CH drug, R1 and R2 loaded patches have been represented as A1, A2 and A3 respectively. Free EB drug, S1 and S2 loaded patches have been represented as B1, B2 and B3 respectively. Free PM drug, T1 and T2 loaded patches have been represented as C1, C2 and C3 respectively. The formulations were characterized by several characterisation techniques such as BET, DLS, FTIR, SEM, HR-TEM, XRD, and ZETA POTENTIAL. Freshly prepared nanomedicines were subjected to *in vitro* drug release study at two different pHs (5.5 and 7.4) to assess the release behaviour under these conditions. Moreover, the skin irritation and ex vivo skin permeation studies were conducted with the patches followed by *ex vivo* drug release kinetics analysis to establish the suitable kinetic model and the release mechanism associated with both the burst and sustained release. The efficacy of the patches was also examined by *in vivo* analgesic activities via the hot-plate and tail-flick methods. The results obtained from the above experiments have been discussed below.

5A.2. Results and Discussion:

5A.2.1. Analysis of DLS Data of SNPs:

Dynamic Light Scattering (DLS) is a powerful technique for characterizing the size distribution of particles in a solution, particularly for nanoparticles and macromolecules. It is widely used in various fields including pharmaceuticals, colloidal science, and biotechnology for quality control, research, and development.

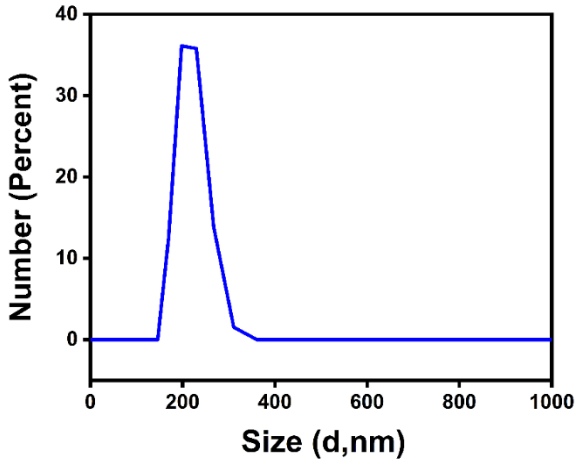

Fig 5A.1. Particle size distribution curve of acid-catalyzed SNPs, P1

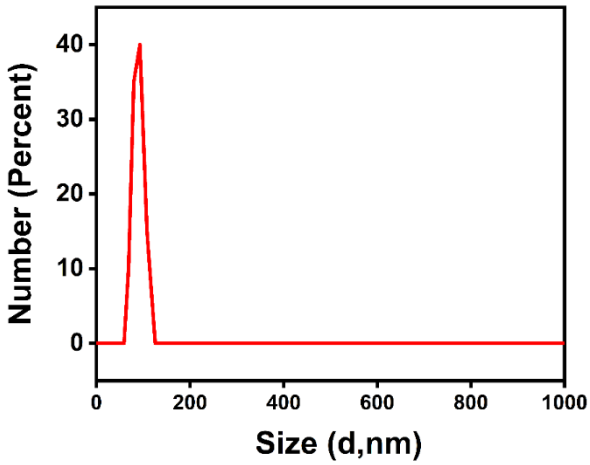

Fig 5A.2. Particle size distribution curve of base-catalyzed SNPs, P2

The single peak obtained from dynamic light scattering (DLS) suggested that the particle size distribution was uniform. The mean particle diameter for P1 and P2 formulations was c.a. 200 nm and 93 nm, respectively (Fig 5A.1-5A.2).

5A.2.2. Analysis of SEM Images of SNPs:

SEM is a powerful imaging technique used to visualize the surface morphology of materials at high magnification.

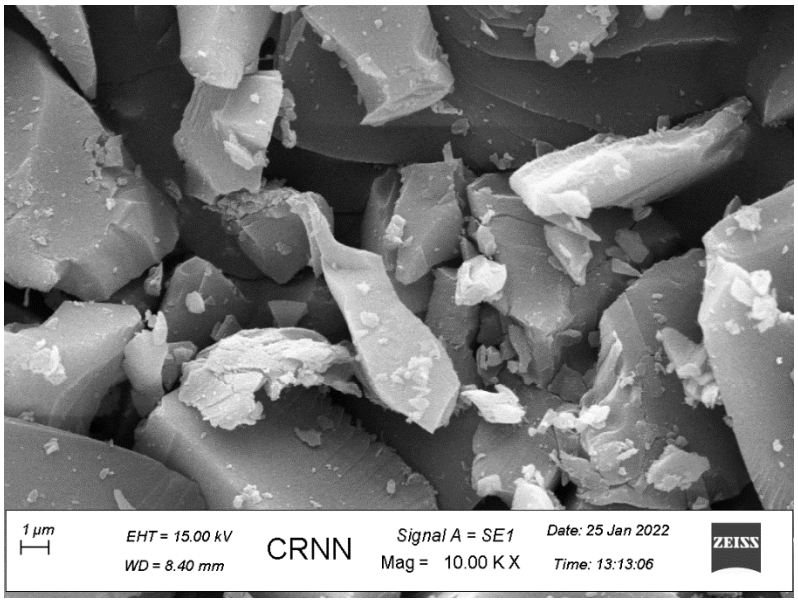

Fig 5A.3. SEM image of acid-catalyzed SNPs, P1 showing irregular morphology of the particles

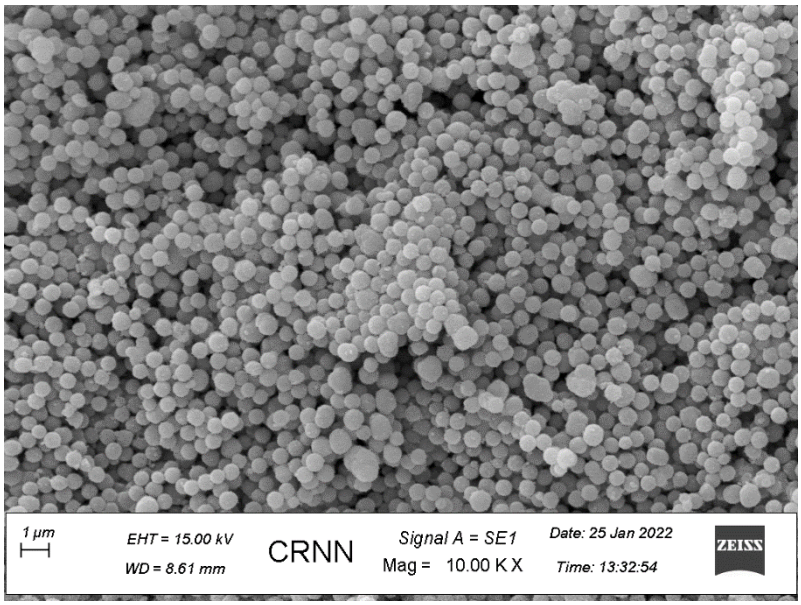

Fig 5A.4. SEM image of base-catalyzed SNPs, P2 showing spherical morphology of the particles

SEM images revealed that most of the acid-catalyzed SNPs, P1 existed as microparticles along with nanoparticles and formed irregular clusters (Fig 5A.3). All the base-catalysed SNPs, P2, were spherical (Fig 5A.4). The primary silica particles obtained through polymeric bonding of silica monomers aggregated to larger SiO_2 particles in an acidic medium. Therefore, most of the particles existed as irregular cluster-shaped microparticles. However, the particles became spherical and monodispersed in the basic medium due to controlled nucleation and growth of the particles in a slower hydrolysis process; hence all the particles were in the nano dimension. DLS data indicated that very few aggregates were formed in the solution. However, the particle size that appeared in SEM images was larger (P1$\simeq$ 550 nm and P2 $\simeq$ 272 nm) compared to DLS data due to the formation of aggregates. This could result from the drying procedure used to prepare the sample.

5A.2.3. Drug Loading Capacity and Loading Efficiency of SNPs:

Drug loading capacity refers to the maximum amount of drug that can be loaded into the carrier system per unit weight or volume. Drug loading efficiency measures the effectiveness of the drug loading process, indicating the percentage of the drug that is successfully incorporated into the carrier system relative to the total amount of drug used in the formulation. The loading capacity of CH-loaded acid-catalyzed SNPs, R1, was 5.73±0.167%, and base-catalyzed SNPs, R2, was 7.93±0.149%. In the case of EB-loaded acid-catalysed SNPs, S1 and, EB-loaded base-catalysed SNPs, S2, the loading capacity was 6.01±0.105% and 6.92±0.057%, respectively. For PM-loaded acid-catalyzed SNPs, T1, and PM-loaded base-catalyzed SNPs, T2, the value of loading capacity was determined to be 5.47±0.292% and 7.75±0.031% respectively. Additionally, the drug loading efficiency of R1 and R2 formulations was 89.70±0.389% and 90.89±0.453%, respectively. The values of drug loading efficiency obtained for S1 and S2 formulations were 83.72±0.229% and 88.43±0.136%, respectively. The loading efficiency calculated for T1 was 88.46±0.042% and, T2 was 89.15 ± 0.057%. The combination of high

drug loading efficiency and a moderate drug loading capacity of SNPs indicates an effective drug delivery system capable of delivering therapeutically relevant doses of the drug while minimizing waste and ensuring consistent dosing. This contributes to the overall efficacy, safety, and cost-effectiveness of the pharmaceutical formulations.

5A.2.4. BET and BJH Data Analysis for Bare and Drug-loaded SNPs:

BET analysis, short for Brunauer-Emmett-Teller analysis, is a crucial technique used in the field of surface area measurement, particularly in materials science and catalysis. BJH analysis, which stands for Barrett-Joyner-Halenda analysis, is a technique used for the characterization of porous materials, particularly in determining pore size distribution and pore volume.

The sharp uptake of BET isotherm for P1 at low relative pressures (Fig 5A.5) corresponds to the efficient filling of micropores. This high uptake at lower pressures supports the conclusion that the primary adsorption took place within micropores, and larger pores were largely absent. The moderate rise of BET isotherm for P2 at low relative pressures (Fig 5A.5) reflects the limited presence of micropores, with most adsorption occurring at intermediate to high relative pressures. This pattern indicates that surface area contributions were largely from mesopores rather than micropores. The nature of isotherms corroborated with the surface area values for P1 and P2 formulations which were found to be 570.035 m^2/g and 227.214 m^2/g, respectively. The pore diameters for those formulations were 0.70 nm and 1.32 nm, respectively. Also, the pore volumes were 0.3174 cc/g and 1.2571 cc/g, respectively. After the encapsulation of all three drugs, the surface area and pore volume decreased, whereas an increase in pore diameter was observed (Table 5A.1). The pore size distribution curves for bare and drug-loaded SNPs are shown in Fig 5A.6-5A.13.

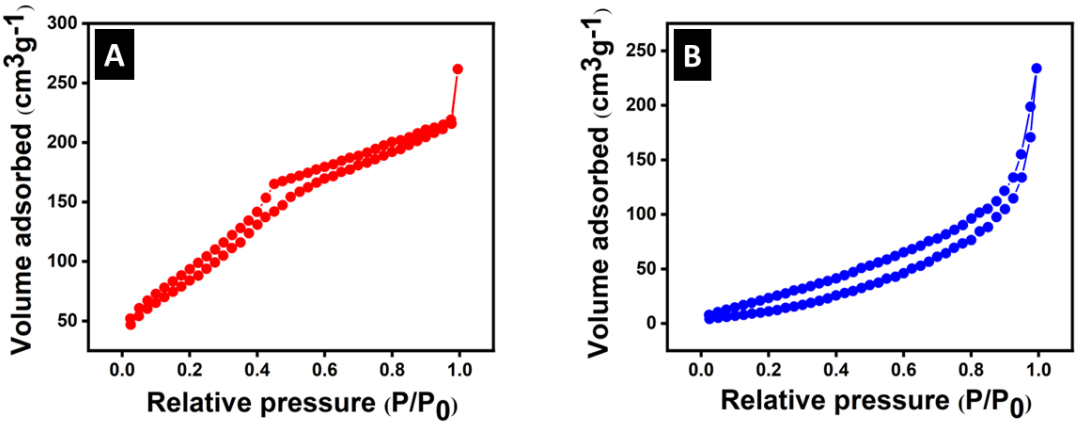

Fig 5A.5. BET adsorption-desorption isotherms of A) bare acid-catalyzed SNPs, P1, and B) bare base-catalyzed SNPs, P2

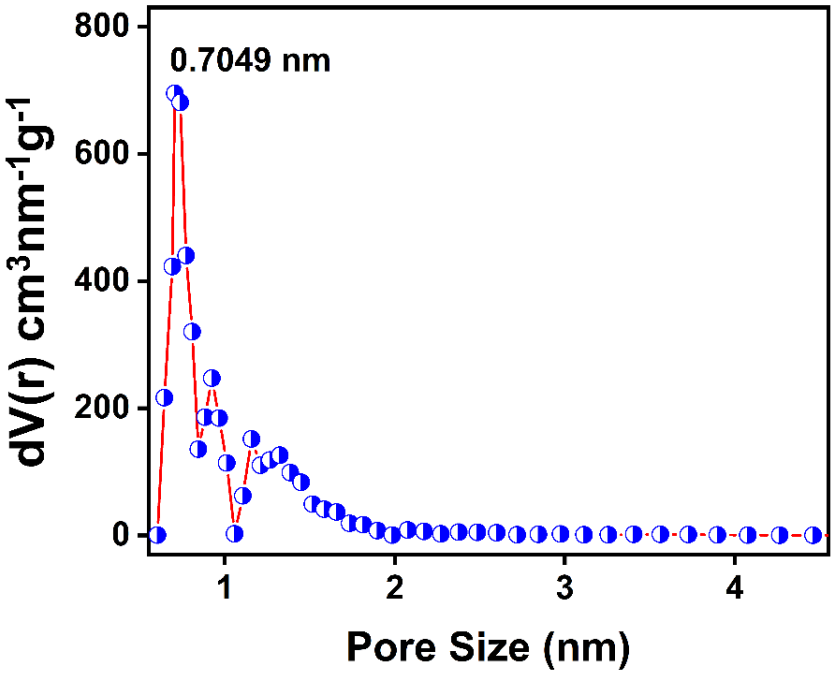

Fig 5A.6. Pore size distribution of bare acid-catalyzed SNPs, P1

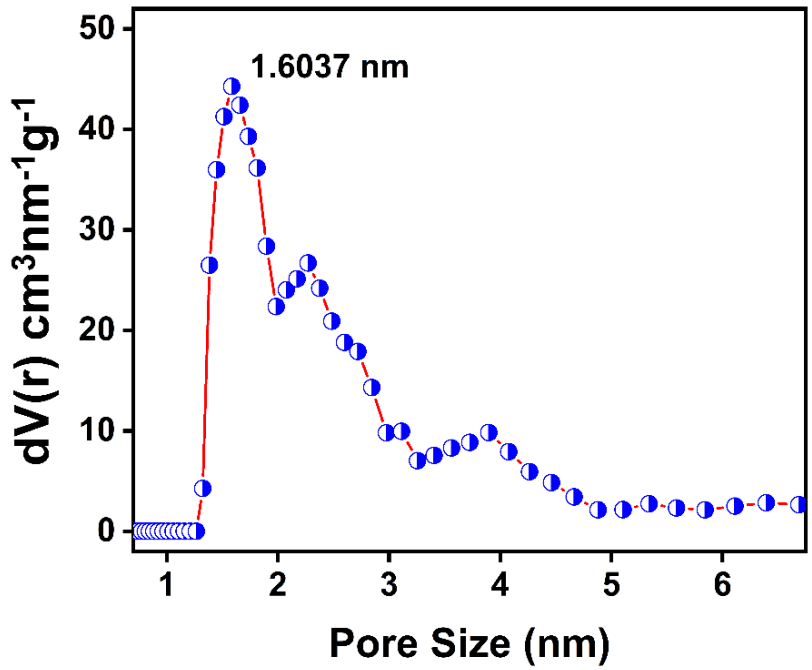

Fig 5A.7. Pore size distribution of CH-loaded acid-catalyzed SNPs, R1

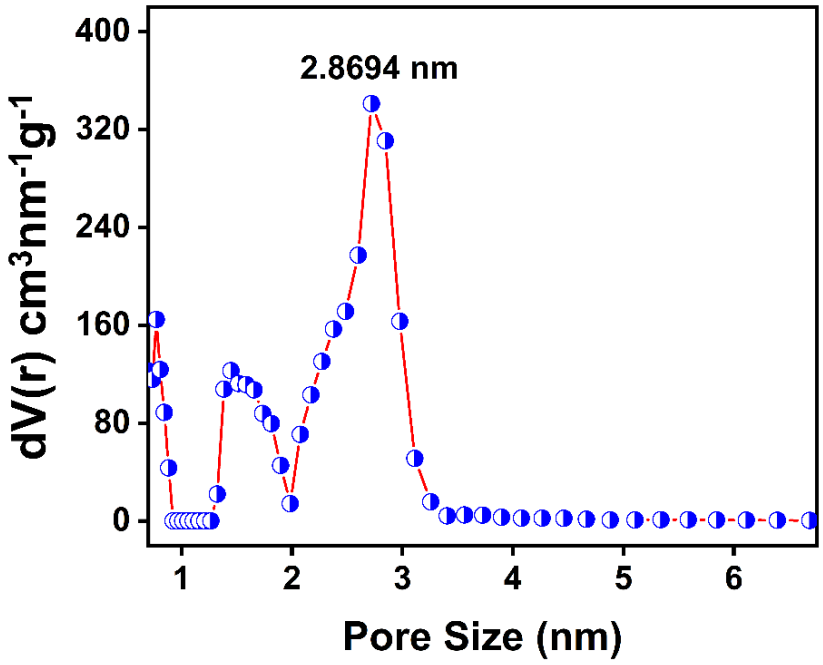

Fig 5A.8. Pore size distribution of EB-loaded acid-catalyzed SNPs, S1

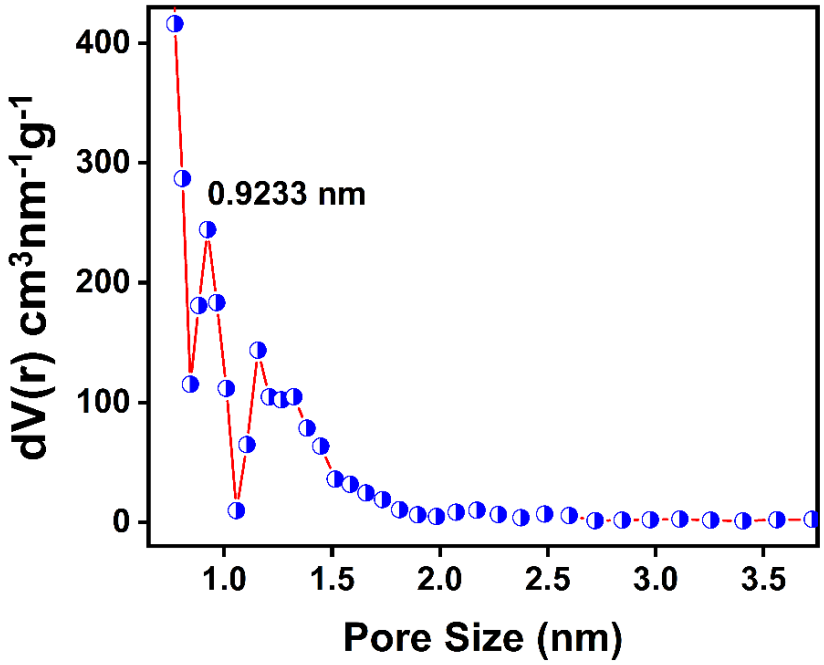

Fig 5A.9. Pore size distribution of PM-loaded acid-catalyzed SNPs, T1

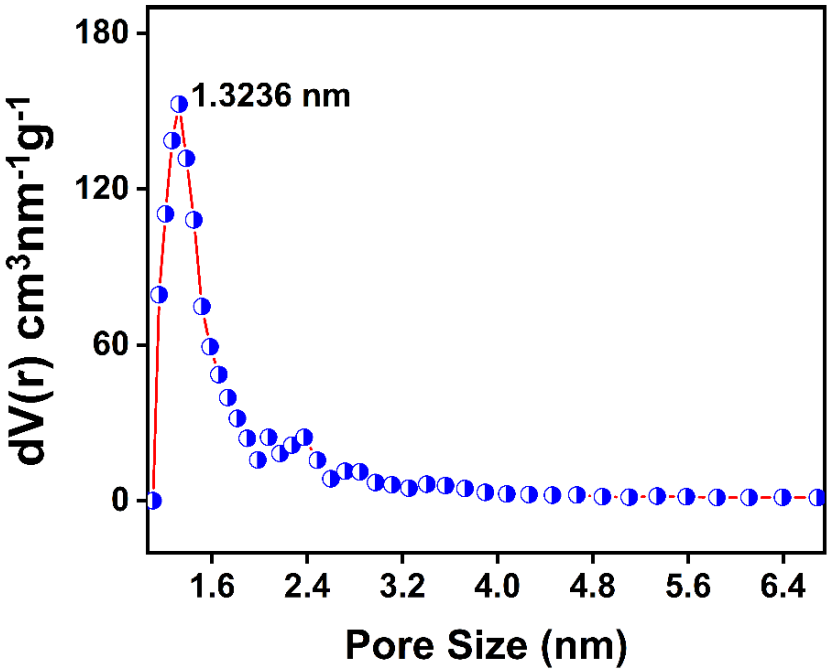

Fig 5A.10. Pore size distribution of bare base-catalyzed SNPs, P2

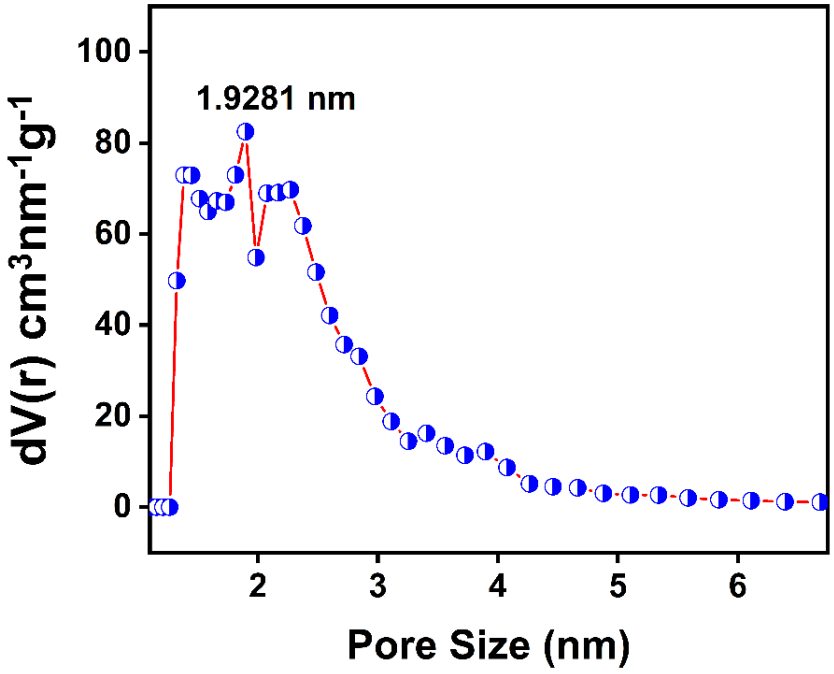

Fig 5A.11. Pore size distribution of CH-loaded base-catalyzed SNPs, R2

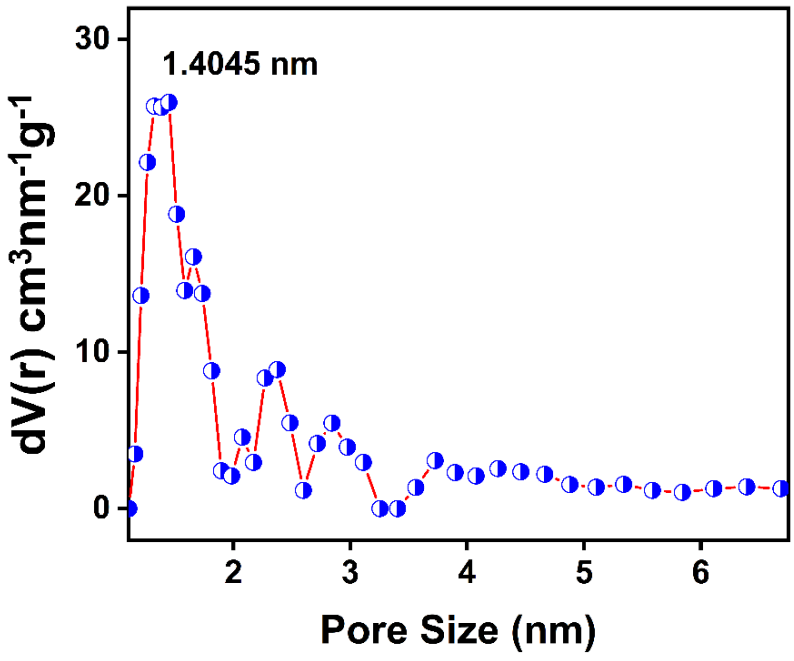

Fig 5A.12. Pore size distribution of EB-loaded base-catalyzed SNPs, S2

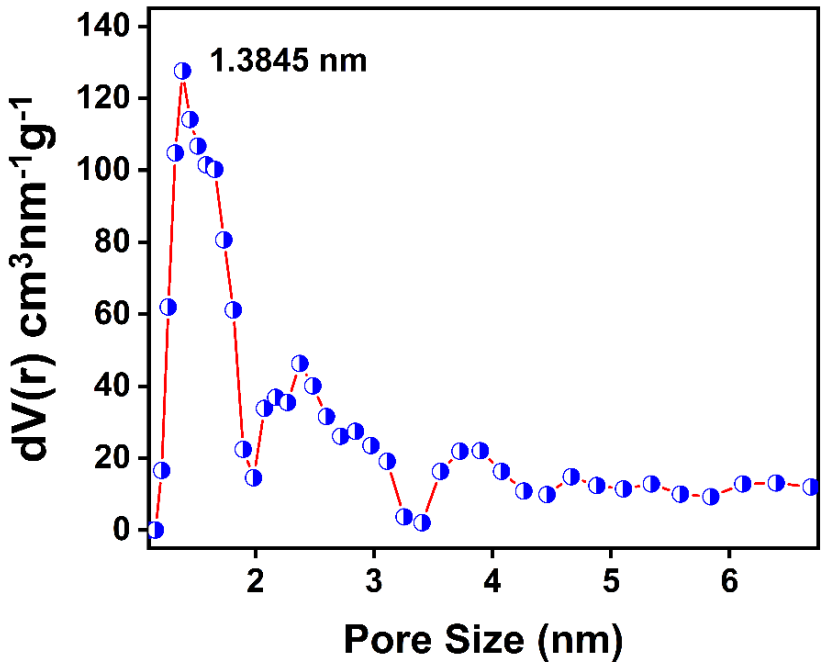

Fig 5A.13. Pore size distribution of PM-loaded base-catalyzed SNPs, T2

Table 5A.1. BET and BJH data for bare and drug-loaded SNPs

SNP Formulations	Surface Area (m^2/g)	Pore Diameter (nm)	Pore Volume (cc/g)
Acid-catalyzed SNPs, P1	570.035	0.7049	0.3174
R1	236.157	1.6037	0.0924
S1	184.006	2.8694	0.0808
T1	255.198	0.9233	0.1705
Base-catalyzed SNPs, P2	227.214	1.3236	1.2571
R2	120.488	1.9281	0.8021
S2	161.129	1.4045	0.8365
T2	187.823	1.3845	0.9080

Enhancement of the pore diameter of both P1 and P2 formulations after drug loading may be attributed to the adherence of a small number of drug molecules to the pore's entrance. P2 had a relatively lower surface area with pore size enlargement by the dissolution-precipitation process (Ostwald ripening) of silica particles in a basic medium. The acid catalyst favours a hydrolysis reaction, mainly leading to the formation of the long polymeric chain. The base catalyst favours condensation reaction, which increases the cross-linking and, therefore, spherical-shaped particles are obtained [1]. This phenomenon could explain the lowering of surface area and thus increasing of pore diameter as well as pore volume in the case of P2 as compared to that of P1.

5A.2.5. XRD Analysis of Pure Drugs, Bare SNPs, and Drug-loaded SNPs:

The peaks observed in XRD patterns correspond to the diffraction of X-rays by the crystal planes within the sample. The sharpness and narrowness of these peaks depend on the degree of crystallinity of the material. Crystalline materials have a regular, repeating atomic arrangement, with well-defined crystal planes. When X-rays interact with crystalline materials, they undergo constructive interference as they scatter off these planes, resulting in sharp and narrow diffraction peaks. Amorphous materials lack long-range order in their atomic arrangement and do not possess well-defined crystal planes. Instead, their atoms are arranged in a disordered, random manner. When X-rays interact with amorphous materials, they scatter in all directions due to the lack of ordered crystal planes. As a result, the diffraction peaks observed in XRD patterns are broad and diffuse, with lower intensity.

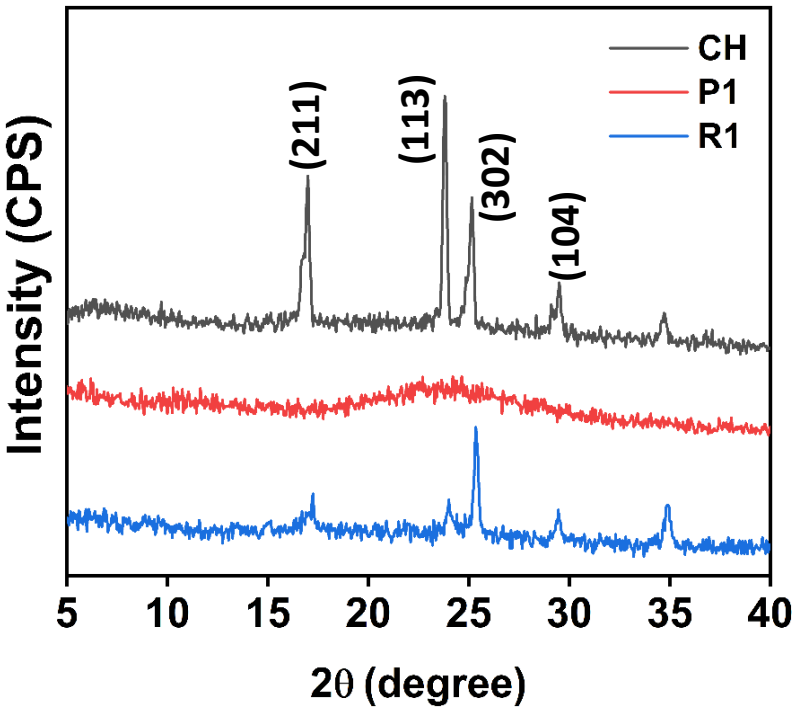

Fig 5A.14. XRD patterns of CH drug, acid-catalyzed SNPs (P1), and CH-loaded P1 (R1)

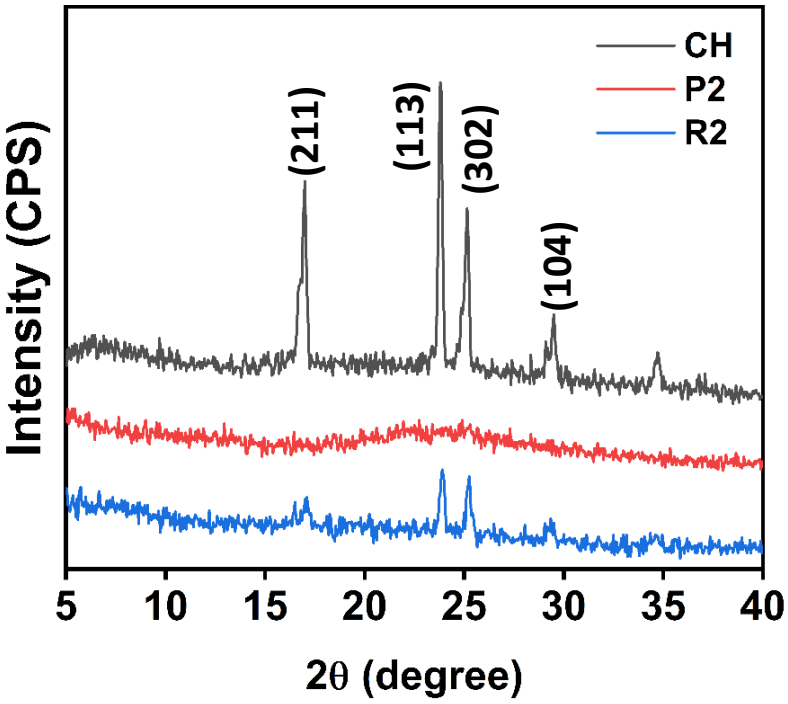

Fig 5A.15. XRD patterns of CH drug, base-catalyzed SNPs (P2), and CH-loaded P2 (R2)

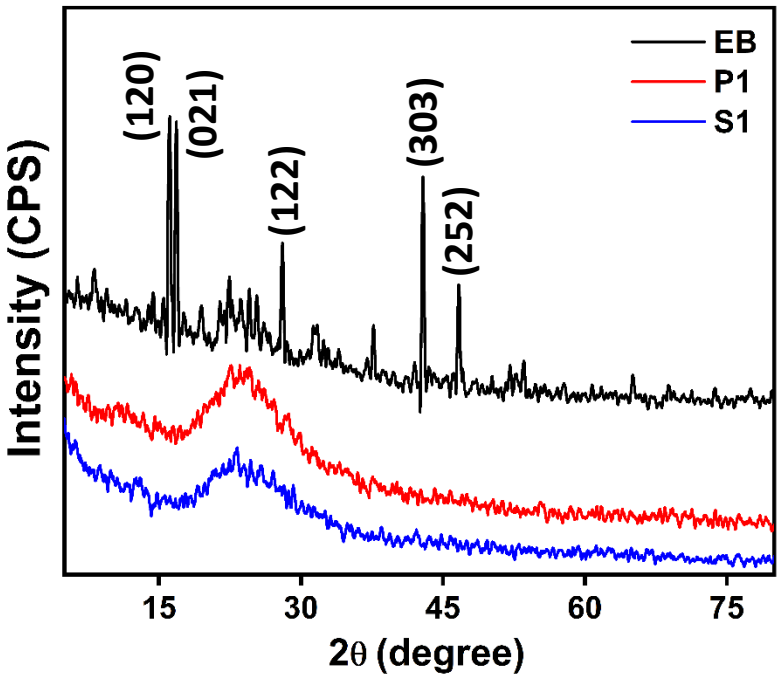

Fig 5A.16. XRD patterns of EB drug, acid-catalyzed SNPs (P1), and EB-loaded P1 (S1)

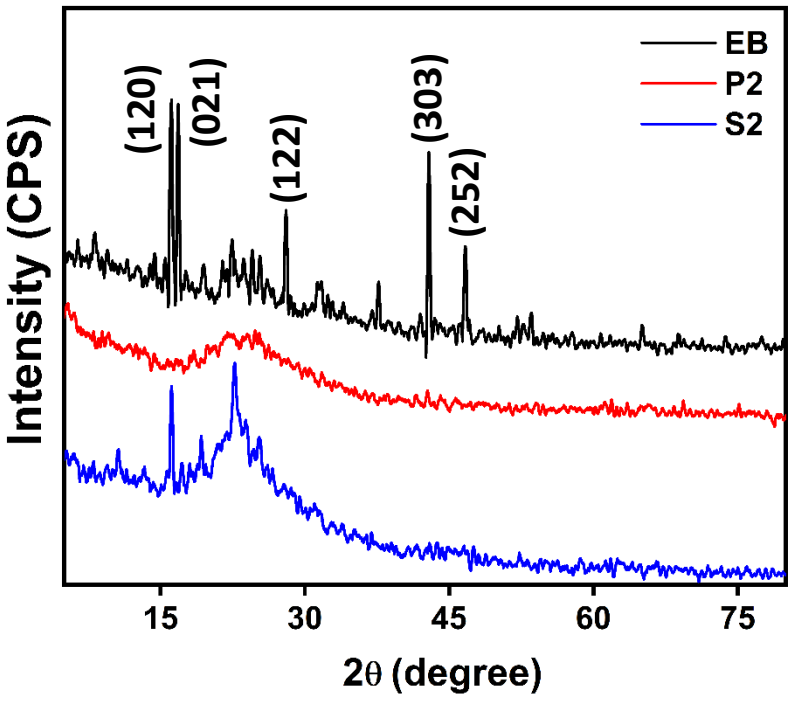

Fig 5A.17. XRD patterns of EB drug, base-catalyzed SNPs (P2), and EB-loaded P2 (S2)

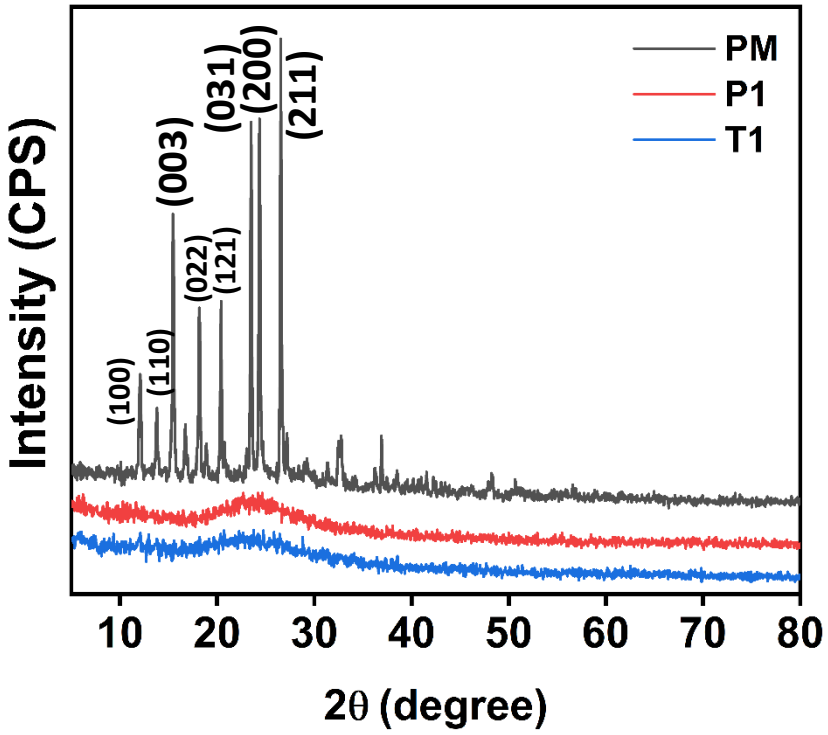

Fig 5A.18. XRD patterns of PM drug, acid-catalyzed SNPs (P1), and PM-loaded P1 (T1)

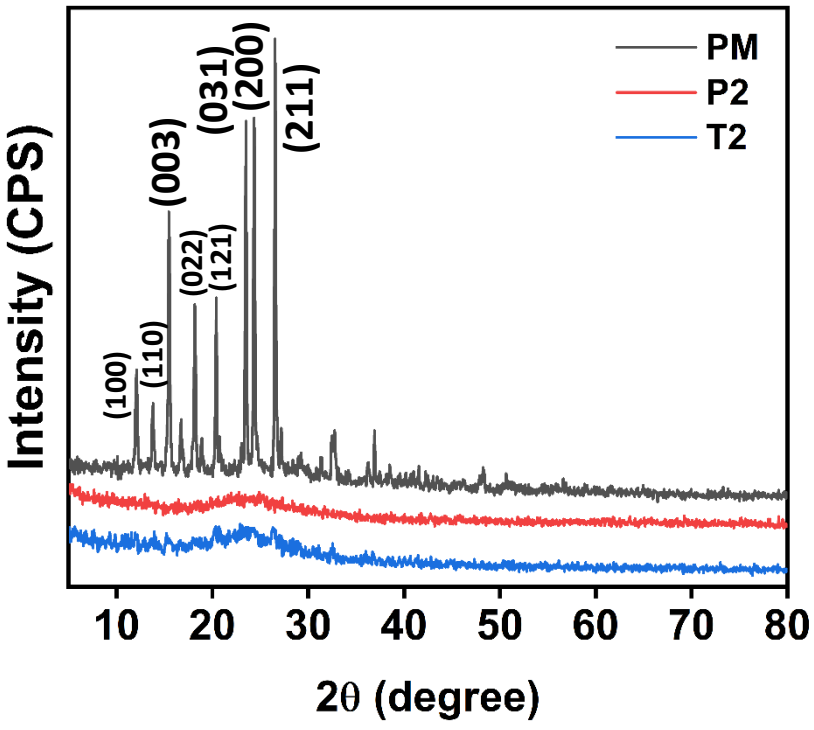

Fig 5A.19. XRD patterns of PM drug, base-catalyzed SNPs (P2), and PM-loaded P2 (T2)

In Fig 5A.13-5A.18, the absence of high-intensity diffraction peaks for SNPs implied its amorphous nature. Highly intense narrower diffraction peaks were the indications of the crystalline characteristic of the drugs. However, a small amount of crystalline drug was detected in the XRD patterns of drug-loaded SNPs. The loss of crystallinity of pure drug molecules after incorporation into silica nanoparticles is primarily attributed to the confinement effects, surface interactions etc. When drug molecules were incorporated into SNPs, they were confined within the nanoparticle matrix. The limited space available within the nanoparticles may prevent the drug molecules from adopting their crystalline lattice arrangement, leading to a loss of crystallinity. Drug molecules might interact with the surface of the SNPs through chemical or physical interactions. These interactions (i.e. surface adsorption or chemical bonding) can disrupt the regular arrangement of drug molecules and inhibit the formation of crystalline structures [2].

5A.2.6. *In Vitro* Drug Release Study from the Drug-loaded SNPs:

In vitro drug release studies from nanoparticles involve evaluating the release profile of a drug from nanoparticle carriers in simulated physiological conditions outside of a living organism. This process typically involves placing the drug-loaded nanoparticles in a solution that mimics the conditions of the body, such as pH, temperature, and fluid composition, and monitoring the release of the drug over time. These studies play a vital role in the development and evaluation of nanoparticle-based drug delivery systems, helping to optimize their performance, predict their behaviour *in vivo*, and ensure their safety and efficacy.

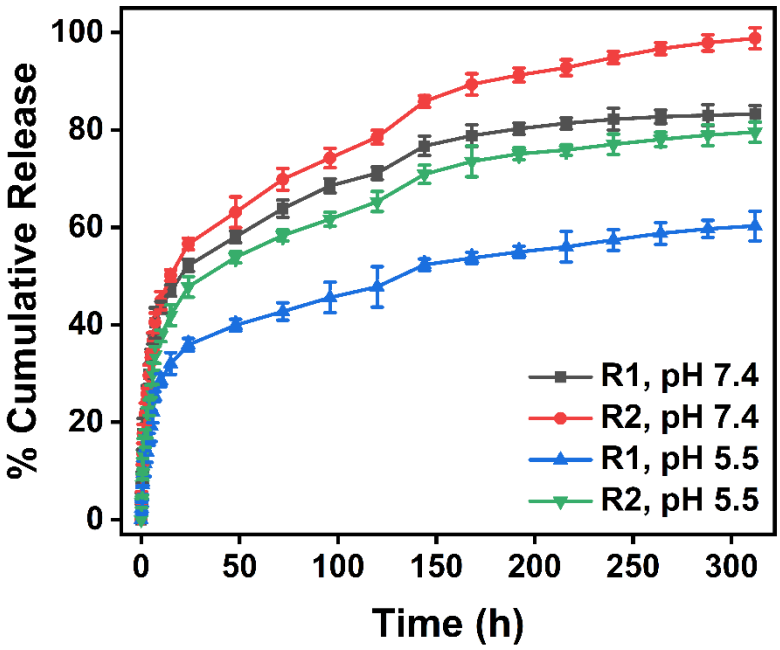

Fig 5A.20. In vitro CH drug release study from both SNPs. The results were expressed as mean ± S.D, n=3

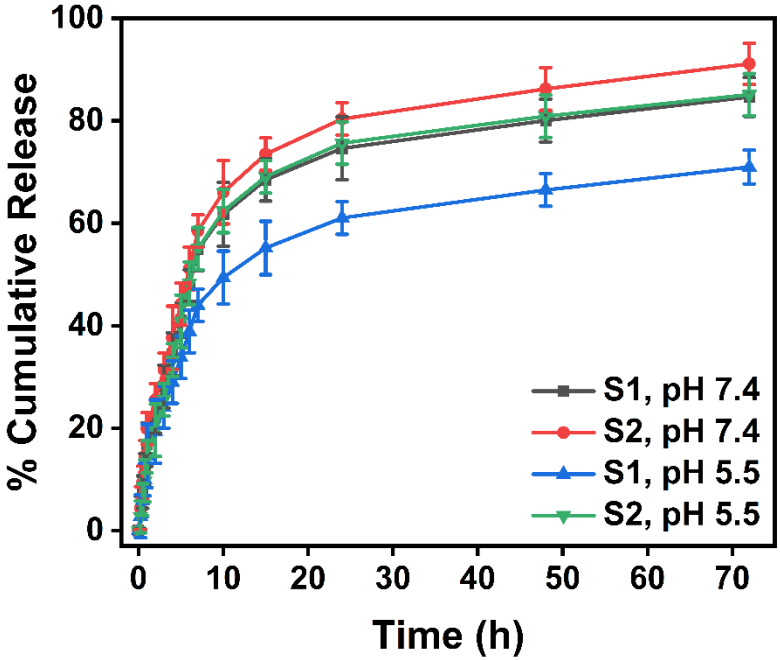

Fig 5A.21. In vitro EB drug release study from both SNPs. The results were expressed as mean ± S.D, n=3

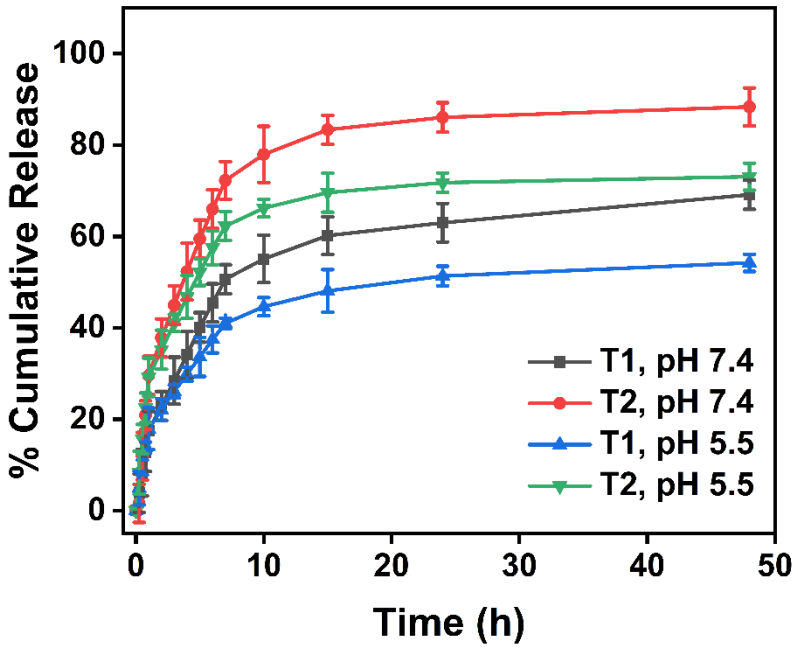

Fig 5A.22. In vitro PM drug release study from both SNPs. The results were expressed as mean ± S.D, n=3

In vitro drug release studies showed that a poorly aqueous soluble drug could be dissolved to an extent using a nanocarrier. From the release profiles (Fig 5A.19-5A.21), it was revealed that the release was sharp initially, and after that, the sustained release was observed in the second phase, which was gradually slowed down at around 312 h for R1 & R2, 72 h for S1 & S2, and, 48 h for T1 and T2 formulations. The cumulative release percentages in sodium acetate buffer (pH 5.5; skin and small intestine pH) were about 60.27% and 79.53% from R1 and R2 respectively, 70.97% and 85.10% from S1 and S2 respectively, 54.2% and 73.07% from T1 and T2 respectively whereas in phosphate buffer (pH 7.4; physiological pH) the cumulative release percentages were 83.24% and 98.79% from R1 and R2 respectively, 84.65% and 91.11% from S1 and S2 respectively, 69.12% and 88.34% from T1 and T2 respectively.

The pH 7.4 corresponds to the physiological pH of human blood and extracellular fluid. The drug release studies at pH 7.4 assessed how the drug formulation behaves under conditions like those in the bloodstream after systemic administration. This is particularly important for drugs intended for intramuscular, intravenous, or transdermal administration. The pH 5.5 corresponds roughly to the pH of the skin and the small intestine, particularly in the duodenum and proximal jejunum. The drug release at pH 5.5 was conducted to evaluate the stability of the formulation under conditions relevant to skin application and to simulate the conditions that the drug encounters upon oral administration and passage through the gastrointestinal tract. The drug molecules adsorbed on the surface of SNPs released rapidly during the initial period (first 15 h). Also, it could be said that there was a high drug concentration gradient initially between the silica matrices and bulk solution, which was the driving force for the higher dissolution of the drug in the first phase. The release was sustained in the second phase for a long period as the drug molecules diffused out from the three-dimensional polymeric network region where an internal tension exists. Since. P2 has larger pores compared to P1 (as obtained from BJH analysis), the larger pores provide more space for drug loading and facilitate the release of the drug molecules. The enhanced dissolution of aqueous soluble drug CH and poorly aqueous soluble drugs (EB & PM) may be explained by its state change from crystalline to amorphous after loading into SNPs, as illustrated in Fig 5A.13-5A.18. Amorphous materials lack the long-range order whereas regular ordered structure was found in crystalline materials. As a result, amorphous substances often have higher surface areas per unit mass compared to their crystalline counterparts. This increased surface area provides more sites for solvent molecules to interact with, facilitating faster dissolution kinetics. Moreover, the crystalline materials are in a more stable energy state compared to amorphous materials, which often have higher internal energy due to their disordered nature. As a result, amorphous materials have a greater tendency to interact with solvent molecules and dissolve to reach a lower energy state [3]. The

percentage of release for each drug was lower at pH 5.5 as compared to pH 7.4. The electrostatic attraction between positive charges over the cationic form of each drug molecule and negative charges over the SNP surface (Zeta potential = -21.62 mV for P1 and -17.97 mV for P2; Fig 5A.22 & 5A.23 respectively) was high at pH 5.5 which led to a lower percentage of drug release. The number of cationic forms of the drugs was low at pH 7.4 for which the extent of electrostatic force mentioned earlier decreased at that pH leading to a higher amount of drug release.

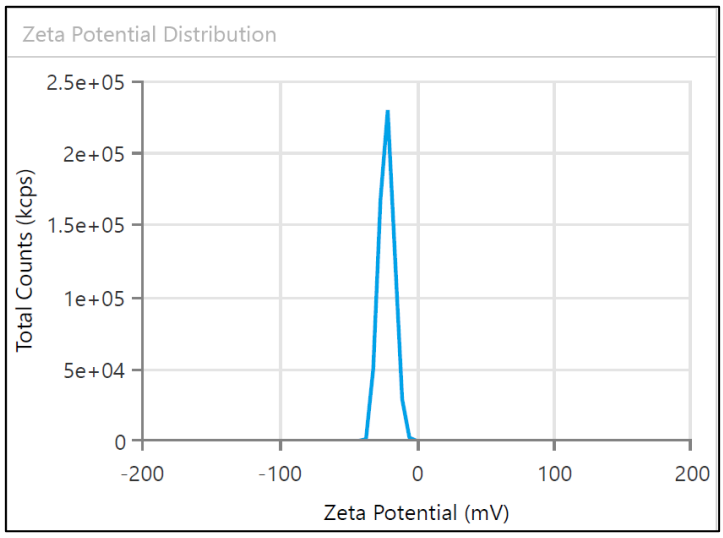

Fig 5A.23. Zeta potential distribution curve of acid-catalyzed SNPs, P1

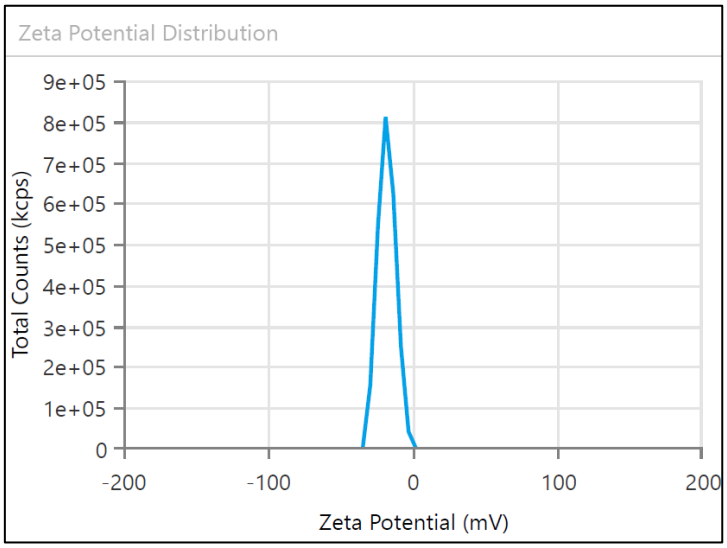

Fig 5A.24. Zeta potential distribution curve of base-catalyzed SNPs, P2

5A.2.7. Preliminary Screening of the Transdermal Patches:

The patches showed low moisture content ranging from 3.02 to 10.77% (CH patches), 3.99 to 10.08% (EB patches), and 3.74 to 9.51% (PM patches) according to Fig 5A.24-5A.26. These patches also exhibited low moisture uptake in the range of 6.38 to 10.84% (CH patches), 7.77 to 10.42% (EB patches), and 6.28 to 11.40% (PM patches) as shown in Fig 5A.24-5A.26. The percentage swelling index increment for all patches was observed with time as depicted in Fig 5A.27-5A.29. The surface pH of patches lay in the skin pH region (pH: 4.5-6.0) as shown in Fig 5A.30-5A.32. Furthermore, the patches were shown to have promising values of folding endurance which exceeded 250 times on average. The values of percentage elongation varied in the range of 28.31 to 29.04% for CH patches, 25.74 to 26.66% for EB patches, and 25.45 to 31.18% for PM patches. The thickness of the patches was found to be in the range of 0.20 and 0.81 mm. All transdermal formulations were uniform in weight as well. The consistency in all parameters mentioned above was ensured by the low standard deviation values in the measurements presented in Table 5A.2.

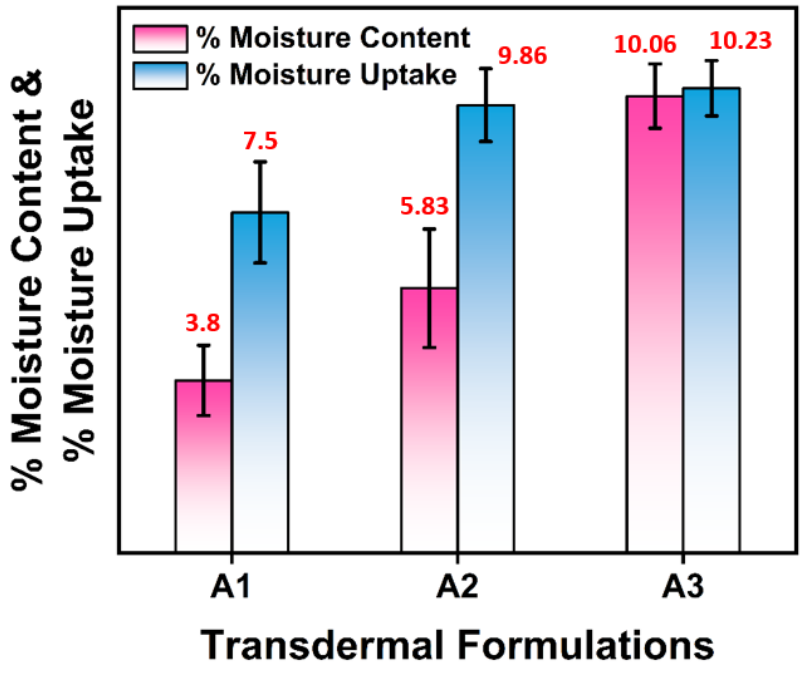

Fig 5A.25. Percentage of moisture content and moisture uptake of CH patches

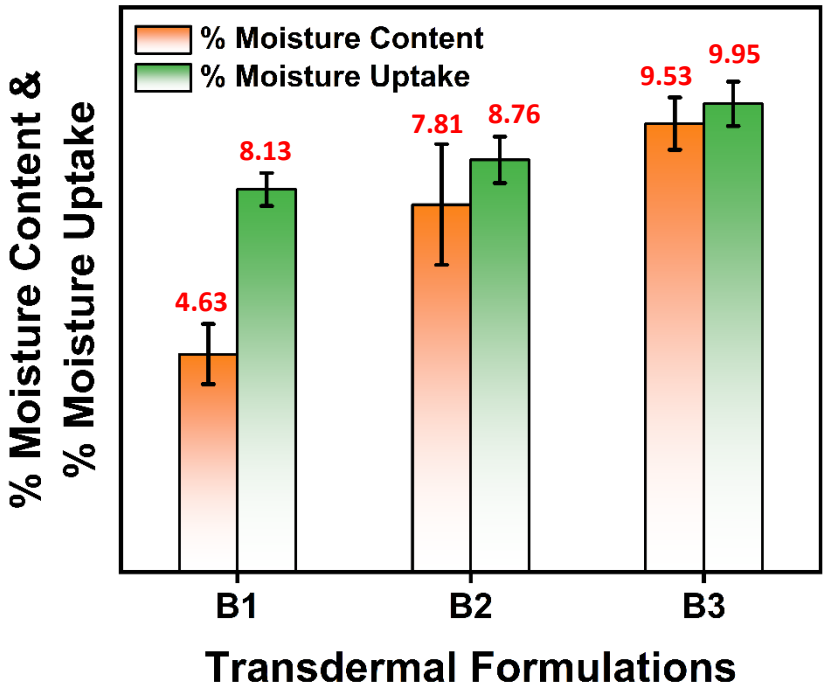

Fig 5A.26. Percentage of moisture content and moisture uptake of EB patches

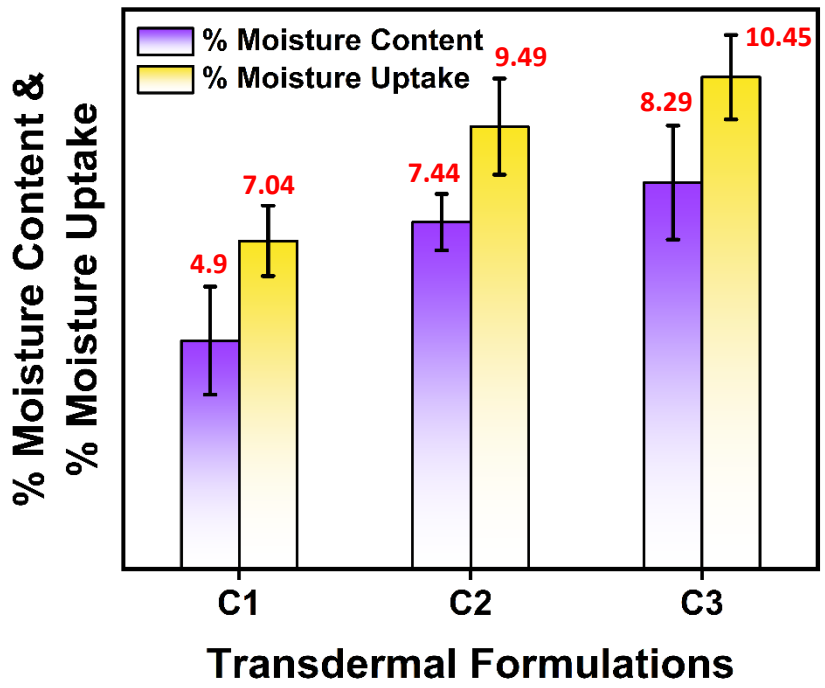

Fig 5A.27. Percentage of moisture content and moisture uptake of PM patches

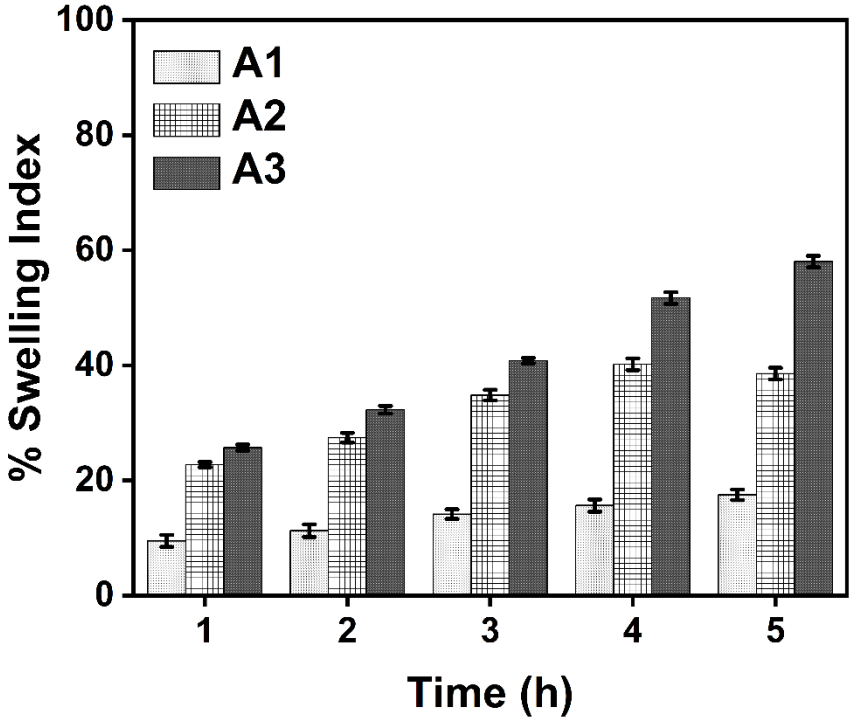

Fig 5A.28. Percentage swelling index of CH patches

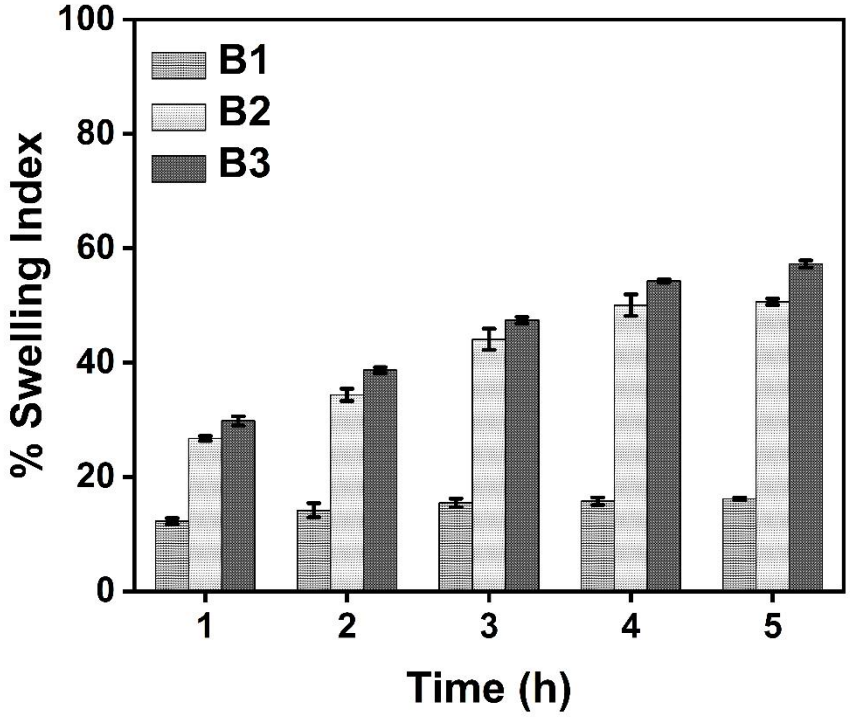

Fig 5A.29. Percentage swelling index of EB patches

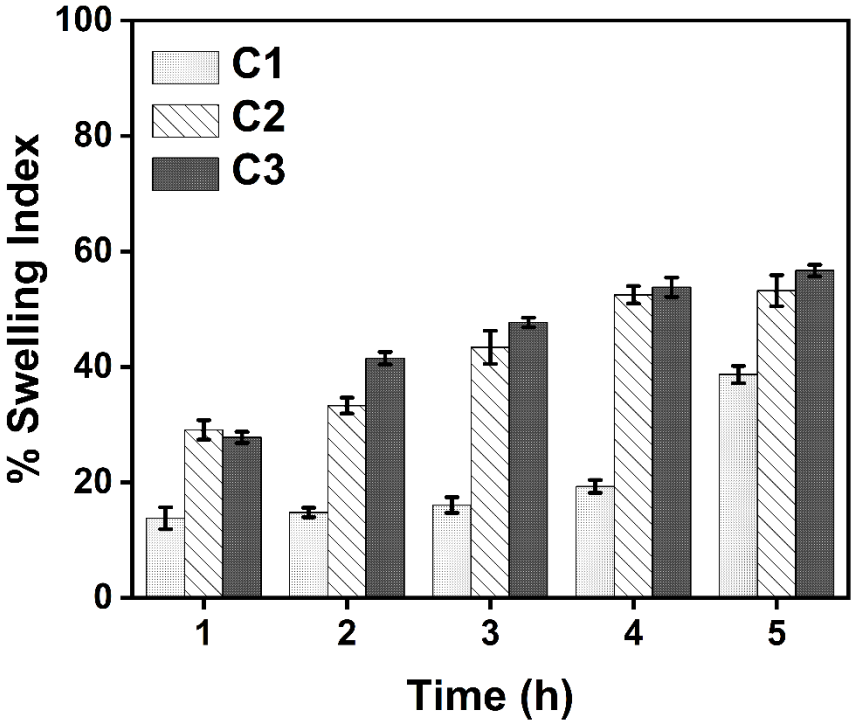

Fig 5A.30. Percentage swelling index of PM patches

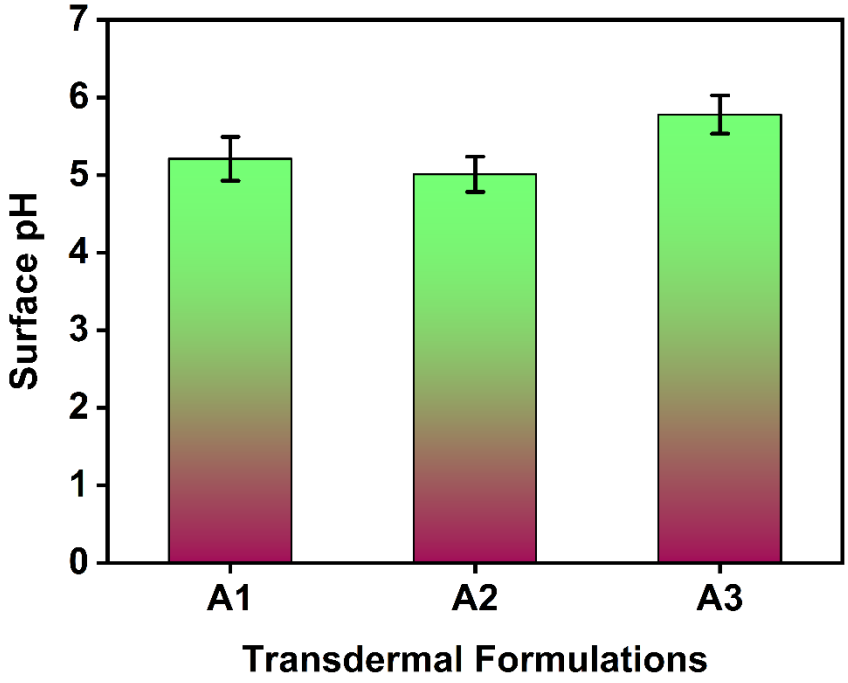

Fig 5A.31. Surface pH of the CH patches

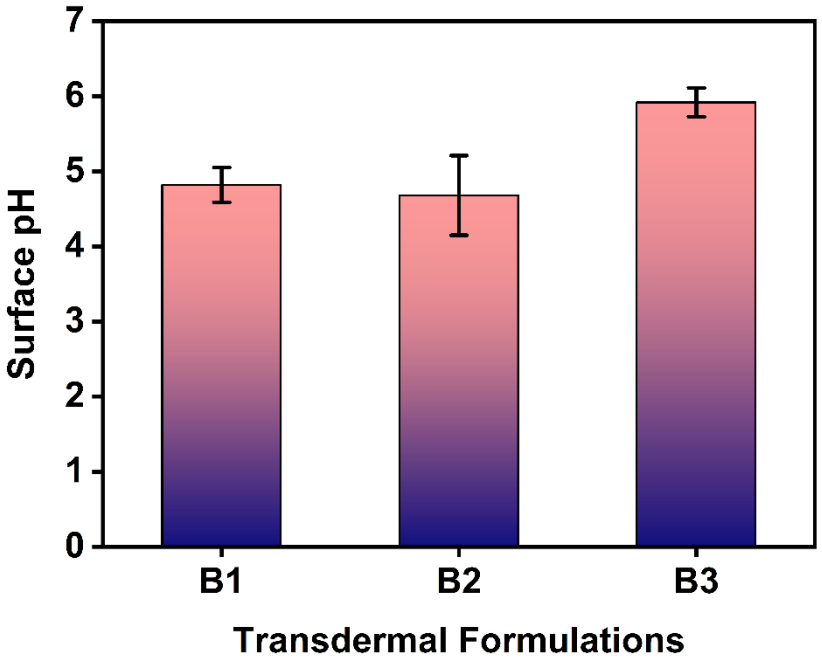

Fig 5A.32. Surface pH of the EB patches

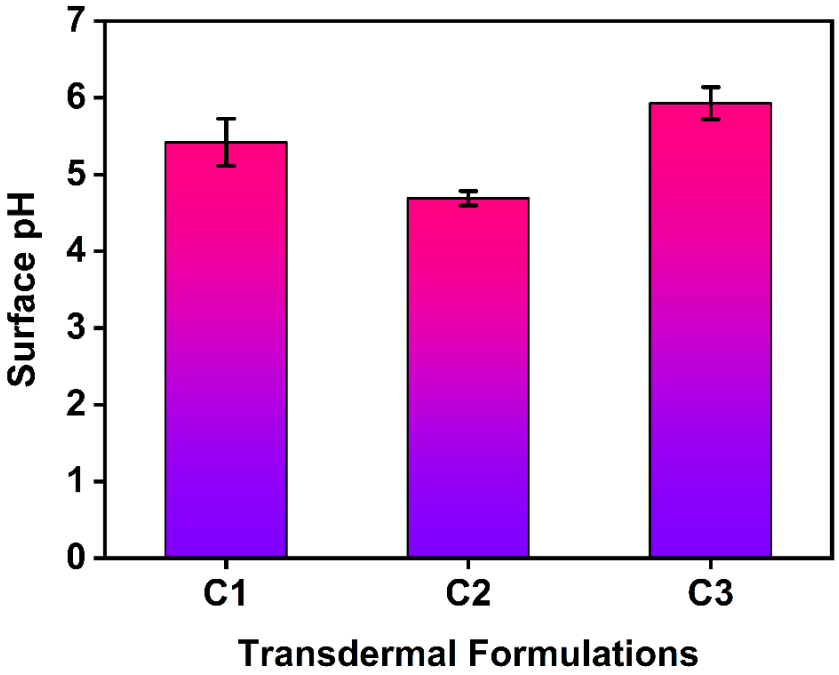

Fig 5A.33. Surface pH of the PM patches

Table 5A.2. Folding endurance, % elongation, thickness, and weight uniformity of the patches

Transdermal Formulations	Folding Endurance	% Elongation	Thickness (mm)	Weight Uniformity (mg)
A1	267 ± 0.667	28.32 ± 0.014	0.38 ± 0.019	101.82 ± 0.024
A2	293 ± 0.663	29.01 ± 0.028	0.36 ± 0.015	102.36 ± 0.059
A3	294 ± 0.732	28.76 ± 0.042	0.33 ± 0.015	100.04 ± 0.042
B1	265 ± 0.838	25.76 ± 0.015	0.39 ± 0.025	95.03 ± 0.059
B2	271 ± 0.509	26.44 ± 0.092	0.47 ± 0.041	98.66 ± 0.018
B3	285 ± 0.517	26.60 ± 0.065	0.46 ± 0.018	93.72 ± 0.018
C1	238 ± 0.867	25.47 ± 0.022	0.21 ± 0.008	98.14 ± 0.017
C2	249 ± 0.833	25.84 ± 0.017	0.43 ± 0.010	95.21 ± 0.015
C3	246 ± 0.971	31.16 ± 0.024	0.79 ± 0.014	101.29 ± 0.021

Preliminary screening of transdermal patches is essential for assessing their effectiveness, safety, and formulation optimization, as well as for guiding further development efforts towards successful clinical translation. Low moisture content preserved the integrity of the patches' components, such as the active pharmaceutical ingredients (API) and adhesive. Also, low moisture uptake protected the patches from microbial contamination and lessened bulkiness. Silica particles are hydrophilic because of the polar Si-O bond, which can form hydrogen bonds with water molecules [4]. The addition of hydrophilic SNPs enhanced surface wettability and water penetration within the matrix. Hence, A2, A3, B2, B3, C2, and C3 formulations showed a higher percentage swelling index as compared to that of A1, B1, and C1. Although the swelling was slightly higher in those transdermal patches containing SNPs,

the materials maintained their original density, resulting in thin and less bulky patches. The skin has a slightly acidic pH, typically 4.5 to 6.0 [5]. Maintaining a similar pH on the surface of transdermal patches ensures compatibility with the skin. Significant deviations from the skin's pH can cause irritation, discomfort, or even damage to the skin barrier. The surface pH values of the prepared patches showed their safety and skin compatibility.

The drug content for the transdermal formulations of CH A1, A2, and, A3 were 89.06±0.243%, 87.32±0.854%, and 88.56±0.405%, respectively. EB-transdermal patches B1, B2, and B3 showed 91.32±0.646%, 84.79±0.290%, and, 87.93±0.212% of drug content respectively. In the case of PM-transdermal formulations, the drug content of C1, C2, and C3 was found to be 80.61±0.031%, 74.54±0.055%, and 78.22±0.039%, respectively. Achieving high drug content can help to minimize the use of additional excipients or adhesives in the patch formulation, reducing the risk of skin irritation or allergic reactions. High drug content can allow for less frequent patch changes which will enhance patient convenience and adherence to the prescribed treatment regimen. Furthermore, high drug content can result in reduced manufacturing costs per dose and improved cost-effectiveness of the treatment.

5A.2.8. FTIR Analysis:

FTIR spectroscopy is widely used to identify chemical functional groups present in a sample. By analyzing the absorption of infrared light by molecular vibrations, FTIR can provide information about the types of chemical bonds present in the molecules. This is valuable for characterizing unknown compounds or confirming the identity of known substances. In pharmaceuticals and other industries, FTIR analysis is used in formulation development to monitor chemical changes during product development and optimize formulations. It helps

researchers understand how different components interact and how formulation changes affect the chemical composition of the product.

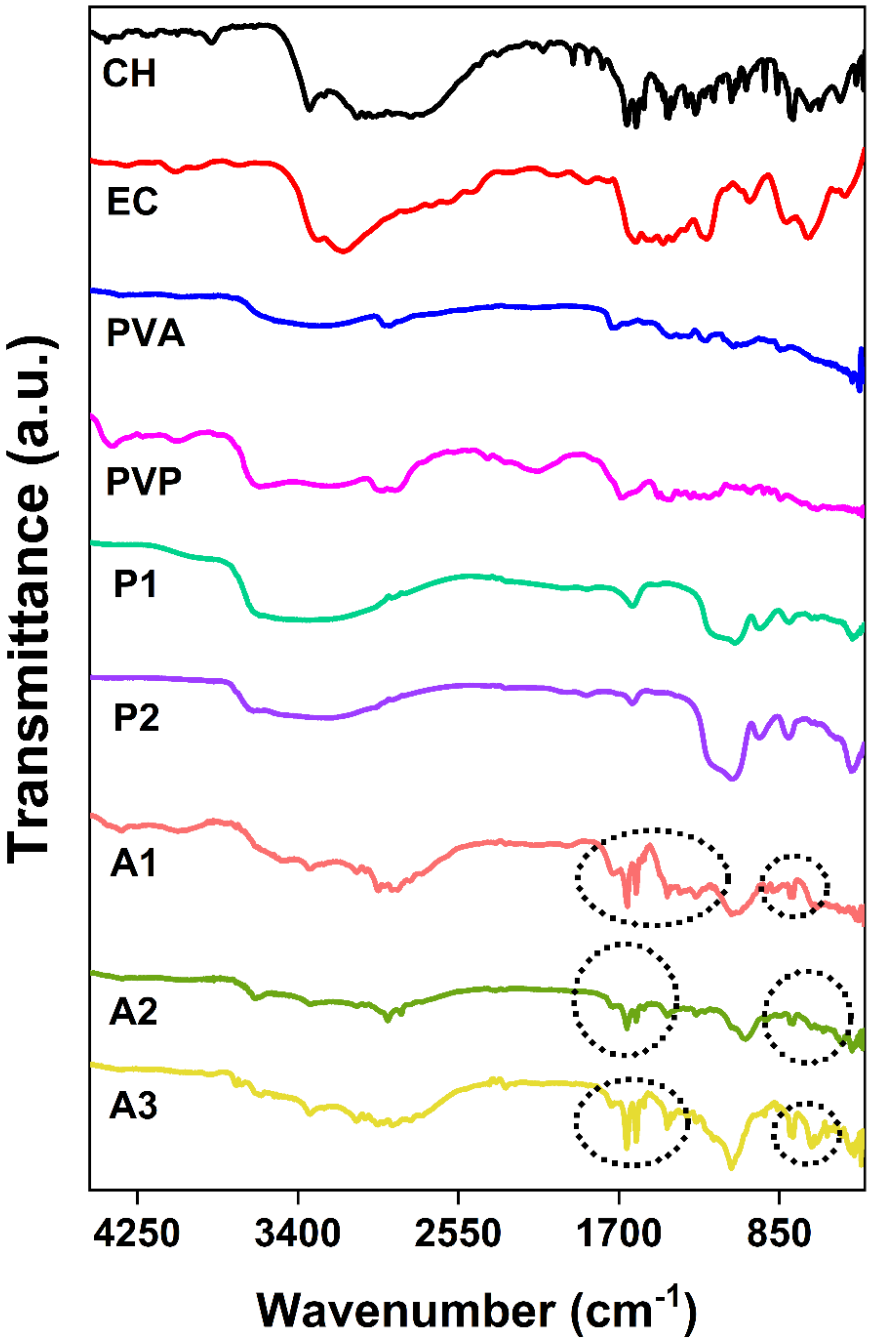

Fig 5A.34. FTIR spectra of CH drug, polymers (EC, PVA & PVP), SNPs (P1 & P2), and patches (A1, A2 & A3)

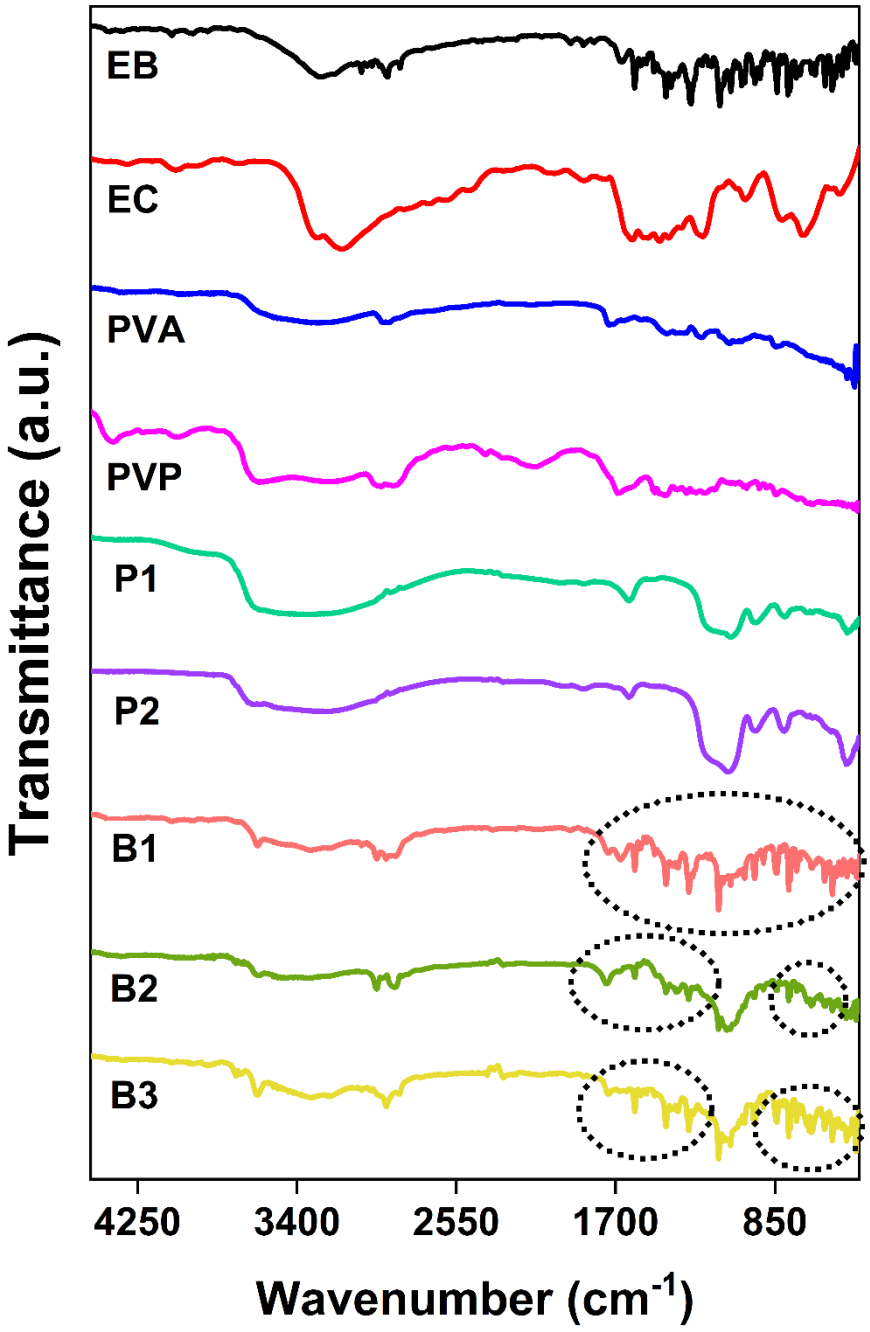

Fig 5A.35. FTIR spectra of EB drug, polymers (EC, PVA & PVP), SNPs (P1 & P2), and patches (B1, B2 & B3)

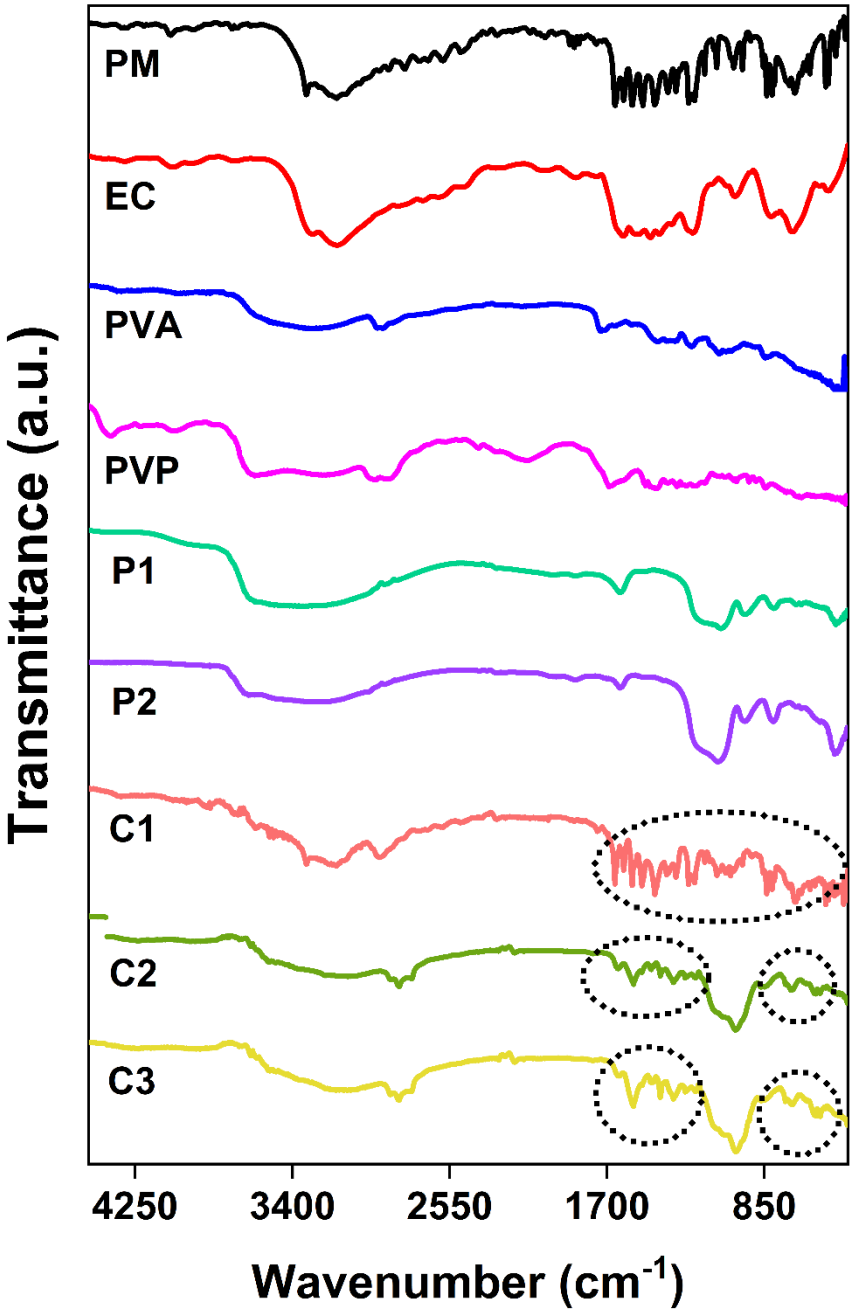

Fig 5A.36. FTIR spectra of PM drug, polymers (EC, PVA & PVP), SNPs (P1 & P2), and patches (C1, C2 & C3)

FTIR spectra of the pure drug, polymers, and transdermal patches were taken within the range of 400–4000 cm^{-1}. This analysis showed that the characteristic peaks of pure CH drug were observed at 3340 cm^{-1} for N-H stretching, 3077 cm^{-1} for C-H stretching,1650 cm^{-1} for C-N stretching,1441 cm^{-1} for in-plane deformation mode of C-H stretching,1299 cm^{-1} for wagging mode of -CH_2 group, and 780 cm^{-1} out-plane deformation mode of C-H stretching (Fig 5A.33) [6]. On the other hand, the major peaks for pure EB drug were found at 1597 and 1492 cm^{-1} due to aromatic C=C stretching, 1145 and 1084 cm^{-1} for S=O stretching vibrations (Fig 5A.34) [7]. The significant peaks of PM appeared at 3324 cm^{-1} for O-H stretching, 3162 cm^{-1} for C-H stretching, 1656 cm^{-1} for C=O stretching, and 1609 cm^{-1} for C=C stretching, 1565 cm^{-1} for N-H bending and 1507 cm^{-1} for asymmetrical C-H bending (Fig 5A.35) [8]. In the FTIR spectra of all the CH transdermal patches, significant peaks of the drug were observed within the range of 1400-1660 cm^{-1} as shown by the dotted circle in Fig5A.33. The spectra of EB transdermal patches showed principal peaks of the drug in the range of 1300-1600 cm^{-1}, as illustrated by the dotted circle in Fig5A.34. The major peaks of pure PM drug in its transdermal formulations were observed between 1220 to 1680 cm^{-1}, as portrayed by the dotted circle in Fig 5A.35. Moreover, the patches containing nanomedicines (A2, A3, B2, B3, C2 & C3) proved the presence of SNPs by showing a broad strong band around 1085 cm^{-1} for the stretching of the C-O bond present in TEOS. However, few additional peaks were observed in all patches due to the presence of other constituting polymers.

5A.2.9. Analysis of SEM Images of the Patches:

SEM analysis is essential for quality control during the production of both blank and drug-loaded patches. It allows the makers to inspect patches for defects, ensure uniformity in drug distribution, and identify any issues that may impact product performance or safety. SEM images of the patches (Fig 5A.36-5A.45) confirmed that the pure drug and drug-loaded SNPs were homogeneously dispersed in the transdermal formulations.

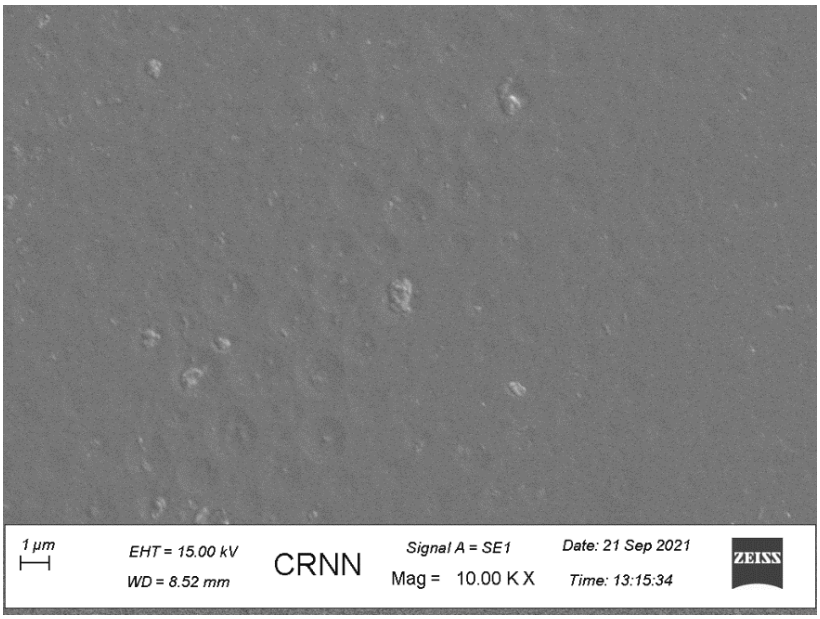

Fig 5A.37. SEM image of blank transdermal patch

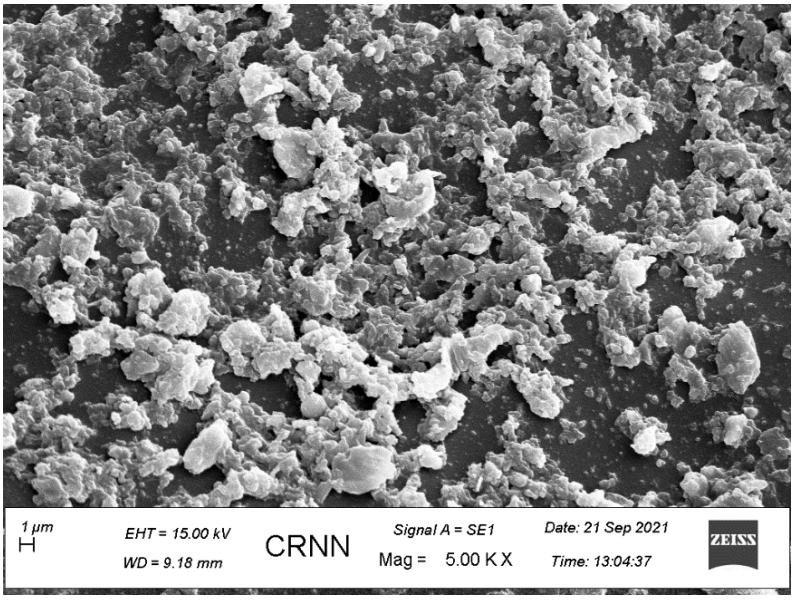

Fig 5A.38. SEM image of the transdermal patch containing free CH, A1

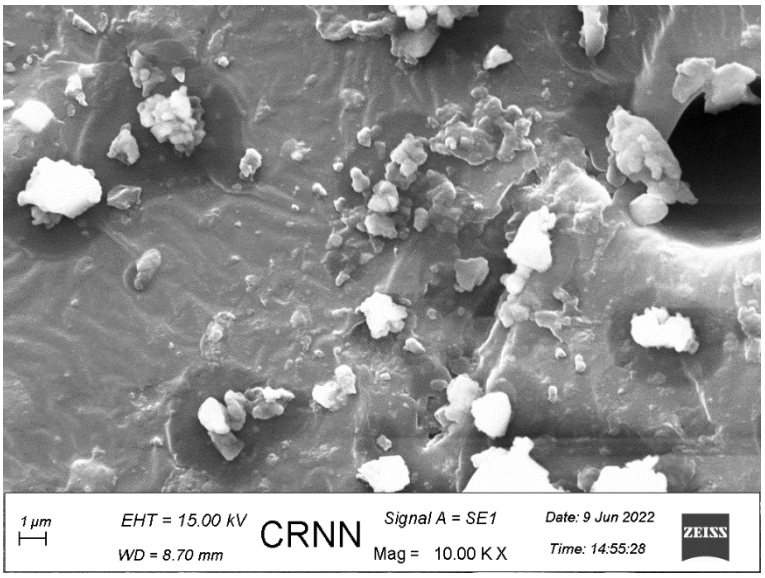

Fig 5A.39. SEM image of the transdermal patch containing CH-loaded acid-catalyzed SNPs, A2

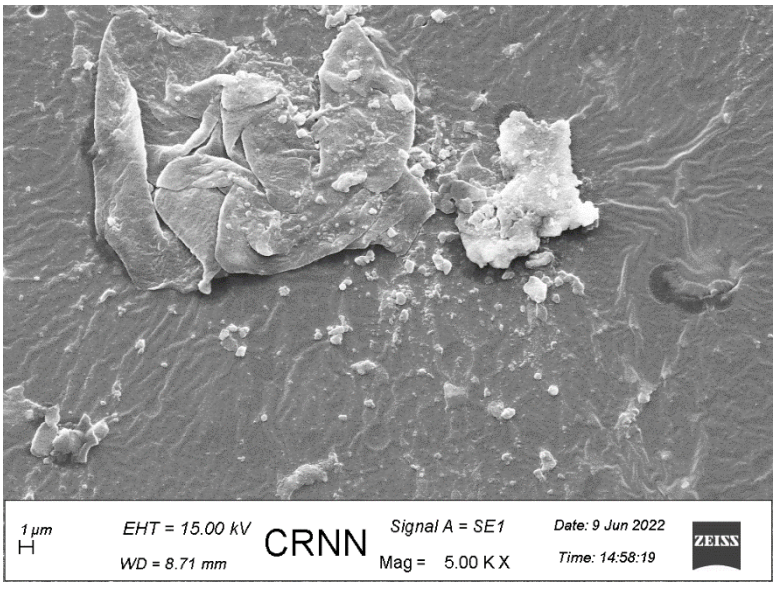

Fig 5A.40. SEM image of the transdermal patch containing CH-loaded base-catalyzed SNPs, A3

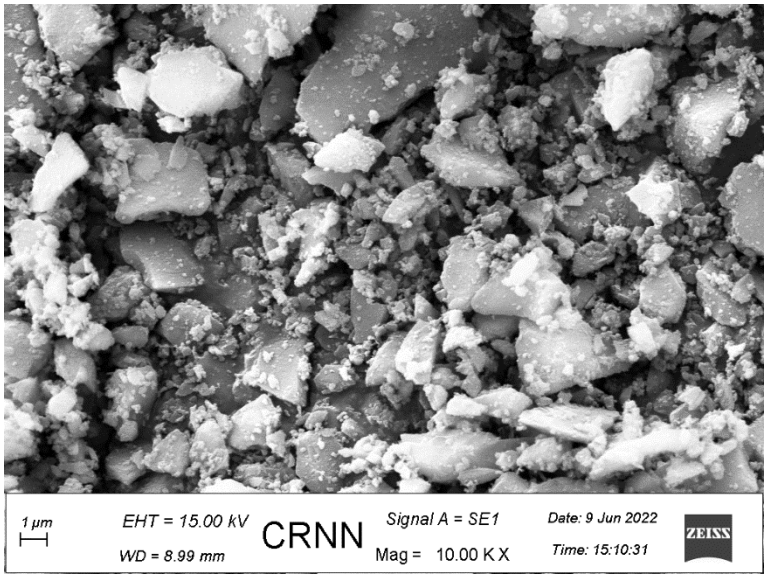

Fig 5A.41. SEM image of the transdermal patch containing free EB, B1

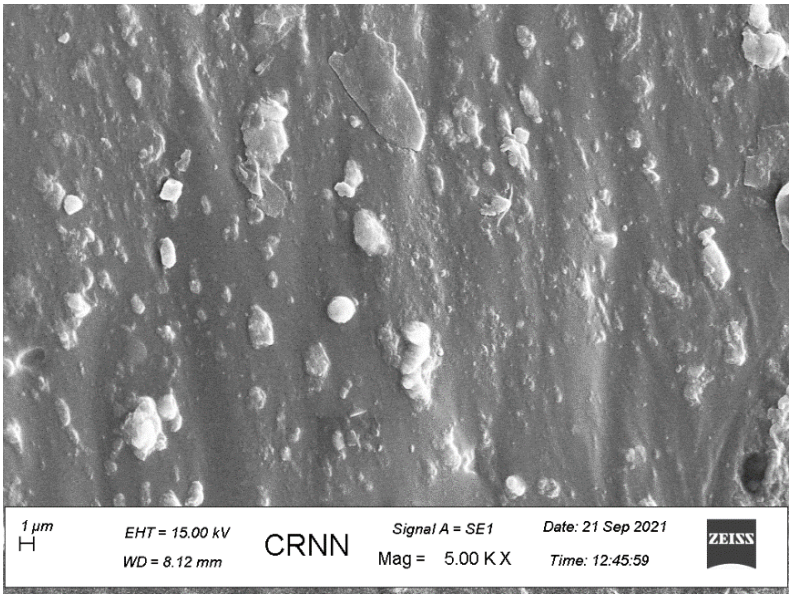

Fig 5A.42. SEM image of the transdermal patch containing EB-loaded acid-catalyzed SNPs, B2

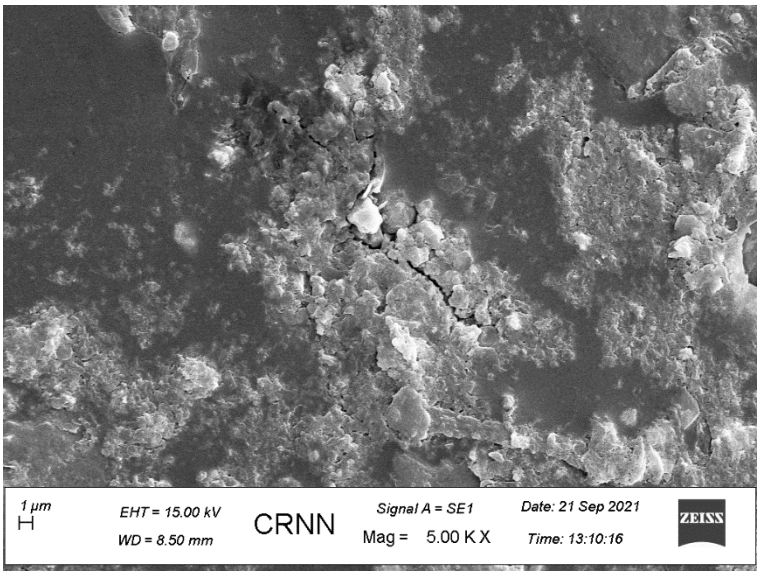

Fig 5A.43. SEM image of the transdermal patch containing EB-loaded base-catalyzed SNPs, B3

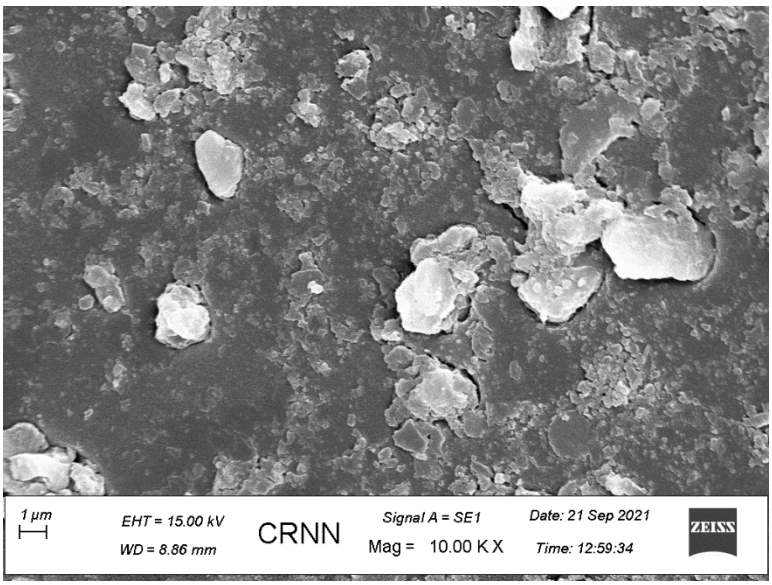

Fig 5A.44. SEM image of the transdermal patch containing free PM, C1

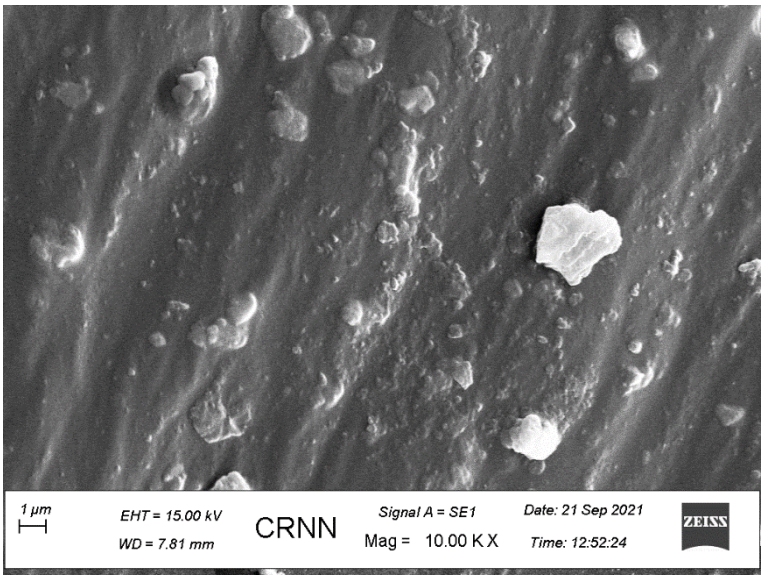

Fig 5A.45. SEM image of the transdermal patch containing PM-loaded acid-catalyzed SNPs, C2

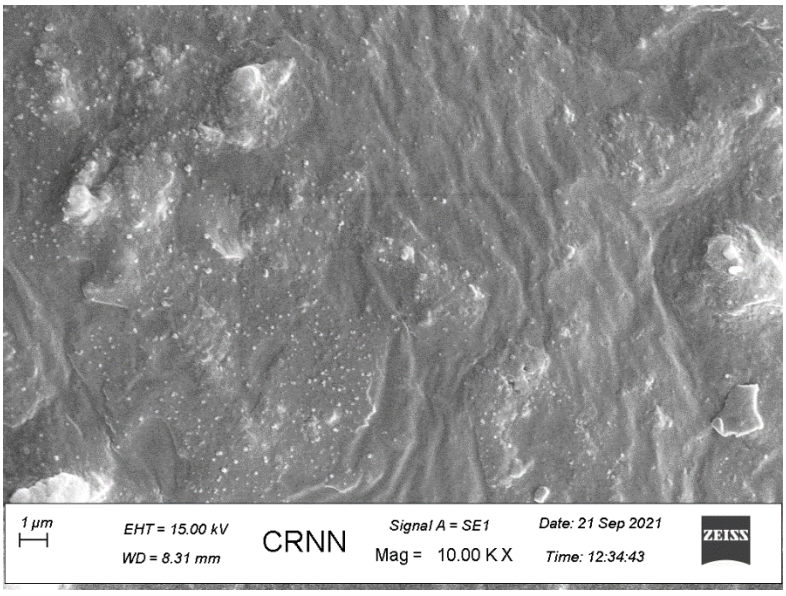

Fig 5A.46. SEM image of the transdermal patch containing PM-loaded base-catalyzed SNPs, C3

5A.2.10. Skin Irritation Study of the Patches:

Skin irritation can reduce patient comfort and compliance with transdermal patch therapy. Skin irritation study can help to identify any formulation or manufacturing factors that may contribute to skin irritation, such as the choice of adhesive, excipients, or manufacturing processes. Product quality and safety can be improved by addressing these factors.

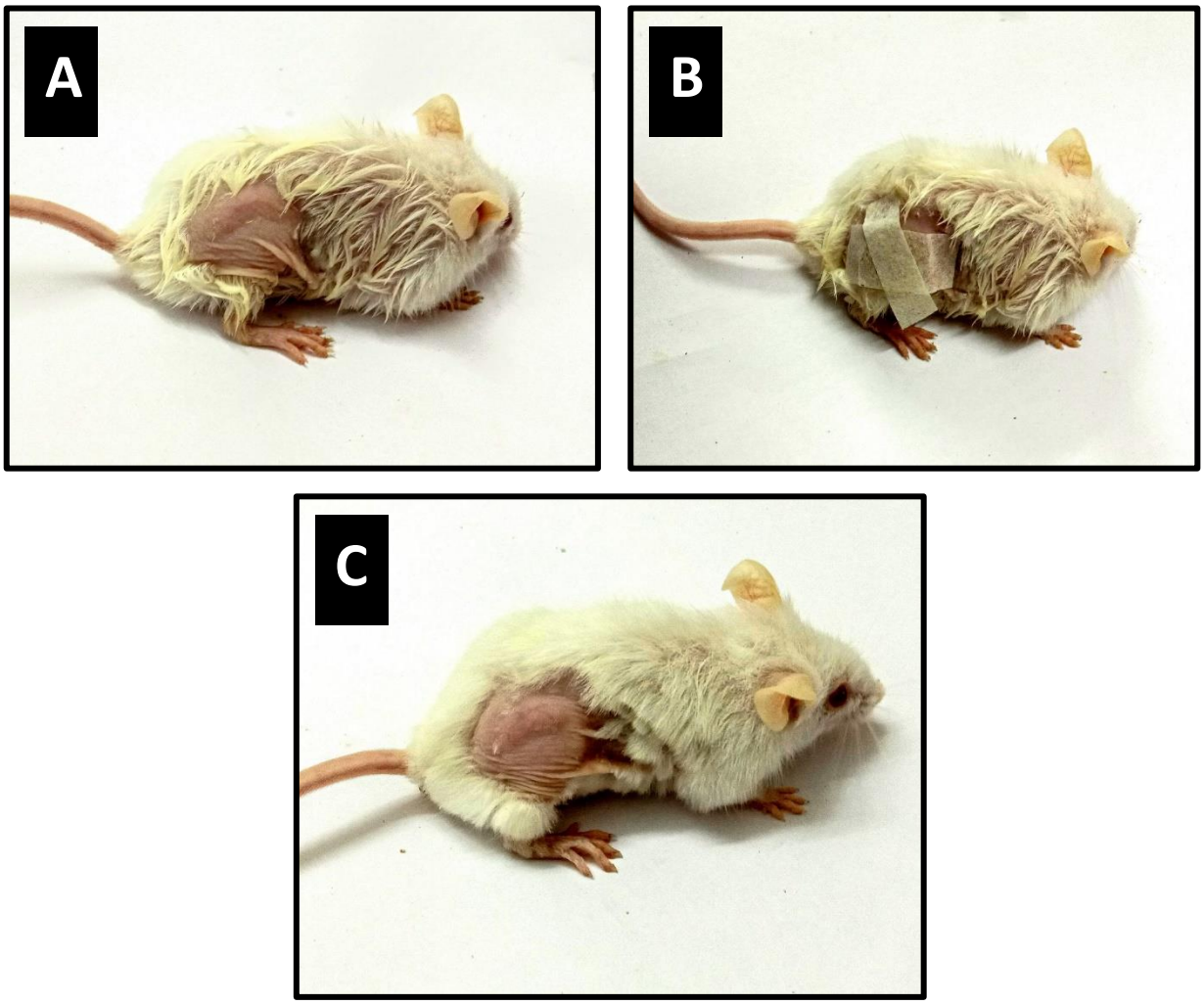

Fig 5A.47. Skin irritation test of the transdermal patches on mice; A) Before application of the patch, B) After application of the patch, and C) After removal of the patch

Skin irritation study (Fig 5A.46) displayed that no erythema (redness and itching) accompanied by edema (swelling) appeared at the application site of the transdermal patches. In the case of

PM patches, a mild erythema reaction (light pink) was observed on the mice skin of each group after 48 h which disappeared within ~5 minutes, but no edema was formed.

5A.2.11. *Ex Vivo* Skin Permeation Study of the Drugs Released from the Patches:

Ex vivo skin permeation studies allow researchers to evaluate the ability of drug molecules to penetrate through the layers of the skin and reach the systemic circulation. This provides vital information about the drug's bioavailability and potential efficacy when delivered via the transdermal route. Also, the researchers can use *ex vivo* skin permeation studies to compare the permeation profiles of different transdermal patch formulations. This allows for the selection of the most promising formulation for further development based on its ability to achieve the desired drug permeation characteristics. In addition, the researchers can design more effective transdermal delivery systems and predict *in vivo* performance by understanding the factors influencing drug transport.

To prepare the transdermal patches, EC and PVP were taken in three different ratios (EC:PVP = 1:1, 2:1 & 3:1) initially in which the ratio of 2:1 was chosen to form the transdermal matrix further (Fig 5A.48). The patches with EC:PVP = 1:1 showed rapid drug release during the *ex vivo* skin permeation study (Fig 5A.47) whereas the matrix with a 3:1 ratio exhibited very slow drug release (Fig 5A.49). The percentages of drug release from transdermal patches decreased with an increase in the ratio of EC to PVP due to several factors. First, EC is known for its ability to form a dense and impermeable film [9]. The increment of the EC to PVP ratio results in the formation of a thicker and more impermeable barrier layer, which may hinder the diffusion of the drug molecules through the patch and into the skin, leading to reduced drug release. Second, PVP is often used in transdermal patches due to its solubilizing and wetting properties, which can enhance the release of drugs from the patch [10]. As the ratio of EC to PVP increases, the amount of PVP available for solubilization decreases. This may result in

reduced swelling of the polymer matrix and decreased solubilization of the drug, leading to slower drug release rates.

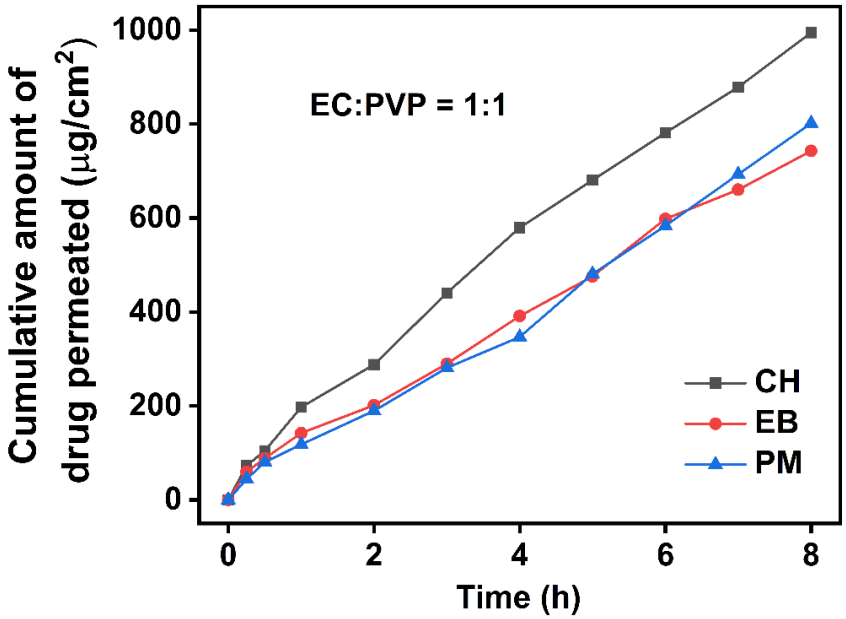

Fig 5A.48. Ex vivo skin permeation study from the free drug-loaded patches having EC:PVP = 1:1

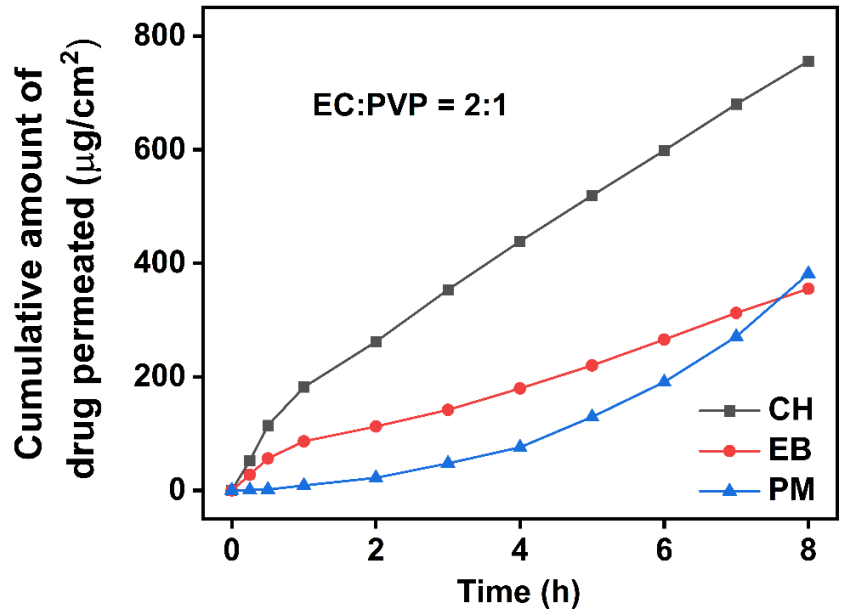

Fig 5A.49. Ex vivo skin permeation study from the free drug-loaded patches having EC:PVP = 2:1

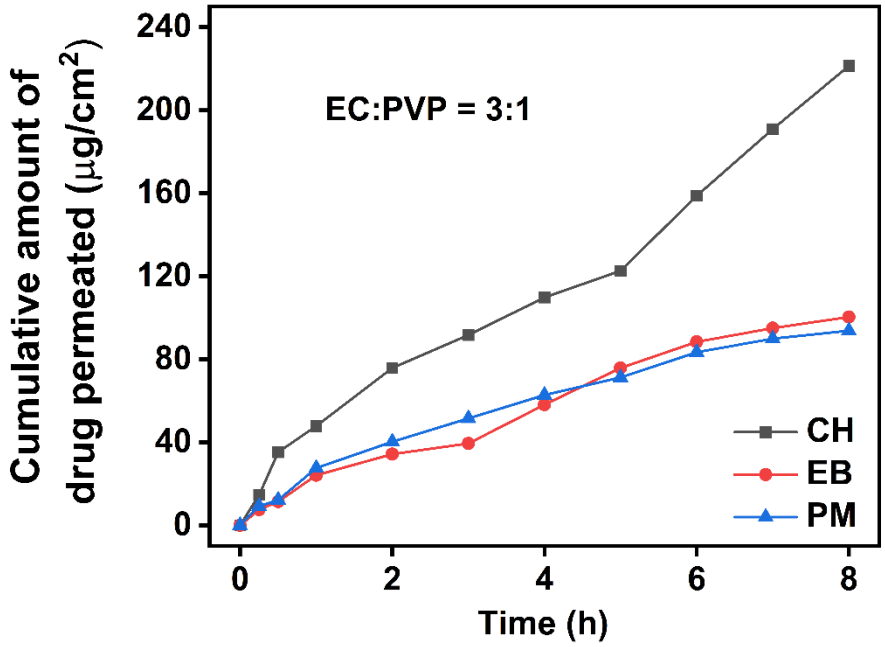

Fig 5A.50. Ex vivo skin permeation study from the free drug-loaded patches having EC:PVP = 3:1

Ex vivo skin permeation study with the patches having EC:PVP=2:1 demonstrated that the cumulative amount of CH permeated per unit area of skin from A1, A2, and A3 formulations (Fig 5A.50) were 904.16±27.59, 464.16±63.16, and 642.50±51.13 μg/cm^2 respectively in first 15 h whereas 1007.50±50.88, 1058.33±81.04, and 1329.17±42.02 μg/cm^2 respectively during 744 h. The steady-state flux (J_{SS}) is obtained by plotting the cumulative amount of drug permeated (μg/cm^2) against time, where the slope is the flux (μg/cm^2.h). The flux for the formulations A1, A2, and A3 were 0.88±0.23, 1.34±0.14, and 1.60±0.18 μg/cm^2.h respectively. On the other hand, the cumulative amount of EB permeated per unit area of skin from B1, B2, and B3 transdermal formulations (Fig 5A.51) were 526.25±65.14, 788.75±101.22, and 1055.62±92.19 μg/cm^2 respectively in first 15 h whereas 1160.62±94.12, 1604.37±83.18, and 1750.62±125.03 μg/cm^2 respectively during 744 h. The J_{SS} values for the formulations B1, B2, and B3 were 1.20±0.15, 1.99±0.66, and 2.15±0.30 μg/cm^2.h respectively. The cumulative amount of PM permeated per unit area of skin from C1, C2, and C3 formulations (Fig 5A.52)

were 1496.13±142.189, 4284.77±143.178, and 6394.42±163.389 μg/cm^2 respectively in the first 15 h whereas 1846.97±172.013, 5591.03±164.414, and 7733.58±122.017 μg/cm^2 respectively during 168 h. The J_{SS} values for the formulations C1, C2, and C3 were found to be 11.98±1.21, 34.137±0.79, and 46.682±0.44 μg/cm^2.h respectively. The skin permeation study helped to understand the formulations' ability to deliver the amount of drug, required to achieve therapeutic effects through the skin barrier. Owing to the particle size between 90-250 nm, the SNPs might be able to permeate the skin barrier efficiently, especially through hair follicles and sweat glands with encapsulated drug molecules. Although the intercellular route is the direct and fast pathway to penetrate stratum corneum (SC), it is hypothesized that the diffusion between cells for rigid-like nanocarriers is somewhat hindered due to their lack of flexibility [5]. SNPs are often composed of silicon dioxide (SiO_2), which forms a rigid and stable structure. At the nanoscale, they can maintain this rigidity, especially if they are synthesized to have a well-defined crystalline or amorphous structure. The strong covalent bonds between silicon and oxygen atoms contribute to the rigidity of the silica nanoparticle matrix. Surface modifications or coatings can impart flexibility to SNPs by introducing organic moieties or altering the surface charge. Hence, SNPs often choose the shunt route (i.e., hair follicles and sweat glands) to penetrate the skin. Thus, many drug molecules as nanomedicine permeated through the skin barrier from the formulations A2, A3, B2, B3, C2 and C3 and dissolved in PBS buffer (pH 7.4). A3, B3, and C3 showed a higher percentage of drug release than A2, B2, and C2 respectively, which was in good agreement with the *in vitro* drug release results.

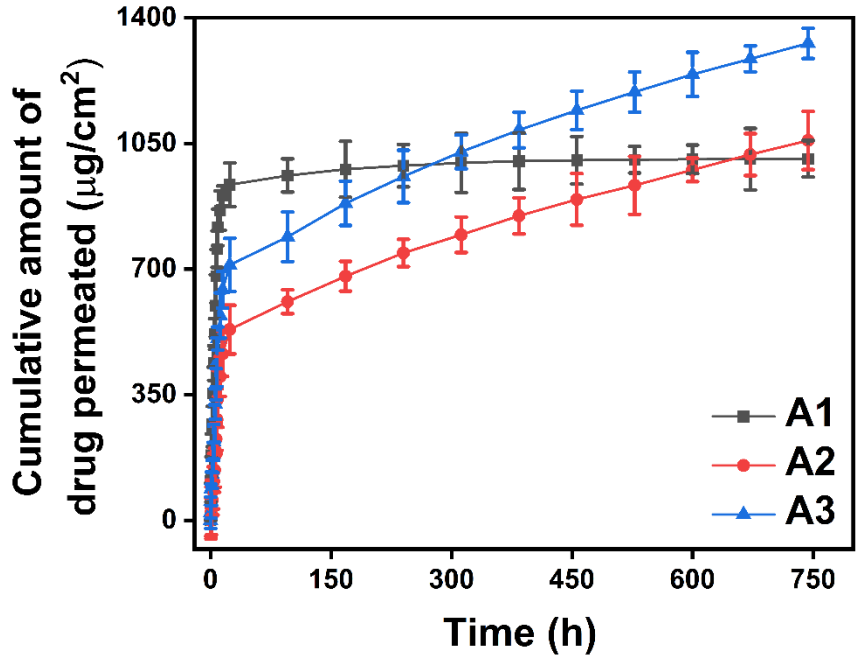

Fig 5A.51. Ex vivo skin permeation study for CH transdermal formulations. The results were expressed as mean ± S.D, n=3

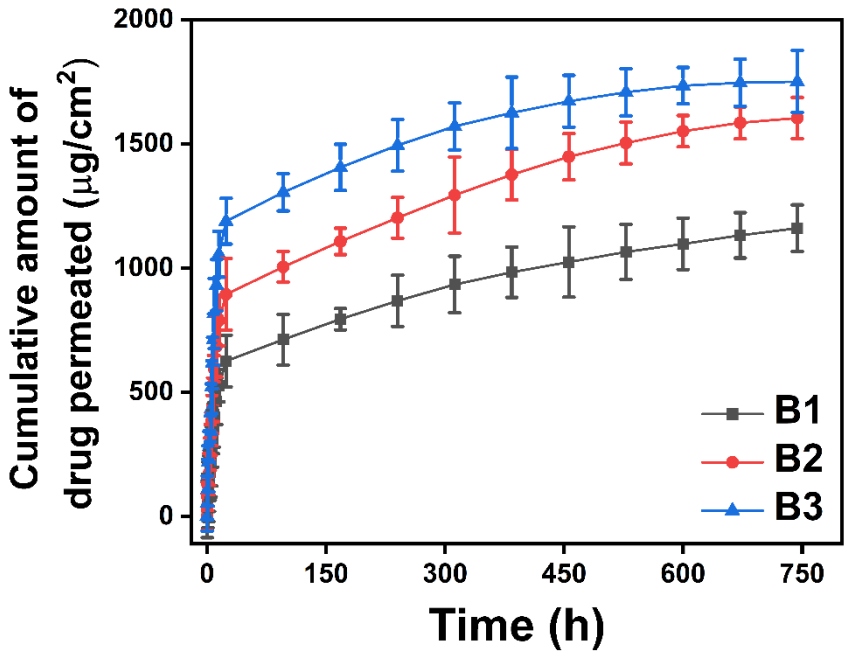

Fig 5A.52. Ex vivo skin permeation study for EB transdermal formulations. The results were expressed as mean ± S.D, n=3

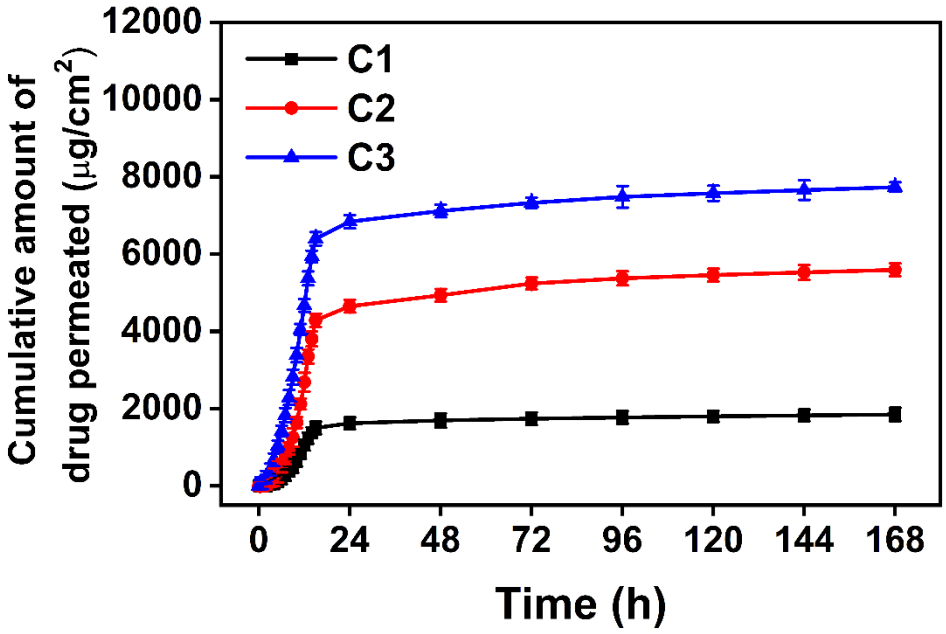

Fig 5A.53. Ex vivo skin permeation study for PM transdermal formulations. The results were expressed as mean ± S.D, n=3

5A.2.12. *Ex Vivo* Drug Release Kinetic Study:

Drug release kinetic models serve as predictive tools to estimate and forecast the release behaviour of drugs from various dosage forms. Researchers can identify optimal formulation parameters to achieve desired release profiles, such as sustained or controlled release by fitting experimental data to mathematical models. Moreover, the researchers can quantitatively compare release profiles and evaluate the performance of various formulations in terms of duration, and mechanism. The R^2 value (regression coefficient) was used as the goodness of fit parameter to evaluate the suitable drug release kinetic model associated with *ex vivo* skin permeation (Tables 5A.3 and 5A.4).

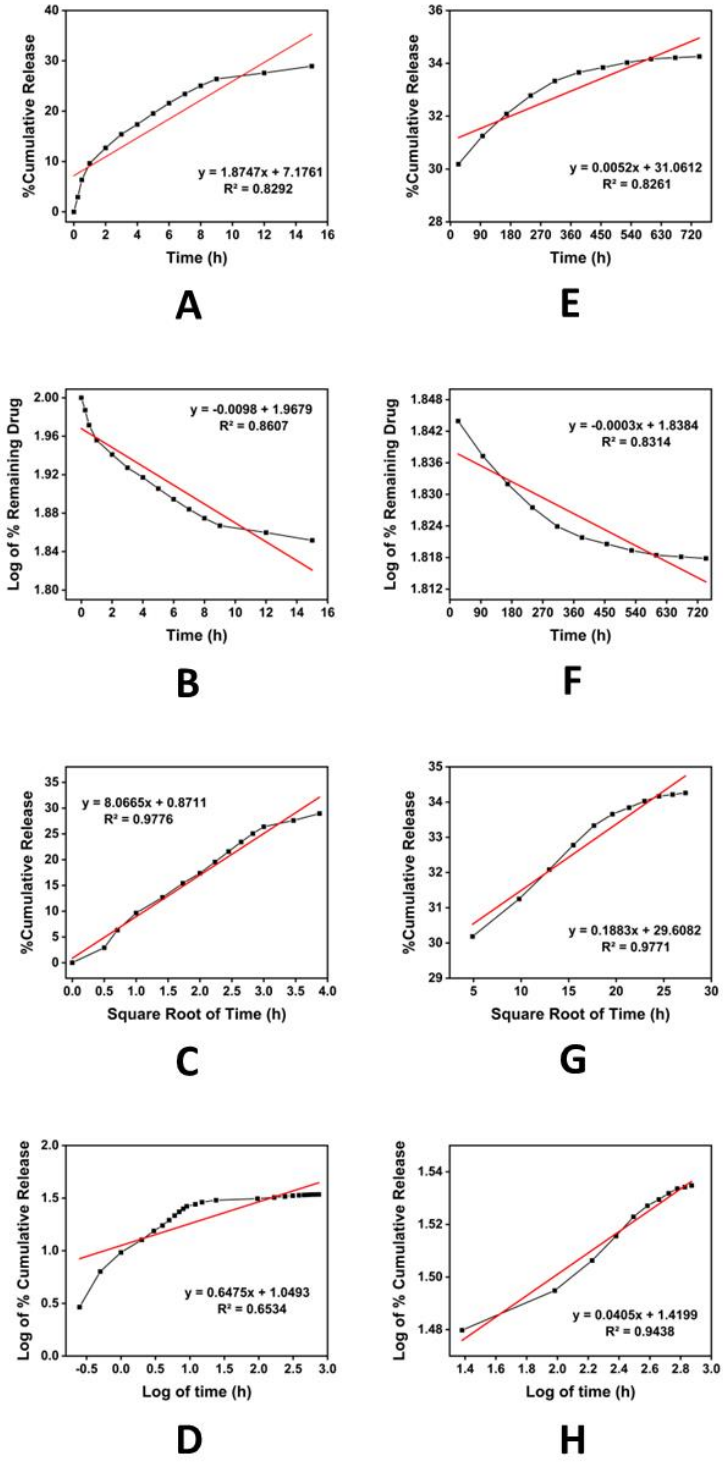

Fig 5A.54. Ex vivo drug release kinetic study of the CH-transdermal formulation A1; A) zero order during burst release. B) first order during burst release, C) Higuchi model during burst release, D) Korsmeyer Peppas model during burst release, E) zero order during sustained release. F) first order during sustained release, G) Higuchi model during sustained release, and H) Korsmeyer Peppas model during sustained release

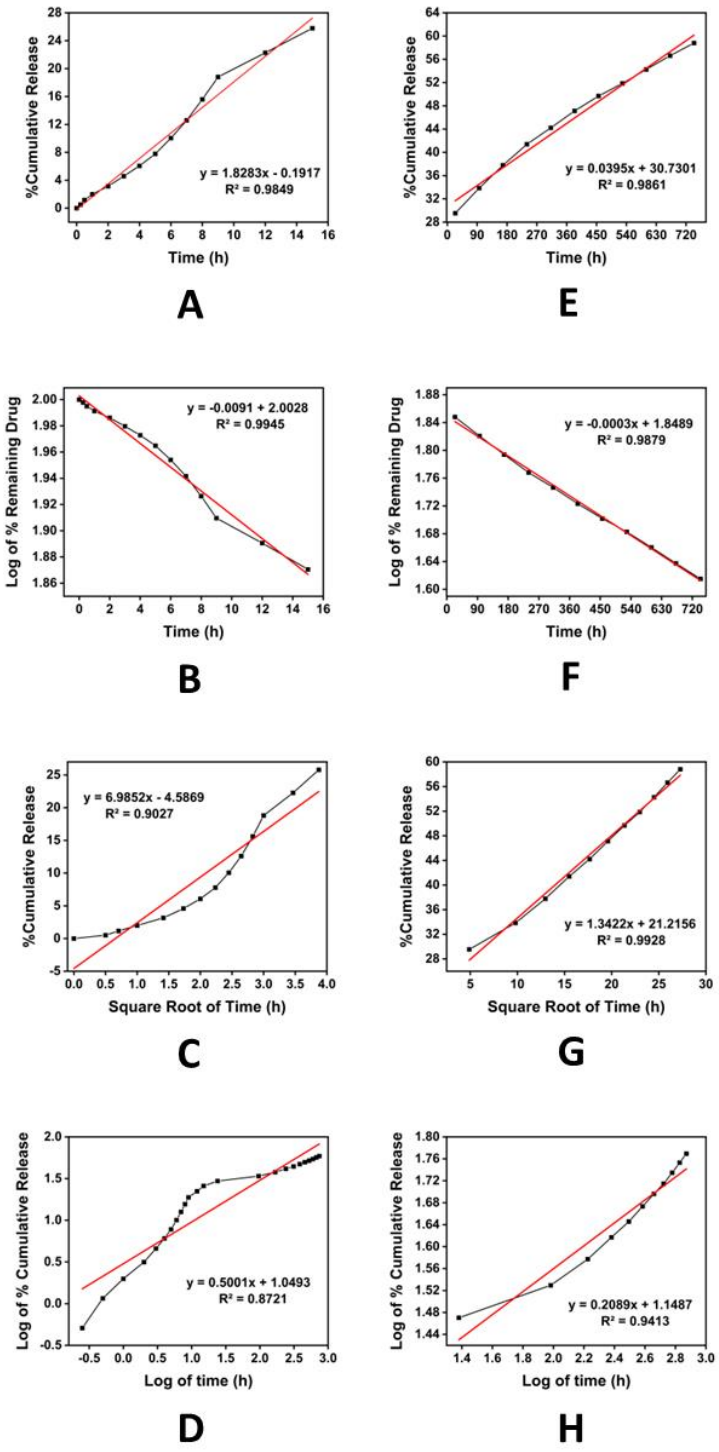

Fig 5A.55. Ex vivo drug release kinetic study of the CH-transdermal formulation A2; A) zero order during burst release. B) first order during burst release, C) Higuchi model during burst release, D) Korsmeyer Peppas model during burst release, E) zero order during sustained release. F) first order during sustained release, G) Higuchi model during sustained release, and H) Korsmeyer Peppas model during sustained release

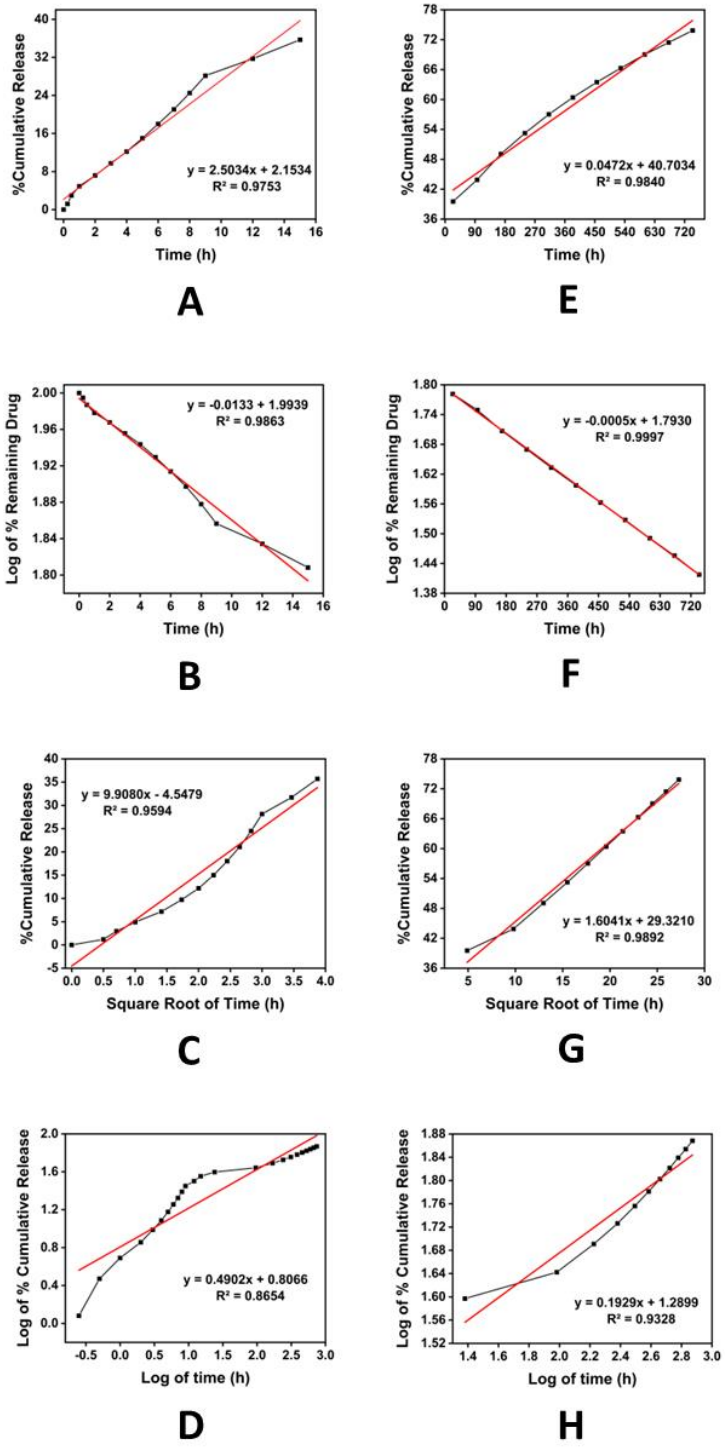

Fig 5A.56. Ex vivo drug release kinetic study of the CH-transdermal formulation A3; A) zero order during burst release. B) first order during burst release, C) Higuchi model during burst release, D) Korsmeyer Peppas model during burst release, E) zero order during sustained release. F) first order during sustained release, G) Higuchi model during sustained release, and H) Korsmeyer Peppas model during sustained release

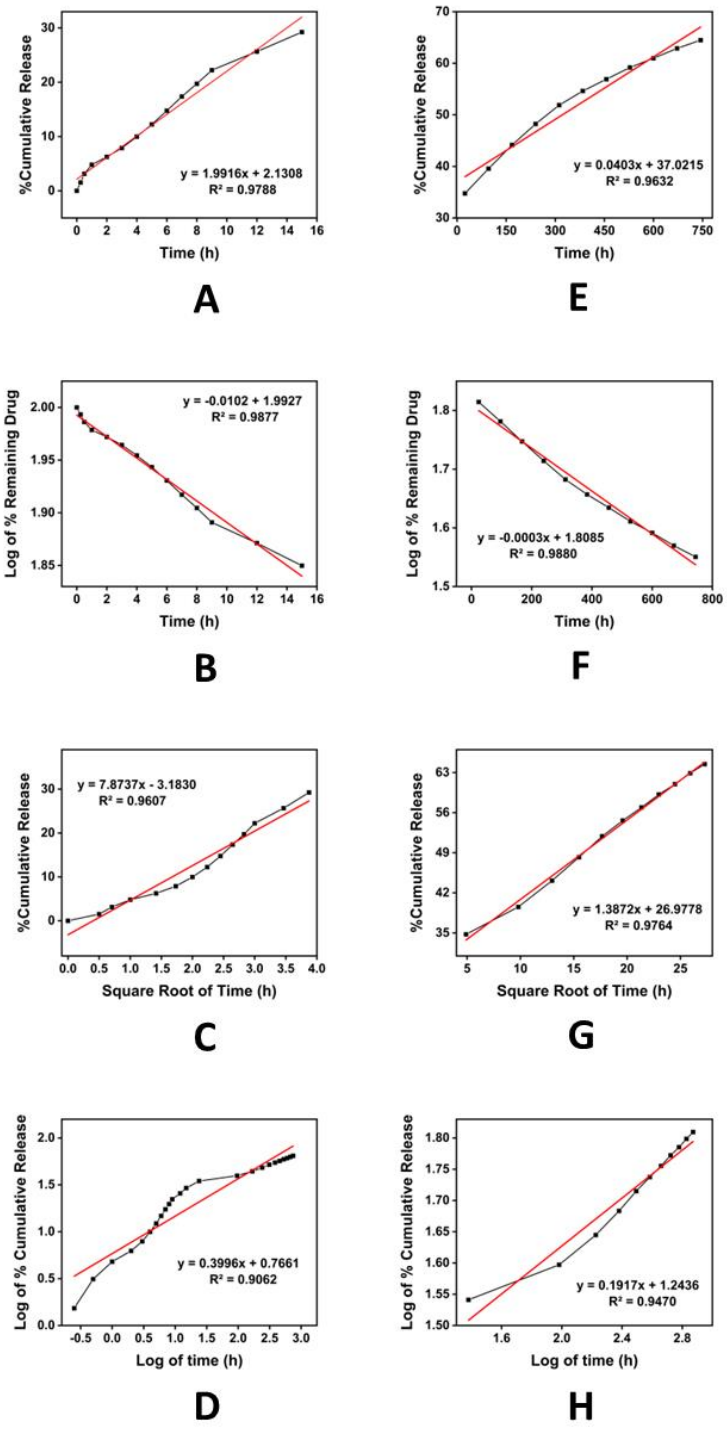

Fig 5A.57. Ex vivo drug release kinetic study of the EB-transdermal formulation B1; A) zero order during burst release. B) first order during burst release, C) Higuchi model during burst release, D) Korsmeyer Peppas model during burst release, E) zero order during sustained release. F) first order during sustained release, G) Higuchi model during sustained release, and H) Korsmeyer Peppas model during sustained release

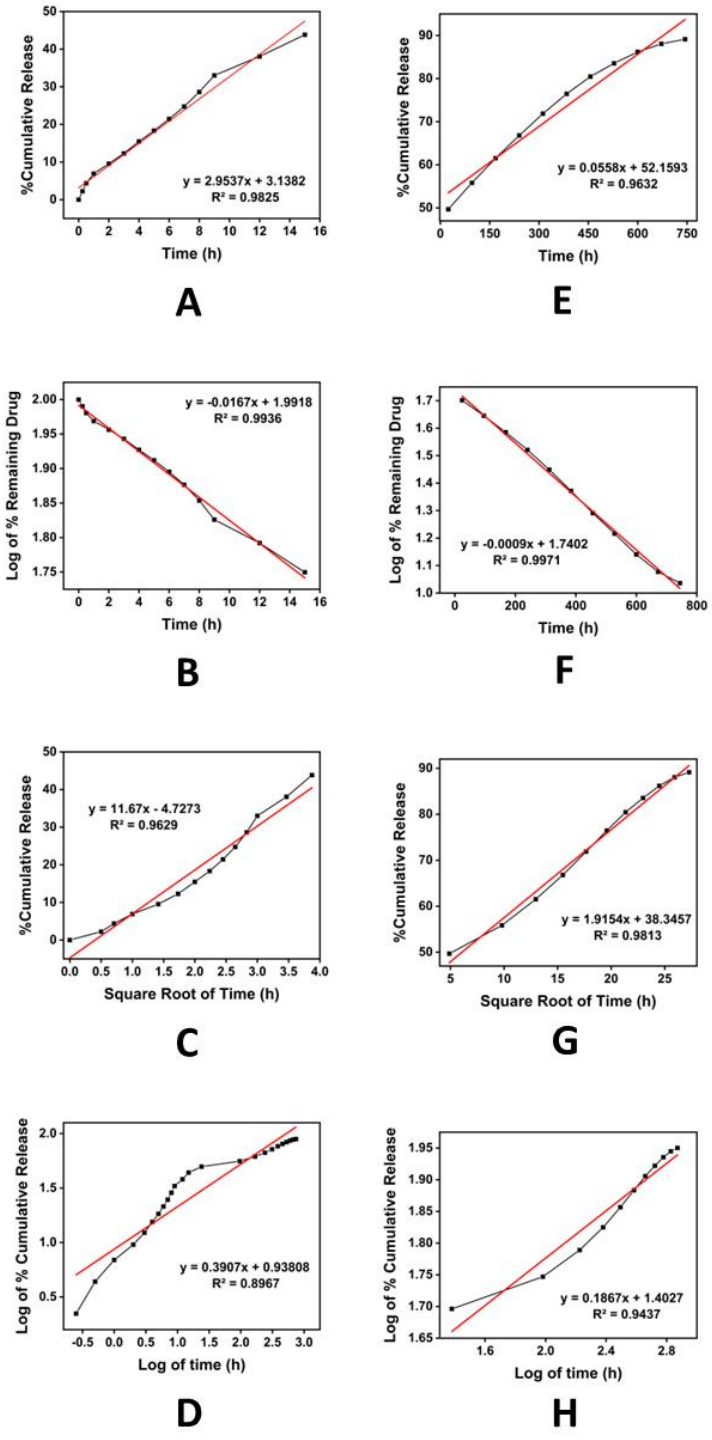

Fig 5A.58. Ex vivo drug release kinetic study of the EB-transdermal formulation B2; A) zero order during burst release. B) first order during burst release, C) Higuchi model during burst release, D) Korsmeyer Peppas model during burst release, E) zero order during sustained release. F) first order during sustained release, G) Higuchi model during sustained release, and H) Korsmeyer Peppas model during sustained release

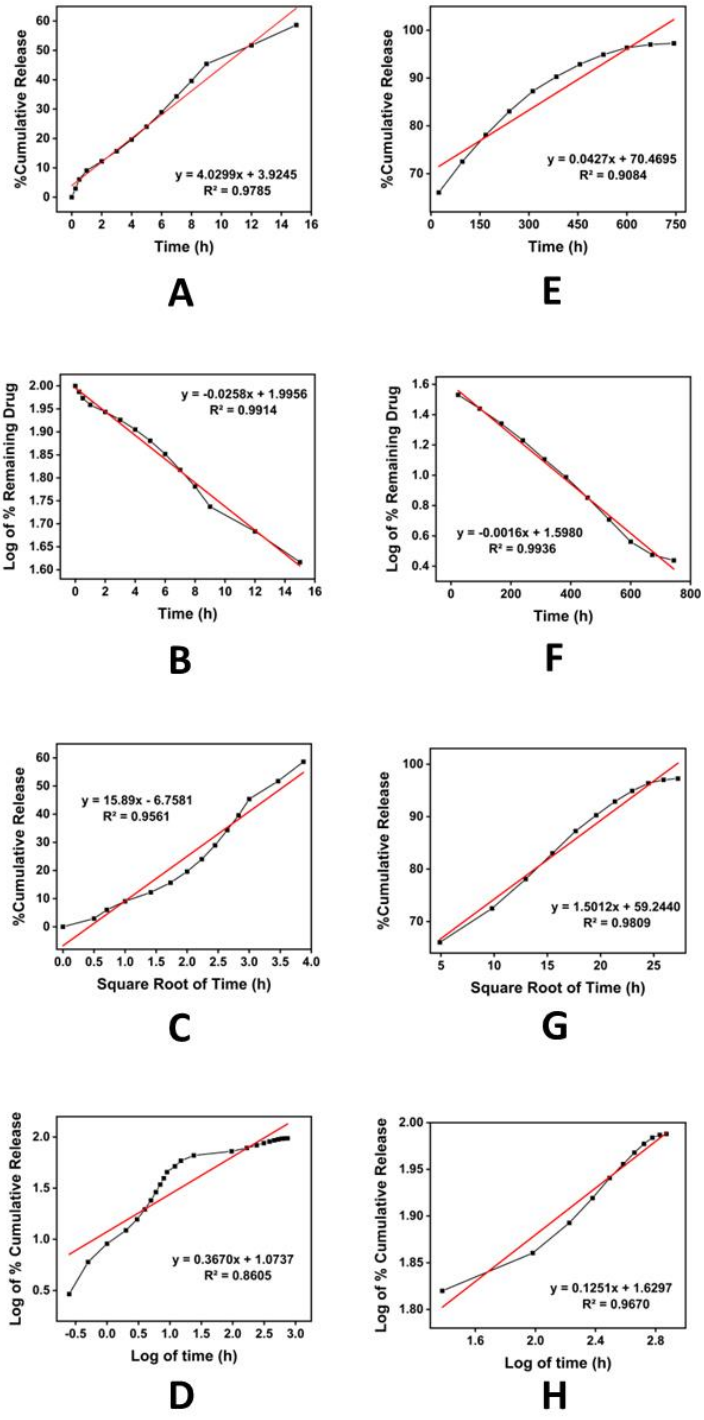

Fig 5A.59. Ex vivo drug release kinetic study of the EB-transdermal formulation B3; A) zero order during burst release. B) first order during burst release, C) Higuchi model during burst release, D) Korsmeyer Peppas model during burst release, E) zero order during sustained release. F) first order during sustained release, G) Higuchi model during sustained release, and H) Korsmeyer Peppas model during sustained release

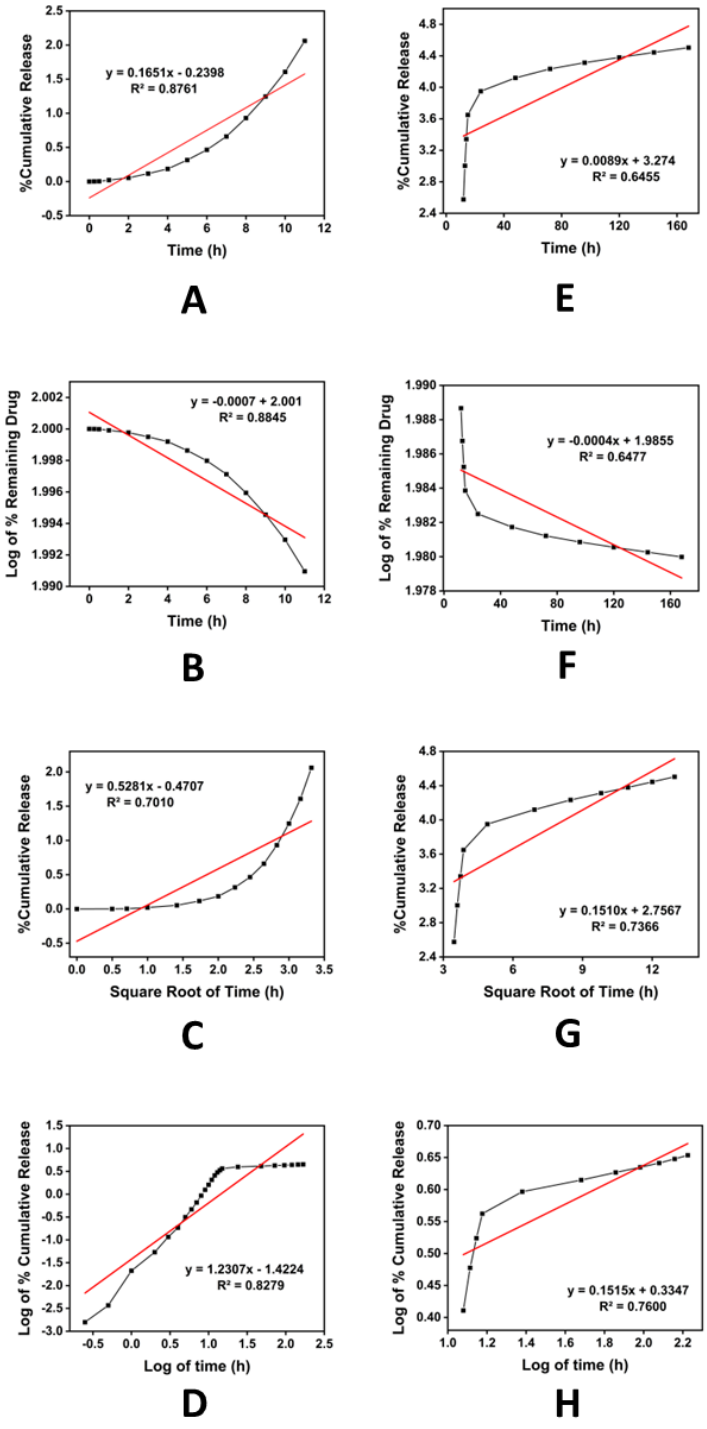

Fig 5A.60. Ex vivo drug release kinetic study of the PM-transdermal formulation C1; A) zero order during burst release. B) first order during burst release, C) Higuchi model during burst release, D) Korsmeyer Peppas model during burst release, E) zero order during sustained release. F) first order during sustained release, G) Higuchi model during sustained release, and H) Korsmeyer Peppas model during sustained release

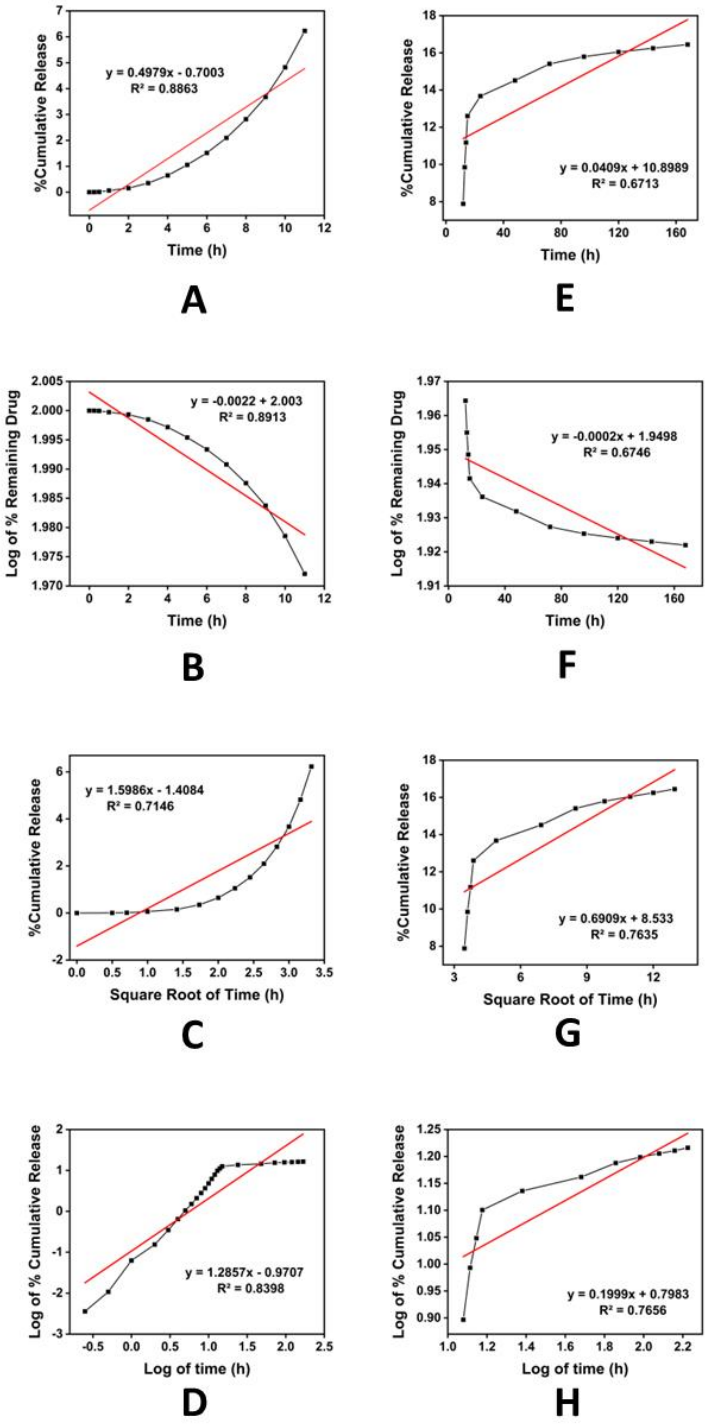

Fig 5A.61. Ex vivo drug release kinetic study of the PM-transdermal formulation C2; A) zero order during burst release. B) first order during burst release, C) Higuchi model during burst release, D) Korsmeyer Peppas model during burst release, E) zero order during sustained release. F) first order during sustained release, G) Higuchi model during sustained release, and H) Korsmeyer Peppas model during sustained release

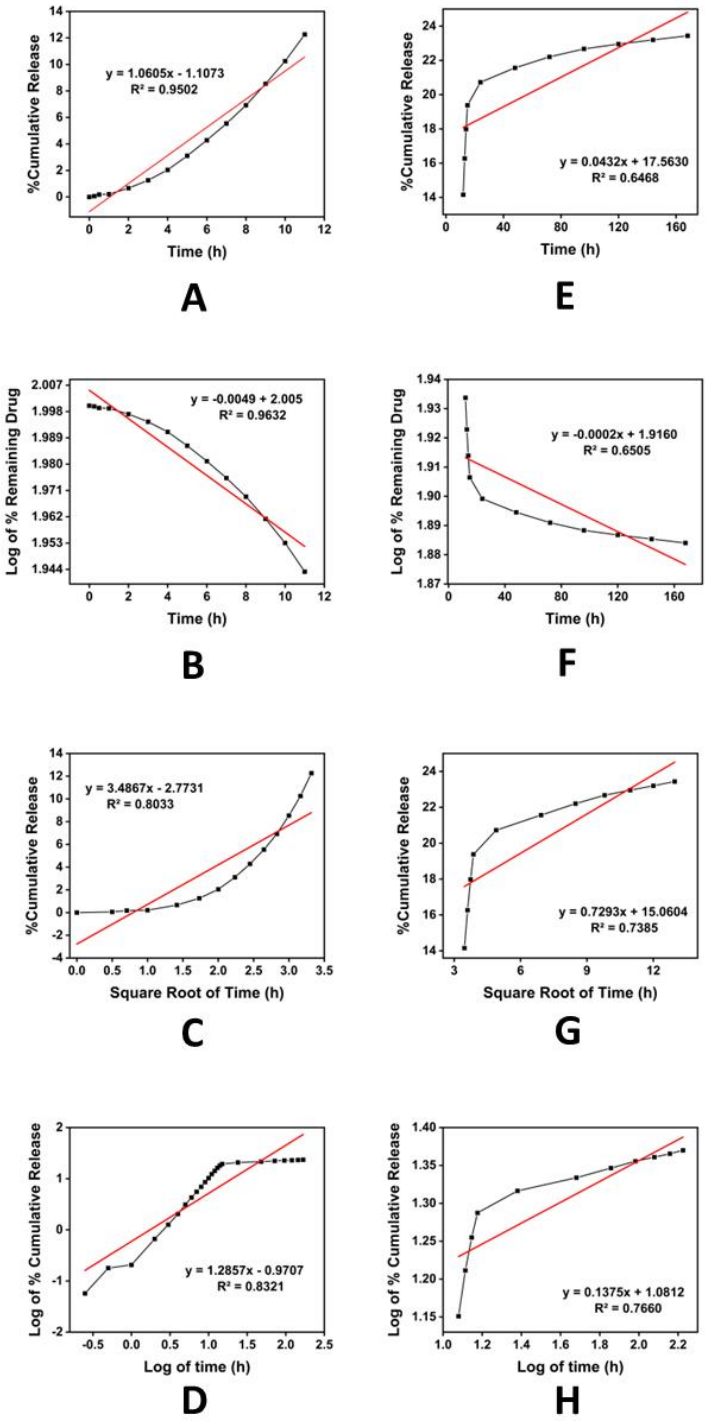

Fig 5A.62. Ex vivo drug release kinetic study of the PM-transdermal formulation C3; A) zero order during burst release. B) first order during burst release, C) Higuchi model during burst release, D) Korsmeyer Peppas model during burst release, E) zero order during sustained release. F) first order during sustained release, G) Higuchi model during sustained release, and H) Korsmeyer Peppas model during sustained release

In the case of CH transdermal formulations, A1 showed fair linearity in Higuchi kinetics during both the burst release phase (for the first 15 h) and the sustained release phase (24-744 h) (Fig 5A.53). A2 and A3 followed first-order kinetics during the burst release whereas they showed combined release kinetics (first-order, Higuchi & zero-order kinetics simultaneously) during the sustained release ((Fig 5A.54-5A.55). Among the EB transdermal formulations, B1, B2, and B3 followed first-order kinetics initially and combined release kinetics (first-order & Higuchi kinetics simultaneously) during the later period (Fig 5A.56-5A.58). Similarly, PM formulations (C1, C2 & C3) followed first-order kinetics during the burst release period whereas combined kinetics (Higuchi & Korsmeyer-Peppas kinetics at a time) during the sustained release period (24–168 h) (Fig 5A.59-5A.61). From the release exponent values (the slope of the Korsmeyer–Peppas equation, Tables 8 and 9), it was established that the release behaviour of CH patches was non-fickian (anomalous) diffusion during the first 15 h. After that, the release followed the fickian diffusion mechanism. EB formulations showed the fickian mechanism throughout the release process for 744 h. The initial release mechanism of PM formulations was super case II transport followed by fickian diffusion during the sustained release phase.

Drug release kinetics can vary for different drug molecules due to several factors related to the physicochemical properties of the drug itself (chemical stability, crystal form, drug-excipient interactions, molecular weight, partition coefficient & solubility), as well as the formulation of the drug delivery system. Among the CH-transdermal patches, A1 followed Higuchi kinetics in both burst and sustained release periods. Higuchi kinetics is primarily controlled by diffusion through a matrix or barrier. Formulations containing high molecular weight polymers, such as ethylcellulose (EC) tend to exhibit Higuchi kinetics. These polymers form dense matrices that impede drug diffusion, resulting in a sustained release profile. Due to the low dose of CH, the amount of the CH molecules adsorbed on the SNP surface was very low. This is why, the A1

formulation was not able to exhibit dissolution-controlled first-order kinetics in both the burst and sustained release periods. However, A2 and A3 followed first-order kinetics during the burst release. It may be attributed to the enhanced solubility of CH molecules after entrapment into SNPs. This property might predominate over the dense texture of the transdermal matrix and the low dose of the drug. Hence, the rate of drug release was primarily governed by the dissolution rate of the drug from the formulations. On the other hand, A2 and A3 exhibited combined release kinetics (first-order, Higuchi, and zero-order) during the sustained release phase which means the overall drug release profile was influenced by multiple mechanisms simultaneously. The drug release was controlled by diffusion through the matrix (Higuchi kinetics) and dissolution (first-order kinetics). Additionally, the release rate might be relatively constant over time (zero-order kinetics). Due to the higher dose of EB compared to CH, all three formulations of EB were stuck into first-order kinetics during the initial period of drug release because the release rate might be dependent on the amount of the drug adsorbed on the SNP surface (dissolution-controlled). These EB patches followed a combined release kinetics (first-order and Higuchi kinetics) after the burst release phase which implied the drug release was driven by unidirectional diffusion through the matrix along with the dissolution of the remainder adsorbed on the SNP surface. Like EB patches, PM patches also adhered to the first-order kinetics during the first 15 h due to the high dose (dissolution-controlled). Moreover, the lower molecular weight of PM (M.W. = 151.16 g/mole) compared to CH (M.W. = 266.60 g/mole) and EB (M.W. = 358.84 g/mole) contributed to the first-order kinetics because smaller PM molecules released more rapidly than any larger molecules. After that, a combination of Higuchi and Korsmeyer-Peppas kinetics was followed by those PM patches which indicated there were no PM molecules left on the SNP surface for dissolution during the sustained release period. The drug release was dominated by diffusion through the matrix involving non-fickian transportation such as relaxation or swelling of the polymeric chain.

CH molecules were released via non-fickian (anomalous) mechanism initially which signified that the magnitude of the solvent diffusion velocity and polymer relaxation was similar. During the sustained release, CH diffused out via fickian mechanism implying the molecular diffusion driven by the chemical potential gradient. EB patches showed fickian release mechanism throughout the release process that carried the same significance mentioned above. The release mechanism was super case II transport during the burst release period for PM patches which meant that the velocity of solvent diffusion was too high leading to polymer disentanglement and erosion [11]. In the later period, PM molecules diffused out due to the chemical potential gradient [12].

Table 5A.3. *Ex vivo* release kinetic study of three drugs from SNP-impregnated transdermal formulations during the burst release period

Formulations	Zero-order (R^2)	First Order (R^2)	Higuchi model (R^2)	Korsmeyer-Peppas model (R^2)	Korsmeyer-Peppas model (n)	Release mechanism
A1	0.82929	0.86075	0.97763	0.65343	0.64757	Non-Fickian (Anomalous)
A2	0.9849	0.9945	0.9027	0.8721	0.5001	Non-Fickian (Anomalous)
A3	0.9753	0.9863	0.9594	0.8654	0.4902	Non-Fickian (Anomalous)
B1	0.9788	0.9877	0.9607	0.9062	0.3996	Fickian diffusion
B2	0.9825	0.9936	0.9629	0.8967	0.3907	Fickian diffusion
B3	0.9786	0.9914	0.9561	0.8605	0.3670	Fickian diffusion
C1	0.8761	0.8845	0.7010	0.8279	1.2307	Super case II transport
C2	0.8863	0.8913	0.7146	0.8398	1.2857	Super case II transport
C3	0.9502	0.9632	0.8033	0.8321	0.9393	Super case II transport

Table 5A.4. *Ex vivo* release kinetic study of three drugs from SNP-impregnated transdermal formulations during the sustained release period

Formulations	Zero-order (R^2)	First Order (R^2)	Higuchi model (R^2)	Korsmeyer-Peppas model (R^2)	Korsmeyer-Peppas model (n)	Release mechanism
A1	0.82610	0.83149	0.97711	0.94386	0.04055	Fickian diffusion
A2	0.9861	0.9879	0.9928	0.9413	0.2089	Fickian diffusion
A3	0.9840	0.9997	0.9892	0.9328	0.1929	Fickian diffusion
B1	0.9632	0.9880	0.9764	0.9470	0.1917	Fickian diffusion
B2	0.9632	0.9971	0.9813	0.9437	0.1867	Fickian diffusion
B3	0.9084	0.9936	0.9809	0.9670	0.1251	Fickian diffusion
C1	0.6455	0.6477	0.7366	0.7600	0.1515	Fickian diffusion
C2	0.6713	0.6746	0.7636	0.7656	0.1999	Fickian diffusion
C3	0.6468	0.6505	0.7385	0.7660	0.1376	Fickian diffusion

5A.2.13. *In Vivo* Analgesic Study via Hot-Plate and Tail-Flick Methods:

The hot-plate and tail-flick assays are well-established methods for evaluating analgesic activity in laboratory animals, providing reliable measures of pain sensitivity and response to analgesic drugs. These methods mimic aspects of acute pain, which is relevant to several types of pain conditions experienced by patients. Researchers can infer the potential effectiveness of transdermal patches in providing relief for acute pain in humans by assessing analgesic efficacy in animal models using these methods.

During *in vivo* analgesic activity via both hot plate and tail flick methods, the highest latency of response in mice was observed for those transdermal formulations in which SNPs acted as nano drug reservoirs and permeation enhancers for a long time (A2, A3, B2, B3, C2 & C3). B1 and C1 formulations showed reactivity almost the same as saline (Fig 5A.64-5A.67) whereas A1 performed (Fig 5A.62-5A.63) well for around 4 days beyond which its reactivity decreased down gradually.

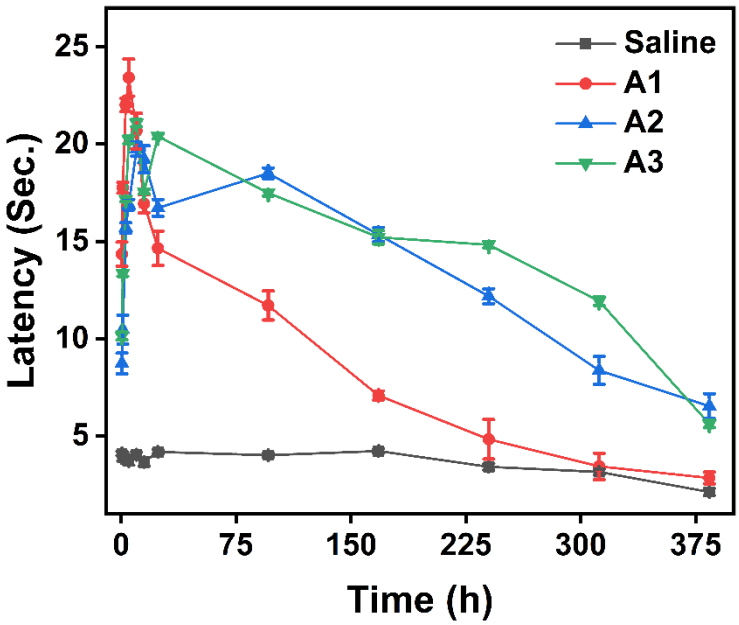

Fig 5A.63. In vivo analgesic study via the "Hot-Plate method" of CH released from three different formulations of transdermal patches on mice. The results were expressed as mean ± S.D, n=3

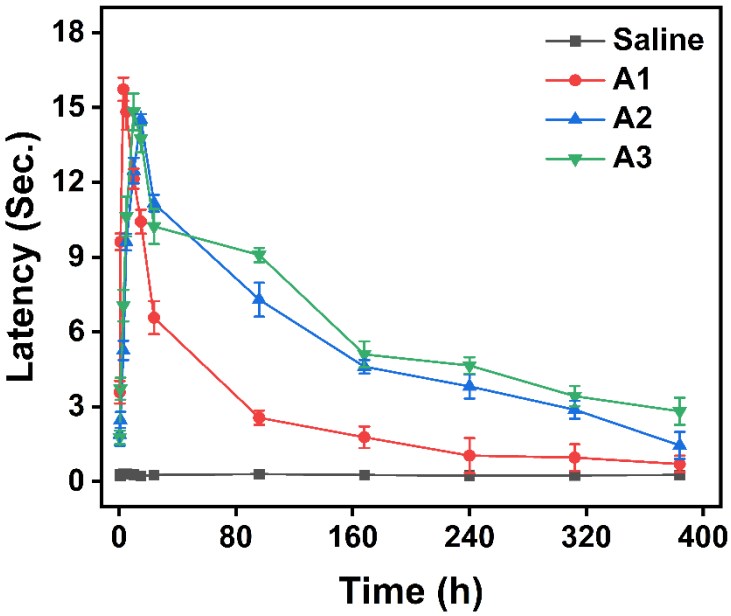

Fig 5A.64. In vivo analgesic study via the "Tail-Flick method" of CH released from three different formulations of transdermal patches on mice. The results were expressed as mean ± S.D, n=3

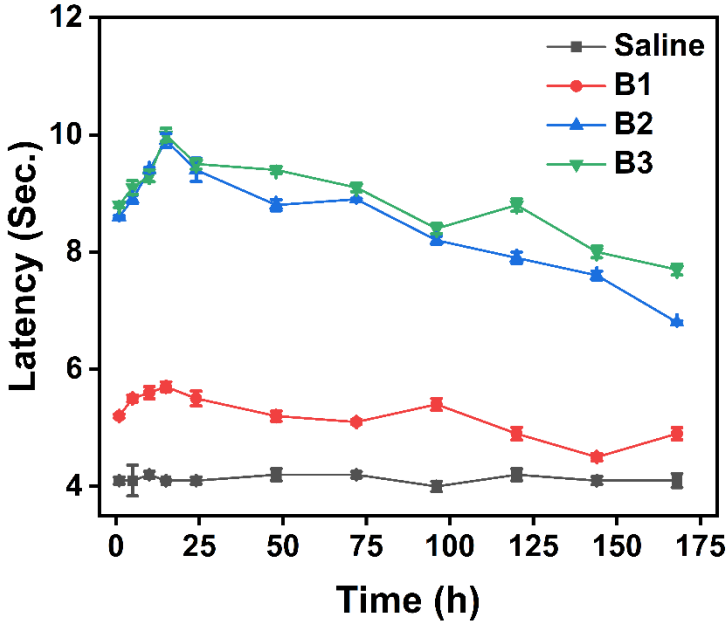

Fig 5A.65. In vivo analgesic study via the "Hot-Plate method" of EB released from three different formulations of transdermal patches on mice. The results were expressed as mean ± S.D, n=3

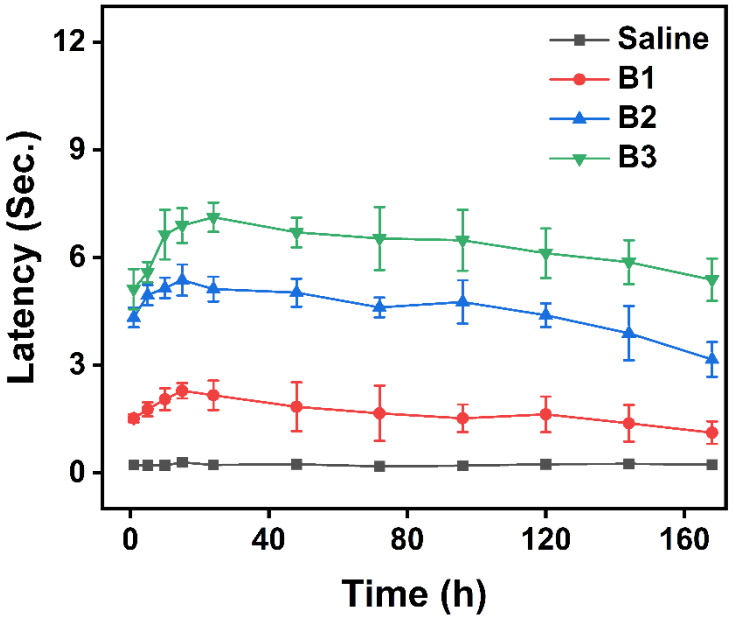

Fig 5A.66. In vivo analgesic study via the "Tail-Flick method" of EB released from three different formulations of transdermal patches on mice. The results were expressed as mean ± S.D, n=3

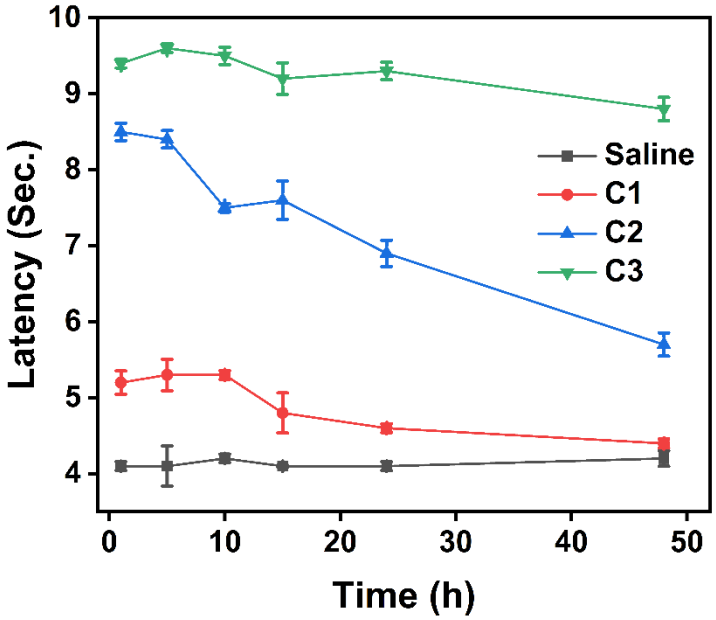

Fig 5A.67. In vivo analgesic study via the "Hot-Plate method" of PM released from three different formulations of transdermal patches on mice. The results were expressed as mean ± S.D, n=3

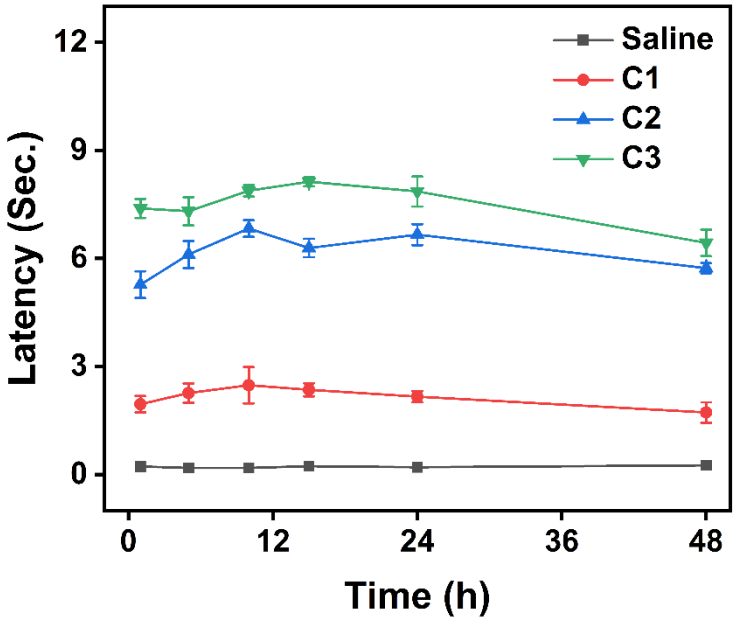

Fig 5A.68. In vivo analgesic study via the "Tail-Flick method" of PM released from three different formulations of transdermal patches on mice. The results were expressed as mean ± S.D, n=3

The responses obtained from *in vivo* analgesic activities (hot plate & tail-flick method) were quite fitted with the results of *in vitro* as well as *ex vivo* drug release studies. In other words, achieving drugs' effective blood plasma concentration for prolonged periods in a single dose using nanomedicine-loaded transdermal formulations might be the reason behind such good responses. The performance of the B1 formulation was poor due to the very low hydrophilicity of EB (0.01 to 0.5 mg/mL) whereas the efficacy of the C1 formulation was inferior due to low hydrophilicity (14.5 mg/mL) and very low lipophilicity (log P = 0.48 to 0.52) of PM molecules. Pure EB molecules could traverse the skin layers to some extent (log P = 2.79) but pure PM molecules were not able to cross the lipid barrier of the skin and dissolve in the blood plasma. Due to the high aqueous solubility (50 mg/ml) and lipophilicity (log P = 2.49) of CH molecules, the A1 patch showed better performance compared to B1 and C1 throughout the experiment.

Conclusions:

1. *In vitro* drug release experiment was conducted for the drugs in two dissolution media of different pH (5.5 and 7.4). The percentage of drug release from base-catalysed SNPs was higher than that from acid-catalysed ones. Furthermore, a higher amount of each drug was released at pH 7.4 compared to pH 5.5. Moreover, the release process became slow and sustained with the decrease in the dose of the drugs.
2. FTIR analysis confirmed the entrapment of the drugs (as free drug molecules and nanomedicines) in the transdermal patches. SEM images showed that the free drug molecules and nanomedicines were homogeneously dispersed in the transdermal matrix.
3. The Skin irritation study revealed that the excipients of prepared transdermal patches did not cause skin irritation, allergy or dermal toxic effects which means the patches might be patient-friendly.
4. *Ex vivo* skin permeation study revealed that a transdermal patch could transport nanomedicine, which effectively penetrates the skin barrier and releases drug molecules for a long time.
5. *In vivo* analgesic studies on mice as well as rats also showed that the permeation of drug molecules released from the patches through skin layers could be enhanced and the effectiveness of the drugs could be extended for a prolonged period with the help of SNPs. It suggested that the effective blood plasma concentration of these drugs might be achieved in humans with the appropriate doses in such transdermal formulations.
6. The kinetic analysis determined the probable mechanisms associated with the drug release from all the transdermal formulations. Apart from the drug release mechanisms, it was observed that the patches with relatively high drug doses (B1, B2, B3, C1, C2, C3) exhibited first-order kinetics during the burst release period followed by the

combination of slow diffusion-controlled Higuchi and Korsmeyer-Peppas model during the sustained release period. However, A2 and A3 followed first-order kinetics during the burst release despite the low dose. It may be attributed to the enhanced solubility of CH molecules after entrapment into SNPs.

Reference:

1. Esposito, S. (2019). " Traditional " Sol-Gel Chemistry as a Powerful Tool for the Preparation of Supported Metal and Metal Oxide Catalysts, 1–25. https://doi.org/10.3390/ma12040668
2. Khan, I., Saeed, K., & Khan, I. (2019, November 1). Nanoparticles: Properties, applications and toxicities. *Arabian Journal of Chemistry*. Elsevier B.V. https://doi.org/10.1016/j.arabjc.2017.05.011
3. Sareen, S., Joseph, L., & Mathew, G. (2012). Improvement in solubility of poor water-soluble drugs by solid dispersion. *International Journal of Pharmaceutical Investigation*, *2*(1), 12. https://doi.org/10.4103/2230-973x.96921
4. Xu, B., & Zhang, Q. (2021). Preparation and Properties of Hydrophobically Modified Nano-SiO2with Hexadecyltrimethoxysilane. *ACS Omega*, *6*(14), 9764–9770. https://doi.org/10.1021/acsomega.1c00381
5. Lambers, H., Piessens, S., Bloem, A., Pronk, H., Finkel, P., & Household, S. L. (2006). *Natural skin surface pH is on average below 5, which is beneficial for its resident flora*. *International Journal of Cosmetic Science* (Vol. 28).
6. Romano, E., Davies, L., & Brandán, S. A. (2017). Structural properties and FTIR-Raman spectra of the anti-hypertensive clonidine hydrochloride agent and their dimeric species. *Journal of Molecular Structure*, *1133*, 226–235. https://doi.org/10.1016/j.molstruc.2016.12.008
7. Das, A., Nayak, A. K., Mohanty, B., & Panda, S. (2011). Solubility and Dissolution Enhancement of Etoricoxib by Solid Dispersion Technique Using Sugar Carriers. *ISRN Pharmaceutics*, *2011*, 1–8. https://doi.org/10.5402/2011/819765
8. Chanda, A. (2015). EVALUATION AND ISOLATION OF NOVEL BINDING AGENT ALSTONIA EVALUATION AND ISOLATION OF NOVEL BINDING AGENT. *World Journal of pharmacy and pharmaceutical sciences*, *4*(04), 1247–1258.

9. Adeleke, O. A. (2019). Premium ethylcellulose polymer based architectures at work in drug delivery. *International Journal of Pharmaceutics: X*, *1*. https://doi.org/10.1016/j.ijpx.2019.100023

10. Kurakula, M., & Rao, G. S. N. K. (2020, December 1). Pharmaceutical assessment of polyvinylpyrrolidone (PVP): As excipient from conventional to controlled delivery systems with a spotlight on COVID-19 inhibition. *Journal of Drug Delivery Science and Technology*. Editions de Sante. https://doi.org/10.1016/j.jddst.2020.102046

11. Fu, Y., & Kao, W. J. (2010, April). Drug release kinetics and transport mechanisms of non-degradable and degradable polymeric delivery systems. *Expert Opinion on Drug Delivery*. https://doi.org/10.1517/17425241003602259

12. Solanki, D., & Motiwale, M. (2020). Studies on Drug Release Kinetics and Mechanism from Sustained Release Matrix Tablets of Isoniazid using Natural Polymer Obtained from Dioscorea Alata. *International Journal of ChemTech Research*, *13*(3), 166–173. https://doi.org/10.20902/ijctr.2019.130313

Chapter: 5B

Drug Delivery by Sodium Montmorillonite Nanoclay (Na-MMT)-Based Transdermal Patch

5B.1. Introduction:

Sodium montmorillonite (Na-MMT) nanoclay was also selected as a nanocarrier for the entrapment of the same three analgesic drugs (CH, EB, and PM) mentioned in previous chapter 6A. Na-MMT was prepared by the modification of purchased montmorillonite clay MMT K 10 with NaCl. Three experimental methods were adopted to produce drug/Na-MMT composites: dispersion, melting, and grinding methods. CH/Na-MMT composites synthesized by dispersion, melting, and grinding methods have been designated as M1, M2, and M3 respectively. EB/Na-MMT composites synthesized by dispersion, melting, and grinding methods have been designated as L1, L2, and L3 respectively. PM/Na-MMT composites synthesized by dispersion, melting, and grinding methods have been designated as G1, G2, and G3 respectively. These drug/Na-MMT composites acted as nanomedicines which were further utilized for the fabrication of the transdermal patches via the solvent-casting method. Besides. a few patches were prepared without nanocarrier keeping the other constituents and amount the same. Free CH drug, M1, M2, and M3 loaded patches have been represented as A1, A4, A5 and A6 respectively. Free EB drug, L1, L2, and L3 loaded patches have been represented as B1, B4, B5, and B6 respectively. Free PM drug, G1, G2, and G3 loaded patches have been represented as C1, C4, C5, and C6 respectively. The formulations were characterized by several characterization techniques such as FTIR, SEM, HR-TEM, and XRD. Two pH values (5.5 and 7.4) were used during *in vitro* drug release study to understand the differences in the release behaviour for all the freshly prepared nanomedicines. Additionally, skin irritation and *ex vivo* skin permeation studies were carried out using the patches. Thereafter, *ex vivo* drug release kinetics analysis was performed to determine the suitable kinetic model and the release mechanism associated with both the burst and sustained release. Furthermore, *in vivo* analgesic studies via hot-plate and tail-flick methods were executed to analyse the performance of the patches. The results obtained from the above experiments have been discussed below.

5B.2. Results and Discussion:

5B.2.1. Drug Loading Capacity and Loading Efficiency of Na-MMT:

Drug loading capacity directly impacts the amount of drug that can be delivered by the system. A higher loading capacity means more drugs can be delivered, potentially leading to improved therapeutic efficacy. High loading capacity can reduce the need for excess excipients, lower production costs, and minimize potential side effects associated with excipient use. Drug loading efficiency measures the proportion of the drug that is successfully incorporated into the delivery system. High efficiency ensures optimal utilization of resources and minimizes waste.

The loading capacity of CH/Na-MMT composites M1, M2, and M3 were 6.783±0.171%. 6.142±0.193%, and 3.057±0.165%, respectively. Meanwhile, the loading efficiency of the same composites was 84.98±0.308%, 79.20±0.349%, and 63.11±0.465%, respectively. In the case of EB/Na-MMT composites, the loading capacity of L1, L2, and L3 was determined to be 5.496±0.222%, 5.218±0.139%, and 4.053±0.181%, respectively whereas the loading efficiency was calculated as 74.59±0.210%, 71.77±0.313%, and 69.23±0.148%, respectively. The loading capacity displayed by PM/Na-MMT composites G1, G2, and G3 was 10.217±0.113%, 5.048±0.179%, and 4.847±0.085%, respectively. The loading efficiency for the same PM/Na-MMT composites was found to be 85.57±0.071%, 81.93±0.119%, and 76.12±0.053%, respectively. The combination of high drug loading efficiency along with reasonable drug loading capacity of all composites resulted in an overall high drug content in the nanoclay-based delivery system. This ensures that a significant proportion of the total weight of the delivery system consists of the drug.

5B.2.2. Importance of pH on the Intercalation of the Drugs into Na-MMT:

The intercalation of drugs into Na-MMT typically involves ion exchange, where cations in the interlayer space of Na-MMT are replaced by the cationic form of the drug molecules. The pH of the solution affects the ionization state of both the drug molecules and the clay mineral, influencing the ion exchange process. The pH can also influence the swelling behaviour and layer spacing of Na-MMT. Changes in pH can alter the hydration state and electrostatic interactions within the clay mineral structure, affecting its ability to accommodate drug molecules between its layers.

In the dispersion method, both CH and PM intercalation were maximum at pH 5.0 (Fig 5B.1 & 5B.3 respectively). In contrast, the intercalation decreased gradually above pH 5.0. Then a rapid drop was observed beyond pH 9.0 for CH and 8.0 for PM (Fig 5B.1 & 5B.3 respectively). On the other hand, maximum EB intercalated at pH 3.0 followed by a gradual decrease above pH 3.0 and a sharp decrease beyond pH 10.0 (Fig 5B.2). Also, there was a decrease in intercalation of each drug below their maximum pH of loading. CH exists as a cationic form below pH 6.5 (pKa of CH = 8.21) and the number of cationic forms increases with a decrease in the pH of the solution. CH remains as an uncharged species mostly at pH 12. The protonation of PM starts below pH 7.4 (pKa of PM = 9.50) and the maximum number of negatively charged species exists beyond 9.50. A significant portion of etoricoxib exists in its cationic form below pH 4.0 (pKa of EB = 4.96). Also, there was a decrease in intercalation below pH 5.0 for CH and PM and below pH 3.0 for EB owing to a competition between the cationic form of drugs and H^+ ions present in the acidic solution as exchangeable ions. Being a smaller ion than cation form of drugs, H^+ ions tend to have higher mobility than larger ones. This is why, more H^+ ions accumulated into the interlayer space of Na-MMT in the strongly acidic pH of the solution.

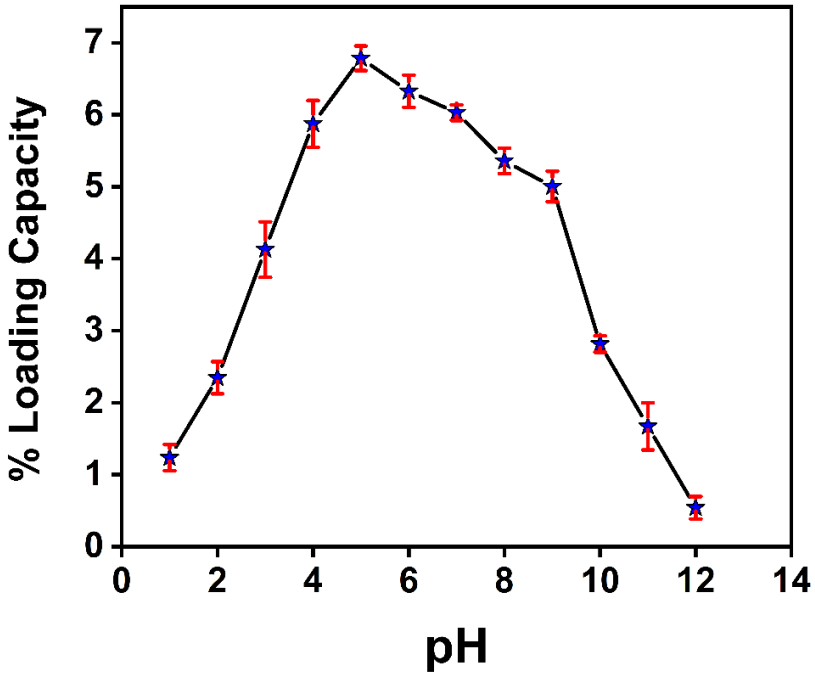

Fig 5B.1. Effect of pH on intercalation of the CH drug into the interlayer space of Na-MMT

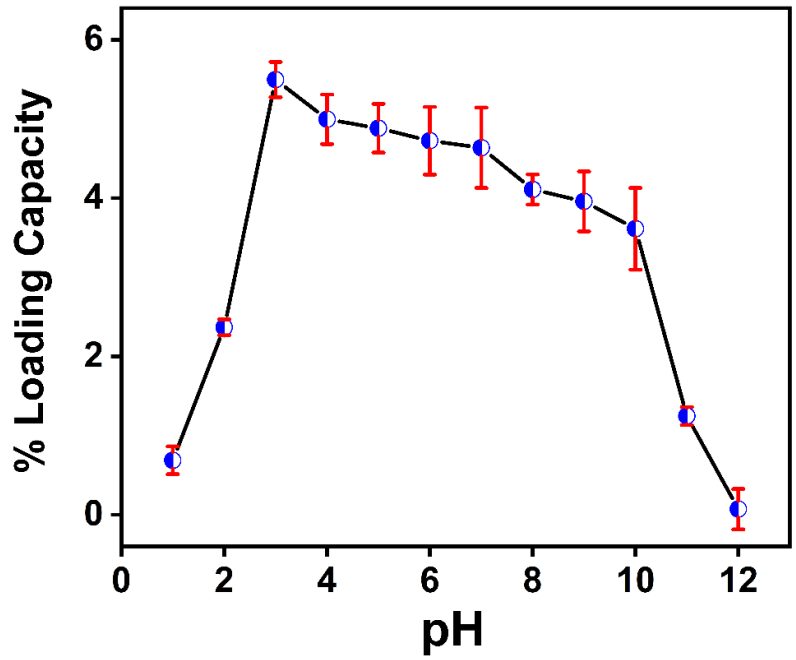

Fig 5B.2. Effect of pH on intercalation of the EB drug into the interlayer space of Na-MMT

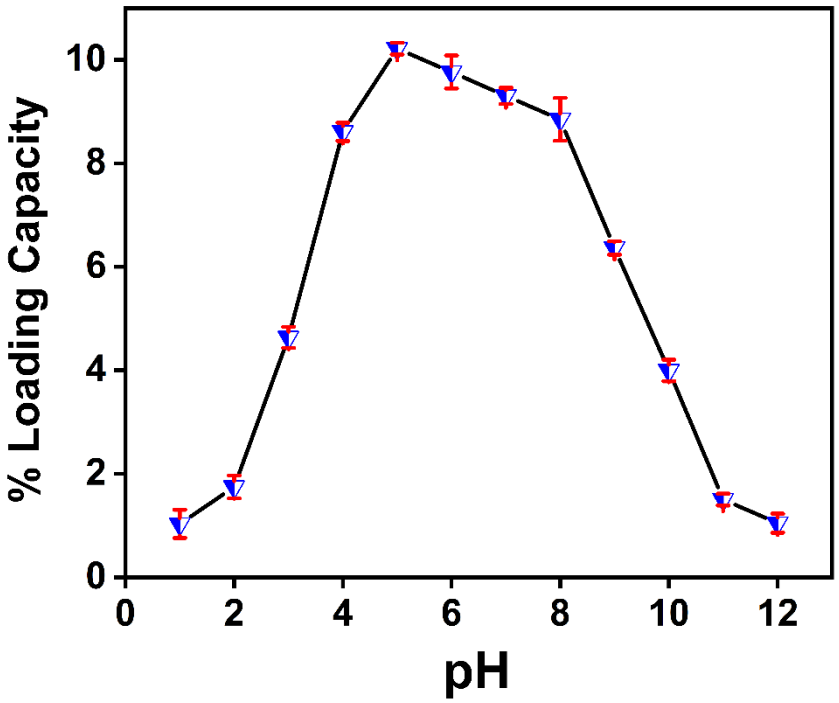

Fig 5B.3. Effect of pH on intercalation of the PM drug into the interlayer space of Na-MMT

5B.2.3. Analysis of XRD Patterns to Confirm the Intercalation of Drugs in Na-MMT:

XRD is a powerful technique used to analyze the crystal structure and composition of materials. In the case of nanoclays, intercalation of the molecules between the layers of the clay mineral leads to changes in the XRD pattern. Specifically, the interlayer spacing of the clay mineral increases upon intercalation. Therefore, XRD analysis can also provide direct evidence of intercalation, detecting the changes in interlayer spacing.

XRD patterns (Fig 5B.4-5B.6) depicted an increment in basal spacing (d-value) after the successful entrapment of the drug into the interlayer space of Na-MMT. The characteristic XRD peak for the (001) plane of pure Na-MMT was observed at 6.91˚ i.e. the value of basal spacing (d) was 1.23 nm whereas M1, M2, and M3 composites showed peaks at 5.08˚, 5.08˚, and 6.45˚ with d-spacing of 1.74, 1.74, and 1.37 nm respectively (Fig 5B.4). The XRD peaks

for L1, L2, and L3 composites were shifted to 6.10˚,6.10˚, and 6.14˚ respectively whose corresponding d-values are 1.45, 1.45, and 1.44 nm respectively (Fig 5B.5). The peaks for G1, G2, and G3 composites appeared at 4.88˚, 4.88˚, and 5.21˚ respectively which corresponds to 1.81, 1.81, and 1.70 nm d-spacing respectively (Fig 5B.6). Bragg's law states that an increase in d-spacing causes the corresponding XRD peak to move from a higher to a lower diffraction angle. Thus, the peak shifting for all the drug/Na-MMT composites implied that the drug molecules were successfully intercalated into the interlayer of Na-MMT. The drug/Na-MMT composites prepared by dispersion and melting methods exhibited similar increments in d-spacing values due to the fundamental principles of intercalation, but they differed in their response to grinding methods due to the lack of specific interactions like ion exchange, adsorption, or diffusion of molten drug molecules into clay layers. Grinding relies solely on mechanical energy. This mechanical energy may not promote the formation of specific interactions between the drug molecules and the clay layers necessary for effective intercalation. As a result, the degree of intercalation achieved by grinding may be limited, leading to a smaller increase in d-spacing value. Besides, grinding typically results in the reduction of particle size and increased surface area of the clay and drug particles. While this may enhance the physical mixing of the components, it does not necessarily translate to a significant increase in interlayer spacing. Instead, the increase in surface area may lead to greater particle-particle interactions and agglomeration, which can inhibit the intercalation of drug molecules between clay layers.

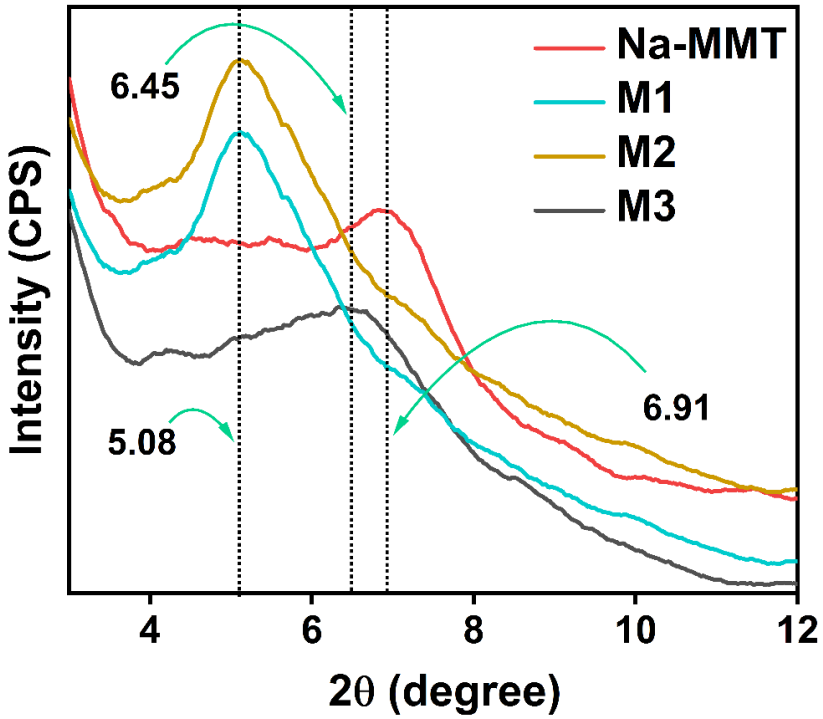

Fig 5B.4. XRD patterns for pure Na-MMT and CH/Na-MMT composites

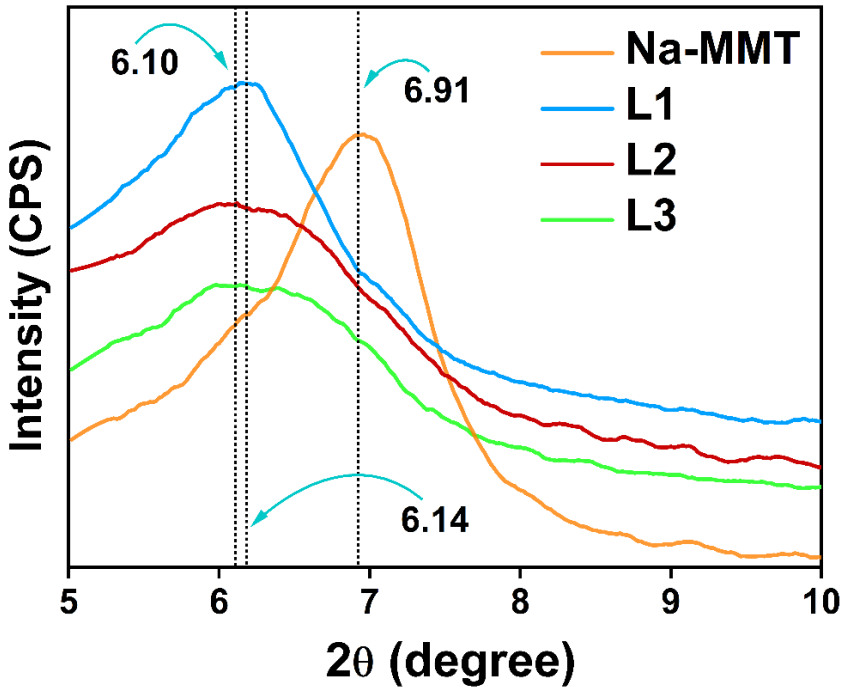

Fig 5B.5. XRD patterns for pure Na-MMT and EB/Na-MMT composites

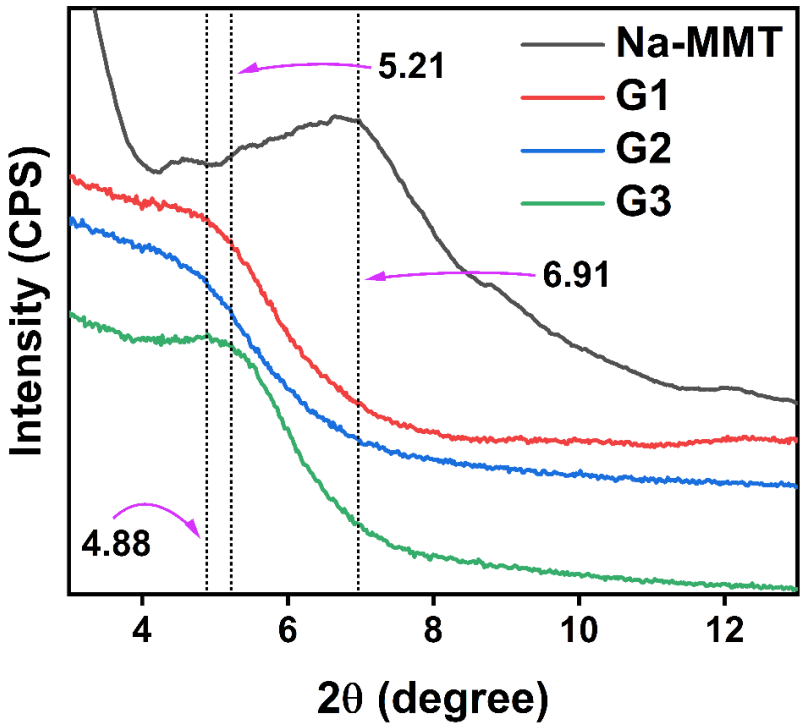

Fig 5B.6. XRD patterns for pure Na-MMT and PM/Na-MMT composites

5B.2.4. Analysis of TEM Images to Confirm the Intercalation of Drugs in Na-MMT:

When studying the intercalation of drugs into nanoclay, TEM can confirm this process by observing changes in the lattice structure of the nanoclay. Nanoclays typically have a layered structure with repeating units arranged in a lattice pattern. If the drugs intercalate into the interlayer spaces of the nanoclay, there may be an observable increment in the spacing between the lattice strips (basal spacing) of the nanoclay compared to the bare nanoclay sample. This increase in basal spacing indicates that additional material has been inserted between the clay layers, which is consistent with intercalation. The results obtained from the XRD analysis mentioned above were quite fitted with the information regarding the change in basal spacing revealed by TEM images. TEM images as shown in Fig 5B.7-5B.16 confirmed the intercalation by showing the enhancement of spacing between two lattice strips which correspond to basal planes.

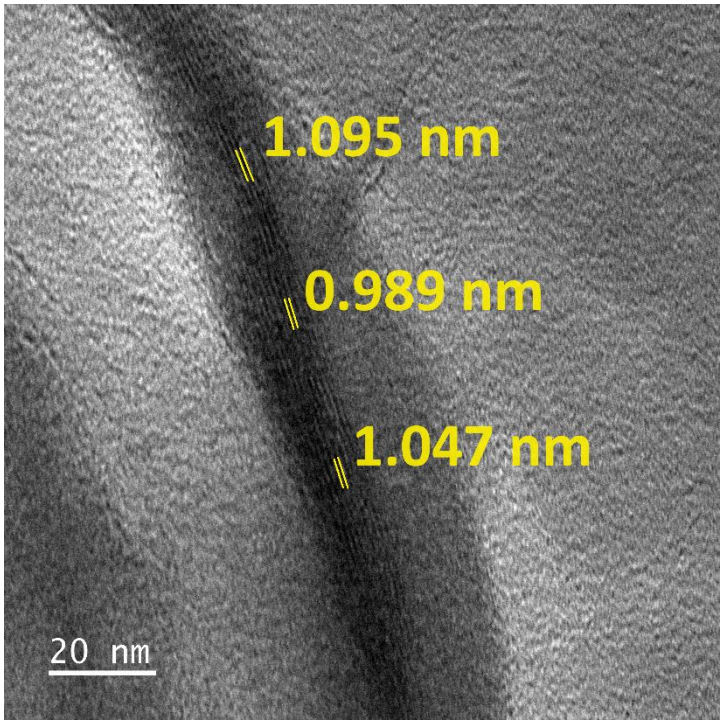

Fig 5B.7. TEM image of interlayer spacing of pure Na-MMT

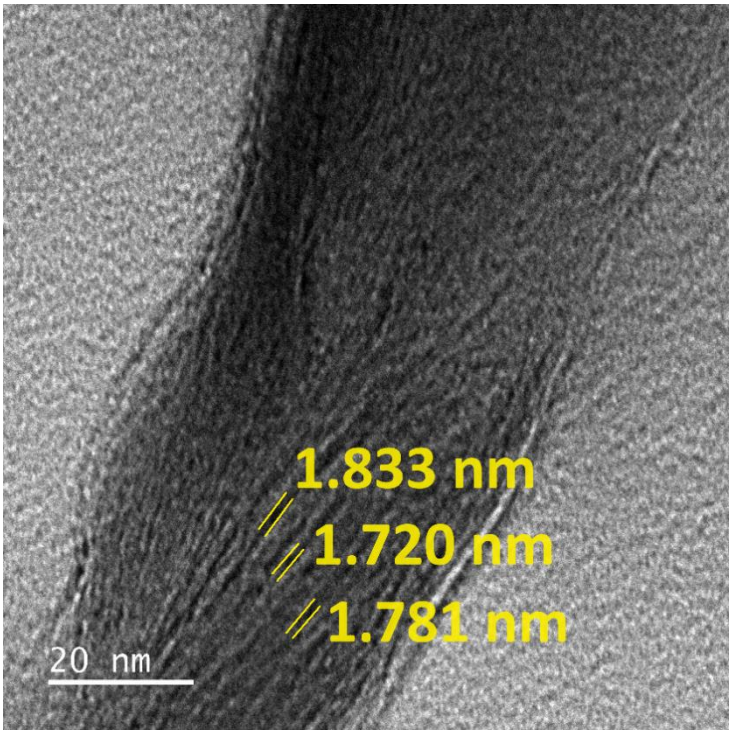

Fig 5B.8. TEM image of enhanced interlayer spacing of Na-MMT in M1 composite

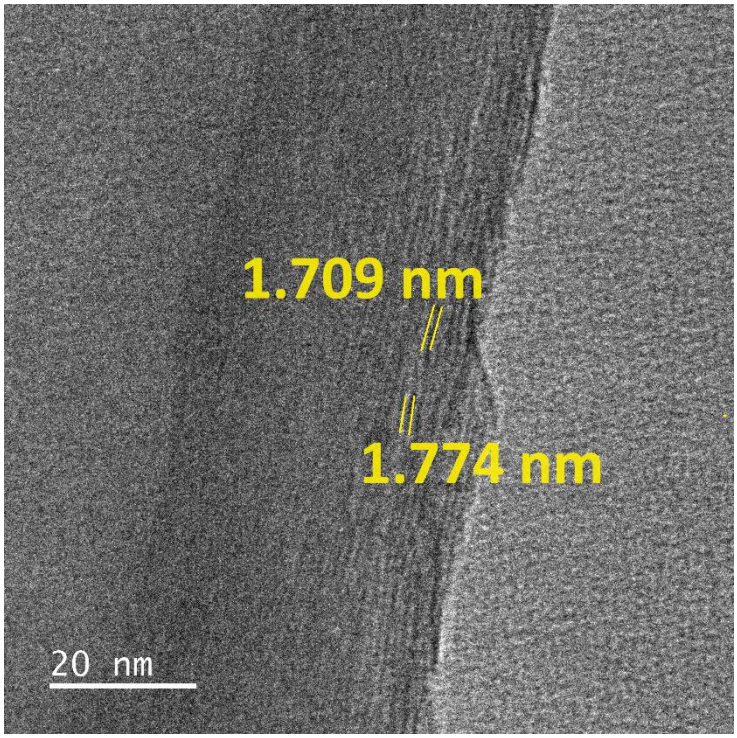

Fig 5B.9. TEM image of enhanced interlayer spacing of Na-MMT in M2 composite

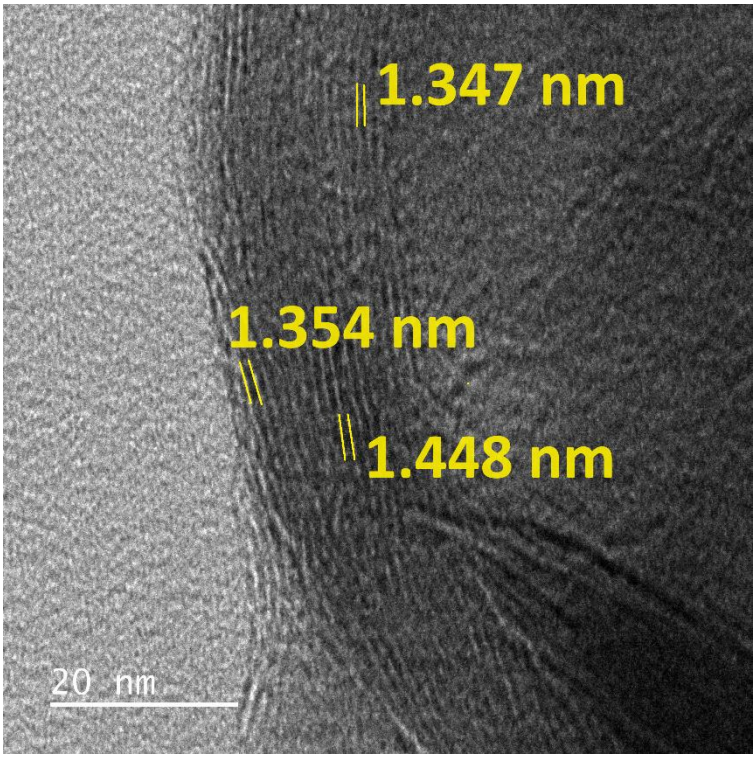

Fig 5B.10. TEM image of enhanced interlayer spacing of Na-MMT in M3 composite

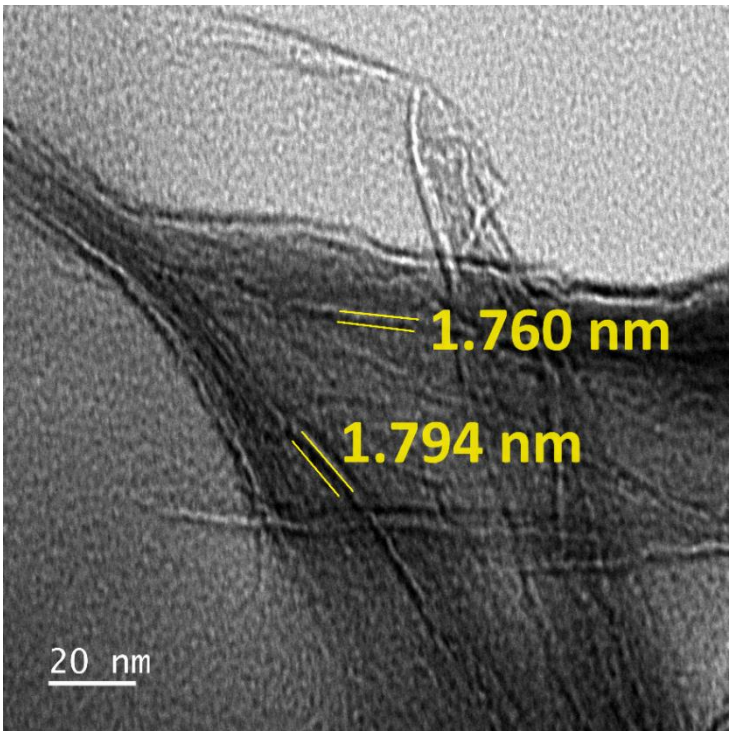

Fig 5B.11. TEM image of enhanced interlayer spacing of Na-MMT in L1 composite

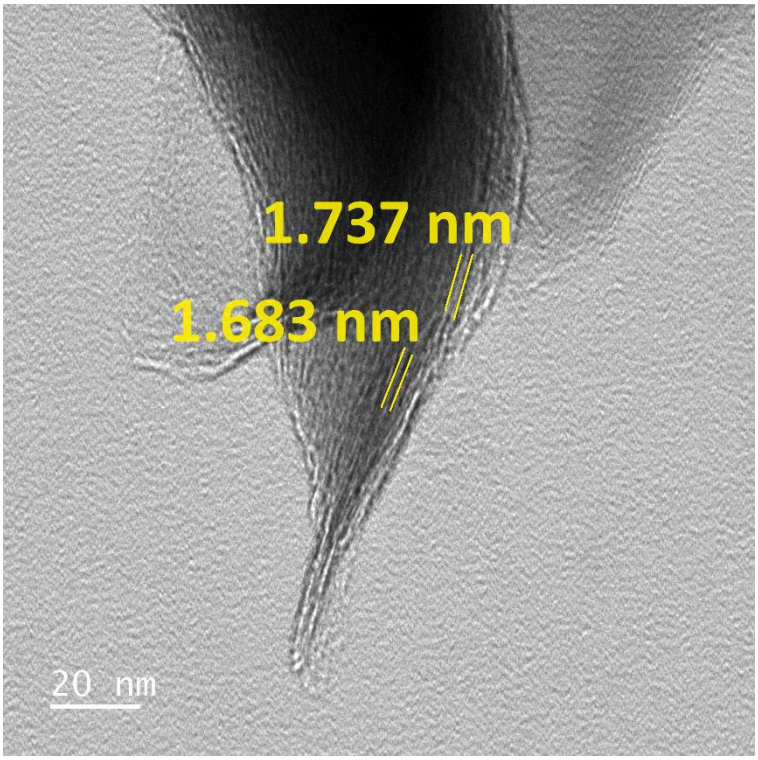

Fig 5B.12. TEM image of enhanced interlayer spacing of Na-MMT in L2 composite

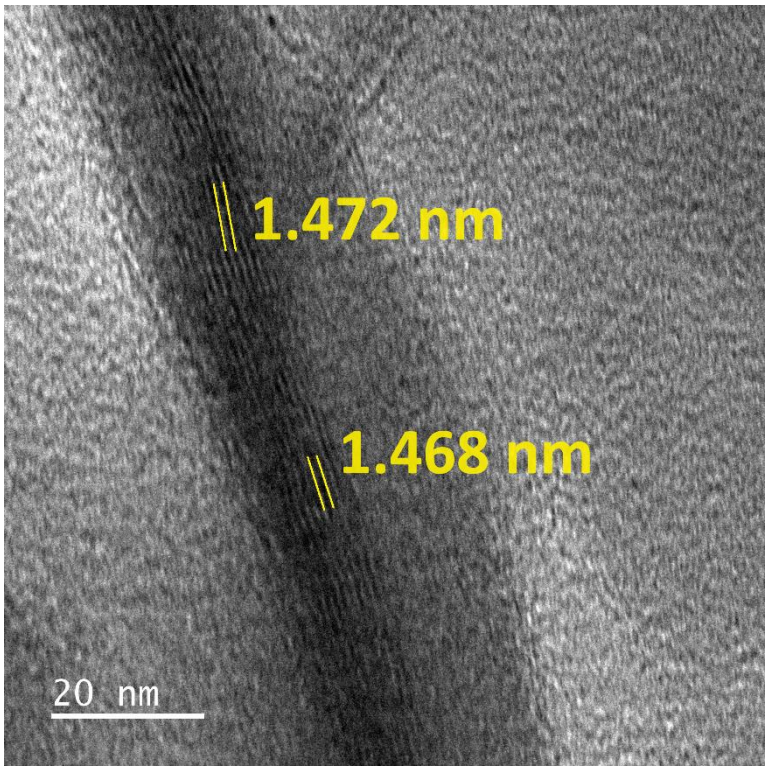

Fig 5B.13. TEM image of enhanced interlayer spacing of Na-MMT in L3 composite

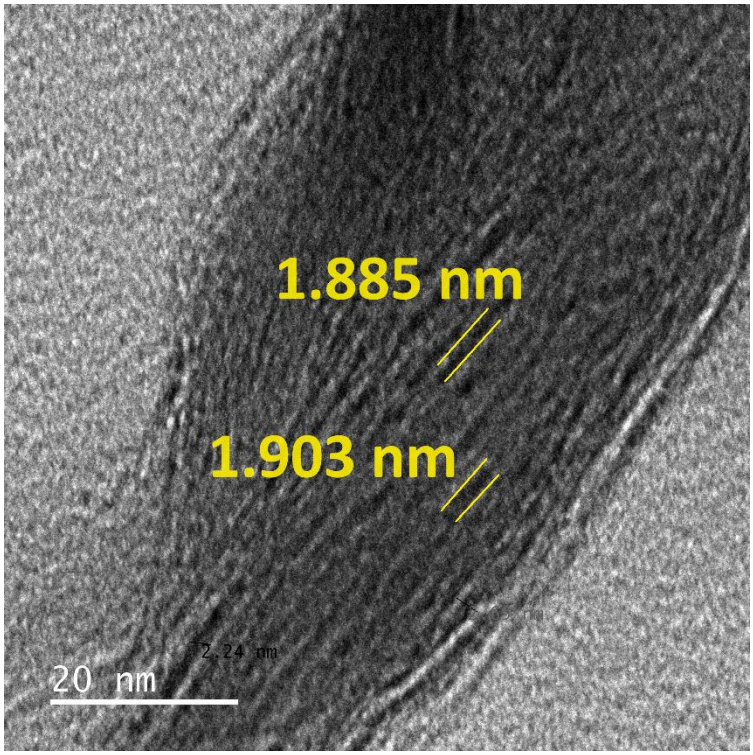

Fig 5B.14. TEM image of enhanced interlayer spacing of Na-MMT in G1 composite

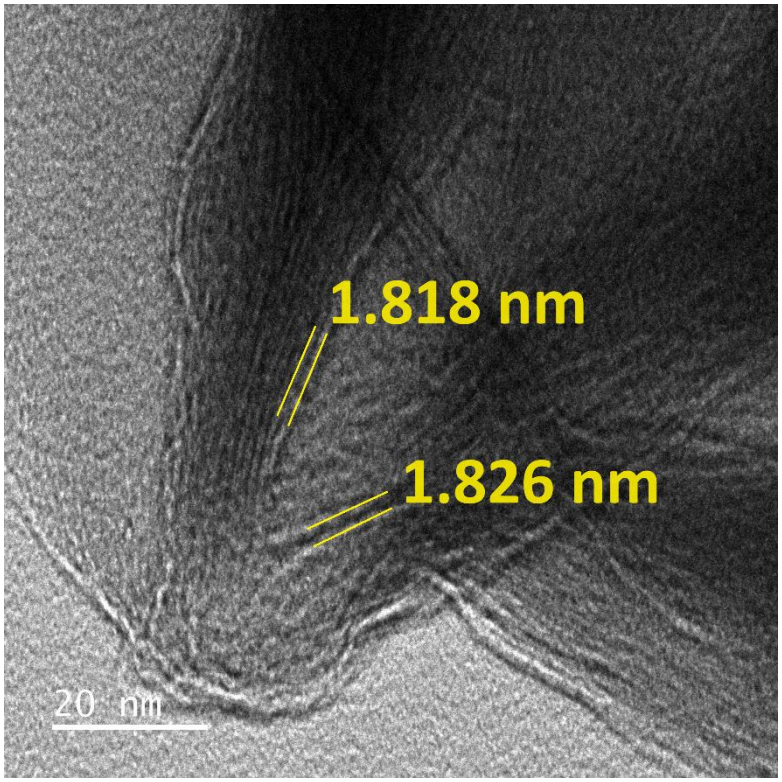

Fig 5B.15. TEM image of enhanced interlayer spacing of Na-MMT in G2 composite

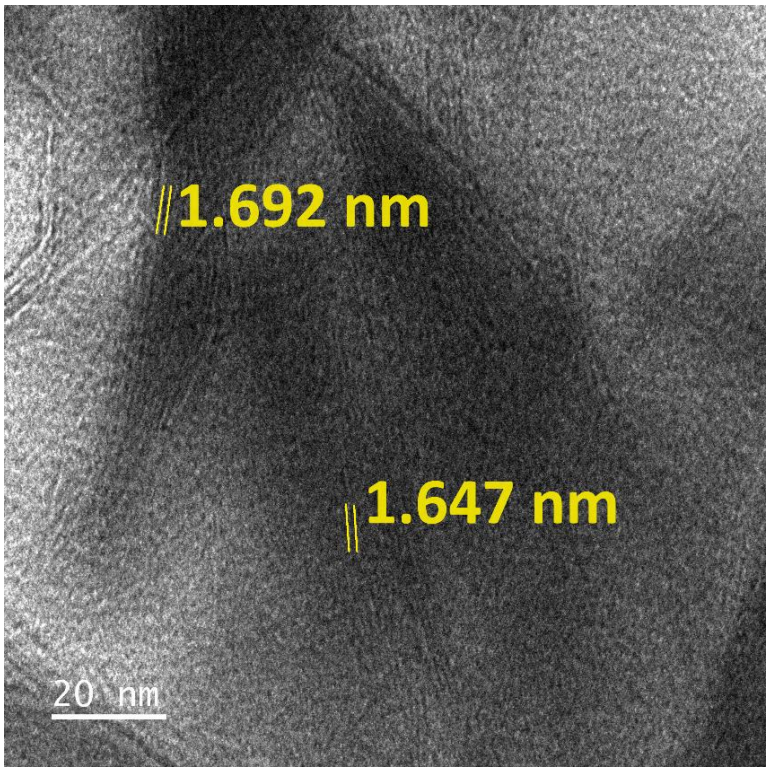

Fig 5B.16. TEM image of enhanced interlayer spacing of Na-MMT in G3 composite

5B.2.5. Analysis of SEM Image of Na-MMT:

The importance of SEM images lies in their ability to provide information about the external morphology of the Na-MMT nanoclay. SEM image (Fig 5B.17) showed that Na-MMT nanoclay consists of flakes or agglomerates of various sizes. It was also shown that layers of clay particles were stacked on top of each other which corroborated the TEM images.

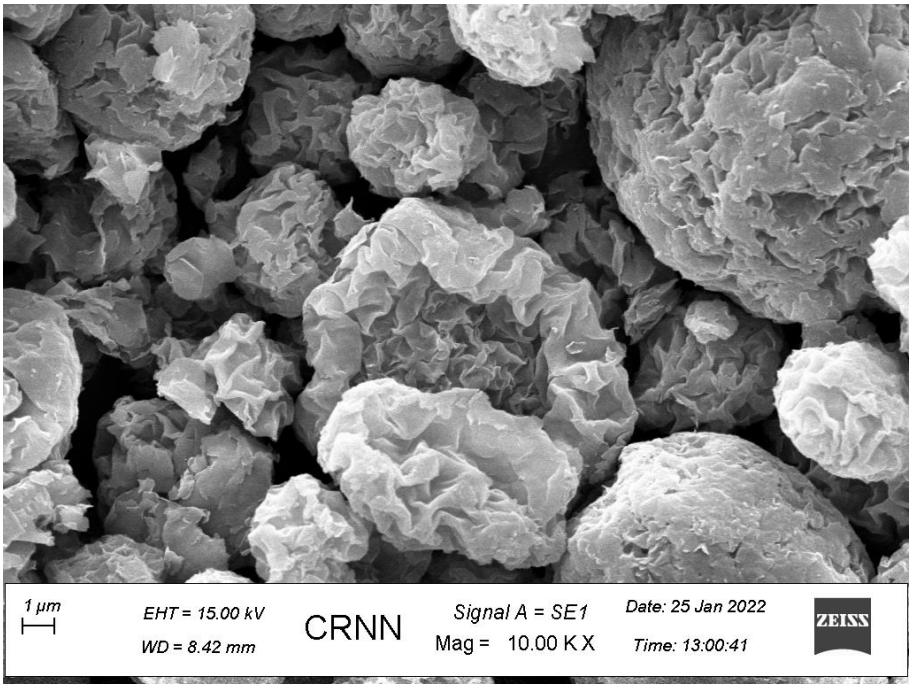

Fig 5B.17. SEM image of pure Na-MMT

5B.2.6. *In Vitro* Drug Release Study from the Drug/Na-MMT Composites:

In vitro studies allow researchers to precisely control experimental parameters such as pH, temperature, and agitation, which may be challenging to control *in vivo*. Moreover, this study reduces the need for animal experimentation, addressing ethical concerns associated with animal testing and helps to mitigate risks associated with formulation failure or unexpected drug release behaviour in later stages of development.

In vitro release profiles (Fig 5B.18-5B.20) indicated an initial rapid release, followed by a sustained release in the second phase, gradually slowing down at approximately 744 h for CH/Na-MMT composites (M1, M2 & M3) and EB/Na-MMT composites (L1, L2 & L3). The sustained release was observed for 336 h for PM/Na-MMT composites (G1, G2 & G3). The cumulative release percentages in sodium acetate buffer (pH 5.5; skin and small intestine pH) were approximately 63.15%, 49.95%, and 42.77% from M1, M2, and M3, respectively; 83.05%, 71.67%, and 55.55% from L1, L2, and L3, respectively; 72.22%, 64.09%, and 60.20% from G1, G2, and G3, respectively. In phosphate buffer (pH 7.4; physiological pH), the cumulative release percentages were 82.13%, 71.52%, and 59.72% from M1, M2, and M3, respectively; 92.74%, 91.59%, and 72.36% from L1, L2, and L3, respectively; 84.08%, 82.55%, and 77.26% from G1, G2, and G3, respectively.

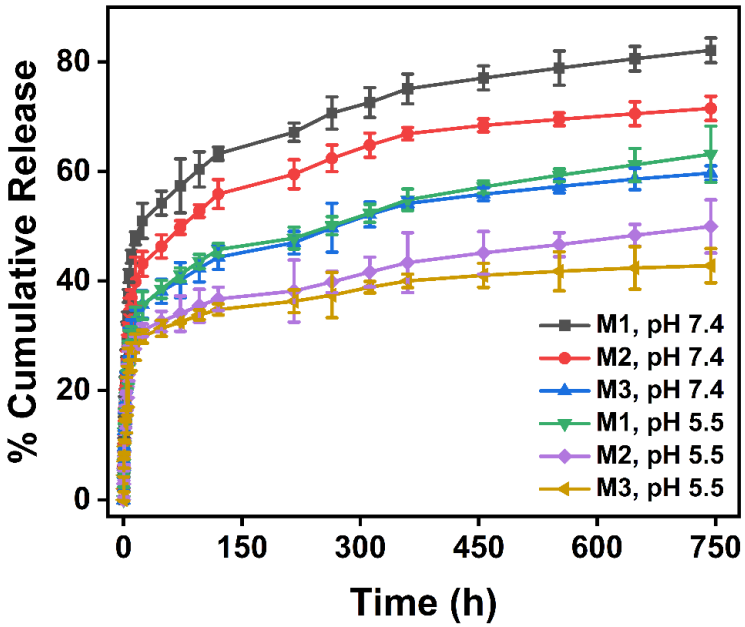

Fig 5B.18. In vitro CH drug release study from three CH/Na-MMT composites. The results were expressed as mean ± S.D, n=3

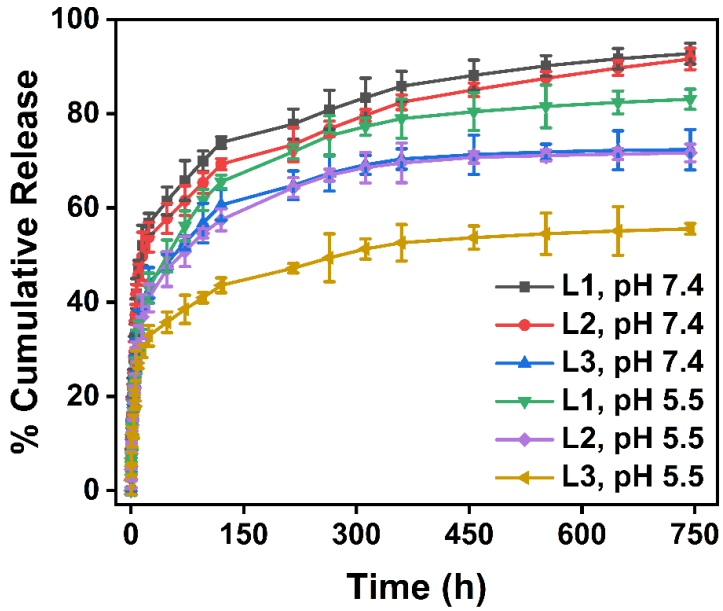

Fig 5B.19. In vitro EB drug release study from three EB/Na-MMT composites. The results were expressed as mean ± S.D, n=3

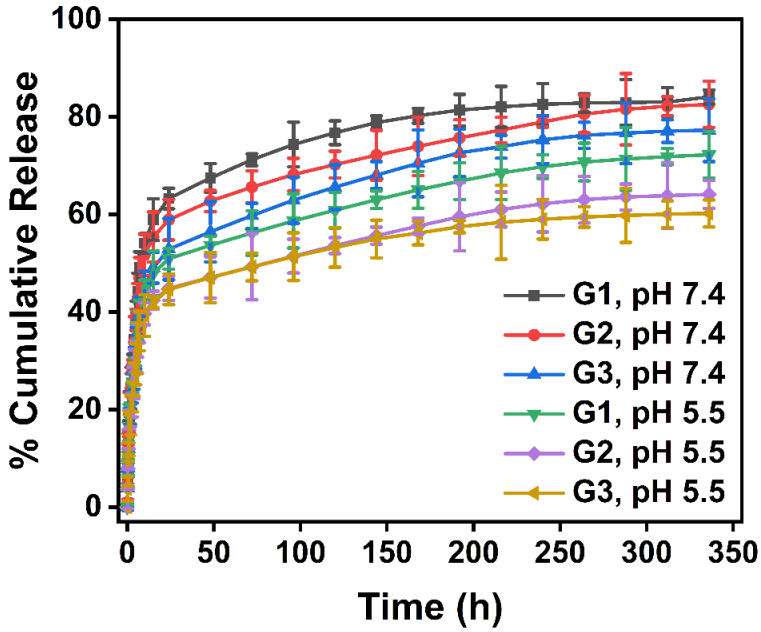

Fig 5B.20. In vitro PM drug release study from three PM/Na-MMT composites. The results were expressed as mean ± S.D, n=3

The *in vitro* release profile demonstrated that the release process from each composite was slow and persistent in both buffer solutions (pH 5.5 & 7.4). The sustained release may be elucidated based on the "ion-exchange" process between alkali metal ions present in buffer solutions and the cationic form of drug molecules intercalated in the nanoclay. Also, it was observed that 100% drug was not released i.e., the intercalated drugs could not be entirely exchanged due to the equilibrium nature of the ion-exchange phenomenon [1]. It is worth mentioning that the nanoclay was more capable of sustaining the drug release for an extended period in comparison to that of SNPs. Nanoporous SNPs typically lack such ion-exchange properties, limiting their ability to sustain drug release through this mechanism. Besides, the nanoclay can swell in the presence of water or biological fluids due to its ability to absorb and retain water molecules within its layers. This hydration and swelling behaviour can slow down the release of drugs intercalated within layers by creating diffusion barriers, thus extending the release period. On the other hand, while SNPs may also interact with water, their swelling behaviour and the impact of swelling on drug release are typically not as pronounced as that of Na-MMT nanoclay. The percentage release of all three drugs from the Na-MMT nanoclay was lower at pH 5.5 as compared to pH 7.4. This may be attributed to the presence of many protonated forms of the drug molecules at pH 5.5. The extent of electrostatic attraction between positive charges over the cationic form of each drug molecule and negative charges over the Na-MMT surface was high at pH 5.5 which led to a lower percentage of drug release. Moreover, this electrostatic force might be another reason for the incomplete release of the drug at both pH [1]. In addition, the release process was slow and extended with the decrease in the dose of drugs from both Na-MMT and SNPs. A large amount of drug molecules was adsorbed on the surface of the nanoparticles with the increase in the dose which led to the maximum amount of drug release during the burst release period.

5B.2.7. Preliminary Screening of the Transdermal Patches:

The prepared patches showed low moisture content ranging from 3.02 to 1.20% (CH patches), 3.99 to 11.00% (EB patches), and 3.74 to 11.85% (PM patches) whereas low moisture uptake in the range of 6.38 to 18.48% (CH patches), 7.77 to 16.38% (EB patches) and 6.28 to 14.42% (PM patches) as depicted in Fig 5B.21-5B.23. The percentage swelling indices of all patches were found to increase with time (Fig 5B.24-5B.26). The pH levels on the surface of all four transdermal formulations were within the range of skin pH (pH: 4.5-6.0) as displayed in Fig 5B.27-5B.29. Additionally, the patches exhibited promising folding endurance values, surpassing an average of 300 times. The percentage elongation values ranged from 28.31 to 28.93% for CH patches, 25.74 to 28.97% for EB patches, and 25.45 to 30.65% for PM patches. The thickness of the patches varied between 0.20 mm and 0.48 mm. Moreover, all transdermal formulations showed uniform weight. Consistency in all the parameters mentioned above was confirmed by the low standard deviation values and the results are summarized in Table 5B.1.

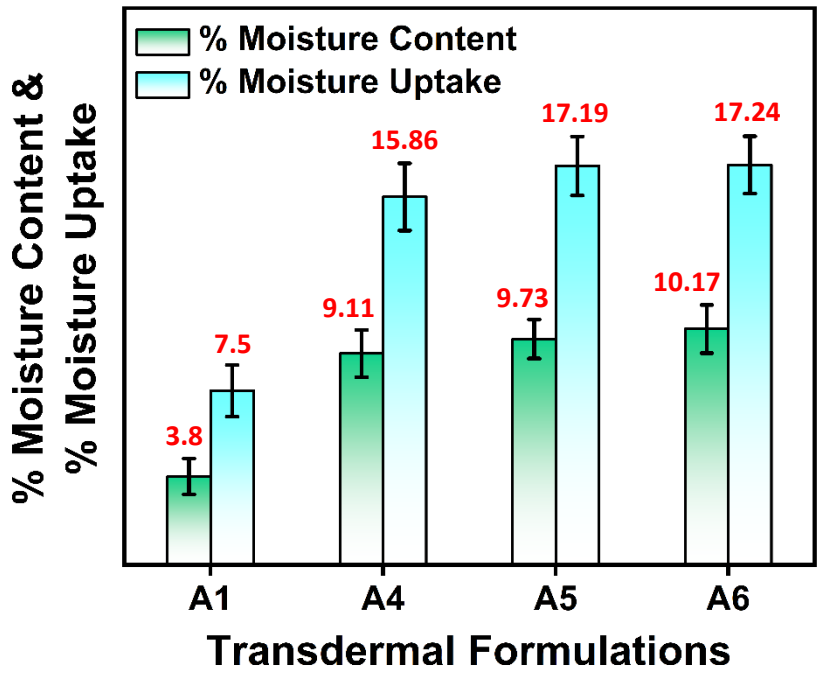

Fig 5B.21. Percentage of moisture content and moisture uptake of CH patches

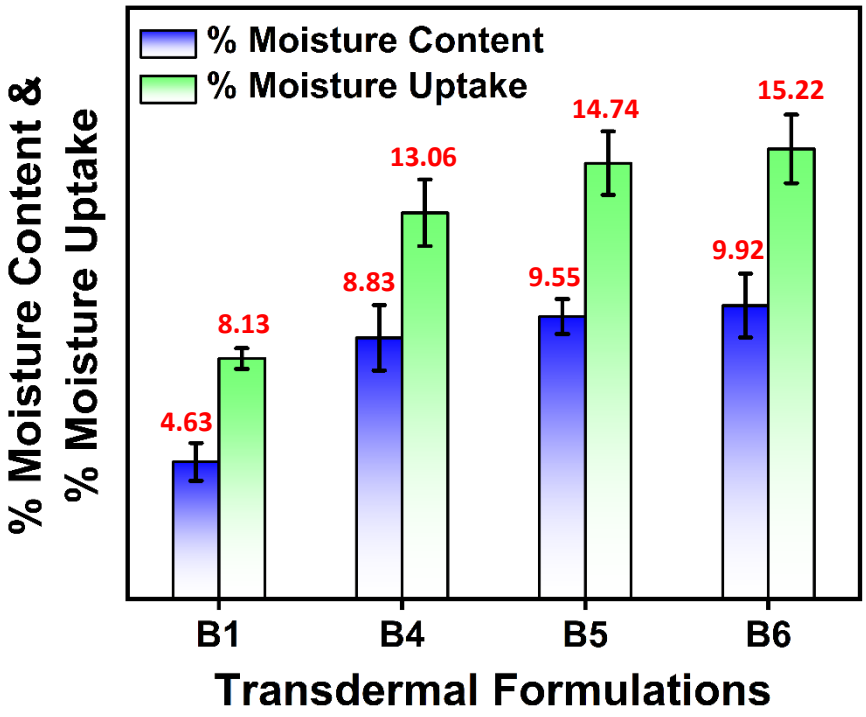

Fig 5B.22. Percentage of moisture content and moisture uptake of EB patches

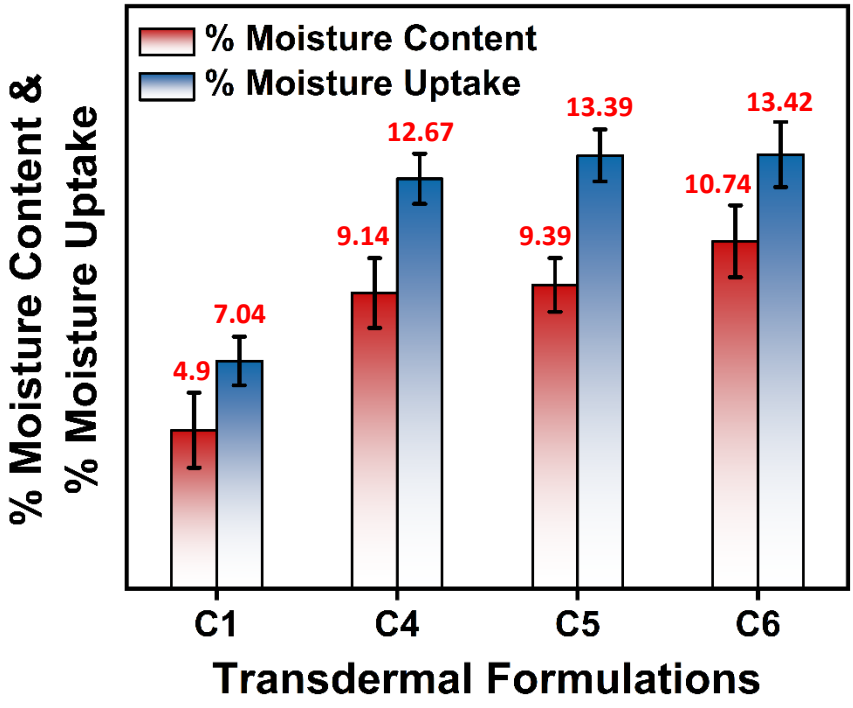

Fig 5B.23. Percentage of moisture content and moisture uptake of PM patches

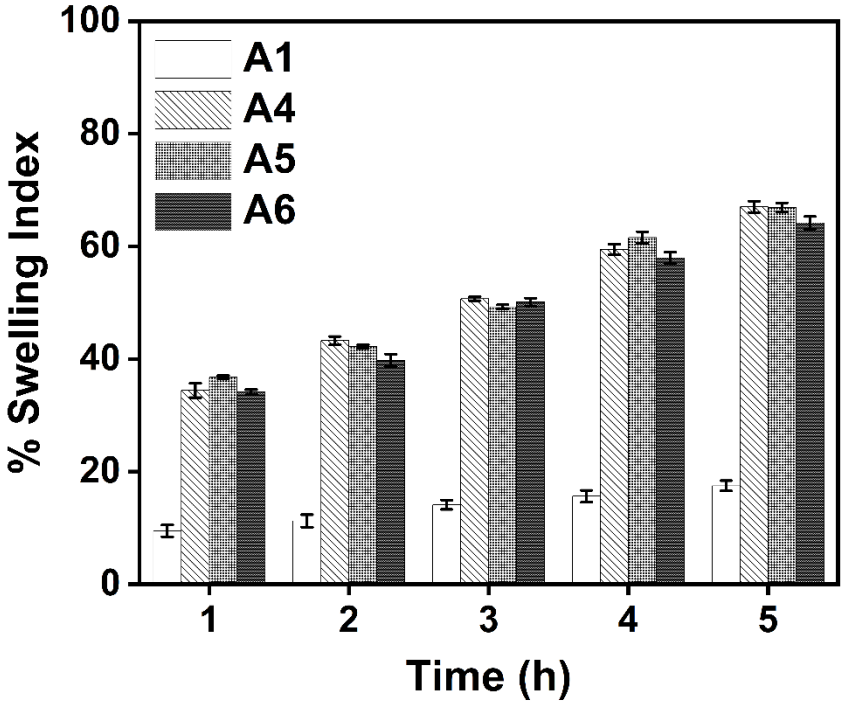

Fig 5B.24. Percentage swelling index of CH patches

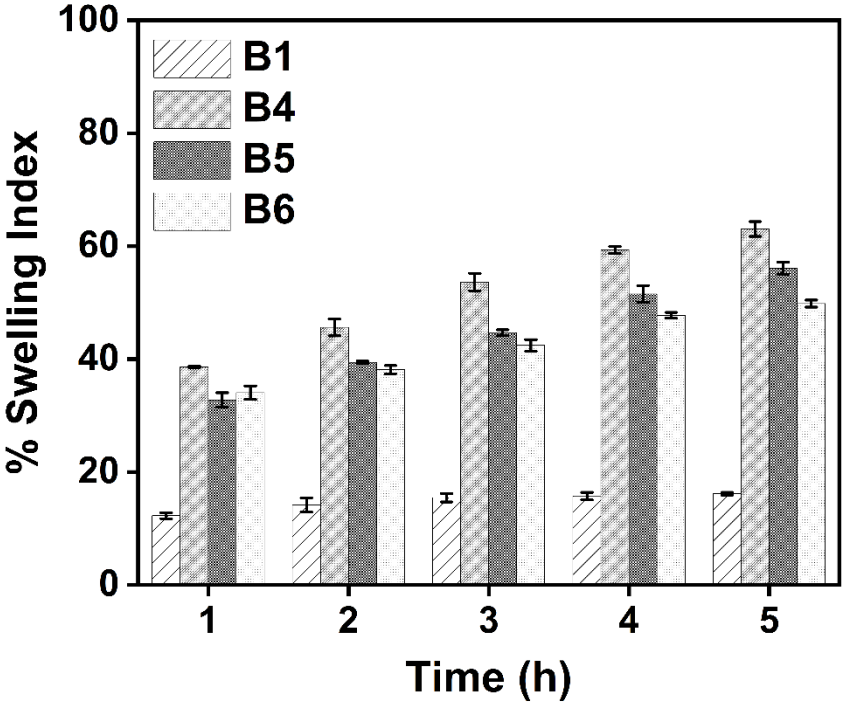

Fig 5B.25. Percentage swelling index of EB patches

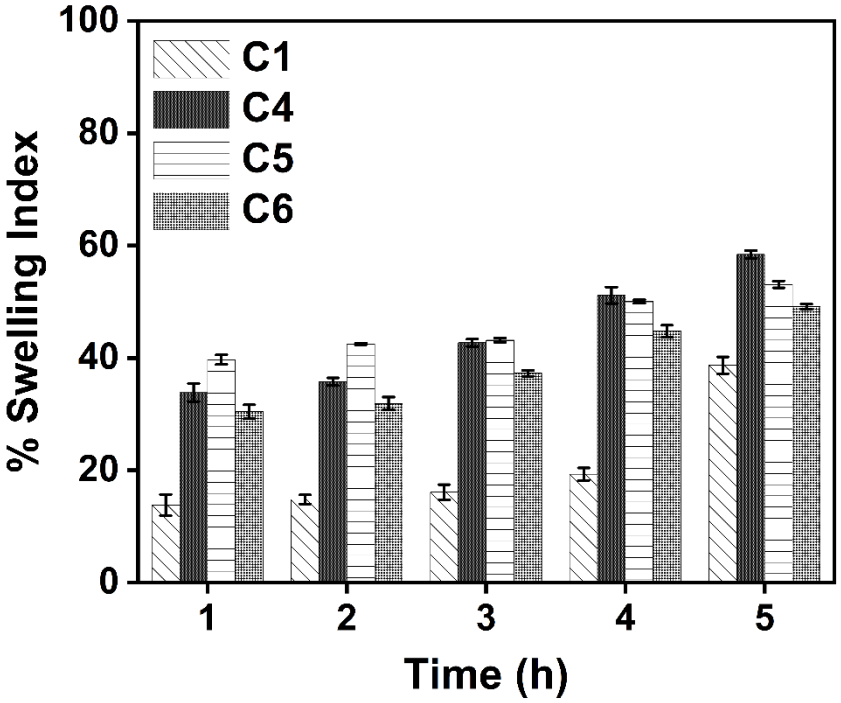

Fig 5B.26. Percentage swelling index of PM patches

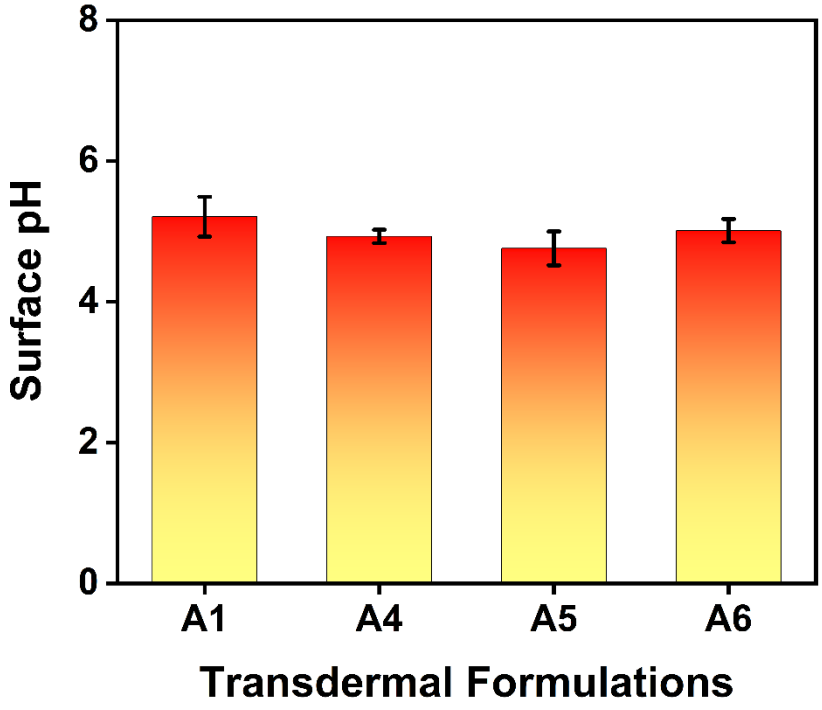

Fig 5B.27. Surface pH of the CH patches

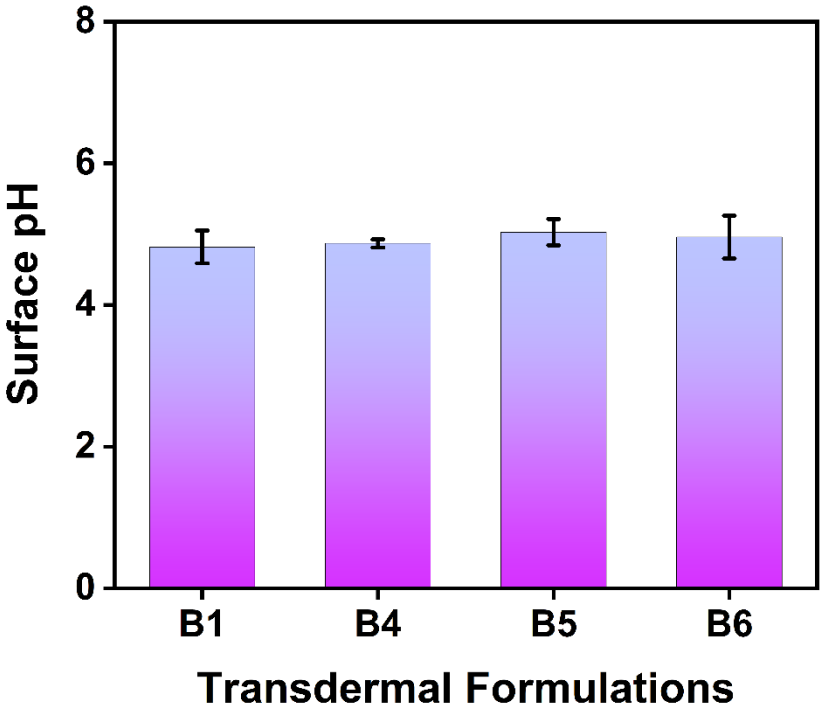

Fig 5B.28. Surface pH of the EB patches

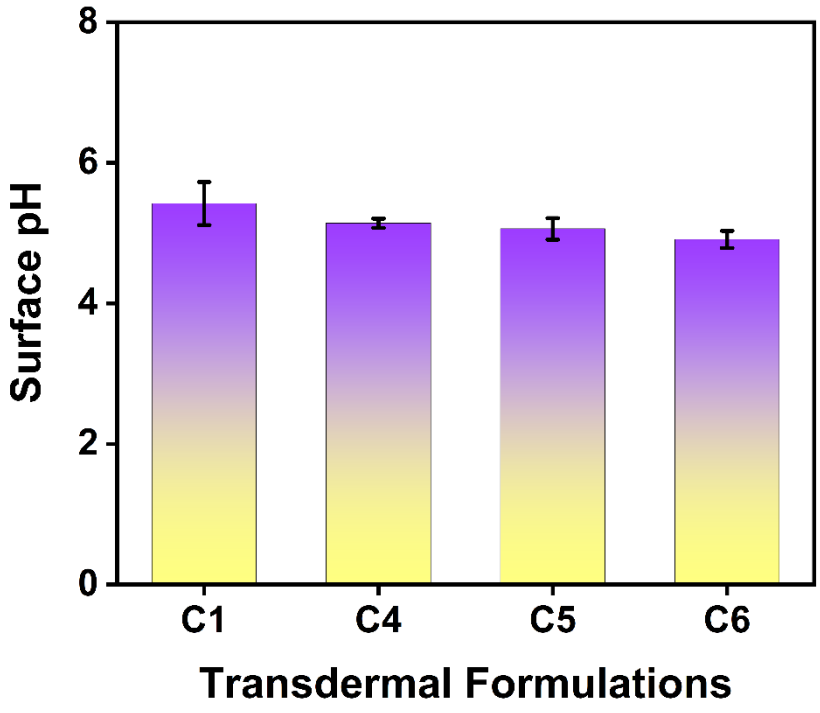

Fig 5B.29. Surface pH of the PM patches

Transdermal patches were stable since they contained less moisture. Moreover, microbial contamination could be avoided due to the low moisture uptake of the patches. Microorganisms require moisture to thrive and reproduce, so minimizing moisture content in the patches reduced the available water for microbial colonisation. The transdermal formulations containing CH/Na-MMT composites (A4, A5, A6, B4, B5, B6, C4, C5 & C6) had a higher swelling index as compared to that of A1, B1, and C1 because montmorillonite exhibits hydrophilic properties and swells with water [2]. When montmorillonite clay encounters water, the water molecules are attracted to the surface of the clay particles and can penetrate between the layers of the mineral structure. This causes the clay to swell as the layers expand to accommodate the water molecules. Folding endurance and percentage elongation values of the patches suggested that the concentration of Di-n-butyl phthalate present in transdermal patches could be sufficient to maintain the elasticity, flexibility, and integrity of the patches with skin folding. The surface pH of the patch must be close to that of the skin pH to prevent irritation when the patch is applied. The surface pH values of freshly prepared patches demonstrated their safety and skin compatibility [3].

The drug content for the transdermal formulations of CH, labelled as A1, A4, A5, and A6, was determined to be 89.06±0.243%, 88.21±0.751%, 88.43±0.565%, and 86.09±0.797%, respectively. For EB-transdermal patches, designated as B1, B4, B5, and B6, the drug content was found to be 91.32±0.646%, 76.55±0.811%, 75.22±0.375%, and 74.48±0.273%, respectively. In the case of PM-transdermal formulations, the drug content of C1, C4, C5, and C6 was 80.61±0.031%, 78.43±0.014%, 70.22±0.028%, and 68.58±0.041%, respectively. High drug content allows for less frequent patch changes or smaller patch sizes, which can enhance patient convenience and adherence to the prescribed treatment regimen. Besides, high drug content ensures a sufficient reservoir of the drug within the patch, allowing for prolonged release kinetics and consistent plasma concentrations of the drug over time. Additionally, high

drug content can result in reduced manufacturing costs per dose and improved cost-effectiveness of the treatment.

Table 5B.1. Folding endurance, % elongation, thickness, and weight uniformity of the patches

Transdermal Formulations	Folding Endurance	% Elongation	Thickness (mm)	Weight Uniformity (mg)
A1	267 ± 0.667	28.32 ± 0.014	0.38 ± 0.019	101.82 ± 0.024
A4	312 ± 0.854	28.91 ± 0.023	0.33 ± 0.012	100.37 ± 0.031
A5	305 ± 0.821	27.36 ± 0.026	0.42 ± 0.017	99.51 ± 0.034
A6	308 ± 0.783	28.55 ± 0.019	0.31 ± 0.025	99.84 ± 0.031
B1	265 ± 0.838	25.76 ± 0.015	0.39 ± 0.025	97.03 ± 0.059
B4	295 ± 0.627	28.31 ± 0.061	0.38 ± 0.011	98.73 ± 0.024
B5	298 ± 0.575	28.93 ± 0.040	0.34 ± 0.005	99.26 ± 0.085
B6	293 ± 0.648	28.03 ± 0.063	0.41 ± 0.015	100.14 ± 0.054
C1	238 ± 0.867	25.47 ± 0.022	0.21 ± 0.008	98.14 ± 0.017
C4	299 ± 0.881	28.72 ± 0.028	0.46 ± 0.017	99.70 ± 0.011
C5	286 ± 0.785	30.65 ± 0.030	0.39 ± 0.009	97.13 ± 0.024
C6	290 ± 0.793	29.15 ± 0.023	0.43 ± 0.032	97.48 ± 0.036

5B.2.8. FTIR Analysis:

FTIR analysis is essential for assessing drug loading and understanding the interaction between the drug and the patch components. The FTIR spectra of the three drugs, polymers, Na-MMT nanoclay, and the freshly prepared transdermal patches using the above constituents were measured within the range of 400-4000 cm^{-1}. FTIR analysis showed that the characteristic peaks of pure CH drug were observed at 3340 cm^{-1} for N-H stretching, 3077 cm^{-1} for C-H stretching,1650 cm^{-1} for C-N stretching,1441 cm^{-1} for in-plane deformation mode of C-H stretching,1299 cm^{-1} for wagging mode of -CH_2 group, and 780 cm^{-1} out-plane deformation mode of C-H stretching (Fig 5B.30) [4]. On the other hand, the major peaks for pure EB drug were found at 1597 and 1492 cm^{-1} due to aromatic C=C stretching, 1145 and 1084 cm^{-1} for S=O stretching vibrations (Fig 5B.31) [5]. The significant peaks of PM drug appeared at 3324 cm^{-1} for O-H stretching, 3162 cm^{-1} for C-H stretching, 1656 cm^{-1} for C=O stretching, and 1609 cm^{-1} for C=C stretching, 1565 cm^{-1} for N-H bending and 1507 cm^{-1} for asymmetrical C-H bending (Fig 5B.32) [6]. In the FTIR spectra of all the CH transdermal patches, significant peaks of the drug were observed within the range of 1280-1670 cm^{-1}, as shown by the dotted circle in Fig 5B.30. The spectra of EB transdermal patches showed principal peaks of the drug in the range of 1140-1670 cm^{-1}, as illustrated by the dotted circle in Fig 5B.31. The major peaks of pure PM drug in its transdermal formulations were observed between 1250 to 1660 cm^{-1}, as portrayed by the dotted circle in Fig 5B.32. Moreover, the patches containing nanomedicines (A4, A5, A6, B4, B5, B6, C4, C5 & C6) proved the presence of Na-MMT nanoclay by showing a broad strong band around 1040 cm^{-1} corresponds to Si–O bond stretching present in the clay. However, few additional peaks were observed in all patches due to the presence of other constituting polymers.

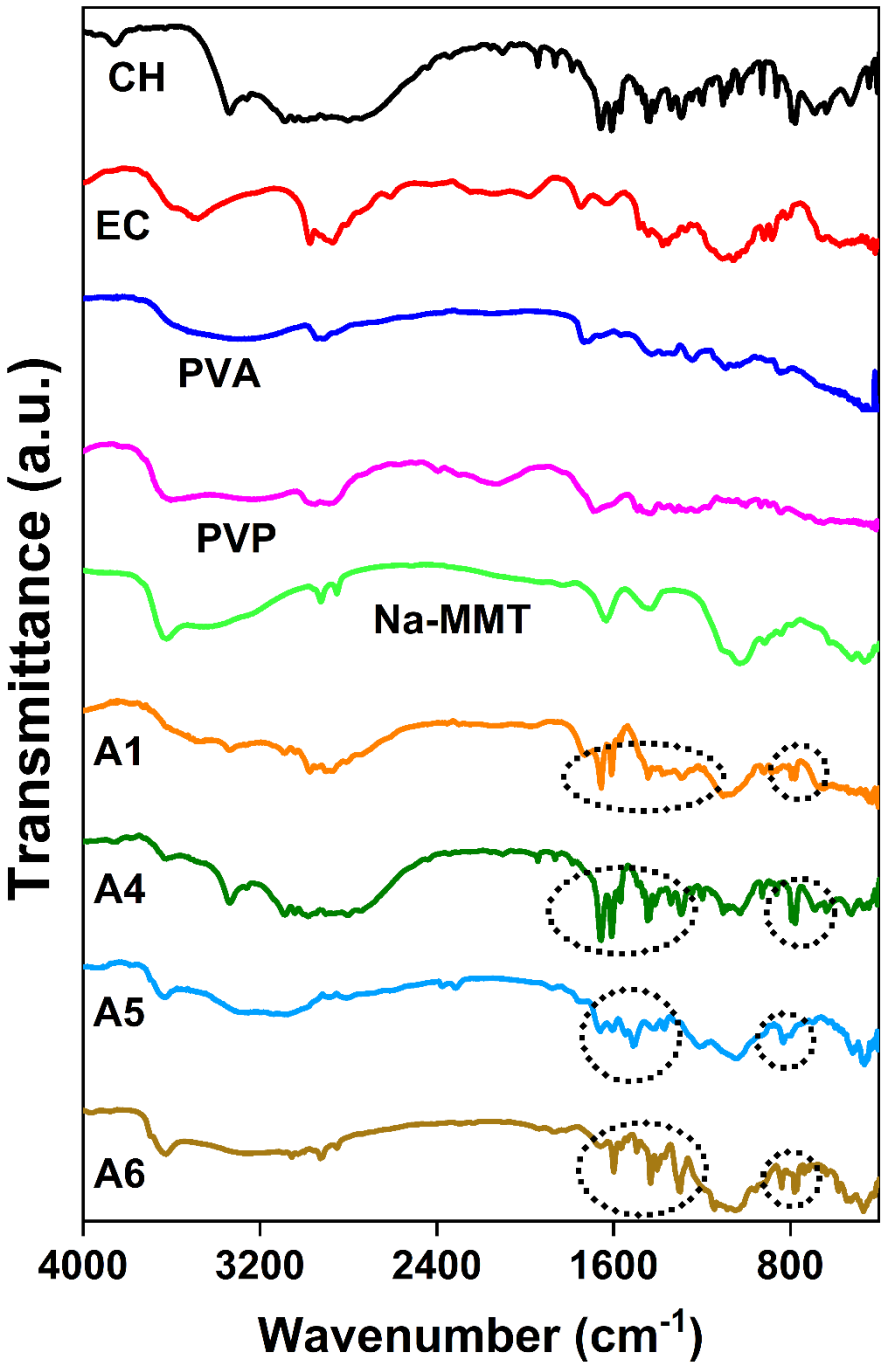

Fig 5B.30. FTIR spectra of CH drug, polymers (EC, PVA & PVP), Na-MMT and patches (A1, A4, A5 & A6)

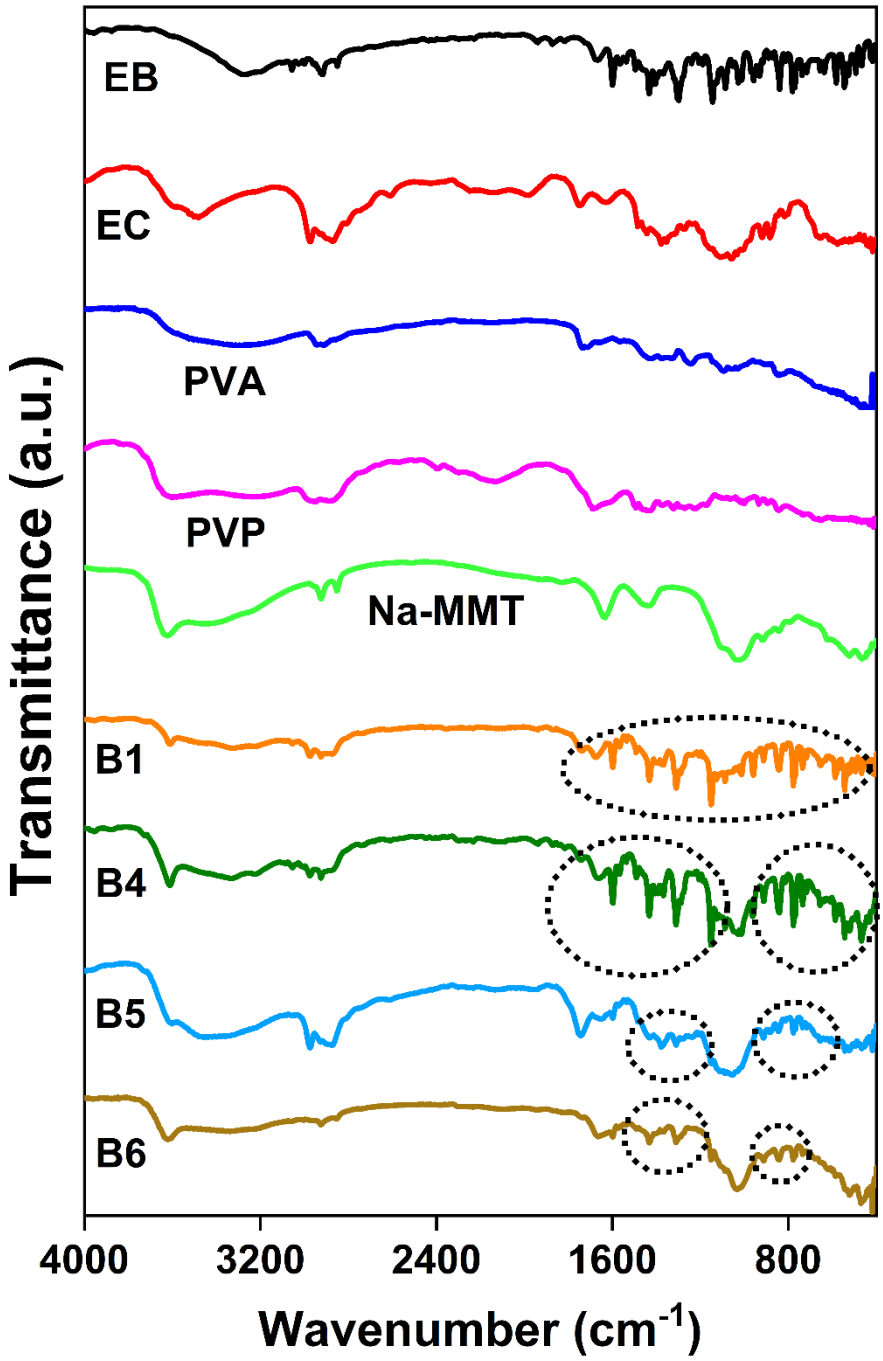

Fig 5B.31. FTIR spectra of EB drug, polymers (EC, PVA & PVP), Na-MMT and patches (B1, B4, B5 & B6)

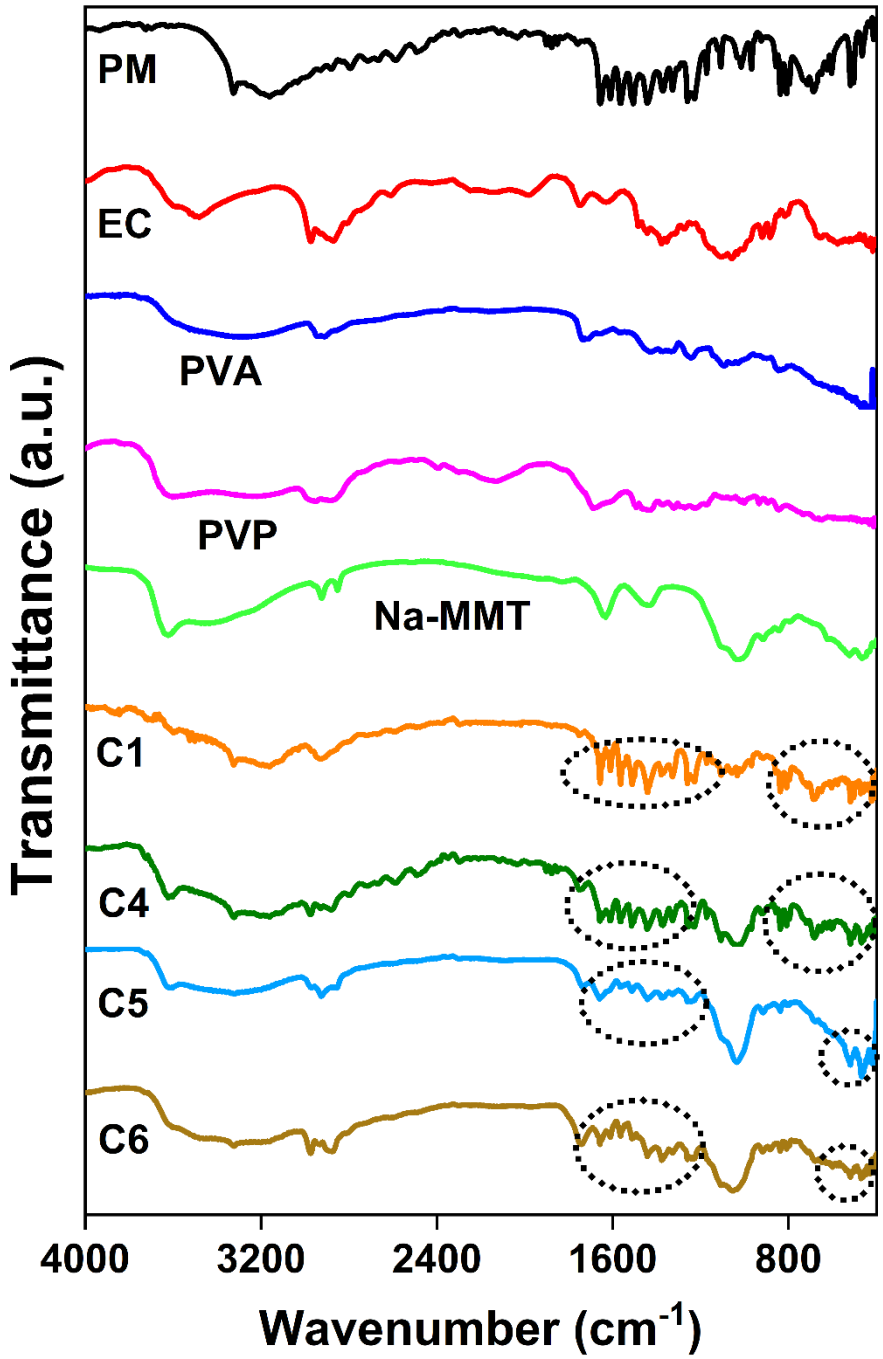

Fig 5B.32. FTIR spectra of PM drug, polymers (EC, PVA & PVP), Na-MMT and patches (C1, C4, C5 & C6)

5B.2.9. Analysis of SEM Images of the Patches:

SEM images can reveal the distribution and localization of the drug within the patch matrix. This information is important for understanding how effectively the drug is dispersed throughout the patch and whether there are any regions of aggregation or uneven distribution. The comparison among the SEM images of different formulations (e.g., different polymers, drug concentrations) can provide insights into how formulation parameters affect the microstructure and drug distribution within the patches. This information is valuable for optimizing patch formulations to achieve desired drug release kinetics and therapeutic efficacy. SEM images of the freshly prepared patches exhibited homogeneous dispersion of the drug/Na-MMT composites in the transdermal matrices (Fig 5B.33-5B.42). The homogeneous dispersion of the free drug molecules throughout the transdermal matrices (A1, B1 and C1) was already shown in section 5A.2.9. of the previous chapter 5A.

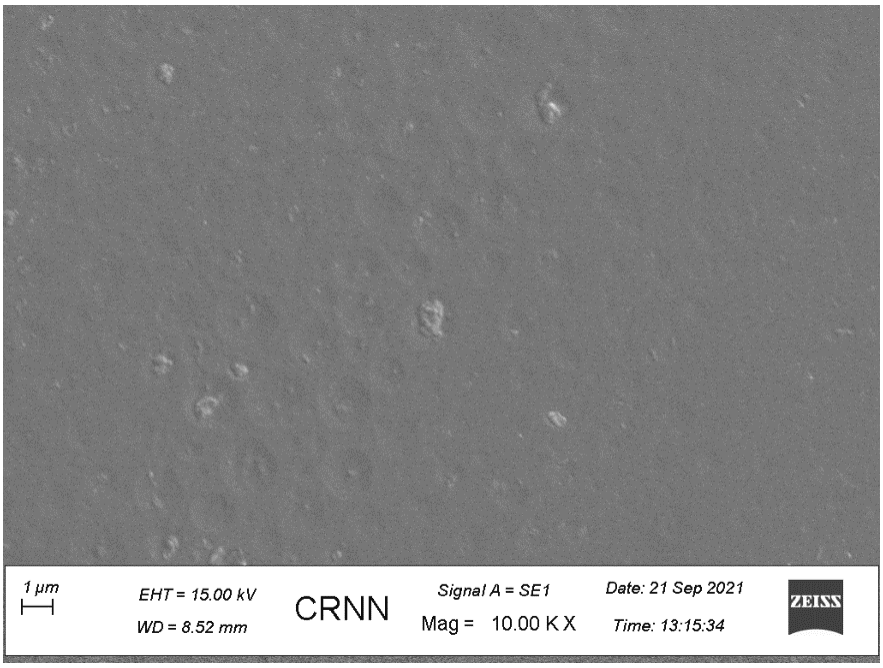

Fig 5B.33. SEM image of blank transdermal patch

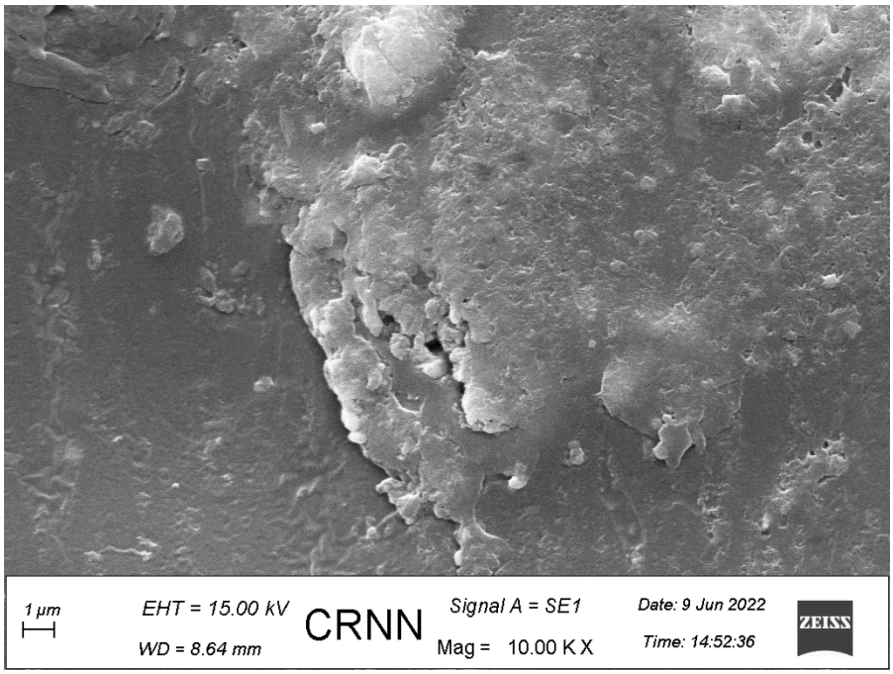

Fig 5B.34. SEM image of the transdermal patch containing M1 composite, A4

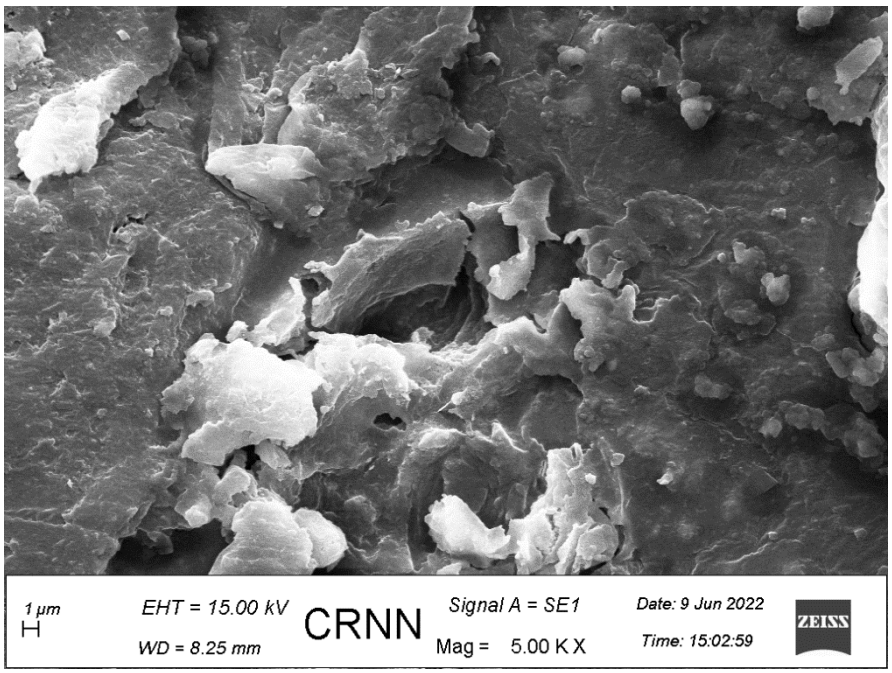

Fig 5B.35. SEM image of the transdermal patch containing M2 composite, A5

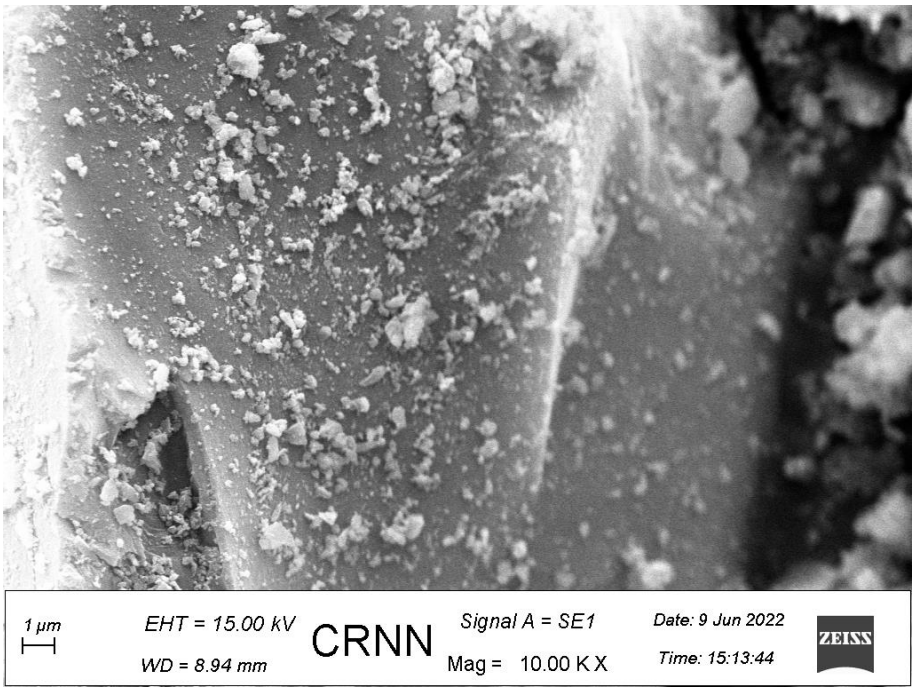

Fig 5B.36. SEM image of the transdermal patch containing M3 composite, A6

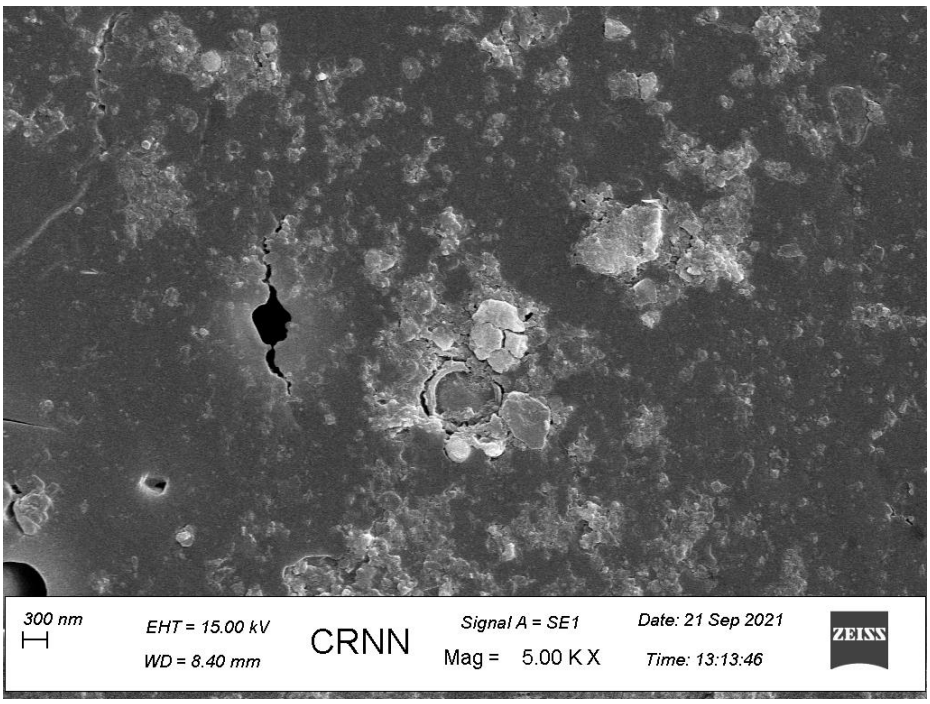

Fig 5B.37. SEM image of the transdermal patch containing L1 composite, B4

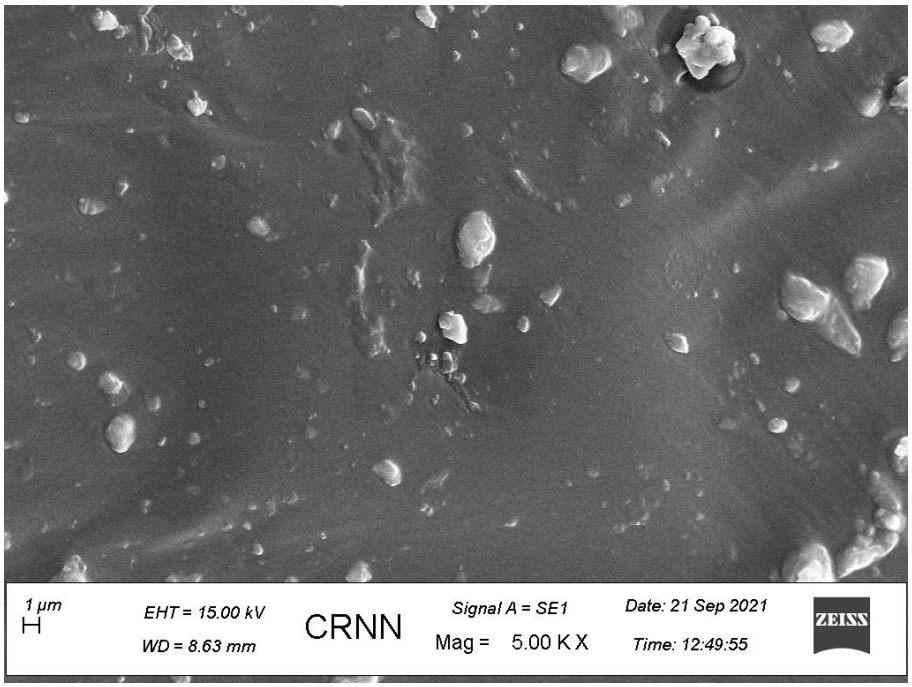

Fig 5B.38. SEM image of the transdermal patch containing L2 composite, B5

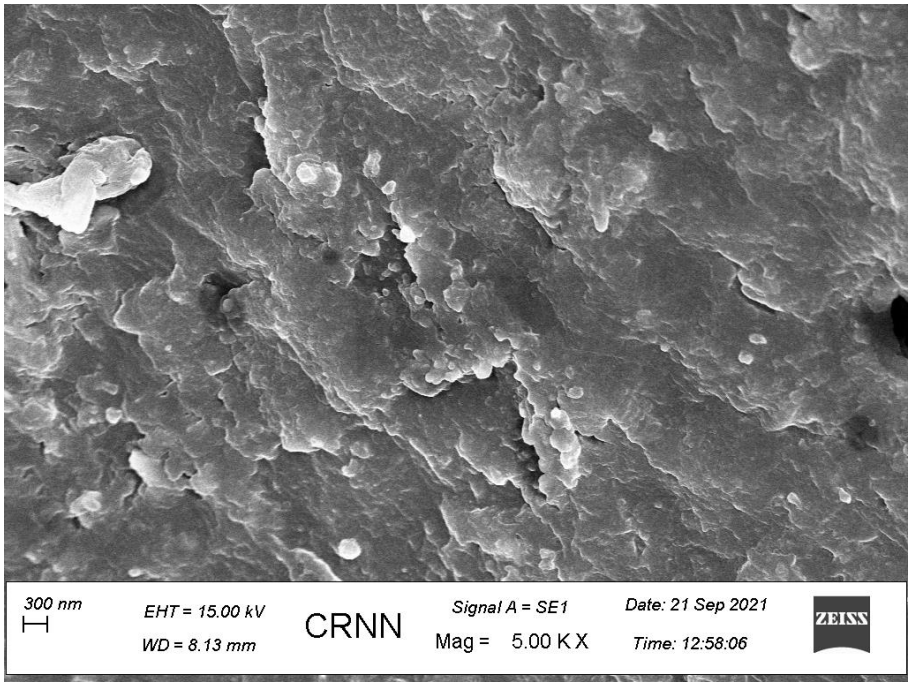

Fig 5B.39. SEM image of the transdermal patch containing L3 composite, B6

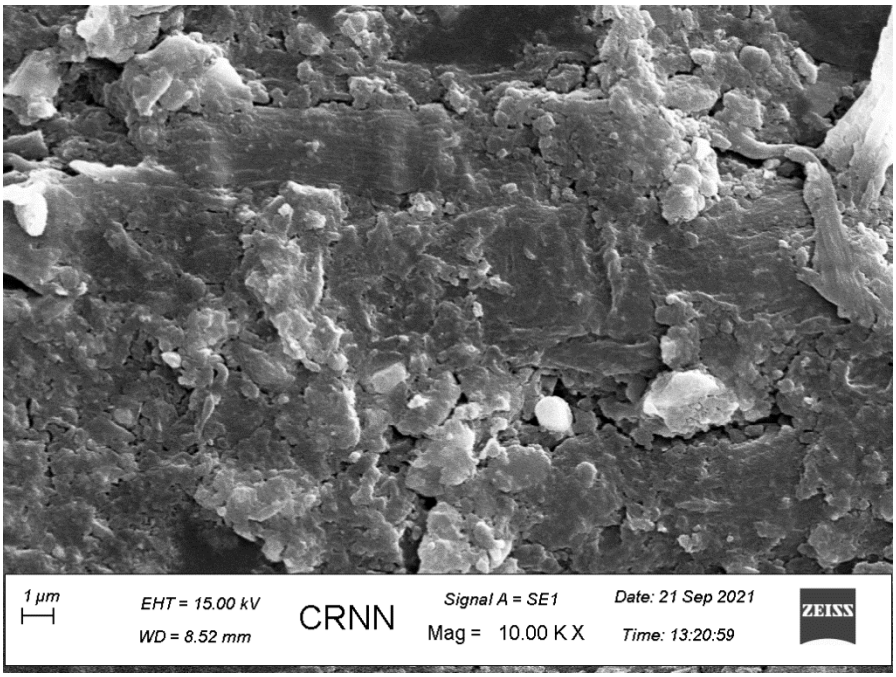

Fig 5B.40. SEM image of the transdermal patch containing G1 composite, C4

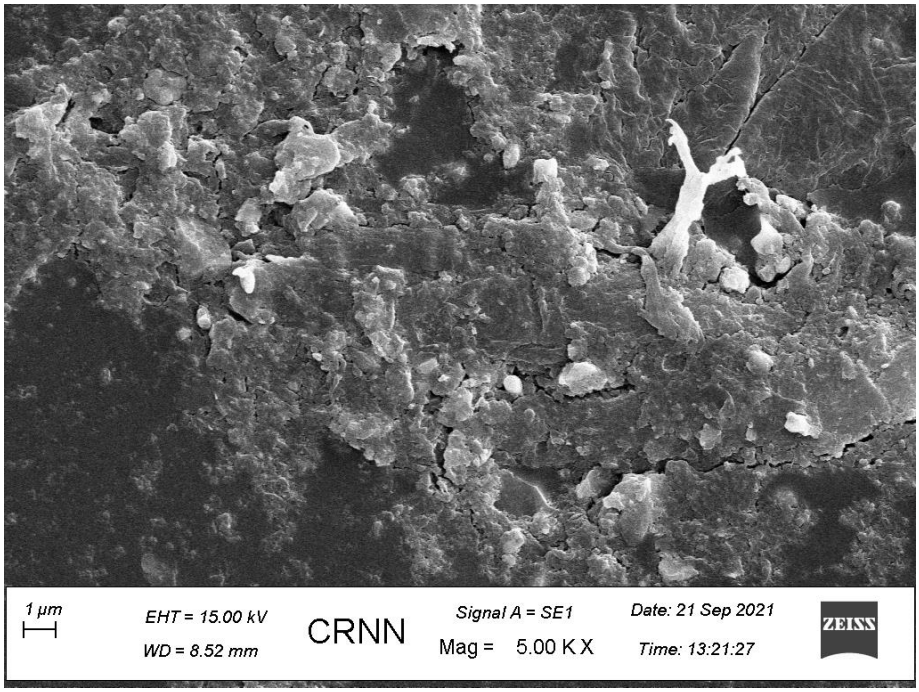

Fig 5B.41. SEM image of the transdermal patch containing G2 composite, C5

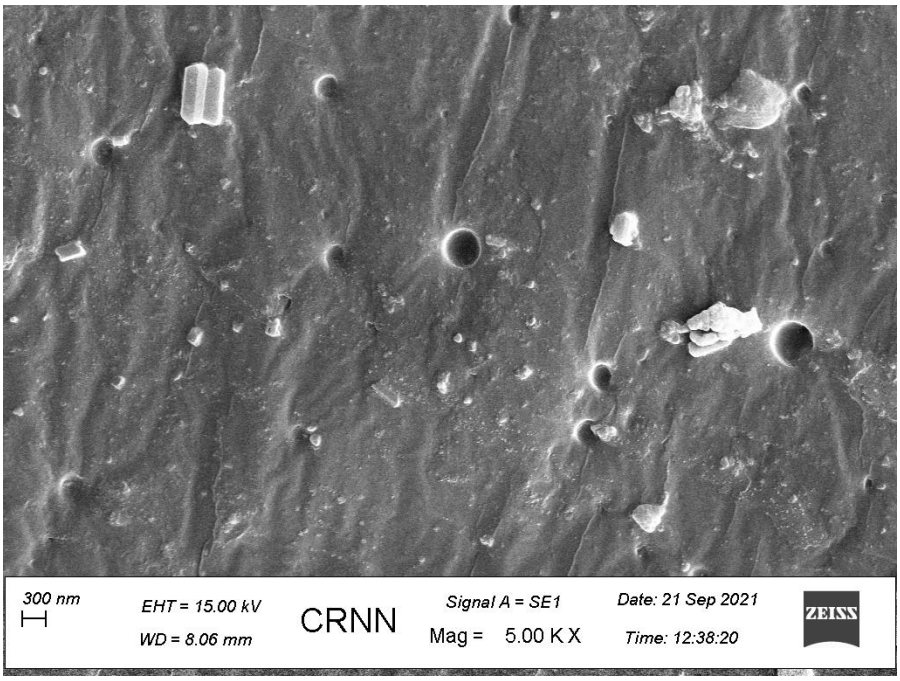

Fig 5B.42. SEM image of the transdermal patch containing G3 composite, C6

5B.2.10. Skin Irritation Study of the Patches:

Skin irritation studies evaluate the potential of transdermal patches to cause irritation or allergic reactions when applied to the skin. This is especially important because the skin serves as a barrier and any irritation can lead to discomfort or adverse reactions in patients. Skin irritation studies allow for comparative analysis of different patch formulations or delivery systems. Researchers can select the most suitable formulation with minimal skin irritation for further development by comparing the irritation potential of various formulations.

The skin irritation study on rats showed that there were no signs of erythema (redness and itching) or edema (swelling) at the application site of the transdermal patch (Fig 5B.43).

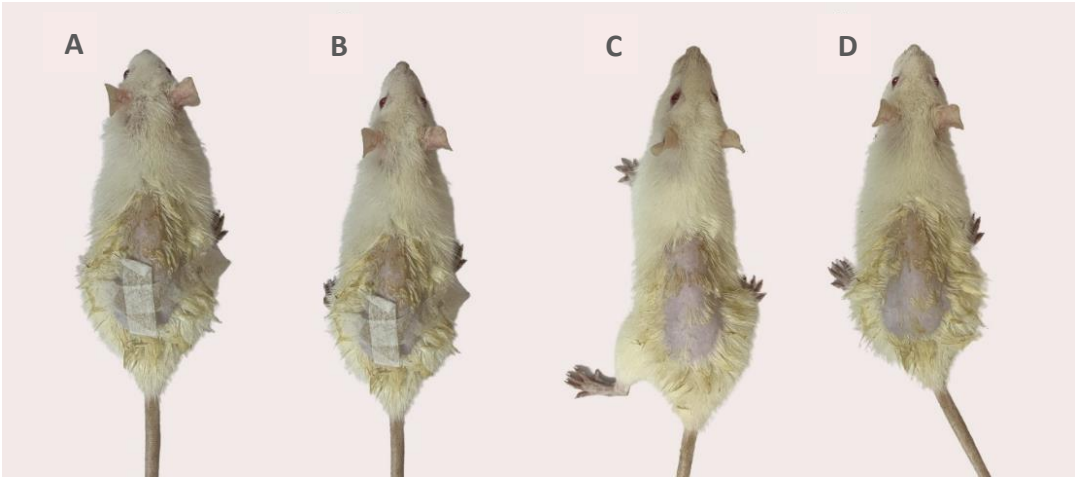

Fig 5B.43. Skin irritation test of the transdermal patches on rats; A-B) After application of the patch and C-D) After removal of the patch

5B.2.11. *Ex Vivo* Skin Permeation Study of the Drugs Released from the Patches:

Ex vivo studies serve as a useful preclinical model for predicting *in vivo* performance, reducing the need for extensive animal testing, and providing early-stage data on patch permeation characteristics. Analyzing a few factors such as drug diffusion rates, permeation profiles, and skin penetration depths, researchers can gain insights into the kinetics and dynamics of drug transport across the skin, which is essential for optimizing patch formulations and delivery strategies.

Ex vivo skin permeation study showed that the cumulative amount of CH permeated per unit area of skin from A1, A4, A5, and A6 formulations (Fig 5B.44) were 904.16±27.59, 585±39.13, 497.50±78.14, and 526.67±46.22 μg/cm^2 respectively in first 15 h whereas 1007.50±50.88, 913.33±63.12, 802.50±66.76, and 748.33±50.1 μg/cm^2 respectively during 744 h. The steady-state flux (J_{SS}) is obtained by plotting the cumulative amount of drug permeated (μg/cm^2) against time, where the slope is the flux (μg/cm^2.h). The flux for the

formulations A1, A4, A5, and A6 were 0.88±0.23, 0.76±0.11, 0.72±0.13, and 0.66±0.13 μg/cm^2.h respectively. The cumulative amount of EB permeated per unit area of skin from B1, B4, B5, and B6 formulations (Fig 5B.45) were 526.25±65.14, 572.50±92.15, 622.50±83.17, and 655.62±92.19 μg/cm^2 respectively in first 15 h whereas 1160.62±94.12, 1485±52.21, 1415±93.19, and 1355±55.08 μg/cm^2 respectively during 744 h. The J_{SS} values for the formulations B1, B4, B5, and B6 were 1.20±0.15, 1.88±0.16, 1.83±0.18, and 1.62±0.15 μg/cm^2.h respectively. The cumulative amount of PM permeated per unit area of skin from C1, C4, C5, and C6 formulations (Fig 5B.46) were 1496.13±142.189, 3126.13±152.111, 2926.24±172.213, and 1479.31±174.154 μg/cm^2 respectively in first 15 h whereas 1846.97±172.013, 6895.94±183.167, 6071.92±151.641, and 4510.69±193.178 μg/cm^2 respectively during 168 h. The J_{SS} values for the formulations C1, C4, C5, and C6 were found to be 11.98±1.21, 43.53±0.62, 37.89±0.56, and 30.73±0.91 μg/cm^2.h respectively. *Ex vivo* skin permeation study showed that the drug/Na-MMT composites from the patches (A4, A5, A6, B4, B5, B6, C4, C5 & C6) penetrated the layers of skin more effectively as compared to that of pure drugs (B1 & C1), most probably accumulated in hair follicles, and sweat glands (shunt route) to a greater amount and released the drug molecules for a long period in a single dose maintaining an effective concentration in the release medium of pH 7.4 (PBS) [7, 8]. The cation exchange properties of Na-MMT could potentially enhance the solubility of poorly aqueous soluble EB (aqueous solubility = 0.01 to 0.5 mg/mL at 25°C) and PM (aqueous solubility = 14.5 mg/mL at 25°C) drugs. When the clay-drug composites were exposed to the release medium PBS, cations present in the PBS replaced the exchangeable cationic form of the drug molecules present in the interlayer spaces through the ion exchange process. It is noticeable that the A1 formulation released a higher amount of drug exceptionally within a short period as compared to that of the other two formulations containing free drug (B1 & C1). The reason might be the higher aqueous solubility (aqueous solubility = 50 mg/mL at 25°C) along with the

reasonable lipophilicity (log P = 2.49) of CH. Hence, a large number of CH molecules were able to diffuse through the intercellular spaces of the epidermis layer to reach the dermis layer from where they entered into the PBS.

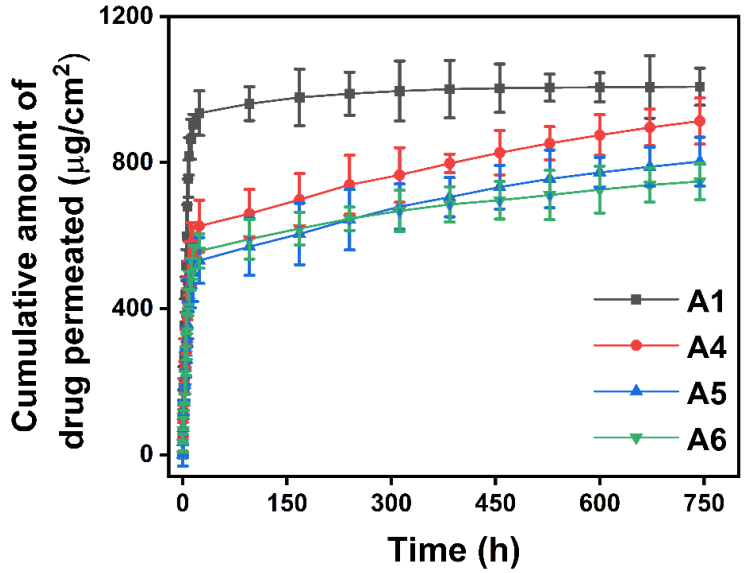

Fig 5B.44. Ex vivo skin permeation study for CH transdermal formulations. The results were expressed as mean ± S.D, n=3

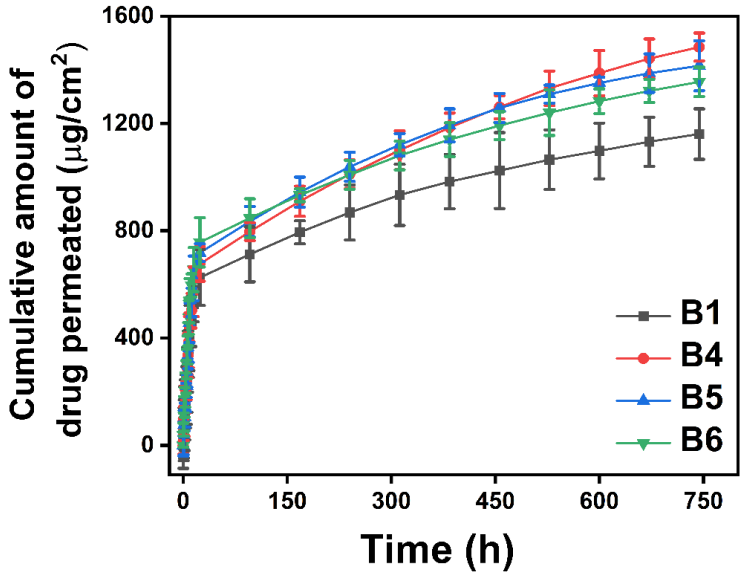

Fig 5B.45. Ex vivo skin permeation study for EB transdermal formulations. The results were expressed as mean ± S.D, n=3

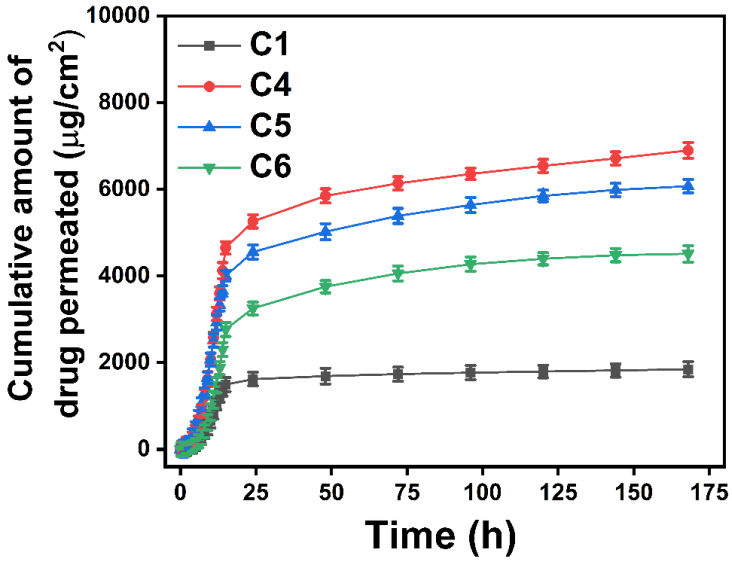

Fig 5B.46. Ex vivo skin permeation study for PM transdermal formulations. The results were expressed as mean ± S.D, n=3

5B.2.12. *Ex Vivo* Drug Release Kinetic Study:

Drug release kinetic studies help to identify potential risks associated with drug formulations, such as dose dumping, skin irritation, or systemic toxicity due to rapid release. By quantifying release rates and profiles, researchers can assess the safety profile of the formulations and implement measures to mitigate any potential risks. Kinetic studies also help to elucidate the mechanisms governing drug release from the formulations. It is important to understand whether release occurs primarily through diffusion, erosion, or a combination of mechanisms, for designing effective formulations and predicting their behaviour *in vivo*. The R^2 value, serving as the regression coefficient, was employed as a measure of goodness of fit to assess the suitable kinetic model associated with *ex vivo* drug release (Tables 5B.2 and 5B.3).

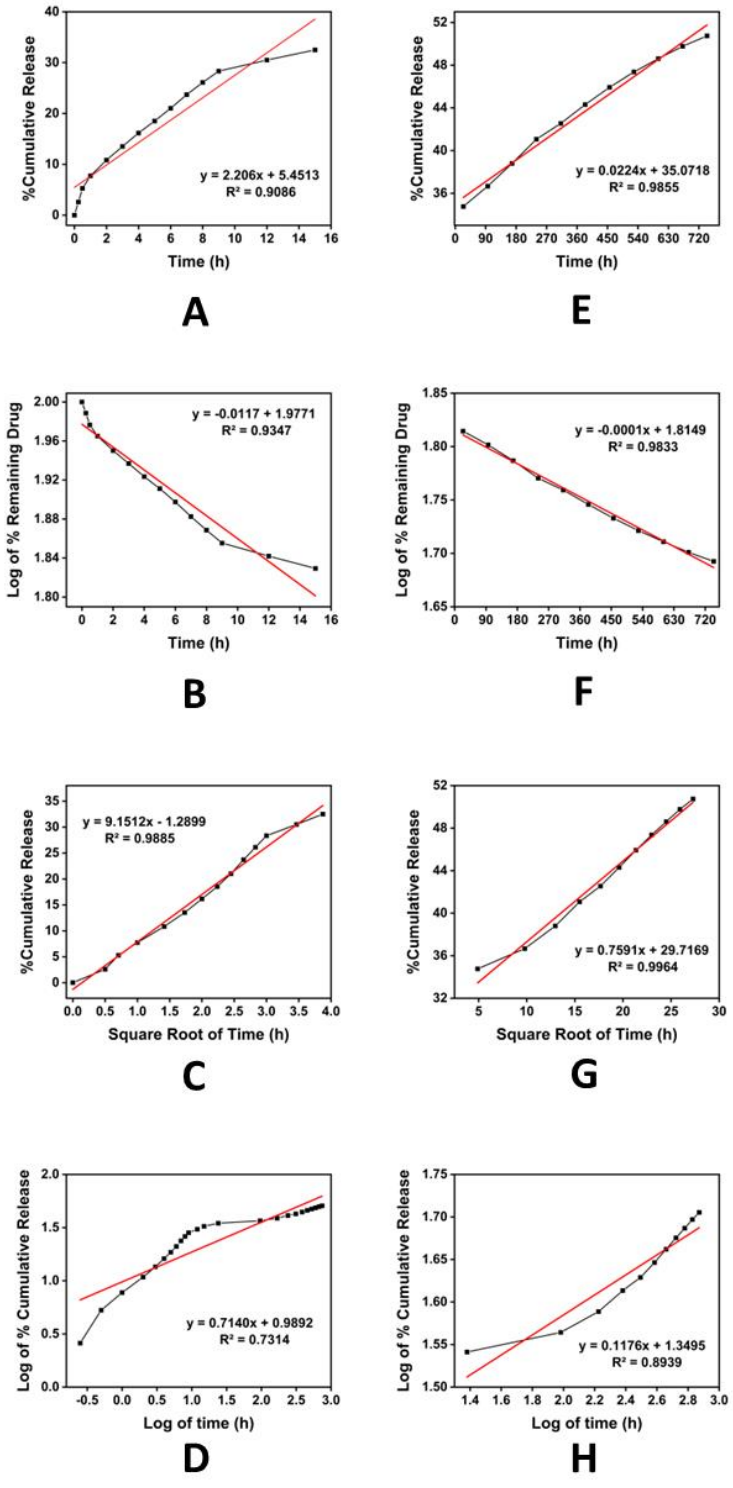

Fig 5B.47. Ex vivo drug release kinetic study of the CH-transdermal formulation A4; A) zero order during burst release. B) first order during burst release, C) Higuchi model during burst release, D) Korsmeyer Peppas model during burst release, E) zero order during sustained release. F) first order during sustained release, G) Higuchi model during sustained release, and H) Korsmeyer Peppas model during sustained release

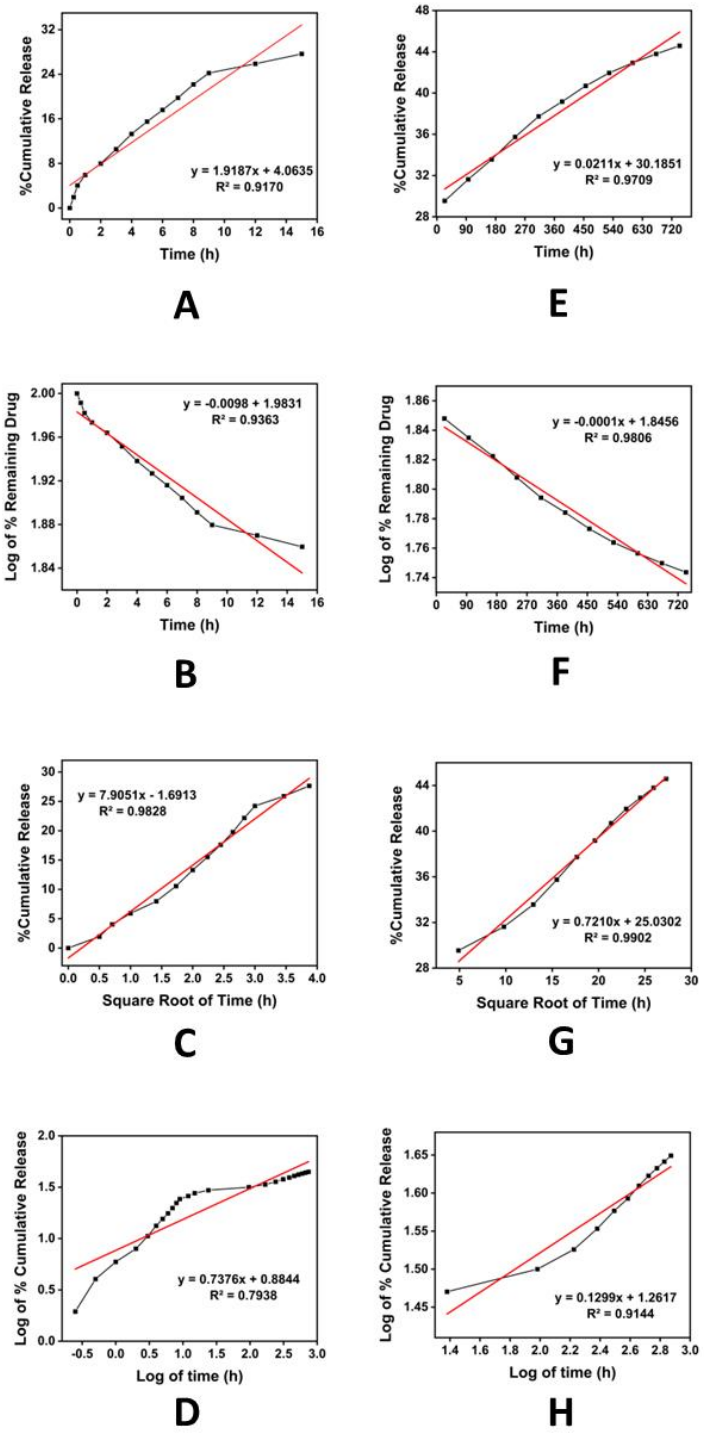

Fig 5B.48. Ex vivo drug release kinetic study of the CH-transdermal formulation A5; A) zero order during burst release. B) first order during burst release, C) Higuchi model during burst release, D) Korsmeyer Peppas model during burst release, E) zero order during sustained release. F) first order during sustained release, G) Higuchi model during sustained release, and H) Korsmeyer Peppas model during sustained release

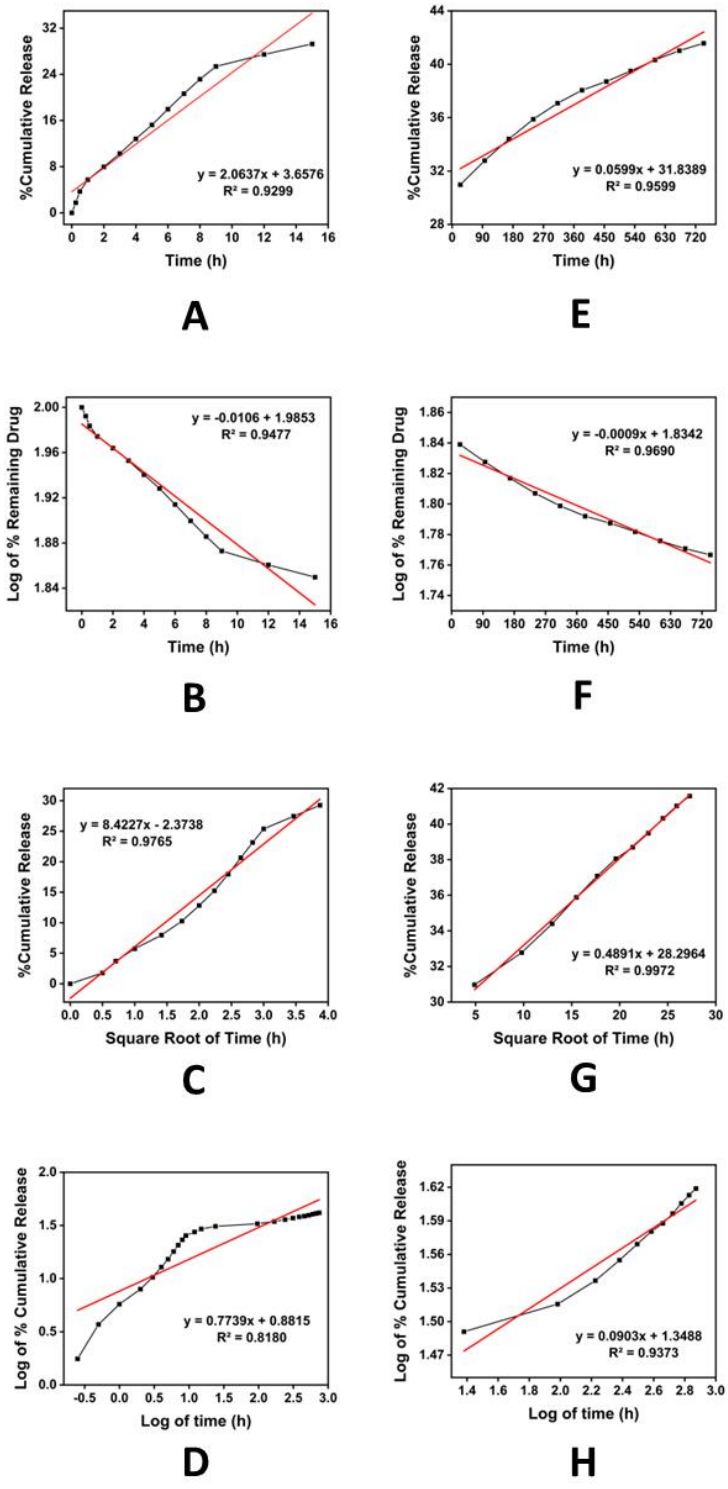

Fig 5B.49. Ex vivo drug release kinetic study of the CH-transdermal formulation A6; A) zero order during burst release. B) first order during burst release, C) Higuchi model during burst release, D) Korsmeyer Peppas model during burst release, E) zero order during sustained release. F) first order during sustained release, G) Higuchi model during sustained release, and H) Korsmeyer Peppas model during sustained release

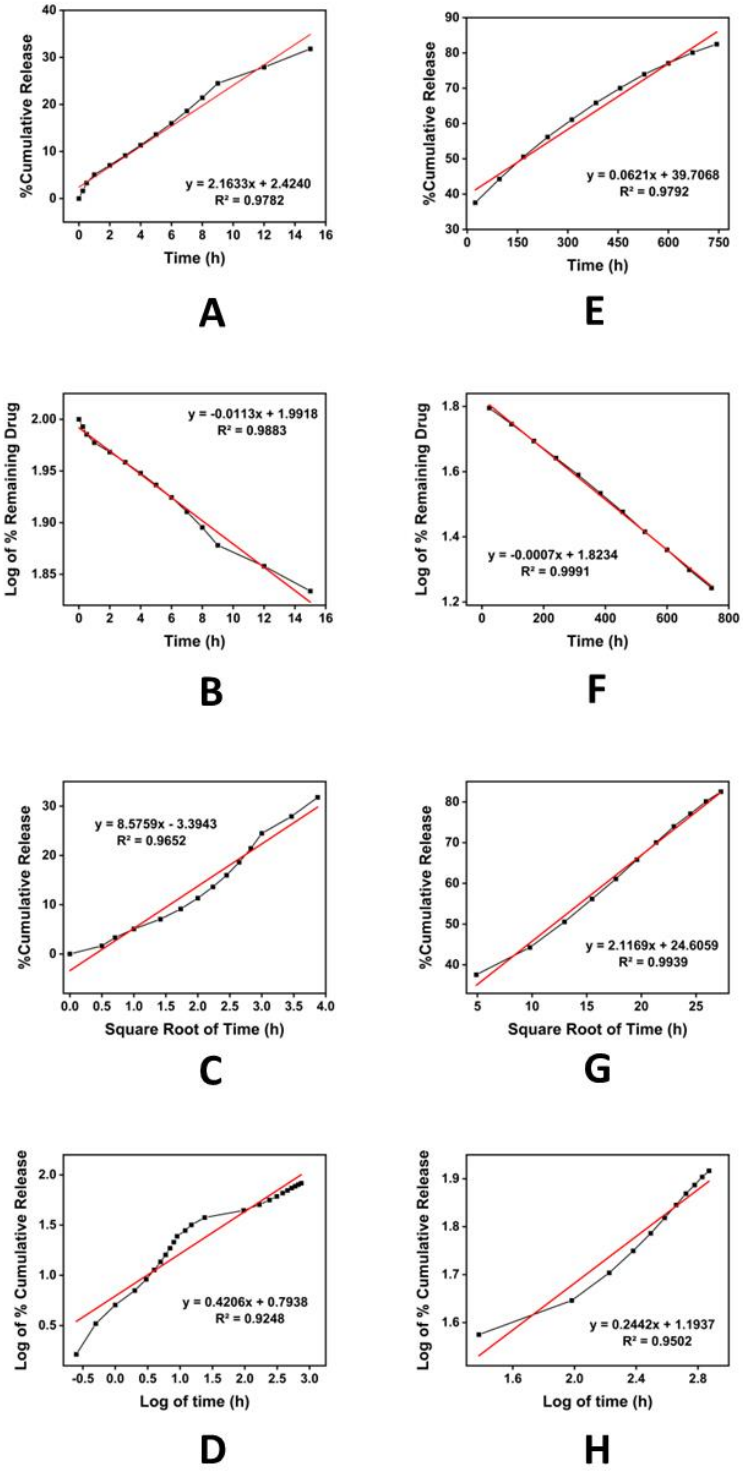

Fig 5B.50. Ex vivo drug release kinetic study of the EB-transdermal formulation B4; A) zero order during burst release. B) first order during burst release, C) Higuchi model during burst release, D) Korsmeyer Peppas model during burst release, E) zero order during sustained release. F) first order during sustained release, G) Higuchi model during sustained release, and H) Korsmeyer Peppas model during sustained release

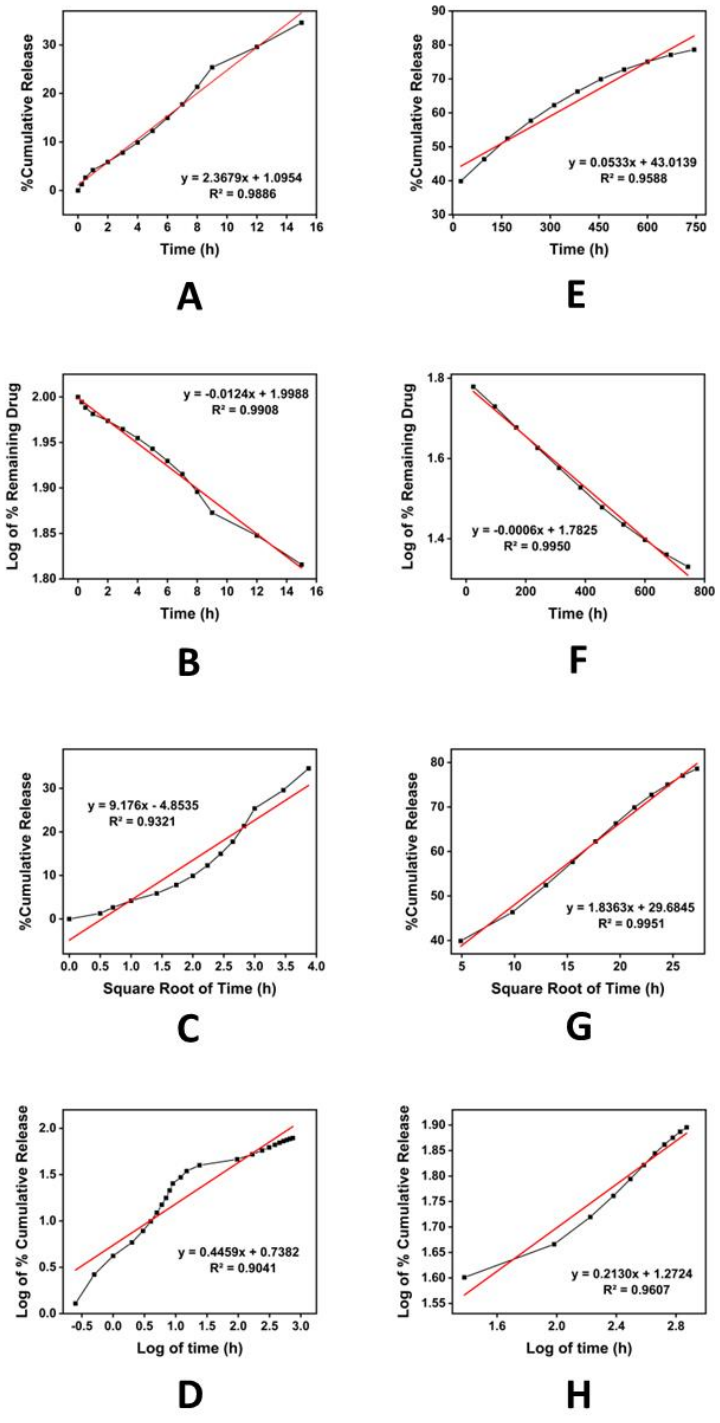

Fig 5B.51. Ex vivo drug release kinetic study of the EB-transdermal formulation B5; A) zero order during burst release. B) first order during burst release, C) Higuchi model during burst release, D) Korsmeyer Peppas model during burst release, E) zero order during sustained release. F) first order during sustained release, G) Higuchi model during sustained release, and H) Korsmeyer Peppas model during sustained release

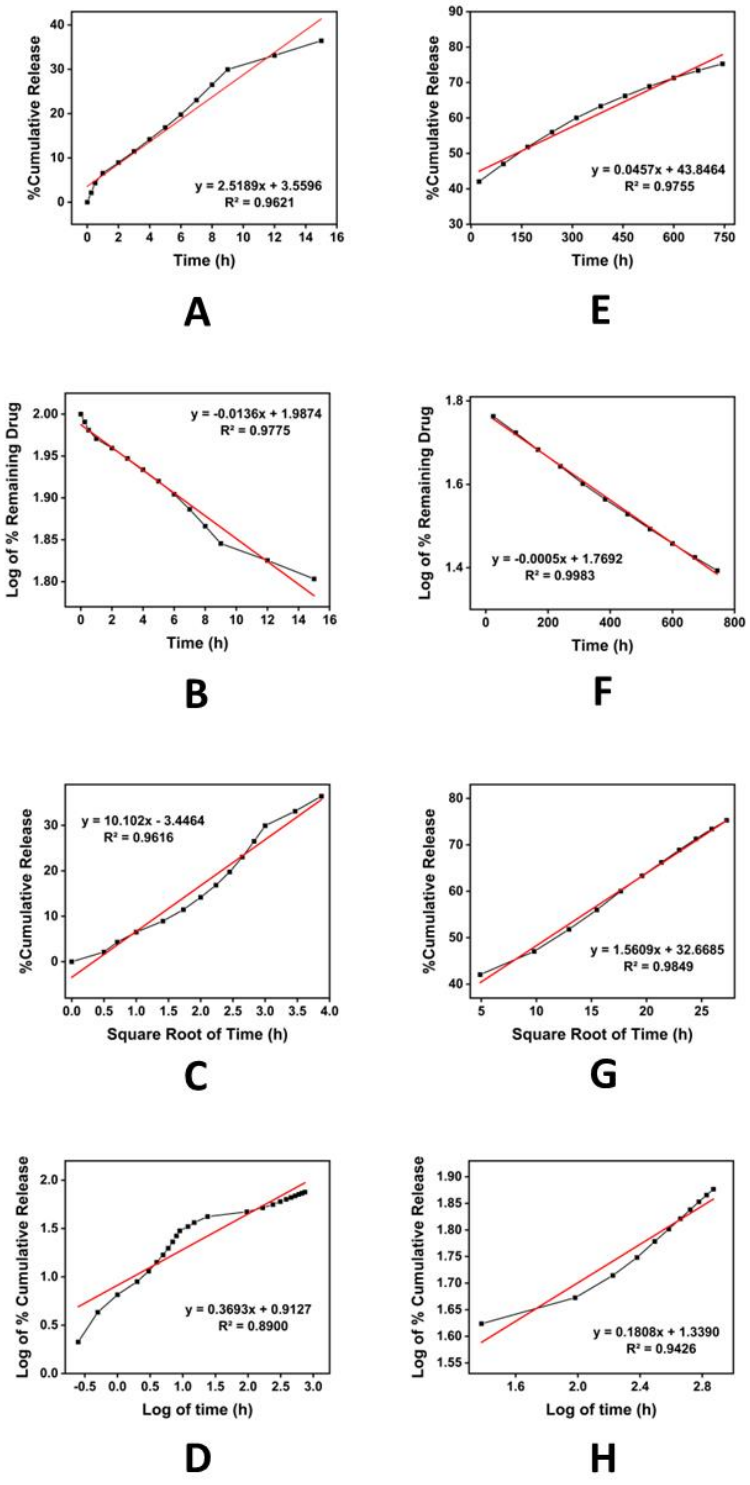

Fig 5B.52. Ex vivo drug release kinetic study of the EB-transdermal formulation B6; A) zero order during burst release. B) first order during burst release, C) Higuchi model during burst release, D) Korsmeyer Peppas model during burst release, E) zero order during sustained release. F) first order during sustained release, G) Higuchi model during sustained release, and H) Korsmeyer Peppas model during sustained release

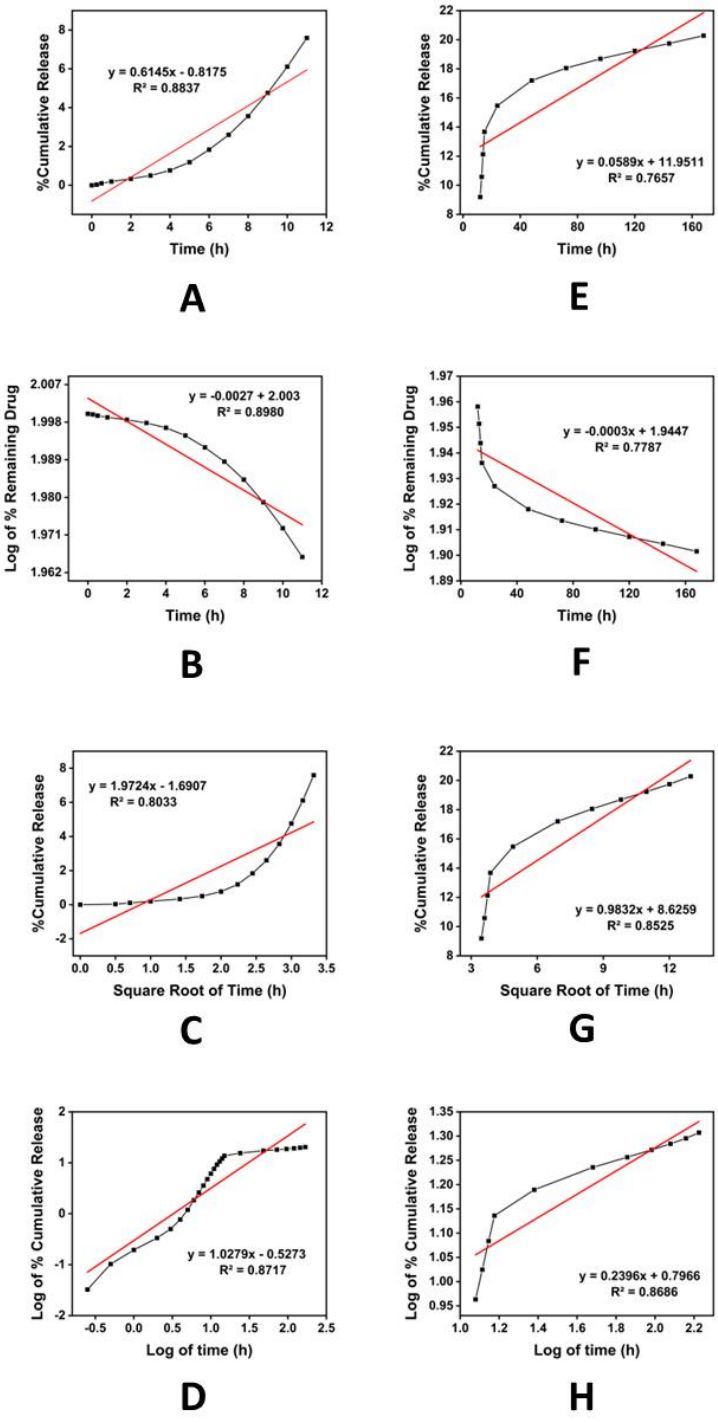

Fig 5B.53. Ex vivo drug release kinetic study of the PM-transdermal formulation C4; A) zero order during burst release. B) first order during burst release, C) Higuchi model during burst release, D) Korsmeyer Peppas model during burst release, E) zero order during sustained release. F) first order during sustained release, G) Higuchi model during sustained release, and H) Korsmeyer Peppas model during sustained release

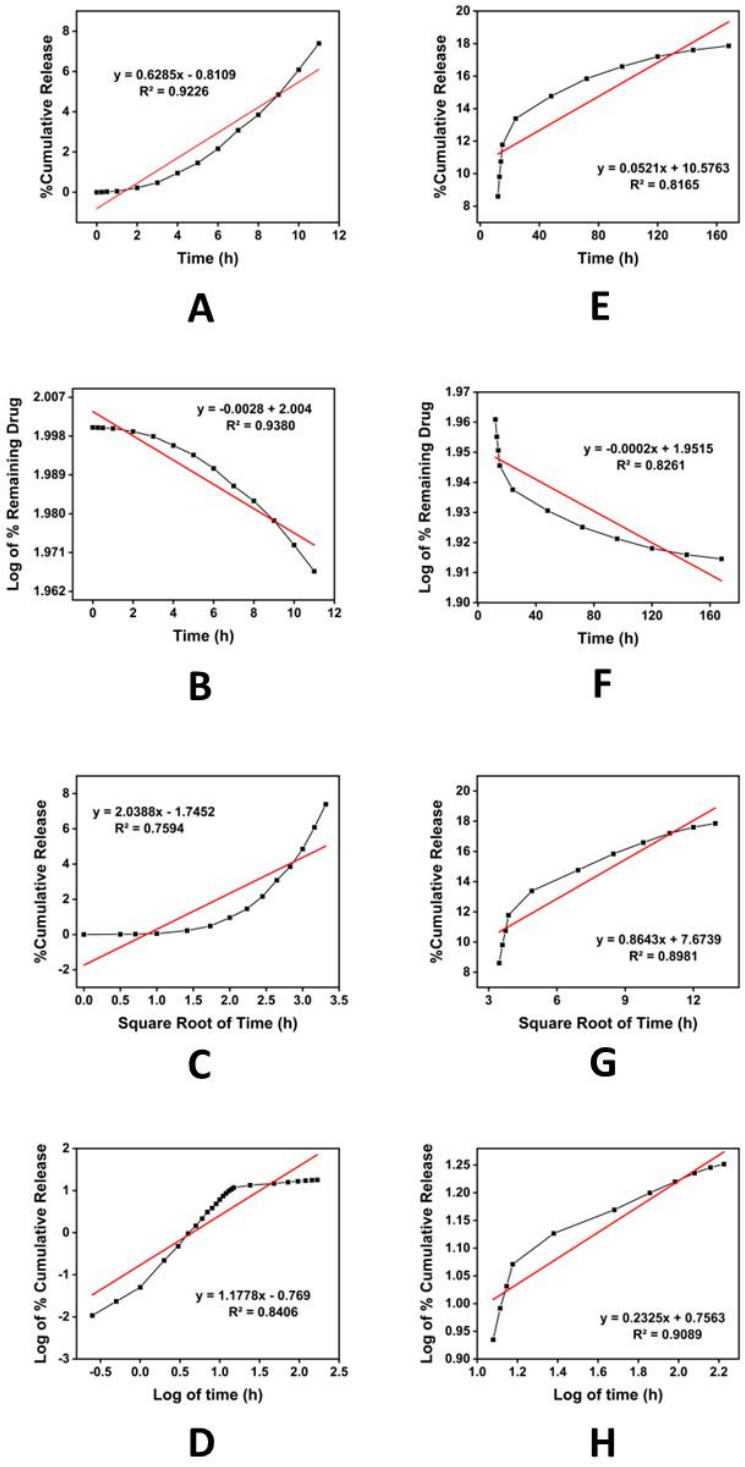

Fig 5B.54. Ex vivo drug release kinetic study of the PM-transdermal formulation C5; A) zero order during burst release. B) first order during burst release, C) Higuchi model during burst release, D) Korsmeyer Peppas model during burst release, E) zero order during sustained release. F) first order during sustained release, G) Higuchi model during sustained release, and H) Korsmeyer Peppas model during sustained release

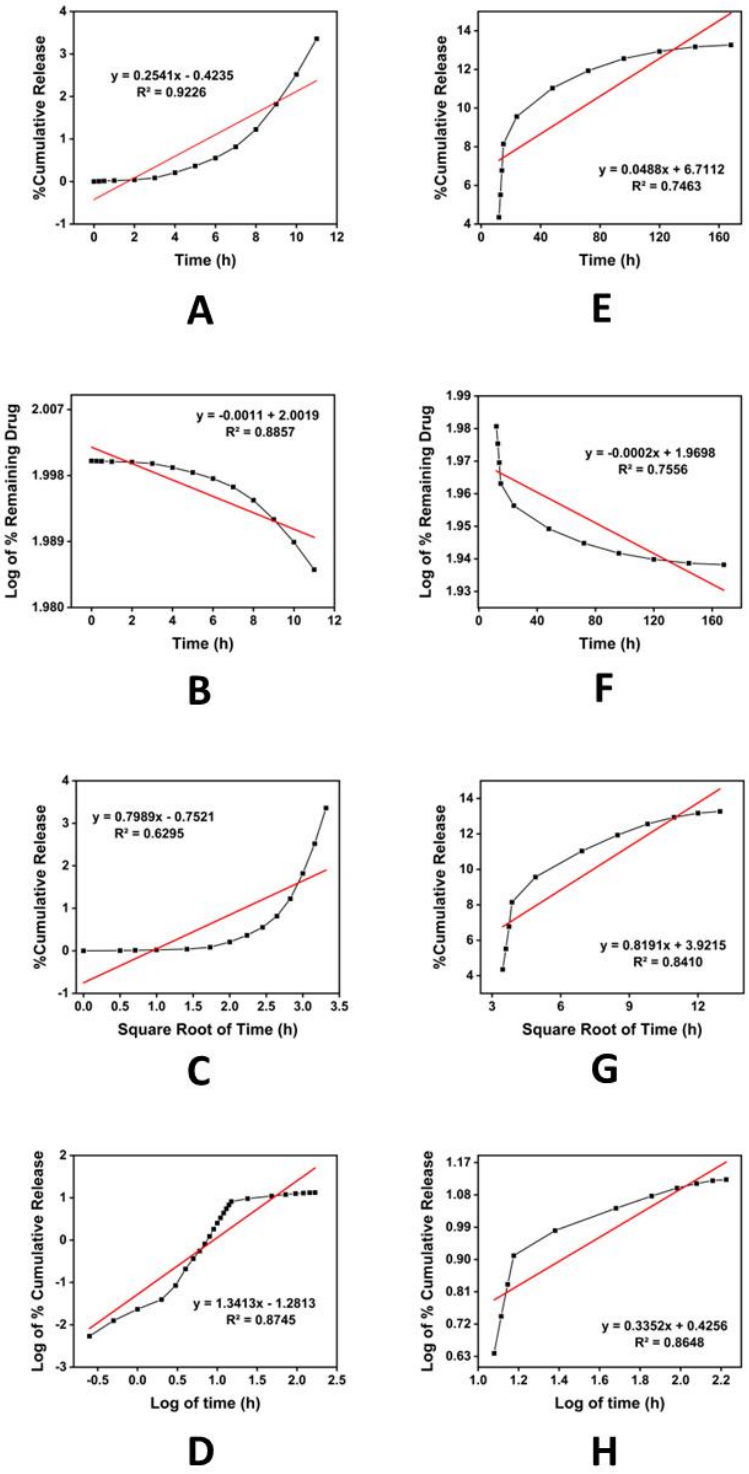

Fig 5B.55. Ex vivo drug release kinetic study of the PM-transdermal formulation C6; A) zero order during burst release. B) first order during burst release, C) Higuchi model during burst release, D) Korsmeyer Peppas model during burst release, E) zero order during sustained release. F) first order during sustained release, G) Higuchi model during sustained release, and H) Korsmeyer Peppas model during sustained release

All CH patches (A4, A5 and A6) adhered to Higuchi kinetics during the burst release phase (for the first 15 h) and the sustained release phase (24-744 h) (Fig 5B.47-5B.49). The release exponent values (the slope of the Korsmeyer–Peppas equation, Tables 5B.2 and 5B.3) established that the release mechanism of CH was non-fickian during the burst release and fickian during the sustained release period. All EB transdermal formulations (B1, B4, B5 & B6) followed first-order kinetics during the burst release phase. In the later period, the same formulations exhibited combined release kinetics (first-order & Higuchi kinetics simultaneously) (Fig 5B.50-5B.52). The release mechanism was fickian from all EB patches throughout the whole release process. Furthermore, all PM formulations (C1, C4, C5 & C6) adhered to first-order kinetics along with the super case II transport release mechanism during the burst release period and combined kinetics of Higuchi and Korsmeyer-Peppas model along with fickian release mechanism during the sustained release period (Fig 5B.53-5B.55). *Ex vivo* drug release kinetic plots of the transdermal formulations loaded with free drugs (i.e., A1, B1 & C1) have already been placed in section 5A.2.12. of the previous chapter 5A.

All transdermal formulations of CH adhered to the Higuchi kinetic model during both burst and sustained release periods as the release rate might depend on the square root of time, not on the remaining concentration of drug adsorbed on the surface of Na-MMT. The dense matrices made of the polymer EC were responsible for the slow release [9]. In other words, the initial drug concentration in the matrix could be substantially greater than the solubility of drug molecules (dissolution of the adsorbed drug molecules), the diffusion was unidirectional, the size of drug molecules might be smaller than the thickness of the system, the dissolution or swelling of the matrix was negligible, the release environment created ideal sink conditions, and the diffusivity of drug molecules might remain constant [10, 11]. Here one thing should be mentioned A4, A5 and A6 exhibited Higuchi kinetics unlike the patches of the other two drugs during the burst release periods despite the presence of nanomedicine in the transdermal matrix.

This could be explained based on the very low dose of CH drug and the slower drug delivery property of the Na-MMT nanoclay as compared to that of SNPs which was also in quite good agreement with the results obtained in *in vitro* and *ex vivo* drug release studies.

With the increase in dose, the maximum number of drug molecules remain adsorbed on the surface of the nanocarriers. Since the dose of EB and PM was higher than CH, all EB patches showed first-order kinetics during the burst release phase as the amount of drug might decrease exponentially over time on the surface of Na-MMT i.e. the release rate depended on the remaining concentration of the drug molecules adsorbed on the surface (dissolution-controlled release). In the later period, the drug molecules might spread from the matrix in one dimension (diffusion-controlled release) and no swelling or dissolution of the matrix occurred. Similarly, the drug release rate from PM patches was dependent on the remaining concentration of the drug adsorbed on the surface of Na-MMT during the burst release period (dissolution-controlled release). Next, the drug release was controlled by a slow diffusion mechanism from the matrix along with the dissolution or swelling of the clay particles.

Table 5B.2. *Ex vivo* release kinetic study of three drugs from Na-MMT-impregnated transdermal formulations during the burst release period

Formulations	Zero-order (R^2)	First Order (R^2)	Higuchi model (R^2)	Korsmeyer-Peppas model (R^2)	Korsmeyer-Peppas model (n)	Release mechanism
A1	0.82929	0.86075	0.97763	0.65343	0.64757	Non-Fickian (Anomalous)
A4	0.90867	0.93472	0.98859	0.73145	0.71402	Non-Fickian (Anomalous)
A5	0.91703	0.93639	0.98284	0.79389	0.73761	Non-Fickian (Anomalous)
A6	0.92997	0.94774	0.97653	0.81802	0.77399	Non-Fickian (Anomalous)
B1	0.9788	0.9877	0.9607	0.9062	0.3996	Fickian diffusion
B4	0.9782	0.9883	0.9652	0.9248	0.4206	Fickian diffusion
B5	0.9886	0.9909	0.9321	0.9041	0.4459	Fickian diffusion
B6	0.9621	0.9775	0.9616	0.8900	0.3693	Fickian diffusion
C1	0.8761	0.8845	0.7010	0.8279	1.2307	Super case II transport
C4	0.8837	0.8980	0.7122	0.8717	1.0279	Super case II transport
C5	0.9226	0.9380	0.7594	0.8406	1.1778	Super case II transport
C6	0.8144	0.8857	0.6295	0.8745	1.3413	Super case II transport

Table 5B.3. *Ex vivo* release kinetic study of three drugs from Na-MMT-impregnated transdermal formulations during the sustained release period

Formulations	Zero-order (R^2)	First Order (R^2)	Higuchi model (R^2)	Korsmeyer-Peppas model (R^2)	Korsmeyer-Peppas model (n)	Release mechanism
A1	0.82610	0.83149	0.97711	0.94386	0.04055	Fickian diffusion
A4	0.98554	0.98333	0.99644	0.89398	0.11762	Fickian diffusion
A5	0.97094	0.98066	0.99020	0.91449	0.12990	Fickian diffusion
A6	0.95994	0.96905	0.99726	0.93731	0.09038	Fickian diffusion
B1	0.9632	0.9880	0.9764	0.9470	0.1917	Fickian diffusion
B4	0.9792	0.9991	0.9939	0.9502	0.2442	Fickian diffusion
B5	0.9588	0.9950	0.9951	0.9607	0.2130	Fickian diffusion
B6	0.9755	0.9983	0.9849	0.9426	0.1808	Fickian diffusion
C1	0.6455	0.6477	0.7366	0.7600	0.1515	Fickian diffusion
C4	0.7657	0.7787	0.8525	0.8686	0.2396	Fickian diffusion
C5	0.8165	0.8261	0.8981	0.9089	0.2325	Fickian diffusion
C6	0.7463	0.7556	0.8410	0.8648	0.3352	Fickian diffusion

5B.2.13. *In Vivo* Analgesic Study via Hot-Plate And Tail-Flick Methods:

The hot-plate and tail-flick tests are widely used experimental models for evaluating analgesic effects in rodents by measuring their response to noxious stimuli. By administering the patches and observing changes in pain thresholds or response latencies, researchers can determine the extent to which the patches alleviate pain.

Both hot plate and tail flick methods displayed that, the highest latency of response in rats was observed for those transdermal formulations in which Na-MMT nanoclay acted as a permeation enhancer for an extended period (A4, A5, A6, B4, B5, B6, C4, C5 & C6). B1 and C1 formulations showed reactivity almost the same as saline (Fig 5B.58-5B.61) whereas A1 performed well for around 4 days beyond which its reactivity decreased gradually (Fig 5B.56-5B.57).

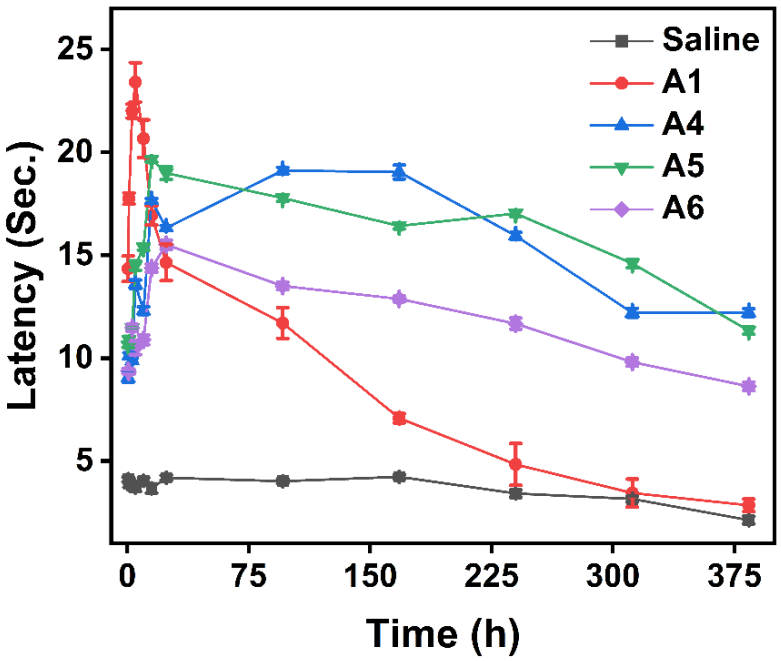

Fig 5B.56. In vivo analgesic study via the "Hot-Plate method" of CH released from four different formulations of transdermal patches on rats. The results were expressed as mean ± S.D, n=3

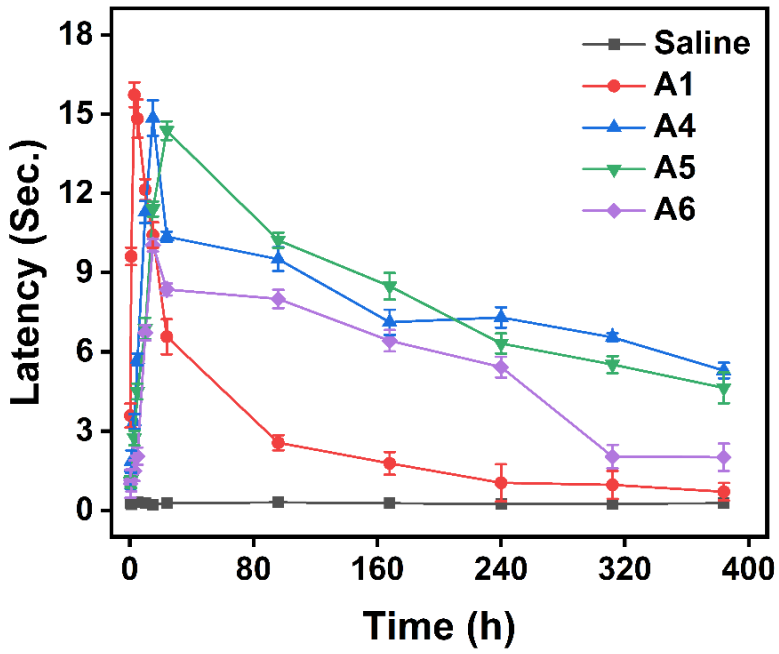

Fig 5B.57. In vivo analgesic study via the "Tail-Flick method" of CH released from four different formulations of transdermal patches on rats. The results were expressed as mean ± S.D, n=3

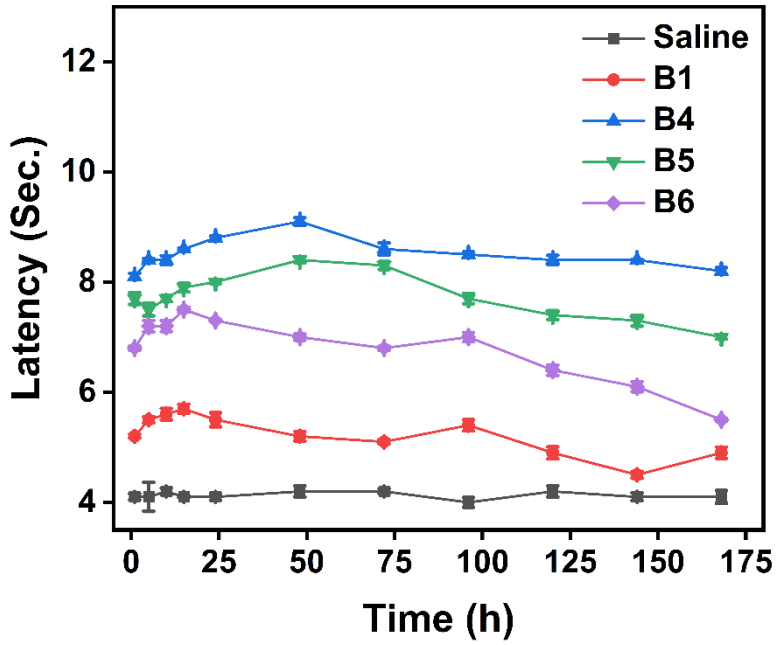

Fig 5B.58. In vivo analgesic study via the "Hot-Plate method" of EB released from four different formulations of transdermal patches on rats. The results were expressed as mean ± S.D, n=3

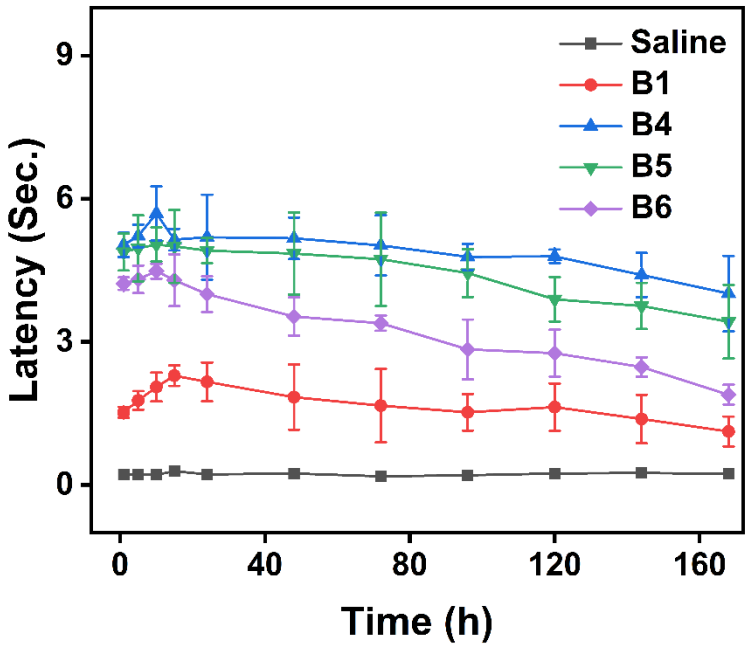

Fig 5B.59. In vivo analgesic study via the "Tail-Flick method" of EB released from four different formulations of transdermal patches on rats. The results were expressed as mean ± S.D, n=3

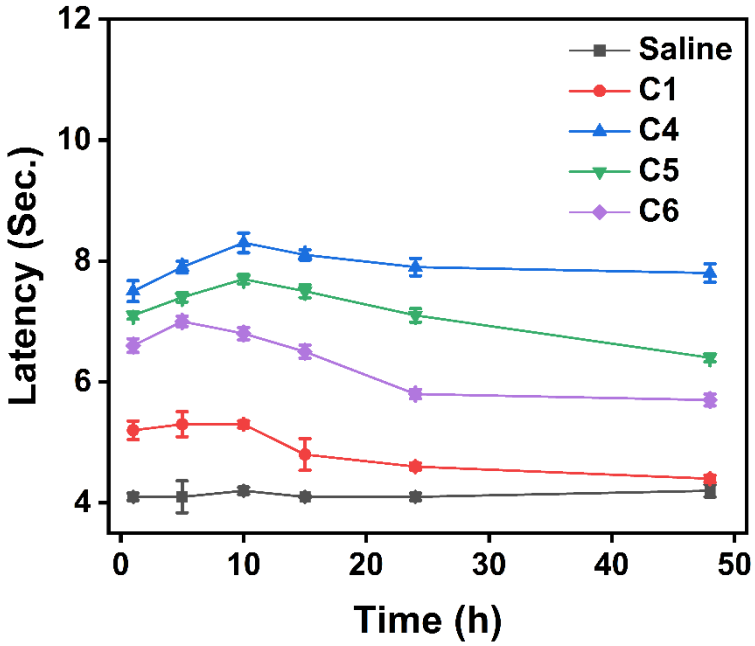

Fig 5B.60. In vivo analgesic study via the "Hot-Plate method" of PM released from four different formulations of transdermal patches on rats. The results were expressed as mean ± S.D, n=3

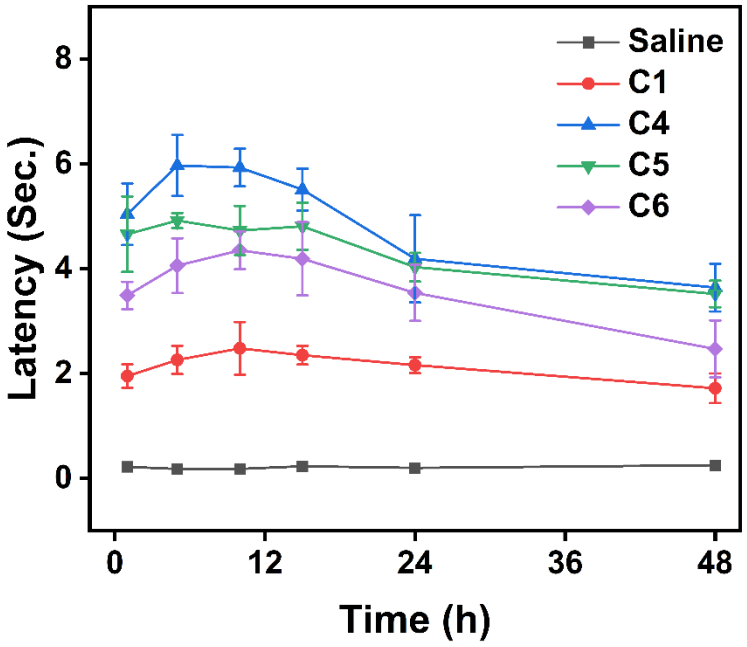

Fig 5B.61. In vivo analgesic study via the "Tail-Flick method" of PM released from four different formulations of transdermal patches on rats. The results were expressed as mean ± S.D, n=3

The responses produced from *in vivo* analgesic activities (hot plate & tail flick methods) fitted well with the findings of both *in vitro* and *ex vivo* drug release studies. Achievement of effective blood plasma concentration of each drug for an extended period in a single dose with the help of nanoclay-based patches could be a reason for long-term analgesia in rats. Thus, the analgesic activity was found to be sustained after the application of A4, A5, A6, B4, B5, B6, C4, C5, and C6 transdermal patches on rats' skin. The overall performance of CH patches was better compared to the other two drugs due to an adequate amount of hydrophilicity as well as lipophilicity of CH molecules.

Conclusions

1. Three different methods were employed to intercalate the drug molecules in the interlayer space of alumina-silicate layers of nanoclay. The aqueous dispersion method exhibited the highest drug loading among the three methods of intercalation. Different pH of the solution was maintained in the dispersion method in which a high amount of CH and PM loading was observed at pH 5 and EB loading was observed at pH 3. TEM, as well as XRD analysis, confirmed the intercalation of drugs in nanoclay.
2. *In vitro* drug release using nanomedicines showed that the percentage of drug release from the nanomedicines prepared via dispersion method was highest and the release percentage from the nanomedicines prepared via grinding method was lowest. This may be attributed to the highest drug loading efficiency in the dispersion method and the lowest loading efficiency in the grinding method. Furthermore, a higher amount of each drug was released at pH 7.4 compared to pH 5.5.
3. The entrapment of the drugs (as free drug molecules and nanomedicines) in the transdermal patches was confirmed by FTIR analysis. SEM images showed that the free drug molecules and nanomedicines were homogeneously dispersed in the transdermal matrix.
4. The Skin irritation study revealed that the excipients of prepared transdermal patches did not cause skin irritation, allergy or dermal toxic effects which means the patches might be patient-friendly.
5. *Ex vivo* skin permeation study revealed that a transdermal patch could transport nanomedicine, which effectively penetrates the skin barrier and releases drug molecules for a long time.
6. *In vivo* analgesic studies on mice as well as rats also showed that the permeation of drug molecules released from the patches through skin layers could be enhanced and the

effectiveness of the drugs could be extended for a prolonged period with the help of Na-MMT. It suggested that the effective blood plasma concentration of these drugs might be achieved in humans with the appropriate doses in such transdermal formulations.

7. The kinetic analysis determined the probable mechanisms associated with the drug release from all the transdermal formulations. Apart from the drug release mechanisms, it was observed that the patches with relatively high drug doses (B4, B5, B6, C4, C5, C6) exhibited first-order kinetics during the burst release period followed by the combination of slow diffusion-controlled Higuchi and Korsmeyer-Peppas model during the sustained release period. A4, A5, and A6 exhibited Higuchi kinetics unlike the patches of the other two drugs during the burst release periods despite the presence of nanomedicine in the transdermal matrix. This could be explained based on the very low dose of CH drug and the slower drug delivery property of the Na-MMT nanoclay as compared to that of SNPs.

Reference:

1. Mohamed, W. S., Mostafa, A. B., & Nasr, H. E. (2014). Characterization and Application of Intercalated Montmorillonite with Verapamil and its Polymethyl Methacrylate Nanocomposite in Drug Delivery. *Polymer - Plastics Technology and Engineering*, *53*(14), 1425–1433. https://doi.org/10.1080/03602559.2014.909462

2. Uddin, F. (2018). Montmorillonite: An Introduction to Properties and Utilization. In M. Zoveidavianpoor (Ed.), *Current Topics in the Utilization of Clay in Industrial and Medical Applications* (p. Ch. 1). Rijeka: IntechOpen. https://doi.org/10.5772/intechopen.77987

3. Lambers, H., Piessens, S., Bloem, A., Pronk, H., Finkel, P., & Household, S. L. (2006). *Natural skin surface pH is on average below 5, which is beneficial for its resident flora*. *International Journal of Cosmetic Science* (Vol. 28).

4. Romano, E., Davies, L., & Brandán, S. A. (2017). Structural properties and FTIR-Raman spectra of the anti-hypertensive clonidine hydrochloride agent and their dimeric species. *Journal of Molecular Structure*, *1133*, 226–235. https://doi.org/10.1016/j.molstruc.2016.12.008

5. Das, A., Nayak, A. K., Mohanty, B., & Panda, S. (2011). Solubility and Dissolution Enhancement of Etoricoxib by Solid Dispersion Technique Using Sugar Carriers. *ISRN Pharmaceutics*, *2011*, 1–8. https://doi.org/10.5402/2011/819765

6. Chanda, A. (2015). EVALUATION AND ISOLATION OF NOVEL BINDING AGENT ALSTONIA EVALUATION AND ISOLATION OF NOVEL BINDING AGENT. *World Journal of pharmacy and pharmaceutical sciences*, *4*(04), 1247–1258.

7. Akram, M. W., Jamshaid, H., Rehman, F. U., Zaeem, M., Khan, J. zeb, & Zeb, A. (2022). Transfersomes: a Revolutionary Nanosystem for Efficient Transdermal Drug Delivery. *AAPS PharmSciTech*, *23*(1). https://doi.org/10.1208/s12249-021-02166-9

8. Lademann, J., Patzelt, A., Richter, H., Antoniou, C., Sterry, W., & Knorr, F. (2009). Determination of the cuticula thickness of human and porcine hairs and their potential influence on the penetration of nanoparticles into the hair follicles. *Journal of Biomedical Optics*, *14*(2), 021014. https://doi.org/10.1117/1.3078813

9. Adeleke, O. A. (2019). Premium ethylcellulose polymer based architectures at work in drug delivery. *International Journal of Pharmaceutics: X*, *1*. https://doi.org/10.1016/j.ijpx.2019.100023

10. Siepmann, J., & Peppas, N. A. (2011, October 10). Higuchi equation: Derivation, applications, use and misuse. *International Journal of Pharmaceutics*. https://doi.org/10.1016/j.ijpharm.2011.03.051

11. Elmas, A., Akyüz, G., Bergal, A., Andaç, M., & Andaç, Ö. (2020, December 1). Mathematical modelling of drug release. *Research on Engineering Structures and Materials*. MIM RESEARCH GROUP. https://doi.org/10.17515/resm2020.178na0122

Chapter: 6

Overall Conclusion, Limitations, IPR Issues and Future Scope of Work

♦ **Overall Conclusion:**

This research has pioneered the development of nanomedicine-loaded transdermal patches, offering innovative solutions for the delivery of pain-relief drugs such as clonidine hydrochloride (CH), etoricoxib (EB), and paracetamol (PM). By addressing the limitations of conventional drug delivery, this study has demonstrated significant improvements in sustained release and enhanced analgesic effects through SNPs and Na-MMT nanocarriers. The patches have proven to be both effective and biocompatible, with no adverse effects observed in *in vivo* models, paving the way for new, more effective therapeutic options for managing acute and chronic pain. The findings have revealed the versatility of nanomedicine-based transdermal systems, highlighting their potential for prolonged therapeutic effects, reduced side effects, and applicability across a range of pain relief drugs.

➢ **Findings:**

1. A higher percentage of drug loading efficiency was observed for SNPs as compared to Na-MMT nanoclay.
2. *In vitro* as well as *ex vivo* drug release studies showed that the drug release from drug/Na-MMT composites and the patches containing drug/Na-MMT composites occurred at a slower rate as compared to from SNPs and the patches containing SNPs. Due to high drug loading efficiency, a significant amount of the drug was present on the surface of the SNPs. The surface-bound drug is more readily available for immediate release, resulting in a maximum amount of drug release during the burst release period. In the case of Na-MMT, a substantial amount of drug was released from the interlayer region where the drug molecule remains stabilized via different types of interactions (H-bonding, electrostatic interaction, etc.) and therefore the release process occurred very slowly. Hence, the nanoclay was more capable of sustaining the drug

release for an extended period in comparison to that of SNPs. For example, CH, EB, and PM drugs were released approximately 80% in 744 h, 264 h, and 168 h respectively at pH 7.4 from the drug/Na-MMT composites prepared by dispersion method during the *in vitro* drug release study. In contrast, these three drugs were released in the same amount at the same pH from the drug-loaded base-catalyzed SNPs in 120 h, 24 h, and 15 h respectively. This indicates that Na-MMT nanoclay could sustain drug release over a long period, maintaining therapeutic concentrations at each time interval. A similar trend was observed for all remaining nanomedicine formulations at both pH levels (5.5 and 7.4) during the *in vitro* drug release study, as discussed in Chapters 5A (5A.2.6) and 5B (5B.2.6). Additionally, the *ex vivo* drug release study with these nanomedicines incorporated into transdermal patches showed a similar trend at pH 7.4, as presented in detail in Chapters 5A (5A.2.11) and 5B (5B.2.11).

3. Among the three drugs, CH exhibited a higher analgesic effect in both Hot-Plate and Tail-Flick methods for a prolonged period than the other drugs released from both SNPs and Na-MMT-based transdermal patches. A low dose results in a reduced concentration gradient between the dosage form and the surrounding medium, leading to a slower diffusion rate of the drug out of the formulation. Furthermore, the drug molecules may be distributed more evenly throughout the matrix with a low dose. This can extend the diffusion pathway for each drug molecule, resulting in a slow overall release as the drug takes a long time to migrate from the inner parts of the matrix to the outer surface. This is why, CH (dose: 2 mg) showed longer-term analgesia as compared to EB (dose: 60 mg) and PM (dose: 100 mg). Besides, the extent of analgesia for CH was high due to its high aqueous solubility i.e., high solubility in the body fluid. For CH patches, the reaction latency of mice and rats was observed to be up to 21 seconds, and the latency was noticed for 384 h using both the hot-plate and tail-flick methods. In contrast, the

reaction latency of mice and rats was observed to be a maximum of 9.9 and 9.6 seconds for EB and PM patches respectively and this effect did not persist as long as that of the CH patches in either the hot-plate or tail-flick methods. EB and PM patches exhibited analgesia for 168 h and 48 h respectively. The reaction latencies for all transdermal formulations are described in detail in Chapters 5A (5A.2.13) and 5B (5B.2.13).

4. Moreover, *In vivo* analgesic activity of the three drugs in mice/rats via both Hot-Plate and Tail-Flick methods showed that the transdermal patches containing nanomedicines maintained the effective plasma concentration for a few weeks. In contrast, the patches with free CH drug maintained the effective concentration for a few days whereas the patches with free EB and PM drugs were not able to maintain such an effective plasma concentration in a single dose.
5. The transdermal patches caused no dermal toxic effects on mice and rats' skin.
6. Both SNP and Na-MMT-based transdermal patches exhibited mainly first-order kinetics during the burst release period followed by combined kinetics of the Higuchi model and Korsmeyer-Peppas model during the sustained release period of the *ex vivo* release process. This implied that initially, the release rate was highly dependent on the concentration gradient of the drugs i.e., the dose of the drugs in the nanocarriers. Therefore, the release rate gradually decreased with time as the concentration gradient decreased and the release process started to follow a slow diffusion-controlled Higuchi and Korsmeyer-Peppas model. Only CH showed slow diffusion-controlled Higuchi kinetics during the burst release period due to its very low dose.

The overall conclusions on the characteristics of both SNPs and Na-MMT-based transdermal patches are presented as a comparative chart below in Table 6.1.

Table 6.1. The comparative chart between SNPs and Na-MMT-based transdermal patches

Parameters	**SNPs-based Transdermal Patches**	**Na-MMT-based Transdermal Patches**
Differences:		
Shelf Life	They had a longer shelf life due to lower moisture uptake as compared to Na-MMT-based patches, reducing the risks of swelling or degradation.	They had a shorter shelf life due to higher moisture uptake than SNP-based patches.
In Vitro Drug Release Study	The faster release was observed due to the presence of a significant amount of surface-bound drug. For example, CH, EB, and PM drugs were released at approximately 80% in 120 h, 24 h, and 15 h respectively at pH 7.4 from the drug-loaded base-catalyzed SNPs.	The slower drug release was observed due to the intercalation of the drug within the clay layers and the stabilization of drugs within layers via H-bonding or electrostatic interactions. The same 80% release of CH, EB, and PM occurred in 744 h, 264 h, and 168 h respectively from the drug/Na-MMT composites prepared by the dispersion method at the same pH. This implied that prolonged sustained release and better control for extended therapeutic effects can be achieved by Na-MMT nanocarrier.

Ex Vivo Drug Release Study	A faster release from the patches was observed as observed during the *in vitro* drug release study. For example, CH, EB, and PM drugs were permeated through per unit area of human skin at an amount of 642.50±51.13, 1055.62±92.19, and 6394.42±163.389 μg/cm^2 respectively at pH 7.4 within 15 h from the patches containing drug-loaded base-catalyzed SNPs.	The slower drug release from the patches was observed. For example, CH, EB, and PM drugs were permeated through per unit area of human skin at an amount of 585±39.13, 572.50±92.15, and 3126.13±152.111 μg/cm^2 respectively at pH 7.4 within 15 h from the patches containing drug/Na-MMT composites prepared by dispersion method. These findings also indicated that the Na-MMT-based patches can sustain the drug release for a longer period than SNPs-based patches.
Similarities:		
Drug Release Kinetics	Both SNP and Na-MMT-based transdermal patches exhibited mainly first-order kinetics during the burst release period followed by the combined kinetics of the Higuchi model and Korsmeyer-Peppas model during the sustained release period of the *ex vivo* release process. First order kinetics signified that the drug was released at a rate proportional to the concentration of the drug remaining in the nanocarriers. The combined kinetics of the Higuchi and Korsmeyer-Peppas model implied that the release process was diffusion-controlled.	
Analgesic Effect of the Drugs	For both patches, CH exhibited the highest analgesic effect with prolonged relief in both Hot-Plate and Tail-Flick tests (up to 384 h). EB and PM showed lower analgesic effects as compared to CH, lasting 168 h and 48 h, respectively.	

- **Advantages of the Prepared Patches over the Commercially Available Products:**

I. The sustained drug release of the prepared patches, especially with the Na-MMT nanocarrier, ensured prolonged drug delivery over extended periods. For instance, the drug release was sustained for over 744 hours (about 31 days) in some formulations. This is superior to many commercially available patches, which typically only sustain release for a shorter duration.

II. The research highlighted that minimal doses of drugs were required due to the enhanced skin permeation and improved bioavailability. This reduced the potential side effects often associated with high doses in conventional formulations.

III. The patches were effective for various drugs e.g., CH, EB, and PM - demonstrating their versatility in delivering drugs of different solubilities and molecular sizes. This adaptability offers an advantage over commercial patches, often limited to specific drugs due to formulation constraints.

☞ **Interpretation:** The nanomedicine-loaded transdermal patches were successfully prepared for the three types of pain-relief drugs: clonidine hydrochloride (CH), etoricoxib (EB) and paracetamol (PM). The novelty of the research lies in the delivery of drugs as nanomedicine from the transdermal patch. This attempt was made to enhance the skin permeation as well as the solubility of sparingly aqueous soluble pain relief drugs which are unavailable commercially as patches. The prepared patches showed no adverse effects such as redness, itching, inflammation, or rash after the application on mice and rats' skin i.e., the patches can be concluded as user-friendly. Therefore, this research revealed that a nanomedicine-loaded transdermal patch could transport the drug for an extended period which would make it suitable for children, and patients suffering from pain such as any mild pain, cancer pain, inflammation, post-operative pain etc.

♦ **Limitations:**

I. The research is primarily based on *in vivo* studies using animal models (mice and rats), which may not fully replicate the human physiological responses to nanomedicine-based transdermal patches. This introduces a translational gap between the animal model findings and potential human clinical outcomes.

II. The preparation techniques, while effective at a laboratory scale, might face challenges in being scaled up for commercial production without affecting the drug loading efficiency and release kinetics.

III. Na-MMT-based patches demonstrated higher moisture uptake, potentially affecting their stability in humid environments. This limitation may restrict their storage conditions and shelf life, especially in regions with high humidity.

♦ **Intellectual Property Rights (IPR) issues:**

I. The drugs used in the research - Clonidine Hydrochloride (CH), Etoricoxib (EB), and Paracetamol (PM) - are already well-known and extensively used. Therefore, the patentability of the research will not cover the drugs themselves, but rather the method of delivery through the nanoparticle-based transdermal patches. Any further improvements in drug stability, bioavailability, or reduced side effects through this novel delivery system could strengthen patent claims.

II. Since portions of the research have already been published in academic journals, care must be taken to assess whether the published data may have compromised novelty, especially regarding the formulations or methods disclosed.

♦ **Future Scope of Work:**

I. Nanomedicine can be engineered to target specific pain receptors or inflammatory pathways, minimizing off-target effects, and maximizing therapeutic efficacy. This targeted approach could lead to more personalized pain management strategies.

II. Nanotechnology offers opportunities for combining multiple therapeutic agents or modalities within a single transdermal patch. This approach could synergistically enhance pain relief by targeting different aspects of the pain pathway or addressing comorbid conditions simultaneously.

III. In addition to symptomatic relief, nanotechnology-enabled transdermal patches could incorporate bioactive molecules or stem cells to promote tissue regeneration and repair. This regenerative approach holds promise for addressing the underlying causes of certain types of chronic pain and accelerating healing processes.

ANNEXURES

যাদবপুর বিশ্ববিদ্যালয়
কলকাতা-৭০০০৩২, ভারত

*JADAVPUR UNIVERSITY
KOLKATA-700 032, INDIA

FACULTY OF ENGINEERING & TECHNOLOGY
DEPARTMENT OF PHARMACEUTICAL TECHNOLOGY

Certificate

This is to certify that the project proposal no. **JU/IAEC-22/11** entitled **"Design and synthesis of nanocarriers for sustained release of analgesic drugs through different media"**, submitted by **Subrata Goswami** has been approved/recommended by the IAEC of Department of Pharmaceutical Technology, Jadavpur University, in its meeting held on 01.06.2022 and 10: Wistar Rats (Number and Species of animals) have been sanctioned under this proposal for a duration of next 12 months.

Authorized by	Name	Signature	Date
Chairman	Prof. Sanmoy Karmakar	Sanmoy Karmakar	01/6/22
Member Secretary	Prof. Pallab Kanti Haldar	P. Haldar	01/06/2022
Main nominee of CPCSEA	Dr. Sankar Maiti	Sankar Maiti	01-06-2022